SPOTLIGHT ON THE BACKGROUND ACTORS – PHYSIOLOGY AND PATHOPHYSIOLOGY OF SUPPORTING, ACCESSORY AND LESS COMMON CELL TYPES IN THE GASTROINTESTINAL TRACT

EDITED BY: Pawel Ferdek, Wei Huang, Monika Jakubowska and Ole Holger Petersen

frontiers Research Topics

About Frontiers

Frontiers is more than just an open-access publisher of scholarly articles: it is a pioneering approach to the world of academia, radically improving the way scholarly research is managed. The grand vision of Frontiers is a world where all people have an equal opportunity to seek, share and generate knowledge. Frontiers provides immediate and permanent online open access to all its publications, but this alone is not enough to realize our grand goals.

Frontiers Journal Series

The Frontiers Journal Series is a multi-tier and interdisciplinary set of open-access, online journals, promising a paradigm shift from the current review, selection and dissemination processes in academic publishing. All Frontiers journals are driven by researchers for researchers; therefore, they constitute a service to the scholarly community. At the same time, the Frontiers Journal Series operates on a revolutionary invention, the tiered publishing system, initially addressing specific communities of scholars, and gradually climbing up to broader public understanding, thus serving the interests of the lay society, too.

Dedication to Quality

Each Frontiers article is a landmark of the highest quality, thanks to genuinely collaborative interactions between authors and review editors, who include some of the world's best academicians. Research must be certified by peers before entering a stream of knowledge that may eventually reach the public - and shape society; therefore, Frontiers only applies the most rigorous and unbiased reviews.
Frontiers revolutionizes research publishing by freely delivering the most outstanding research, evaluated with no bias from both the academic and social point of view. By applying the most advanced information technologies, Frontiers is catapulting scholarly publishing into a new generation.

What are Frontiers Research Topics?

Frontiers Research Topics are very popular trademarks of the Frontiers Journals Series: they are collections of at least ten articles, all centered on a particular subject. With their unique mix of varied contributions from Original Research to Review Articles, Frontiers Research Topics unify the most influential researchers, the latest key findings and historical advances in a hot research area! Find out more on how to host your own Frontiers Research Topic or contribute to one as an author by contacting the Frontiers Editorial Office: researchtopics@frontiersin.org

SPOTLIGHT ON THE BACKGROUND ACTORS - PHYSIOLOGY AND PATHOPHYSIOLOGY OF SUPPORTING, ACCESSORY AND LESS COMMON CELL TYPES IN THE GASTROINTESTINAL TRACT

Topic Editors:
Pawel Ferdek, Jagiellonian University, Poland
Wei Huang, Sichuan University, China
Monika Jakubowska, Jagiellonian University, Poland
Ole Holger Petersen, Cardiff University, United Kingdom

Table of Contents

frontiers
in Physiology

Check for updates

Editorial: Spotlight on the Background Actors - Physiology and Pathophysiology of Supporting, Accessory and Less Common Cell Types in the Gastrointestinal Tract

Pawel E. Ferdek[1]*, Monika A. Jakubowska[2], Wei Huang[3] and Ole H. Petersen[4]

[1] *Faculty of Biochemistry, Biophysics and Biotechnology, Jagiellonian University, Krakow, Poland,* [2] *Malopolska Centre of Biotechnology, Jagiellonian University, Krakow, Poland,* [3] *Department of Integrated Traditional Chinese Medicine and Western Medicine, Sichuan Provincial Pancreatitis Centre and West China-Liverpool Biomedical Research Centre, West China Hospital, Sichuan University, Chengdu, China,* [4] *School of Biosciences, Cardiff University, Cardiff, United Kingdom*

Editorial on the Research Topic

Spotlight on the Background Actors - Physiology and Pathophysiology of Supporting, Accessory and Less Common Cell Types in the Gastrointestinal Tract

The gastrointestinal (GI) tract is an entire system of different organs and tissues, which not only forms a continuous passageway between the mouth and the anus, but also includes the organs that aid food intake and digestion such as the pancreas, liver, gallbladder, or tongue. The primary role of the GI tract is ingestion of food, followed by breakdown and absorption of nutrients as well as removal of the remaining waste. Additionally, the GI tract serves as part of the immune system and maintains the microbial homeostasis by hosting gut microflora and preventing the expansion of potentially harmful bacteria. Given the magnitude and complexity of its roles, it is not surprising that the GI tract comprises vast spectrum of cell types of distinct morphology and specialized functions. However, not all of those cells receive the same amount of scientific attention. Owing to their prevalence or obvious physiological functions, cells such as hepatocytes, enterocytes, or pancreatic acinar cells have been subjects of a large number of studies in the past decades. Many other cell types of lower abundance or less clear physiological roles have not been perceived as equally attractive research targets and as a result have not been extensively investigated or characterized.

As the name of this Research Topic suggests we intended to put in the spotlight somewhat overlooked "background actors" of the GI tract. Although nine articles in this collection might at first seem very diverse in terms of the subjects they touch on, they share a focus on accessory, supporting or less common cell types found in the intestine, stomach, or pancreas. These articles explore physiological roles pertaining to these cells, describe new methodology or provide a concise review of the current knowledge.

An interesting example of an intestinal cell type are Paneth cells. These cells are known for their role in the innate immunity as they secrete antimicrobial peptides. Singh et al. review the literature on metaplastic Paneth cells in order to understand their etiology and the role they play in intestinal metaplasia. The authors conclude that the presence of metaplastic Paneth cells at extra-intestinal mucosal sites could be linked to a protective response induced by the altered microbiome. A study

by Burgueño et al. also touches on the subject of gut microbiota. The authors not only describe methodology for measuring epithelial production of H_2O_2 but also demonstrate very interesting evidence that intestinal epithelial cells (IECs) generate and release H_2O_2 in response to chronic inflammation or as a result of microbial imbalance. This underlies the pivotal role IECs play in the innate defense mechanisms and in maintaining the intestinal homeostasis.

Moving onto the stomach, populations of cells in the gastric epithelium that express a bitter taste receptor Tas2r126 have been identified by Widmayer et al.. Although their role is not yet entirely clear, the authors speculate that these cells may be part of a "surveillance system" that could detect certain constituents of the luminal content and, by conveying this information to the gastric effectors, control appropriate responses of the stomach to the chemical composition of the luminal content. Further, Baratta et al. provide a review of research methodology used in studies on the parietal cells, an epithelial cell type in the stomach whose main function is secretion of hydrochloric acid. The article describes parietal cell isolation and culture as well as discusses the (patho)physiology of these elusive cells and highlights the major research milestones.

Pancreatic cell types have received relatively a lot coverage in this Themed Issue. Gál et al. describe a method of acute isolation of the pancreas that is particularly useful in studying pancreatic ducts and ductal cells. The method is based on injection of low-melting-point agarose into the pancreas via the common bile duct and it allows not only for morphological characterization of these cells but also for functional investigation. A very interesting study comes from DelGiorno et al., who show that chronic pancreatitis (CP) and acinar-to-ductal metaplasia trigger formation of tuft cells in the mouse pancreas and that this process appears to be affected by the mouse genetical background.

Finally, the physiology of pancreatic stellate cells (PSCs), whose activation is a hallmark of pancreatic disorders, has been highlighted by articles from three different groups. Kuntze et al. have investigated the function of mechanosensitive ion channel Piezo1 in these cells and draw conclusions about its role in the pathogenesis of pancreatic ductal adenocarcinoma (PDAC). Stimulation of this channel induces Ca^{2+} influx and

is associated with alterations in the cytoskeletal architecture. According to the repot, Piezo1 is sensitive to extra- and intracellular acidification, which may downregulate its excessive activation in response to the mechanical stress exerted by the PDAC stroma and thus protect PSCs against Ca^{2+} overload and cell death. Hu et al. present the role of Yes-associated protein 1 (YAP) in the regulation of PSC activation, proliferation, and fibroinflammatory responses during CP and PDAC progression. The authors also highlight the crosstalk between the YAP, TGF-β, and PDGF signaling pathways, all of which regulate PSC activation and growth. We can learn even more about signaling pathways in PSCs from the article by Kusiak et al., who set the focus of their brief review on the Hippo, Wnt pathways, Ca^{2+} signaling as well as mechanosensing, highlighting the role of all the above in (patho)physiology of the pancreas.

AUTHOR CONTRIBUTIONS

All authors listed have made a substantial, direct and intellectual contribution to the work, and approved it for publication.

FUNDING

A Novel *in situ* Approach to Studying Pancreatic Ducts in Mice

Eleonóra Gál[1†], Jurij Dolenšek[2,3†], Andraž Stožer[2†], Viljem Pohorec[2], Attila Ébert[1] and Viktória Venglovecz[1*]

[1] Department of Pharmacology and Pharmacotherapy, University of Szeged, Szeged, Hungary, [2] Faculty of Medicine, University of Maribor, Maribor, Slovenia, [3] Faculty of Natural Sciences and Mathematics, University of Maribor, Maribor, Slovenia

Introduction: The tissue slice technique offers several benefits compared to isolated cells and cell clusters that help us understand the (patho)physiology of several organs *in situ*. The most prominent features are preserved architecture and function, with intact homotypic and heterotypic interactions between cells in slices. In the pancreas, this technique has been utilized successfully to study acinar and endocrine islet cells. However, it has never been used to investigate ductal function. Since pancreatic ductal epithelial cells (PDECs) play an essential role in the physiology of the pancreas, our aim was to use this technique to study PDEC structure and function *in situ*.

Materials and methods: Eight- to sixteen weeks old C57BL/6 mice were used for preparation of pancreas tissue slices. Low melting point agarose was injected into the common bile duct and the whole organ was extracted. For morphological studies, pieces of tissue were embedded in agarose and cryosectioned to obtain 15 μm thick slices. In order to visualize pancreatic ducts, (i) the Giemsa dye was added to the agarose and visualized using light microscopy or (ii) immunostaining for the cystic fibrosis transmembrane conductance regulator (CFTR) was performed. For functional characterization, agarose-embedded tissue was immediately cut to 140 μm thick tissue slices that were loaded with the cell permeant form of the Oregon Green 488 BAPTA-1 dye and used for confocal calcium imaging.

Results: Giemsa staining has shown that the injected agarose reaches the head and body of the pancreas to a greater extent than the tail, without disrupting the tissue architecture. Strong CFTR expression was detected at the apical membranes of PDECs and acinar cells, whereas islet cells were completely negative for CFTR. Stimulation with chenodeoxycholic acid (CDCA, 1 mM) resulted in a robust transient increase in intracellular calcium concentration that was readily visible in >40 ductal cells per slice.

Conclusion: Our results confirm that the acutely-isolated pancreas tissue slice technique is suitable for structural and functional investigation of PDECs and their relationship with other cell types, such as acini and endocrine cells *in situ*. In combination with different genetic, pharmacological or dietary approaches it could become a method of choice in the foreseeable future.

Keywords: pancreas, slice, duct, calcium, CFTR, Giemsa, chenodeoxycholic acid

INTRODUCTION

The tissue slice technique is a suitable *in situ* experimental system for investigating structure and function of different tissues, such as the brain, liver, adrenal gland, and retina (Skrede and Westgaard, 1971; Moser and Neher, 1997; Enoki et al., 2006; Graaf et al., 2007). Speier et al. applied and optimized this technique to study pancreatic beta cell function (Speier and Rupnik, 2003). Since then, it was successfully used to study the functional organization and calcium dynamics of beta cells within islets (Dolenšek et al., 2013; Stožer et al., 2013a,b). The technique has also been applied to characterize acinar cell morphology and secretory function (Marciniak et al., 2013, 2014; Liang et al., 2017). Although there are several *in vitro* approaches for the isolation of both islets and acini from the pancreas, importantly, the greatest advantages of tissue slice preparation technique is that it does not require enzymatic digestion and the architecture and viability of the cells are retained in an intact, nearly physiological environment. It is also important to emphasize that this technique is suitable for both morphological and functional imaging, as well as for electrophysiological studies and investigating interactions between neighboring cells or between the exocrine and endocrine part of the pancreas (Marciniak et al., 2013; Klemen et al., 2014).

Basically, there are two major cell types in the exocrine pancreas, the acinar cells and the pancreatic ductal epithelial cells (PDECs). Although PDECs comprise only a very small fraction of the entire organ, they play an essential role in maintaining the integrity of the pancreas. PDECs secrete an HCO_3^--rich, alkaline solution that neutralizes the acidic pH of gastric juice, curtails premature trypsinogen activation, and delivers digestive enzymes from the pancreas to the small intestine (Argent Be, 1994; Argent, 2006; Dolensek et al., 2017). Insufficient or decreased HCO_3^--secretion can lead to cystic fibrosis or trigger acute or chronic pancreatitis (Scheele et al., 1996; Venglovecz et al., 2008, 2011; Hegyi and Rakonczay, 2010). Therefore, intensive research has been conducted to characterize the ductal function both under physiological and pathophysiological conditions (Hegyi et al., 2011; Judák et al., 2014; Katona et al., 2016; Venglovecz et al., 2018). In the 80's, Barry Argent and his colleagues worked out a novel technique that allows the isolation of intact intra-interlobular pancreatic ducts from the pancreas of rodents (Argent et al., 1986). This methodological development was a very important milestone in the physiology of the pancreas, since it pointed out that ductal cells not only provide a framework for acini, but also secrete HCO_3^-. However, this technique has many limitations. Ducts are isolated from the pancreas after an enzymatic digestion that may result in functional changes. The isolation procedure is long and the ducts should be incubated overnight in order to facilitate their regeneration, similarly to isolation and cultivation of islets of Langerhans, which can importantly affect their function (Gilon et al., 1994). In addition, the biggest disadvantage of this

technique is that the ductal cells are isolated from their normal environment and, therefore not influenced by other cell types, which can fundamentally support and influence their function. We strongly believe that the pancreas slice preparation is much closer to the physiological conditions than the duct isolation technique and therefore provides a better experimental model to study the function of PDECs both under physiological and pathophysiological conditions.

Our aim in this study was to use the acutely-isolated pancreas tissue slice technique for the morphological and functional investigation of PDECs. We have shown that the ductal cells preserve their viability after the preparation and that the technique is suitable for functional multicellular calcium imaging.

MATERIALS AND METHODS

Ethical Approval

Animal experiments were conducted in compliance with the *Guide for the Care and Use of Laboratory Animals* (United States, Department of Health and Human Services, NIH publication No 85-23, revised 1985) and the experimental protocol was approved by the local Ethical Board of the University of Szeged, the National Scientific Ethical Committee on Animal Experimentation (Budapest, Hungary), and the Veterinary administration of the Republic of Slovenia (permit number: U34401-12/2015/3).

Chemicals and Solutions

Cystic fibrosis transmembrane conductance regulator (CFTR) human, polyclonal antibody was ordered from Alomone Labs (Jerusalem, Israel). Alexa Fluor Goat Anti-Rabbit IgG secondary antibody was obtained from Abcam (Cambridge, UK). Cell permeant acetoxymethyl ester of Oregon Green 488 BAPTA-1 (OGB-1) was from Invitrogen (Eugene, OR, USA). All other laboratory chemicals were ordered from Sigma-Aldrich Kft. (Budapest, Hungary). Extracellular solution (ECS) contained (in mM): 125 NaCl, 2.5 KCl, 26 $NaHCO_3$, 1.25 NaH_2PO_4, 6 glucose, 6 lactic acid, 3 myo-inositol, 0.5 ascorbic acid, 2 Na-pyruvate, 1 $MgCl_2$, and 2 $CaCl_2$. ECS was gassed with 95% O_2/5% CO_2 to set pH to 7.4. For calcium dye loading, we used a HEPES-buffered solution containing (in mM): 150 NaCl, 10 HEPES, 6 glucose, 5 KCl, 2 $CaCl_2$, 1 $MgCl_2$; titrated to pH = 7.4 using 1 M NaOH. For stimulation of PDECs during confocal imaging, we used 1 mM chenodeoxycholic acid (CDCA) dissolved in ECS.

Preparation of Pancreas Tissue Slices

Eight- to Sixteen weeks old C57BL/6 mice of either sex were used. Preparation of acutely-isolated pancreas tissue slices has been described in detail previously (Speier and Rupnik, 2003; Stožer et al., 2013a; Marciniak et al., 2014). Briefly, after sacrificing the animal, the abdomen was accessed via median laparatomy, the papilla of Vater clamped distally and 1.5–2.5 ml of low-melting-point agarose (1.5–1.8%, with or without Giemsa dye, according to protocol) was injected into the common bile duct using 30 G needles. The injected pancreas was then cooled with

FIGURE 1 | Preparation of pancreas slices. (A) Mouse pancreas after injection with agarose. (B) Higher magnification (40X) of the isolated pancreas with an intralobular duct (black arrow head). (C) Pancreas tissue pieces embedded in agarose cubes.
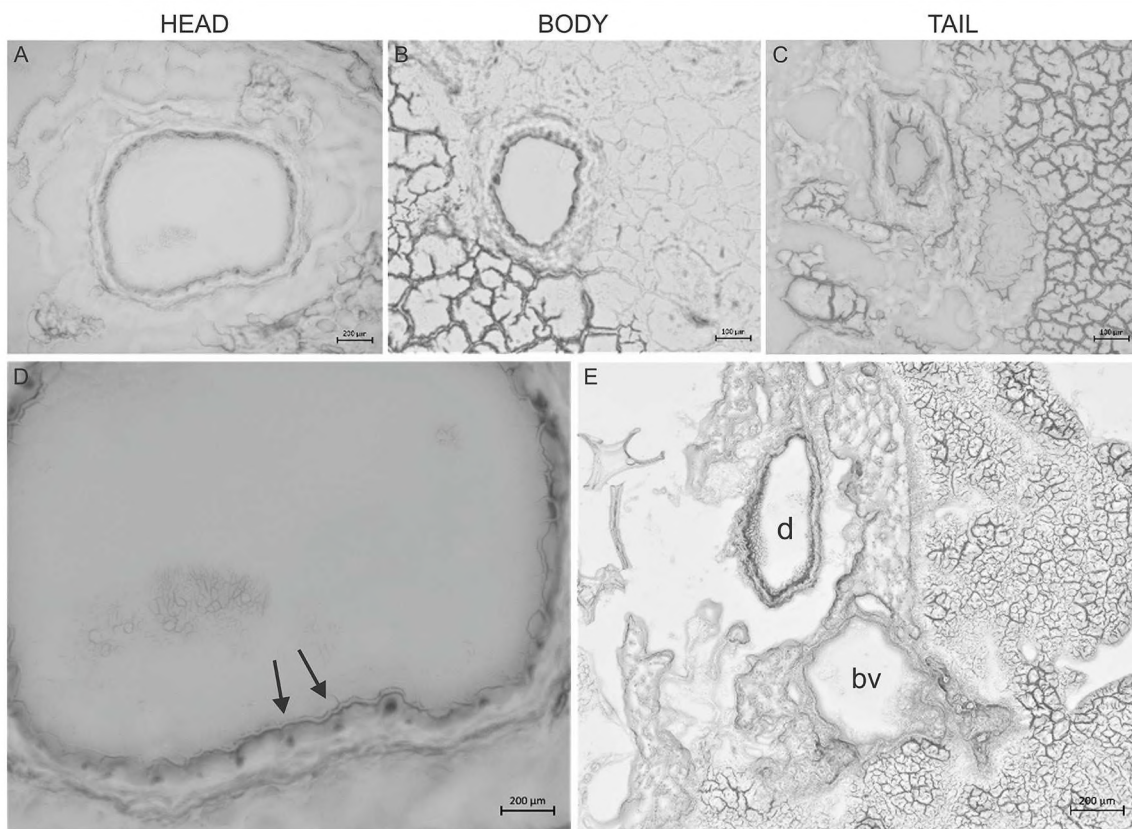
FIGURE 2 | Giemsa staining of the pancreas. Representative cryosections were cut from the head (A), body (B), and tail (C) of the pancreas. Giemsa stain causes dark coloring of the nuclei of inter-intralobular ducts in the head and body of the pancreas and slightly in the tail. (D) Magnified picture of (A). Arrows indicate dark coloring of the nuclei. (E) Representative cryosection from the head of the pancreas shows that Giemsa stained the duct (d) but not the blood vessels (bv).

ice-cold ECS and transferred into a sterile Petri dish containing ice-cold ECS (**Figure 1A**). Higher magnification image of the gland shows the presence of an interlobular duct (**Figure 1B**). In the next step, the pancreas was cleaned from fat and connective tissue, and cut into small pieces (0.25–1.0 cm^3 in size) using surgical scissors. Individual pieces of agarose-injected pancreas were embedded in agarose (1.5–1.8%) (**Figure 1C**) and further sectioned either for immunohistochemistry (IHC) or for calcium imaging. For IHC, the isolated tissue was further embedded in cryomatrix and cut into 15 μm sections using a CM1800 cryostat (Leica Biosystems, Wetzlar, Germany). For calcium imaging, 140 μm thick sections were cut using a VT1000 vibratome (Leica Biosystems, Wetzlar, Germany) while the tissue was continuously buffered with ice-cold gassed ECS. Thirty to forty slices were prepared per animal and used immediately for staining.
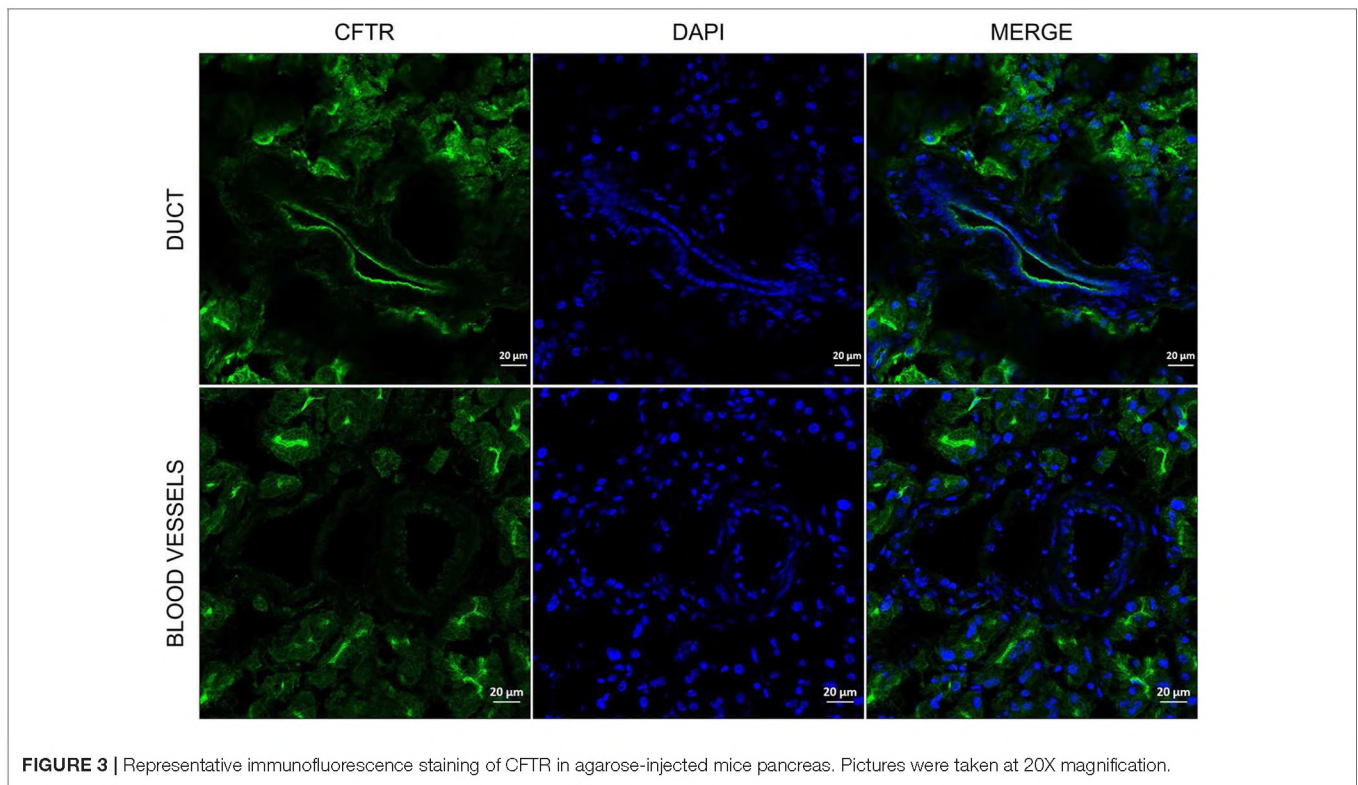
FIGURE 3 | Representative immunofluorescence staining of CFTR in agarose-injected mice pancreas. Pictures were taken at 20X magnification.

Immunohistochemistry

The cryosections were fixed in 4% (v/v) paraformaldehyde for 20 min at room temperature (RT) and washed in PBS 2–3 times. Slices were permeabilized with 0.05% TritonX-100 at RT for 30 min and blocked with the mixture of 1% (v/v) bovine serum albumin/Tris-buffered saline (BSA/TBS) and 10% (v/v) goat serum for 30 min. After the blocking step, slices were incubated with the CFTR rabbit polyclonal antibody (1:100 dilutions) at 4°C, overnight. After the incubation, slices were washed 2–3 times with PBS and incubated with Alexa fluor 488-conjugated goat anti-rabbit IgG secondary antibody (1:400 dilutions) for 3 h at RT. Nuclei were stained with DAPI (1:500 dilutions in BSA/TBS) for 15 min, followed by washing three times in PBS. Slices were mounted using Fluoromount and analyzed using a LSM 880 confocal laser scanning microscope (Carl Zeiss Technika Kft., Budaörs, Hungary). Pancreas slices were excited at 405 (Dapi) and 488 (Alexa fluor 488) nm and emissions were collected at 453 and 516 nm, respectively.

Giemsa Staining

Giemsa was diluted in low-melting-point agarose (1.5%) at a ratio of 1:10, then injected into the common bile duct of the mice as described in the Preparation of Pancreas Tissue Slices section. After the injection, the pancreas was removed cleaned and cut into three pieces (head, body, and tail). Each pieces of the pancreas were then embedded into cryomatrix and cut into 15 µm sections using a CM1800 cryostat (Leica Biosystems, Wetzlar, Germany) and Giemsa staining was analyzed using

an Axio Scope.A1 light microscope (Carl Zeiss Technika Kft., Budaörs, Hungary).

Calcium Imaging

Ten to fifteen slices were incubated in dye-loading solution containing 6 µM of OGB-1, 0.03% Pluronic F-127 (w/v) and 0.12% dimethylsulphoxide (DMSO, v/v, dissolved in HEPES-buffered solution) for 50 min at RT on an orbital shaker (50 turns min^{-1}). Imaging was made within 12 h after staining. Following staining, slices were kept protected from light in a dye-free HEPES-buffered solution, which was exchanged every 2 h. Individual slices were transferred into the recording chamber of either a Leica TCS SP5 II inverted confocal system [Leica HCX PL APO CS 20x immersion objective (NA = 0.7)] or an upright Leica TCS SP5 II confocal system [Leica HCX APO L water immersion objective (20x, NA = 1.0)]. Slices were continuously perfused with gassed ECS at 37°C. OGB-1 was excited by an argon 488 nm laser and fluorescence detected by Leica HyD hybrid detector in the range of 500–650 nm. Eight-bit 512 × 512 pixels images at 1 frame per second were acquired. CDCA stimulation was achieved by manually exchanging delivery tubes of the perifusion system.

RESULTS

Visualization of Pancreatic Ducts in Freshly Prepared Slices

In order to investigate how deep, the agarose penetrates into the ductal tree, Giemsa dye was added to the low melting point agarose (1.5%) in 1:10 dilutions and injected into the

FIGURE 4 | $[Ca^{2+}]_i$ response in ductal cells after stimulation with 1 mM CDCA. **(A)** Confocal fluorescence image of a ductal structure and surrounding acinar tissue with selected regions of interest (ROI) denoting nuclei of individual PDECs. **(B)** Chenodeoxycholic acid (CDCA) induced $[Ca^{2+}]_i$ responses of individual cells corresponding to numbered ROIs in **(B)** (1–6). **(C)** Concurrent transmitted light image. **(D)** Dashed vertical line indicates the start of exposure to 1 mM CDCA. **(E,F)** Bee swarm plots with interquartile ranges and medians for delays of responses after stimulation with 1 mM CDCA ($n = 65$ cells from 4 slices) **(E)** and durations of transient $[Ca^{2+}]_i$ events ($n = 38$ cells from 4 slices) **(F)**.

main pancreatic duct, as described in section Materials and Methods. Freshly prepared pancreas slices of 15 μm thickness from the head, body, and the tail were examined under a stereomicroscope. **Figure 2** shows representative tissue slices with intact pancreas morphology and visible structures of exocrine and endocrine cells. Strong nuclei staining was detected in the intra- and inter-lobular ducts of the head (**Figures 2A,B**) and the body of the pancreas (**Figure 2C**), whereas only weak staining was found in the tail part (**Figure 2D**). Blood vessels were completely negative (**Figure 2E**), indicating that the injection affects only the ductal tree. Using CFTR immunostaining, we were able to identify more specifically the ductal cells in the tissue slices. Under normal conditions, CFTR channel is expressed at the apical membrane of the ductal cells. As shown on **Figure 3**, strong CFTR staining was detected at the apical membrane of PDECs and acini, whereas islet cells and blood vessels were completely negative for CFTR.

CDCA Stimulation Induced a Transient Change in Intracellular Calcium Concentration

To functionally characterize ductal-like structures, we resorted to confocal calcium imaging. Under non-stimulatory conditions, PDECs were brightly stained with OGB-1. Moreover, the dye accumulated in the nuclei producing a typical visual pattern of a mono-layered epithelium (**Figures 4A–C** and **Supplemental Video 1**). The tissue slice technique also enables simultaneous visualization of exocrine acinar cells and islets of Langerhans (**Supplemental Figure 1** and **Supplemental Video 1**). Moreover, calcium activity could be recorded from acinar cells in parallel with PDEC activity, whereas the islets of Langerhans did not respond to the stimulus used in this study (**Supplemental Figure 2**). We stimulated the PDECs using a square pulse-like protocol in which the tissue slices were initially perifused with ECS only, followed by

FIGURE 5 | Spatial displacement of ductal cells after stimulation with 1 mM CDCA. An intralobular duct is shown before **(A)** and during **(B,C)** the stimulation with chenodeoxycholic acid (CDCA). Constructs depicting early **(B)** and late **(C)** $[Ca^{2+}]_i$ response to CDCA display a background of cellular morphology in gray, and an overlay of calcium response in green (see Results section for detailed description). In some PDECs no spatial movement was detected (insets *), whereas in some cells noticeable spatial displacements were observed (insets †). Please note that in the PDECs that were displaced during CDCA response, change in $[Ca^{2+}]_i$ preceded the spatial displacement, therefore not interfering with the calcium response detection.

ECS containing 1 mM CDCA for 10 min. CDCA stimulation evoked a response that was detected in many cells within a single visual field (**Figure 4B**). Individual PDECs responded with a transient increase in $[Ca^{2+}]_i$, followed by a decrease in $[Ca^{2+}]_i$ to a sustained plateau (**Figure 4D**). The median response delay to CDCA stimulation was 14.0 s (Q1 = 11.0 s and Q3 = 24.8 s, **Figure 4E**) and the median duration of the transient change in $[Ca^{2+}]_i$ was 27.5 s (Q1 = 17.0 s and Q3 = 38.0 s, **Figure 4F**).

Coupled with the calcium response, a spatial displacement of PDECs was observed upon stimulation with CDCA (**Figure 5**). In order to exclude the possibility that the detected $[Ca^{2+}]_i$ signal in response to CDCA stimulation was an artifact of cell displacement, we meticulously characterized the movement and compared it with the $[Ca^{2+}]_i$ signal. The calcium response was calculated as $Fresp(t) = F(t) - F_0$, where $Fresp(t)$ presents the calculated calcium response at time t, F_0 the average of the first 100 frames under non-stimulatory conditions and $F(t)$ the calcium signal at time t. A construct was created in which the F_0 frame was displayed in grayscale and $Fresp(t)$ was overlaid in green (**Figure 5** and **Supplemental Video 2**). **Figure 5** shows this construct before CDCA stimulation (**Figure 5A**), as well as the immediate (**Figure 5B**) and late response to CDCA (**Figure 5C**). The initial increase in $[Ca^{2+}]_i$ was coupled with either no (**Figure 5B**, inset *) or minimal (**Figure 5B**, inset †) spatial movement. In contrast, later during the calcium response, some cells failed to display the spatial displacement (**Figure 5C**, inset *), whereas others profoundly changed their location (**Figure 5C**, inset †). The facts that (i) the $[Ca^{2+}]_i$ increase preceded the spatial displacement, and that (ii) $[Ca^{2+}]_i$ transients, similar to the ones in PDECs that did not displace, were recorded from all PDECs that underwent displacement, strongly substantiate that the observed $[Ca^{2+}]_i$ signals are not a motion artifact.

DISCUSSION

We successfully applied the tissue slice preparation technique to study PDECs. The main hallmark of the tissue slice approach, especially in contrast to the majority of studies that were done by isolating ducts using enzymes, is that the homotypic as well as heterotypic interactions are preserved. Histological and functional evaluations of the slices have shown that the slicing procedure did not damage the structure or the function of the tissue indicating that this technique represent an excellent *in situ* model in which the function and the cell-cell interactions of PDECs can be investigated.

For the study of pancreatic acini and islets, the thickness of the tissue slices is critical. The ideal thickness is 100–200 μm, depending on the use of the slice (Marciniak et al., 2014). For the functional cell imaging of PDECs, we found that a practically useful thickness of the slices is 140 μm, enabling the calcium dye to penetrate the cells and allowing for preservation of morphological tissue structure at the same time. Moreover, this thickness allowed for diffusion of gases

and nutrients into the tissue. Tissue slices could be maintained for >8 h in HEPES-buffered solution at RT, however, for even longer studies optimization of the culturing media and use of culture incubators might be needed. One of the critical steps in the preparation of the slices was the injection of agarose. Since pancreas is a "soft" type tissue, injection of agarose serves as a scaffold that stabilized the tissue during cutting. The scaffold effect was achieved by injecting low-melting point agarose at 37°C into the common bile duct, filling the ductal tree retrogradely. Our results have shown that agarose reaches the head and the body of the pancreas and to a smaller extent the tail. We found that the injection procedure did not affect the function or the structure of the ductal cells as confirmed by the histological and functional investigations. Preservation of the intact epithelium has also been confirmed by the fact that the presence of the epithelial-specific ion channel, CFTR, could be detected on the apical membrane of the ductal cells.

Normal calcium signaling plays a central role in the physiological regulation of HCO_3^- secretion by PDECs which is important for neutralization of protons secreted by acinar cells, as well as for keeping trypsinogen in an inactive form and washing it away. Pathologically changed calcium signals, through calcium overload of PEDCs, decreased ATP production due to mitochondrial damage, and impaired HCO_3^- secretion seem to importantly contribute to pathogenesis of acute and chronic pancreatitis (Lee and Muallem, 2008). The toxic calcium signals may be an interesting therapeutic target and thus models that enable studies of PDECs function in normal and pathological conditions are of great practical relevance (Hegyi and Petersen, 2013; Maléth and Hegyi, 2014). To the best of our knowledge, there is only one previous study that analyzed calcium signals in response to bile acids in PDECs. In guinea pig intra-interlobular ducts, low concentration of CDCA, i.e., 0.1 mM, elicited regenerative calcium oscillations that lasted 2–5 min and at this concentration, HCO_3^- secretion was significantly stimulated (Venglovecz et al., 2008). This concentration corresponds with concentrations of taurolithocholic acid sulfate (TLC-S) that elicited calcium responses in the majority of mouse acinar cells. Interestingly, the calcium response in acinar cells was qualitatively very similar to the one in guinea pig PDECs (Voronina et al., 2002). In contrast, 1 mM CDCA produced a transient increase in $[Ca^{2+}]_i$ lasting approximately 5 min, followed by a sustained plateau that returned to the baseline upon termination of stimulation. At this concentration, HCO_3^- secretion was strongly inhibited (Venglovecz et al., 2008). High concentration of TLC-S (0.5 mM) caused a qualitatively very similar response in $[Ca^{2+}]_i$ in mouse acinar cells (Voronina et al., 2002). An important difference in the calcium response between the primary tissue and the slice preparation is that the transient was approximately an order of magnitude shorter (i.e., lasting about 30 s) in the case of slices. Also, in contrast to the behavior in acinar cells, the calcium signals did not seem to be synchronized between different PDECs (Petersen and Findlay, 1987). It needs to be pointed out however, that during supraphysiologically high $[Ca^{2+}]_i$ also acinar cells may be uncoupled (Hegyi and Petersen, 2013). In future studies,

the dose dependence of calcium responses in PDECs needs to be studied into more detail and the slice preparation offers the possibility to simultaneously study the responses of acinar cells. In addition, the specific composition of mouse bile should be taken into account and different bile acids tested for their potential to produce regenerative or sustained calcium responses (Sayin et al., 2013). This shall enable us to assess whether the observed quantitative differences are due to different methodological approaches or due to inter-species differences in responses to bile acids, depending on the relevance of a given bile acid in a given species. Most importantly, a more detailed description of normal and pathological calcium signals in mouse PDECs can help us better understand the etiopathogenesis of pancreatitis and find new therapeutic targets.

An especially interesting observation in this study was that following the CDCA stimulation, we recorded movement of PDECs, a property of PDECs not shown before (**Figure 5**). This active PDEC movement was not uniformly detected in all the cells, moreover it was preceded by the $[Ca^{2+}]_i$ increase, confirming that the recorded $[Ca^{2+}]_i$ signal was not an artifact of this movement. It is not clear what is the mechanism causing the movement of PDECs following CDCA stimulation. A change in osmolality of the local milieu due to the stimulated HCO_3^- secretion may result in an osmotically driven movement. However, we believe this not to be the case since (i) 1 mM CDCA more likely inhibits than stimulates HCO_3^- secretion (Venglovecz et al., 2008), and (ii) the shape of the PDECs as well as of the surrounding acinar cells remained unaffected. More likely, myoepithelial cells in the ducts could provide a mechanistic substrate for active contraction (Puchtler et al., 1975). Therefore, further experiments will be needed to resolve this issue.

In conclusion, we have successfully applied the tissue slice preparation in which the structure and function of PDECs are preserved. This model represents an *in situ* microenvironment that enables studying PDECs under both physiological and pathophysiological conditions and their interaction with the acinar or endocrine cells. This model also opens up the possibilities to investigate human pancreatic function in an intact, *in vivo*-like environment.

DATA AVAILABILITY

All datasets generated for this study are included in the manuscript and/or the **Supplementary Files**.

ETHICS STATEMENT

Animal experiments were conducted in compliance with the Guide for the Care and Use of Laboratory Animals (United States, Department of Health and Human Services, NIH publication No 85-23, revised 1985) and the experimental protocol was approved by the local Ethical Board of the University of Szeged, the National Scientific Ethical Committee on Animal Experimentation (Budapest, Hungary), and the Veterinary

AUTHOR CONTRIBUTIONS

EG was involved in all of the experiments and performed the Giemsa and CFTR staining. JD, AS, and VP performed the calcium imaging, analyzed and interpreted the data, and drafted and edited the manuscript. AÉ was involved in the Giemsa and CFTR staining. VV supervised the project and drafted the manuscript. All authors approved the final version of the manuscript.

FUNDING

SUPPLEMENTARY MATERIAL

The Supplementary Material for this article can be found online at: https://www.frontiersin.org/articles/10.3389/fphys.2019.00938/full#supplementary-material

Supplemental Video 1 | XYZ-stack of OGB-1 loaded acute tissue slice. Morphology of the intralobular duct can be followed, and surrounding acinar and islet cells can be observed. Please note that the structure of acinar cells, as well as an islet of Langerhans, can also be observed in the XYZ-stack.

Supplemental Video 2 | Video demonstrates construct of confocal time series images (see Results section for detailed description). CDCA stimulation from 3.07 s onwards. Background displays cellular morphology in gray, and an overlay of calcium response is depicted in green. See Results section for interpretation.

Supplemental Figure 1 | OGB-1 loaded acute tissue slice demonstrating that different cells types can be visualized simultaneously. The yellow stars depict exocrine acinar cells, the yellow dashed line depicts the border of a pancreatic duct, and the yellow dashed-dotted line depicts the border of an islet of Langerhans.

Supplemental Figure 2 | (A) OGB-1 loaded tissue slice. **(B)** On the same slice, PDECs responding to 1 mM CDCA (red) and spontaneously active acinar cells (blue) are depicted. Numbers correspond with calcium traces in **(C)**. **(C)** Calcium activity of PDECs during stimulation with 1 mM CDCA (red) and spontaneous activity of acinar cells within the slice shown in **(B)**. Numbers correspond with the labels in **(B)**.

REFERENCES

Argent Be, C. R. (1994). "Pancreatic ducts. Cellular mechanism and control of bicarbonate secretion," in *Physiology of the Gastrointestinal Tract*, ed L. Johnson (New York, NY: Raven Press), 1473–1497.

Argent, B. (2006). "Cell physiology of pancreatic ducts," in *Physiology of the Gastrointestinal Tract, 4th Edn,* ed L. Johnson (San Diego, CA: Elsevier), 1376–1396. doi: 10.1016/B978-012088394-3/50057-X

Argent, B. E., Arkle, S., Cullen, M. J., and Green, R. (1986). Morphological, biochemical and secretory studies on rat pancreatic ducts maintained in tissue culture. *Q. J. Exp. Physiol.* 71, 633–648. doi: 10.1113/expphysiol.1986.sp003023

Dolensek, J., Poherec, V., Rupnik, M. S., and Stozer, A. (2017). "Pancreas Physiology," in *Challenges in Pancreatic Pathology*, ed A. Seicean (Romania: IntechOpen), 19–52. doi: 10.5772/65895

Dolenšek, J., Stozer, A., Skelin Klemen, M., Miller, E. W., and Slak Rupnik, M. (2013). The relationship between membrane potential and calcium dynamics in glucose-stimulated beta cell syncytium in acute mouse pancreas tissue slices. *PLoS ONE* 8:e82374. doi: 10.1371/journal.pone.0082374

Enoki, R., Jakobs, T. C., and Koizumi, A. (2006). Horizontal slice preparation of the retina. *J. Vis. Exp.* e108. doi: 10.3791/108

Gilon, P., Jonas, J. C., and Henquin, J. C. (1994). Culture duration and conditions affect the oscillations of cytoplasmic calcium concentration induced by glucose in mouse pancreatic islets. *Diabetologia* 37, 1007–1014. doi: 10.1007/BF00400464

Graaf, I. A., Groothuis, G. M., and Olinga, P. (2007). Precision-cut tissue slices as a tool to predict metabolism of novel drugs. *Expert Opin. Drug Metab. Toxicol.* 3, 879–898. doi: 10.1517/17425255.3.6.879

Hegyi, P., Pandol, S., Venglovecz, V., and Rakonczay, Z. Jr. (2011). The acinar-ductal tango in the pathogenesis of acute pancreatitis. *Gut* 60, 544–552. doi: 10.1136/gut.2010.218461

Hegyi, P., and Petersen, O. H. (2013). The exocrine pancreas: the acinar-ductal tango in physiology and pathophysiology. *Rev. Physiol. Biochem. Pharmacol.* 165, 1–30. doi: 10.1007/112_2013_14

Hegyi, P., and Rakonczay, Z. (2010). Insufficiency of electrolyte and fluid secretion by pancreatic ductal cells leads to increased patient risk for pancreatitis. *Am. J. Gastroenterol.* 105, 2119–2120. doi: 10.1038/ajg.2010.191

Judák, L., Hegyi, P., Rakonczay, Z. Jr., Maleth, J., Gray, M. A., and Venglovecz, V. (2014). Ethanol and its non-oxidative metabolites profoundly inhibit CFTR function in pancreatic epithelial cells which is prevented by ATP supplementation. *Pflugers Arch.* 466, 549–562. doi: 10.1007/s00424-013-1333-x

Katona, M., Hegyi, P., Kui, B., Balla, Z., Rakonczay, Z. Jr., Razga, Z., et al. (2016). A novel, protective role of ursodeoxycholate in bile-induced pancreatic ductal injury. *Am. J. Physiol. Gastrointest. Liver Physiol.* 310, G193–G204. doi: 10.1152/ajpgi.00317.2015

Klemen, M. S., Dolensek, J., Stozer, A., and Rupnik, M. S. (2014). "Measuring exocytosis in endocrine tissue slices," in *Exocytosis Methods. Neuromethods*, ed P. Thorn (Totowa, NJ: Humana Press), 127–146. doi: 10.1007/978-1-62703-676-4_7

Lee, M. G., and Muallem, S. (2008). Pancreatitis: the neglected duct. *Gut* 57, 1037–1039. doi: 10.1136/gut.2008.150961

Liang, T., Dolai, S., Xie, L., Winter, E., Orabi, A. I., Karimian, N., et al. (2017). Ex vivo human pancreatic slice preparations offer a valuable model for studying pancreatic exocrine biology. *J. Biol. Chem.* 292, 5957–5969. doi: 10.1074/jbc.M117.777433

Maléth, J., and Hegyi, P. (2014). Calcium signaling in pancreatic ductal epithelial cells: an old friend and a nasty enemy. *Cell Calcium* 55, 337–345. doi: 10.1016/j.ceca.2014.02.004

Marciniak, A., Cohrs, C. M., Tsata, V., Chouinard, J. A., Selck, C., Stertmann, J., et al. (2014). Using pancreas tissue slices for in situ studies of islet of Langerhans and acinar cell biology. *Nat. Protoc.* 9, 2809–2822. doi: 10.1038/nprot.2014.195

Marciniak, A., Selck, C., Friedrich, B., and Speier, S. (2013). Mouse pancreas tissue slice culture facilitates long-term studies of exocrine and endocrine cell physiology *in situ. PLoS ONE* 8:e78706. doi: 10.1371/journal.pone.0078706

Moser, T., and Neher, E. (1997). Rapid exocytosis in single chromaffin cells recorded from mouse adrenal slices. *J. Neurosci.* 17, 2314–2323. doi: 10.1523/JNEUROSCI.17-07-02314.1997

Petersen, O. H., and Findlay, I. (1987). Electrophysiology of the pancreas. *Physiol. Rev.* 67, 1054–1116. doi: 10.1152/physrev.1987.67.3.1054

Puchtler, H., Waldrop, F. S., Meloan, S. N., and Branch, B. W. (1975). Myoid fibrils in epithelial cells: studies of intestine, biliary and pancreatic pathways, trachea, bronchi, and testis. *Histochemistry* 44, 105–118. doi: 10.1007/BF00494071

Sayin, S. I., Wahlstrom, A., Felin, J., Jantti, S., Marschall, H. U., Bamberg, K., et al. (2013). Gut microbiota regulates bile acid metabolism by reducing the levels of tauro-beta-muricholic acid, a naturally occurring FXR antagonist. *Cell Metab.* 17, 225–235. doi: 10.1016/j.cmet.2013.01.003

Scheele, G. A., Fukuoka, S. I., Kern, H. F., and Freedman, S. D. (1996). Pancreatic dysfunction in cystic fibrosis occurs as a result of impairments in luminal pH, apical trafficking of zymogen granule membranes, and solubilization of secretory enzymes. *Pancreas* 12, 1–9. doi: 10.1097/00006676-199601000-00001

Skrede, K. K., and Westgaard, R. H. (1971). The transverse hippocampal slice: a well-defined cortical structure maintained *in vitro. Brain Res.* 35, 589–593. doi: 10.1016/0006-8993(71)90508-7

Speier, S., and Rupnik, M. (2003). A novel approach to *in situ* characterization of pancreatic beta-cells. *Pflugers Arch.* 446, 553–558. doi: 10.1007/s00424-003-1097-9

Stožer, A., Dolenšek, J., and Rupnik, M. S. (2013a). Glucose-stimulated calcium dynamics in islets of langerhans in acute mouse pancreas tissue slices. *PLoS ONE* 8:e54638. doi: 10.1371/journal.pone.0054638

Stožer, A., Gosak, M., Dolensek, J., Perc, M., Marhl, M., Rupnik, M. S., et al. (2013b). Functional connectivity in islets of Langerhans from mouse pancreas tissue slices. *PLoS Comput. Biol.* 9:e1002923. doi: 10.1371/journal.pcbi.1002923

Venglovecz, V., Hegyi, P., Rakonczay, Z. Jr., Tiszlavicz, L., Nardi, A., Grunnet, M., et al. (2011). Pathophysiological relevance of apical large-conductance Ca2+-activated potassium channels in pancreatic duct epithelial cells. *Gut* 60, 361–369. doi: 10.1136/gut.2010.214213

Venglovecz, V., Pallagi, P., Kemeny, L. V., Balazs, A., Balla, Z., Becskehazi, E., et al. (2018). The importance of aquaporin 1 in pancreatitis and its relation to the CFTR Cl⁻ channel. *Front. Physiol.* 9:854. doi: 10.3389/fphys.2018.00854

Venglovecz, V., Rakonczay, Z. Jr., Ozsvari, B., Takacs, T., Lonovics, J., Varro, A., et al. (2008). Effects of bile acids on pancreatic ductal bicarbonate secretion in guinea pig. *Gut* 57, 1102–1112. doi: 10.1136/gut.2007.134361

Voronina, S., Longbottom, R., Sutton, R., Petersen, O. H., and Tepikin, A. (2002). Bile acids induce calcium signals in mouse pancreatic acinar cells: implications for bile-induced pancreatic pathology. *J. Physiol. (Lond).* 540, 49–55. doi: 10.1113/jphysiol.2002.017525

Yes-Associated Protein 1 Plays Major Roles in Pancreatic Stellate Cell Activation and Fibroinflammatory Responses

Cheng Hu[1,2], Jiayue Yang[2,3], Hsin-Yuan Su[2], Richard T. Waldron[2,4], Mengmeng Zhi[2,3], Ling Li[3], Qing Xia[1], Stephen J. Pandol[2,4] and Aurelia Lugea[2,4]*

[1] Department and Laboratory of Integrated Traditional Chinese and Western Medicine, Sichuan Provincial Pancreatitis Centre and West China-Liverpool Biomedical Research Centre, West China Hospital, Sichuan University, Chengdu, China, [2] Departments of Medicine and Biomedical Sciences, Cedars-Sinai Medical Center, Los Angeles, CA, United States, [3] Department of Endocrinology, Zhongda Hospital Southeast University, Nanjing, China, [4] Department of Medicine, David Geffen School of Medicine at UCLA, Los Angeles, CA, United States

Background: Yes-associated protein 1 (YAP), a transcriptional co-activator and major effector of the Hippo pathway, regulates cell differentiation and morphology in many cell types and supports aberrant tumor growth. Recent studies showed that YAP is expressed in pancreas tissues in pancreatic ductal adenocarcinoma (PDAC) patients and experimental models of PDAC, with YAP largely found in cancer cells and pancreatic stellate cells (PaSC) in the stroma.

Methods and Results: We studied here the role of YAP in the activated phenotype of PaSC. We found that YAP is expressed at low levels in normal mouse pancreas, but protein levels significantly increased after pancreas inflammatory damage induced by repeated cerulein administration in wild-type mice or upon initiation of neoplastic transformation of the pancreas parenchyma in Ptf1-Cre;LSL-Kras$^{G12D/+}$ (KC) mice. In these animal models, YAP upregulation occurred in parallel with activation and proliferation of PaSC. Consistent with these findings, we found robust YAP expression in culture-activated mouse and human PaSC but not in quiescent, freshly isolated cells. Fully activated PaSC isolated from KC mice or PDAC patient tissues exhibited robust nuclear YAP suggesting YAP transcriptional activity. Agents that induce quiescence such as the Bromodomain and Extra-Terminal (BET) inhibitor iBET151 and the p38 MAPK inhibitor SB203580 reduced YAP levels in PaSC. Stimulation of PaSC with the potent mitogen PDGF elicited marked YAP Ser127 phosphorylation. However, unexpectedly, this effect did not diminish YAP nuclear localization, suggesting that YAP phosphorylation at this site does not govern YAP cellular localization in PaSC. siRNA-mediated knockdown of YAP reduced PDGF-induced PaSC expansion in culture and blunted the persistent activation of Akt and ERK elicited by PDGF stimulation, supporting a role for YAP in PDGF-induced cell growth. YAP knockdown also blunted fibroinflammatory gene expression responses both in unstimulated and transforming growth factor beta 1 (TGFβ1)-stimulated PaSC.

Conclusion: Our data suggest a central role for YAP in sustaining the activated phenotype and fibroinflammatory responses in PaSC. Moreover, our findings indicate that a complex crosstalk between YAP, TGFβ1, and PDGF pathways regulates PaSC activity and growth.

Keywords: pancreatic stellate cells, pancreatitis, pancreatic cancer, yes-associated protein 1, fibrosis

INTRODUCTION

Acute (AP), recurrent acute (RAP), and chronic pancreatitis CP are inflammatory disorders of the exocrine pancreas associated with significant morbidity, a high rate of hospitalizations and mortality (Peery et al., 2012; Lew et al., 2017). Further, CP of diverse etiologies significantly increases the risk for pancreatic ductal adenocarcinoma (PDAC) (Lew et al., 2017; Yang and Forsmark, 2017). In this respect, epidemiological studies indicate that CP patients at 5 years after diagnosis have a nearly eight-fold increased risk of acquiring PDAC (Kirkegard et al., 2017). Currently, there are no effective treatments to prevent or attenuate pancreatitis or to prevent RAP and CP from progressing to PDAC, as occurs in some patients.

The precise mechanisms of initiation and progression of CP are unclear. CP is considered to result from unresolved, recurrent fibroinflammation and is characterized by extensive loss of the normal exocrine parenchyma, widespread fibrosis and inflammation, and impairment of both exocrine and endocrine pancreatic functions (Majumder and Chari, 2016; Yang and Forsmark, 2017; Gukovskaya et al., 2019). Accumulating evidence supports the concept that pancreatitis is initiated in the pancreatic acinar cell, the main cell type in the exocrine parenchyma, with stresses causing cellular dysfunction that triggers activation of pro-inflammatory signaling, activation of neighboring quiescent pancreatic stellate cells (PaSC), and immune cell infiltration into the pancreas (Gukovskaya et al., 2019).

PaSC are mesenchymal cells residing in the pancreas. In the normal pancreas, quiescent, non-proliferative PaSC reside in the periacinar space and are estimated to represent about 5–7% of the exocrine parenchymal cells (Omary et al., 2007). Upon pancreas damage, or during the neoplastic transformation of acinar and ductal cells, PaSC acquire a myofibroblast phenotype, a process termed "activation" (Omary et al., 2007; Apte et al., 2013). Characteristics of activated PaSC include high proliferation and growth rates; and expression of marker proteins such as alpha-smooth muscle actin (αSMA), a contractile cytoskeleton protein organized in stress fibers that confer mechanical tension, and cadherin 11 (CDH11), which regulates extracellular matrix (ECM) synthesis and matrix properties (Row et al., 2016). Activated PaSC produce and secrete large quantities of various ECM proteins, cytokines, and growth factors that regulate matrix physical properties, ECM remodeling, and fibrogenesis, as well as immune cell infiltration and inflammatory responses in RAP, CP, and PDAC tumors (Apte et al., 2012, 2013; Erkan et al., 2012; Pandol et al., 2012; Dawson et al., 2013; Chang et al., 2017). Intensive research has demonstrated that PaSC exhibit great plasticity that allows reprogramming in response to multiple inputs from the matrix, neighboring acinar, cancer and immune

cells, and local and systemic factors (Ohlund et al., 2017). Recent work has also shown that PaSC play pivotal roles in other pancreatic disorders including diabetes (Yang et al., 2016). However, despite the critical role of PaSC in pancreas pathobiology, the mechanisms governing their activation, growth, and phenotypic plasticity remain unclear.

Recent studies indicate that Yes-associated protein 1 (YAP) and its homolog WWTR1/TAZ are expressed in pancreatic cells including PaSC during tissue remodeling and PDAC initiation (Morvaridi et al., 2015; Rozengurt et al., 2018; Ansari et al., 2019; Eibl and Rozengurt, 2019). YAP and TAZ are transcriptional regulators that modulate cell proliferation, migration, and apoptosis in developing organs and adult tissues and support aberrant cell growth in many cancers (Eibl and Rozengurt, 2019). By virtue of their sensitivity to mechanical cues such as extracellular matrix rigidity, YAP/TAZ act as mechano-transducers coupling cell-cell and cell-matrix signals with gene expression (Dupont et al., 2011). YAP is found in the cytoplasm and in the nucleus where it interacts with TEF-1/TEC1/abaA (TEA) domain 1-4 (TEAD1-4) and other transcription factors including SMADs involved in cell proliferation, matrix remodeling, and apoptosis (Zheng and Pan, 2019). YAP functions are regulated in a cell type- and context-dependent manner. In myofibroblasts and other cell types, YAP expression and subcellular location are regulated by the Hippo pathway, matrix rigidity, and the mechanical properties of the cellular cytoskeleton (Dupont et al., 2011). Indeed, increased matrix stiffness and high cytoskeletal tension promote YAP nuclear accumulation and transcriptional activity in cancer associated myofibroblasts (Calvo et al., 2013). Recent studies indicate that YAP regulates activation in liver of pro-fibrotic hepatic stellate cells (Mannaerts et al., 2015), a cell type phenotypically similar to PaSC, but the role of YAP in PaSC activation and fibroinflammatory responses has not been defined.

Here, we examined YAP expression and activity during RAP and CP and in quiescent and activated PaSC derived from mouse and human pancreas. We also investigated the effects of agents that we found promote PaSC quiescence, and siRNA-mediated YAP knockdown, on PaSC growth signaling, fibroinflammatory responses, and signaling crosstalk between YAP and two well characterized PaSC activators, platelet-derived growth factor (PDGF) and transforming growth factor beta 1 (TGFβ1).

MATERIALS AND METHODS

Antibodies and Chemicals

The following antibodies were used for Western blotting (WB) and/or immunofluorescence (IF): AKT (#4691), phospho-AKT

(Ser473; #4060), Cadherin11 (CDH11; #4442S), GAPDH (#5174S), CK19 (#12434), p44/42 MAPK (#9102), LATS1 (#3477), phospho-LATS1 (Thr1079; #8654), phospho-p44/42 MAPK (Thr202/Tyr204; #9101), phospho-p70S6 Kinase (Thr389; #9234), SMAD2/3 (#8685), phospho SMAD2 (Ser465/467)/SMAD3(Ser423/425); #8828), YAP (#14074 for WB and IF, #4912 for WB), phospho-YAP (Ser127; #13008), YAP/TAZ (#8418), Caspase-3 (#14220), and corresponding HRP-linked secondary antibodies were from Cell Signaling Technology (Danvers, MA). Antibodies directed against αSMA (#A2547), P4HA2 (#SAB1100773), and β-actin (#A1978) were purchased from Sigma-Aldrich (St. Louis, MO), against GFAP (#ab68428) from Abcam (Cambridge, MA), and against PDGFR-β (#sc-432) from Santa Cruz Biotechnology (Dallas, TX).

Recombinant rat PDGF-BB (PDGF; #520-BB-050), recombinant mouse TGFβ1 (#7666-MB-005), and recombinant human TGFβ1 (#240-B-002) were from R&D Systems, Inc. (Minneapolis, MN). iBet151 (#SML0666) was purchased from Sigma-Aldrich (St. Louis, MO); U0126 (#662005), LY294002 (#440202) and SB203580 (#559389) from MilliporeSigma (Burlington, MA). SuperSignal™ West Pico (or Femto) Chemiluminescent Substrate reagent, 4′,6-diamidino-2-phenylindole (DAPI), ProLong Gold antifade mounting medium, and fluorescence-conjugated secondary antibodies were from ThermoFisher Scientific (Waltham, MA).

Tissue digestion for primary PaSC isolation was performed using Pronase (Roche, #10165921001), Collagenase P (Roche, #11213857001), DNase I (#10104159001) and bovine serum albumin fraction V (BSA; Roche, #3116956001), all obtained from Sigma-Aldrich. Density gradients for PaSC separation were prepared using Nycodenz (#AN1002423; Accurate Chemical & Scientific Corp; Westbury, NY) and Gey's balanced salt solution (GBSS; #G9779; Sigma-Aldrich). Cell culture DMEM/F12 medium (#11330-032), L-Glutamine (#25030-081) were from ThermoFisher Scientific; antibiotics/antimycotics (1% Penicillin–Streptomycin; #25030-081) and fetal bovine serum (FBS; #FB11) were from Omega Scientific (Tarzana, CA). All chemicals and kits were used according to the manufacturer's recommendations, unless otherwise indicated.

Assessment of Yes-Associated Protein 1 Levels in Pancreatic Tissues From Mice Subjected to Cerulein-Induced Pancreatitis

C57BL/6 male mice (Envigo, Placentia, CA) were subjected to repeated episodes of acute cerulein pancreatitis starting at 6–7 weeks of age. Each acute pancreatitis (AP) episode consists of 7 hourly intraperitoneal injections of saline or 50 µg/kg cerulein (Lugea et al., 2006). Recurrent AP (RAP) was characterized in mice subjected to two episodes of cerulein AP, the first one at day 1 (d1) and the second at day 3 (d3). In this RAP model, mice were sacrificed during the acute phase of pancreatitis (1 h after the last cerulein injection, at d1 and d3) and during the recovery phase (at d5). Chronic pancreatitis (CP) was induced by repeated cerulein AP episodes (twice a week for 4 weeks; total eight episodes), and mice were sacrificed 4 days after the last AP episode. At sacrificed, pancreatic tissues were collected and snap-frozen for subsequent

Western blotting analysis (as indicated below) or formalin-fixed for histological assessment of pancreatitis severity, PaSC activation and immunofluorescence analysis of YAP and PaSC activation markers αSMA, Cadherin 11 (CDH11) and PDGF receptor beta (PDGFRβ) expression.

Mice were fed standard chow diet with free access to clean drinking water and maintained at controlled temperature (19–22°C) and 12:12-h light/dark cycle during the duration of the study. Animal studies were approved by the Institutional Animal Care and Use Committee at Cedars-Sinai Medical Center (Los Angeles, CA) in accordance with the NIH Guide for the Care and Use of Laboratory Animals.

Assessment of Yes-Associated Protein 1 Levels in Kras^{G12D} Mice

Wild-type (WT) and Ptf1-Cre;LSL-Kras$^{G12D/+}$ (KC) mice, a genetically engineered mouse model (GEMM) used to study pancreatic ductal adenocarcinoma (PDAC), were generated by breeding as previously described in our studies (Dawson et al., 2013; Chang et al., 2017). Mice were fed standard chow diet and maintained in standard housing conditions [controlled temperature (19–22°C) and 12:12-h light/dark cycle] during the duration of the study. Mice were sacrificed at 3 months and pancreas tissues harvested for histological and Western blotting protein analysis of YAP and PaSC markers as described before (Morvaridi et al., 2015; Chang et al., 2017). Animal studies were approved by the Institutional Animal Care and Use Committee at Cedars-Sinai Medical Center (Los Angeles, CA) in accordance with the NIH Guide for the Care and Use of Laboratory Animals.

Immunofluorescence Analysis of Yes-Associated Protein 1 and Alpha-Smooth Muscle Actin in Mouse Pancreatic Tissues and Cultured Pancreatic Stellate Cells

Formalin-fixed, paraffin-embedded (FFPE) mouse pancreatic tissues were obtained from WT mice subjected to RAP or CP as described above. Four micrometer tissue sections were stained by IF using specific antibodies against YAP (#14074, Cell Signaling Technology) and αSMA (#A2547, Sigma-Aldrich; marker of activated PaSC). Alexa Fluor 488 or Alexa Fluor 594 was used as conjugated secondary antibodies, and 4′6′-diamidino-2-phenylindole (DAPI) as nuclear counterstain. Digitalized images were captured using a Leica TCS SP5 spectral confocal microscope (Leica Microsystems, IL) and analyzed with the Leica Application Suite Advanced Fluorescence Lite 2.6.0 software (LAS-AF-lite; Leica Microsystems Inc., Buffalo Grove, IL) with the assistance of the Cedars-Sinai Medical Center (Los Angeles, CA) Imaging Core. *Similar IF procedures were used to assess YAP and αSMA in cultured PaSC.*

Cellular localization of YAP in cultured PaSC was assessed using Image J by measuring the ratio of nuclear-to-cytoplasmic fluorescence intensity, expressed in each region as integrated intensity per unit area. In these studies, YAP quantification was performed in 70–90 cells from three to five representative microscopic fields.

Pancreatic Stellate Cells Isolation and Culture

Primary mouse PaSC (mPaSC) were obtained from wild-type and KC pancreas tissues as previously described (Pandol et al., 2012; Su et al., 2016; Yang et al., 2016). Briefly, pancreata from one to two mice were excised, minced, and digested in GBSS containing a mixture of pronase, collagenase P and DNase I. The cell suspension was filtered through a 100 μm nylon cell strainer and washed in GBSS supplemented with 0.3% BSA. Then, PaSC were separated by Nycodenz density gradient centrifugation (20 min at 1,400 g). Quiescent PaSC were collected from a fuzzy band at the interface near the top of the gradient and expanded in culture up to passage 2. Myofibroblast-like activated mPaSC were characterized by the presence of αSMA stress fibers, high production of fibronectin, and reduced expression of the quiescent marker GFAP.

Immortalized mouse PaSC (imPaSC) were initially obtained from Dr. Raul Urrutia and characterized in our previous studies (Su et al., 2016; Yang et al., 2016). Human primary PaSC (hPaSC) were obtained from pancreatic cadaveric tissues from organ donors or PDAC surgical resections. Briefly, cadaveric pancreata were digested at City of Hope (Duarte, CA) to isolate islets for clinical transplantation to diabetic patients as described (Song et al., 2015; Lugea et al., 2017). Remnant pancreatic cells after islet isolation (mainly pancreatic acinar, ductal, and PaSC) were further processed at the Cedars-Sinai Medical Center (Los Angeles, CA) to isolate hPaSC following similar procedures indicated above for primary mPaSC. hPaSC from PDAC tissues were obtained by the outgrowth method as previously described (Bachem et al., 2005; Lugea et al., 2006). The studies were performed in accordance with regulations and IRB protocols approved by the Institutional Review Board at Cedars-Sinai Medical Center (Pro31101 and Pro32114).

Primary mPaSC and hPaSC, and imPaSC were grown in DMEM/F12 media supplemented with 10% FBS, 2 mM L-glutamine, and antibiotics/antimycotics, in a humidified 5% CO_2 atmosphere. For experiments, cells were seeded in 60-mm tissue culture dishes in DMEM/F12 and starved in serum-free medium for 12 h, and then treated with the experimental agents at 60–80% confluency, unless otherwise stated.

Knockdown of Yes-Associated Protein 1 *Via* siRNA Transfection

siRNA targeted against mouse YAP1 mRNA were obtained from ThermoFisher Scientific (#4390771Waltham, MA). Control transfections were carried out with Silencer Select Negative Control No. 1 (#4390843, ThermoFisher Scientific). For siRNA transfection, imPaSC (1.5×10^5 cells/plate) were cultured in 60 mm plates until 60% confluence. Silencer nontargeting negative control (10 nmol/L; Mock transfection) or YAP siRNA (10 nmol/L) were mixed with Lipofectamine RNAiMAX (#13778075 ThermoFisher Scientific) according to the manufacturer's recommendations and added to the cells. After transfection, imPaSC were cultured in DMEM/F12 medium containing 10% FBS for 24 h and then used for experiments.

Western Blot Analysis

Cells or tissues were homogenized in RIPA buffer containing 50 mmol/L Tris (pH 7.4), 150 mmol/L NaCl, 1% deoxycholic acid, 1% Triton X-100, 0.1% SDS, and a mix of protease and phosphatase inhibitors (Roche Applied Science, Basel, Switzerland). Protein extracts were resolved by SDS-PAGE for immunoblot analysis. The primary and horseradish peroxidase-conjugated secondary antibodies used here are indicated in the Antibodies and chemicals section. Immunoreactive bands were visualized by chemiluminescence (ThermoFisher Scientific) and densitometrically quantified using the PXi 6 Touch Imaging System (Syngene). To estimate protein levels, optical density values in each blot were expressed relative to those of the loading control (ERK, β-actin or GAPDH).

RNA Analysis by Qualitative Polymerase Chain Recation

Cellular RNA from quiescent and culture-activated PaSC was extracted using the RNeasy® Plus Mini Kit (#74034; Qiagen, Germantown, MD). Reverse transcription was performed with the iScript Reverse Transcription Supermix (#170-8,840; Bio-Rad, Hercules, CA) using 1 μg of total RNA, and the synthesized cDNA samples were used as templates for quantitative real-time PCR (qPCR) analysis. Kits were used according to the manufacturer's instructions. All reactions were performed using the Bio-Rad CFX ConnectTM Real-Time PCR Detection System and the amplifications were done with the iTaq™ Universal SYBR® Green Supermix (Bio-Rad). The gene-specific primers used are listed in **Table 1**. Relative transcript levels were calculated using the comparative $2^{-\Delta\Delta Ct}$ method and normalized to the housekeeping gene, 18S rRNA.

MTT Assay

MTT (Thiazolyl Blue Tetrazolium Bromide) assay was used as indicator of cellular metabolic activity and cell proliferation. PaSC were seeded in 24-well plates at 1×10^4 cells per well. After the indicated treatments, MTT was added to the culture medium to a final concentration of 0.5 mg/ml, and cells were then incubated for 3 h at 37°C in a 5% CO_2 incubator. After removing medium, DMSO was added to dissolve the formazan product. Absorbance was measured at 595 nm using a spectrophotometric plate reader (SpectraMax M3, Molecular Devices, San Jose, CA).

Cell Death

Cell necrosis was assessed by PI uptake. Briefly, cells were treated with the experimental reagents for up to 72 h, and then labeled with PI (2 μg/ml medium) for 10 min. Both attached and floating cells were then collected, washed with PBS to remove excess PI, and lysed in RIPA buffer [50 mmol/L Tris (pH 7.4), 150 mmol/L NaCl, 0.25% deoxycholic acid, 1% Triton X-100, 0.1% SDS containing a mixture of protease and phosphatase inhibitors (Roche Applied Science, Basel, Switzerland)]. PI fluorescence was measured by fluorometry at $535_{ex}/617_{em}$ nm, and values normalized to those of total protein concentration in cell lysates. Caspase 3-dependent apoptosis was assessed by measuring levels of total and cleaved Caspase 3 by Western blotting.

TABLE 1 | Primer sequences for qRT-PCR.

Target	Forward (5′ to 3′)	Reverse (5′ to 3′)
mActa2 (αSMA)	GTTCAGTGGTGCCTCTGTCA	ACTGGGACGACATGGAAAAG
mCol1a1	TAGGCCATTGTGTATGCAGC	ACATGTTCAGCTTTGTGGACC
mCcn1 (Cyr61)	TGCTGTAAGGTCTGCGCTAA	GGTCTGCCTTCTGACTGAGC
mCcn2 (Ctgf)	CTGCCTACCGACTGGAAGAC	CATTGGTAACTCGGGTGGAG
mGfap	AAGAAAACCGCATCACCA	ACAACTTGTATTGTGAGCCT
mHgf	CTTTTTGCCTTCGAGCTATC	GGTCATGCATTCAACTTCTG
mIl6	ACCAGAGGAAATTTTCAATAGGC	TGATGCACTTGCAGAAAACA
mMmp3	AGCCTTGGCTGAGTGGTAGA	CGATGATGAACGATGGACAG
mSerpine1 (PAI-1)	ATCCTGCCTAAGTTCTCTCTG	ATTGTCTCTGTCGGGTTGTG
mTgfb1	CAACCCAGGTCCTTCCTAAA	GGAGAGCCCTGGATACCAAC
mYap1	GCTGCAGCAGTTACAGATGG	GCGCAGAGCTAATTCCTGAC
hACTA2 (αSMA)	CCAGAGCCATTGTCACACAC	CAGCCAAGCACTGTCAGG
hWWTR1 (TAZ)	GTCCTACGACGTGACCGAC	CACGAGATTTGGCTGGGGA
hYAP1	TAGCCCTGCGTAGCCAGTTA	TCATGCTTAGTCCACTGTCTGT
18S rRNA	AGTCCCTGCCCTTTGTACACA	CGATCCGAGGGCCTCACTA

Statistical Analyses

All experiments were performed in triplicate unless otherwise stated. Data are presented as mean ± SD or mean ± SEM. Data were subjected to analysis of variance (ANOVA) followed by Tukey's *post hoc* test, and two tailed Student *t*-test for comparison between 2 groups. Differences between treatments were considered to be statistically significant at $p < 0.05$ as indicated in the figure legends.

RESULTS

Yes-Associated Protein 1 Upregulation During Experimental Pancreatitis and Pancreatic Ductal Adenocarcinoma Progression Parallels Pancreatic Stellate Cells Activation

Previous studies indicate that effectors of the Hippo signaling system including TEAD1 and its transcriptional activator YAP are integral components of the embryonic development of human pancreas (Cebola et al., 2015) and its expression is recapitulated during progression of pancreatic disorders (Kapoor et al., 2014; Zhang et al., 2014; Morvaridi et al., 2015; Hao et al., 2017). Histological analysis of pancreatic tissues from PDAC patients and murine models of pancreatic cancer shows that YAP is upregulated in precancerous lesions (Pancreatic Intraepithelial Neoplasia, PanIN) and cancer cells as well as in activated PaSC in the stroma (Kapoor et al., 2014; Zhang et al., 2014; Morvaridi et al., 2015; Hao et al., 2017). These findings highlight the therapeutic potential of targeting YAP signaling to prevent PaSC activation and fibrosis in PDAC and CP, two pancreatic disorders showing extensive desmoplastic reaction.

To evaluate the relationship between YAP and PaSC activation during pancreatitis, we used experimental mouse models of AP, RAP, and CP. AP was induced by administration of high doses of the cholecystokinin analogue cerulein (50 μg/kg; 7 hourly intraperitoneal injections) and tissues collected during the acute phase (1 h after the last cerulein injection). RAP was induced by two episodes of AP (at days 1 and 3), and mice sacrificed during the acute phase (1 h after the last cerulein injection; day 3) and during the recovery phase (day 5), when pancreas undergo extensive remodeling. CP was induced by repeated episodes of cerulein AP (two episodes per week, for 4 weeks) and mice sacrificed 4 days after the last episode, when marked PaSC activation is evident (Lugea et al., 2006). **Supplementary Figure S1A** shows representative H&E micrographs of pancreas histology in control- and cerulein-treated mice. As shown, repeated cerulein AP leads to loss of normal exocrine parenchyma, acinar cell death, inflammatory cell infiltration and stromal expansion.

In pancreas of control (saline-treated) mice or mice subjected to one episode of AP (day 1), YAP protein expression was negligible (**Figures 1A–C**). YAP levels increased moderately after the second episode of AP (day 3) but markedly 2 days after RAP induction (day 5) and remained elevated during CP (**Figures 1A,B**). YAP upregulation was concomitant with upregulation of the PaSC markers CDH11 and PDGFRβ (**Figure 1A**). Moreover, αSMA positive, activated PaSC in RAP (**Figure 1C**) and CP pancreas (Morvaridi et al., 2015) exhibited marked YAP nuclear staining, suggesting YAP transcriptional activity in these cells.

As our group previously reported (Morvaridi et al., 2015), YAP was markedly upregulated in pancreas of KC mice. Illustrated in **Supplementary Figure S1B**, pancreas tissues of KC mice display abundant PanIN surrounded by stroma enriched in αSMA-positive PaSC. In these mice, pancreatic levels of YAP increased in parallel with PanIN and stromal progression. **Figure 1D** shows significant upregulation of YAP, the PaSC markers PDGFRβ and CDH11, and the ductal marker cytokeratin 19 (CK19) in pancreatic extracts of KC mice compared with wild-type mice.

Yes-Associated Protein 1 Is Expressed in Activated but Not Quiescent Pancreatic Stellate Cells

To further explore the role of YAP in PaSC biology, we measured levels and cellular location of YAP in quiescent and activated cultured PaSC obtained from human (hPaSC) and mouse (mPaSC) tissues. We first used a model of acinar-ductal-metaplasia

FIGURE 1 | YAP levels increase in pancreas during parenchyma remodeling in pancreatic disease. **(A)** Representative immunoblots showing protein levels of YAP and the PaSC markers Cadherin 11 (CDH11) and the PDGF receptor PDGFRβ in pancreas of mice subjected to repeated episodes of cerulein acute pancreatitis: *RAP*; two episodes, 1 day apart; *CP*, chronic pancreatitis, two episodes per week for 4 weeks. As indicated in the "Methods" section, mice were sacrificed during the acute phase of pancreatitis (**d1**, day 1, one AP episode; **d3**, day 3, two AP episodes), 2 days after two AP episodes (**d5**) or 4 days after the last episodes in the **CP** model. ERK1/2 was used as loading control. Each lane shows data from an individual mouse; two mice per group are shown. Data are representative of five mice per group. **(B)** Graph shows quantitation of optical density of YAP bands in immunoblot shown in panel **A** relative to those of ERK1/2. Data are mean ± SEM, *n* = 5 mice/group. **(C)** Paraffin-embedded pancreatic tissues obtained from mice subjected to two episodes of AP (days 1 and 3) and sacrificed at day 5 (**RAP-d5**) or saline-treated mice (**Control**) were analyzed for the PaSC marker αSMA and YAP by immunofluorescence. Nuclei were counterstained with DAPI. Panels **a–f** show representative immunofluorescence staining; Scale bar = 25 μm. Dotted box in panel **f** shows αSMA-positive PaSC displaying YAP staining in the nucleus; the dotted area is shown higher magnified in panel **g**. Arrows in panel **g** show positive YAP nuclei. Scale bar = 10 μm. Control tissues (panels **a–c**) do not exhibit activated PaSC or significant YAP staining. Data are representative of three mice per group. *Representative H&E stained images from control and RAP-5d mice pancreas are shown in* **Supplementary Figure S1A**. **(D)** Representative immunoblots showing protein levels of YAP, the PaSC markers CDH11 and PDGFRβ, the ductal marker Cytokeratin 19 (CK19) in pancreas of 2-month-old wild-type (**WT**) and Ptf1-Cre;LSL-Kras$^{G12D/+}$ (**KC**) mice. GAPDH was used as loading control. Each lane shows data from an individual mouse; three mice per group are shown. *Representative photomicrographs from KC mouse pancreas showing a-SMA positive PaSC are included in* **Supplementary Figure S1B**.

(ADM) generated by culturing pancreatic exocrine cells from human cadaveric donor pancreata without pancreas pathology (Lugea et al., 2017). In this model that mimics parenchymal remodeling during CP initiation and progression, acinar cells rapidly die or dedifferentiate into ductal cells (not shown) and quiescent PaSC become activated and expand. In this system, PaSC exhibited marked upregulation of αSMA and concomitant upregulation of YAP and its homolog TAZ (**Figure 2A**).

We further found that YAP expression is linked to the activated state of PaSC. As shown in **Figures 2B,C**, quiescent, freshly isolated hPaSC, and mPaSC did not express YAP, but YAP levels markedly increased during cell activation in culture and remained elevated during passages. Moreover, as we observed in pancreas tissues, activated PaSC displayed robust YAP nuclear staining in culture conditions, likely associated with YAP transcriptional activity. As illustrated in **Figure 2D**, αSMA-positive PaSC obtained from normal human organ donor pancreata, resected human PDAC tumors or KC mice, all exhibit

nuclear YAP. This staining pattern was also found in culture-activated mPaSC isolated from wild-type mice (not shown). We also found that, unlike reports using cancer and other cell types (Zhao et al., 2007; Hao et al., 2017), the number of PaSC displaying nuclear YAP is not affected by cell density (60–100%; not shown), a property likely related to tension induced by the contractile αSMA filaments in PaSC (Calvo et al., 2013).

Pancreatic Stellate Cells Quiescence Induced by Inhibition of p38 MAPK Signaling and the Bromodomain and Extra-Terminal Bromodomain Family Proteins Results in Yes-Associated Protein 1 Downregulation

We next examined the effects of pharmacologic treatments that induce reversal of PaSC activation state into a quiescent state. This reversion was characterized by downregulation of the

FIGURE 2 | PaSC activation is associated with sustained YAP upregulation. **(A)** Activated PaSC were obtained in culture from an acinar-ductal-metaplasia (ADM) experimental model using pancreatic acini from cadaveric pancreata from human donors. As sown in the graphs, upregulation of YAP and its homolog TAZ in the ADM system was concomitant with upregulation of αSMA, a recognized maker of activated PaSC. αSMA and YAP mRNA expression were determined by qPCR. **(B)** Quiescent PaSC isolated from cadaveric human pancreata (hPaSC) did not express YAP, but YAP levels markedly increased during PaSC activation in culture in parallel with upregulation of αSMA. Similar results were obtained in PaSC obtained from WT mouse pancreas (mPaSC) **(C)**. Graphs in A-C show mean ± SEM; n = 3. **(D)** Immunofluorescence analysis of YAP (red) and αSMA (green) in hPDAC obtained from cadaveric human pancreata (organ donor) or pancreatic adenocarcinoma tumors (PDAC patient) and in mPaSC obtained from KC mice; nuclei were stained with DAPI (blue). Primary cells were expanded in culture using DMEM/F12 medium containing 10% FBS until 70–90% confluency and then immunostained with the indicated targets. Under these culture conditions, both hPaSC and mPaSC display YAP nuclear staining. Similar results were obtained in two additional independent experiments; Scale bar, 50 µM.

activation markers αSMA (encoded by the Acta2 gene) and collagen type I alpha 1 (encoded by the Col1a1 gene), upregulation of the quiescence marker glial fibrillary acidic protein (GFAP) and decrease in cell proliferation (Omary et al., 2007). We found that treatment with the p38 MAPK inhibitor SB203580 (Masamune et al., 2003) and with iBET151, a pan-specific inhibitor of the epigenetic transcriptional regulators Bromodomain and Extraterminal domain (BET) proteins (Kumar et al., 2017), induced quiescence in mPaSC (**Figure 3A**). By contrast, treatment with the known PaSC activator TGFβ1 resulted in marked upregulation of αSMA and Col1a1 in mPaSC (**Figure 3A**). Interestingly, both pharmacological inhibitors also significantly reduced YAP expression levels (62% reduction with 1 µM iBET151, and 48% with 0.5 µM SB203580; **Figure 3B**). Moreover, iBET151 reduced in a dose-dependent manner protein levels of the YAP homolog TAZ and the PaSC markers αSMA, CDH11, PDGFRβ and P4HA2, a collagen synthesizing enzyme (**Figures 3B,C**).

Compared to controls, iBET151 treatment also reduced PaSC metabolic activity, as assessed by MTT assay (**Figure 3D**), and

cell numbers (**Figure 3E**). Differences in MTT absorbance values may reflect changes in cell proliferation and/or cell viability when metabolic events lead to necrosis or apoptosis. To determine whether iBET151 induces cell death, we assessed necrosis by measuring propidium iodide (PI) uptake and apoptosis by measuring protein levels of total and cleaved caspase-3. Our data indicate that iBET151 treatment did not change necrosis (**Figure 3F**) or apoptosis (**Supplementary Figure S2A**), suggesting that the BET inhibitor reduces cell proliferation, an effect consistent with a quiescent state.

Yes-Associated Protein 1 Knockdown *Via* siRNA Transfection Reduces Cell Growth in Pancreatic Stellate Cells and Alters Expression of Genes Involved in Matrix Remodeling

To gain insights into the role of YAP on activated PaSC, we transiently knocked down YAP mRNA in immortalized
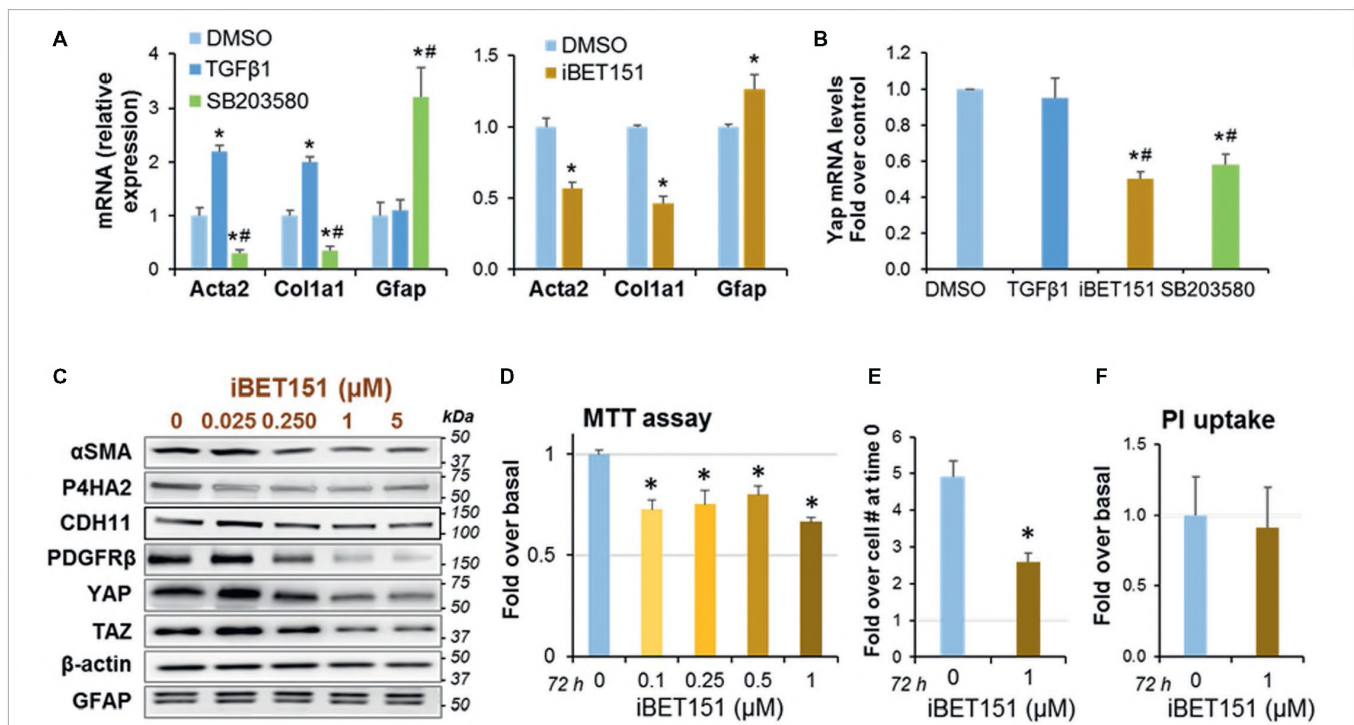
FIGURE 3 | PaSC quiescence induced by a p38 MAP Kinase inhibitor or a BET family inhibitor is associated with YAP downregulation. Immortalized mouse PaSC (imPaSC) were treated with DMSO (control), the p38 MAPK inhibitor SB203580 (5 µM) or the BET inhibitor iBET151 (1 µM) for different times. In selected experiments, TGFβ1 (5 ng/ml) was used as positive control to induce upregulation of proteins found increased in activated PaSC (αSMA and Col1a1). **(A,B)** Graphs show mRNA levels of Acta2 (αSMA), Col1a1, GFAP (a marker of quiescent PaSC) and YAP measured by qPCR in imPaSC treated for 24 h with the indicated agents. Data is representative of three independent experiments. *$p < 0.05$ vs. DMSO; #$p < 0.05$ vs. TGFβ1 treatment. **(C)** Protein extracts from imPaSC treated for 24 h with different concentrations of iBET151 were analyzed to determine levels of YAP and TAZ and the indicated PaSC markers; representative immunoblots are shown. β-actin was used as loading control. As shown, BET inhibition decreases protein levels of several markers of PaSC activation but does not affect levels of the quiescent marker GFAP. Data is representative of three independent experiments. **(D–F)** imPaSC were treated for 72 h with iBET151 at the indicated concentrations, and metabolic activity (MTT assay), cell number and cell necrosis (PI uptake) were assessed. Additionally, **Supplementary Figure S2A** shows protein levels of caspase-3 as a marker of caspase-dependent apoptosis. **(D)** Graph shows MTT assay data after 72 h treatment. (E) Graph shows number of imPaSC after 72 h treatment with or without 1 µM iBET151. The number of cells at 0 and 72 h were assessed by trypan blue exclusion using a hemocytometer; data are expressed as fold increase over the cell number at time 0 (1.25×10^4). **(E)** PI uptake was measured as indicated in "Materials and Methods" section. Graphs show *$p < 0.05$ vs. no-iBET151 control. Data in graphs **(D–F)** represent the means ± SD; $n = 3$.

mPaSC *via* siRNA transfection as indicated in the Materials and Methods section. siRNA treatment resulted in 82% reduction in YAP mRNA levels at 24 h and 49% reduction at 48 h post-transfection (**Figure 4A**). At 48 h, we found in YAP siRNA-treated cells a 50% reduction in MTT absorbance values (MTT assay; **Figure 4B**), and a marked decrease in cell counts (**Figure 4C**). We did not observe morphological evidence of cell death in YAP siRNA-treated cells (not shown), necrosis (**Figure 4D**) or caspase-3-dependent apoptosis (**Supplementary Figure S2B**). Taken together, these data suggest that YAP regulates cell proliferation in activated PaSC.

As illustrated in **Figure 4E**, YAP siRNA knockdown in PaSC reduced a subset of genes including the previously identified YAP gene targets connective tissue growth factor (Ctgf) and cysteine rich angiogenic inducer 61 (Cyr61) that are involved in cell adhesion and ECM remodeling; the PaSC markers αSMA and Col1a1 that participate in PaSC morphology, matrix tension and collagen deposition, and TGFβ1, that stimulates fibroinflammatory responses in these cells. Interestingly, YAP

siRNA treatment markedly increased levels of metalloproteinase 3 (MMP3), a protease involved in degradation of collagens and other ECM proteins during tissue remodeling. These findings support the concept that YAP represses MMP3 transcription in PaSC while promoting the expression of genes favoring collagen deposition and fibrosis. YAP knockdown also led to moderately increased expression of hepatocyte growth factor (HGF; **Figure 4C**), a growth factor that is secreted by PaSC and acts on epithelial and cancer cells regulating angiogenesis, tissue regeneration and cancer cell growth (Pothula et al., 2017). Overall, our findings indicate that YAP controls a variety of transcriptional gene networks in PaSC.

PDGF Activates the Hippo Pathway and Increases Yes-Associated Protein 1 Phosphorylation in Pancreatic Stellate Cells

Rapid upregulation of PDGFRβ is a major event in the activation of PaSC from the quiescent phenotype, and PDGF binding

FIGURE 4 | YAP siRNA decreases PaSC expansion in culture and alters expression of genes involved in matrix remodeling. imPaSC were transfected with nontargeting negative control (**NT**, 10 nmol/L) or a target siRNA (**YAP**, 10 nmol/L) mixed with lipofectamine RNAiMAX, and 24 h later cells were used for experiments. **(A)** Graph shows quantitation of YAP mRNA expression relative to negative control at 48 h post-transfection. Data are mean ± SD, $n = 3$; *$p < 0.05$ vs. NT. **(B)** MTT assay for YAP siRNA-treated cells relative to NT. **(C)** The graph shows imPaSC numbers counted 0 and 48 h after treatment with either NT or YAP siRNA. The cell numbers were assessed by trypan blue exclusion using a hemocytometer, and expressed as a fold increase over time 0 (1.5×10^5). **(D)** PI uptake was measured in cells treated with siRNA to detect any disrupted plasma membrane integrity. After incubation, a portion of cells was permeabilized for 5 min with 0.1% Triton X100 to establish a positive control. Data in graphs **(B–D)** are mean ± SD, $n = 3–6$ independent experiments; *$p < 0.05$ vs. NT. **Supplementary Figure S2B** *shows protein levels of caspase-3 as a marker of caspase-dependent apoptosis*. **(E)** Graph shows mRNA levels of the indicated genes in YAP siRNA treated cells compared to NT. Data is mean ± SD, $n = 5$.

to this receptor acts as a potent mitogen and induces migration in PaSC (Kordes et al., 2005). PDGF is secreted by different cell types including platelets, endothelial cells, and macrophages. In PDAC tissues, cancer cells and macrophages are likely a main source of PDGF and TGFβ1 with distinct effects on PaSC proliferation, migration and production of ECM and cytokines (Bachem et al., 2005; Omary et al., 2007; Apte et al., 2013; Biffi et al., 2019). PDGF induces cell growth and proliferation, in part by activating MAPK and PI3K/AKT signaling pathways (Heldin, 2013).

Here, we investigated potential crosstalk between PDGF and YAP pathways in regulating PaSC growth in culture. Serum-starved imPaSC were treated with 2 or 5 ng/ml PDGF for different times. As expected, we found that PDGF induced rapid (within minutes) activation of ERK1/2 and AKT signaling in imPaSC, as indicated by increased phosphorylation of ERK1/2 at Thr202/Tyr204 and AKT at Ser473 (**Figure 5A**). Similar effects were found in primary human and mouse PaSC (not shown). PDGF treatment also led to rapid phosphorylation of

YAP at Ser127, a site previously reported to be phosphorylated by the Hippo pathway kinase large tumor suppressor kinase 1 (LATS1) and to promote cytoplasmic retention and inactivation of YAP in several cell types (Zhao et al., 2007). In agreement, we found that PDGF induced LATS1 activation in imPaSC (**Figure 5A**).

Serum is a potent growth factor in activated PaSC and was reported to decrease YAP Ser127 phosphorylation and promote YAP nuclear translocation in HEK293A (Yu et al., 2012). To compare the effects of serum and PDGF on YAP activation, we cultured serum-starved imPaSC for 24 h in media containing different concentrations of FBS, and then treated the cells for 30 min with or without 2 ng/ml PDGF. As shown in **Figure 5B**, levels of p-YAP Ser127 decreased in cells treated with 5 and 10% FBS while PDGF increased YAP phosphorylation in both serum-starved and 10% FBS treated imPaSC (**Figure 5B**). To determine whether kinases downstream of ERK1/2 and AKT pathways mediate serum and PDGF effects on YAP phosphorylation at Ser127,
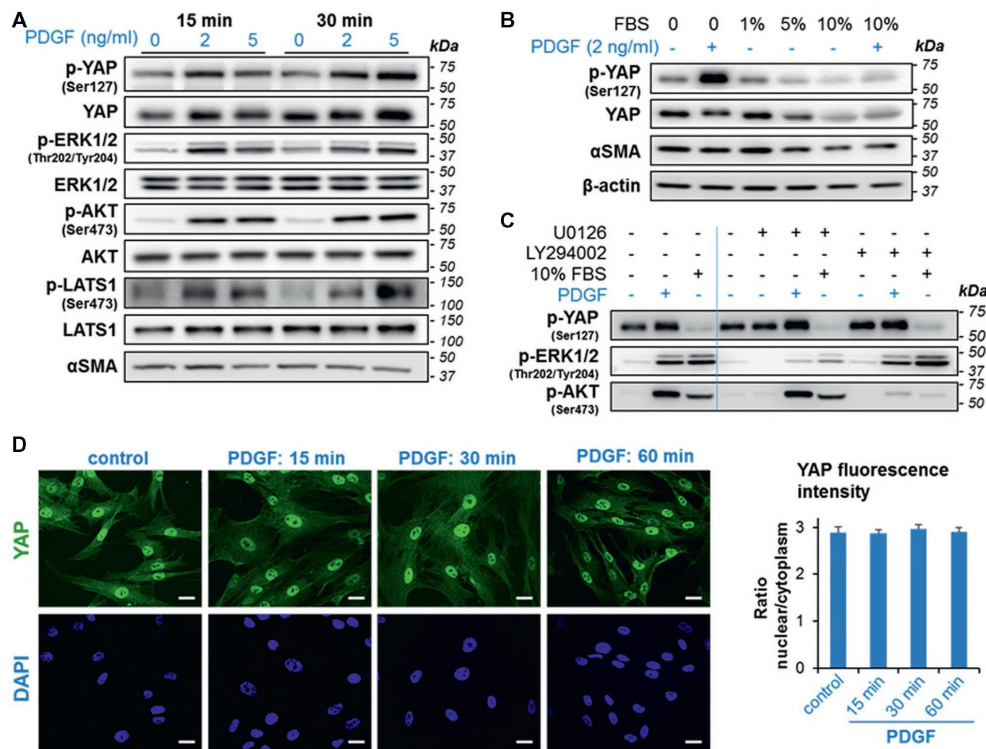
FIGURE 5 | PDGF induces rapid phosphorylation of YAP and activation of growth signaling in imPaSC. **(A)** imPaSC cultured in DMEM containing 10% FBS, were serum-starved for 12 h and then treated with PDGF (2 and 5 ng/ml) for 15- and 30-min. Levels of total and phosphorylated forms of the indicated targets were measured by western blotting. As shown in the immunoblots, PDGF induced rapid activation of ERK1/2, AKT, and Hippo kinases (LATS1) and significantly increased levels of phosphorylated YAP (at Ser127). **(B)** Cells cultured in DMEM containing 10% FBS were serum-starved for 12 h and then cultured in media containing different concentrations of FBS. Twenty-four hours later, cells were treated for 30 min with and without 2 ng/ml PDGF. As shown in the immunoblots, 5 and 10% FBS reduced levels of total and phosphorylated YAP while PDGF markedly induced YAP phosphorylation. **(C)** imPaSC were serum-starved for 12 h, pre-treated with the MEK inhibitor U0126 (10 μM) or the PI3K/AKT inhibitor LY294002 (20 μM) for 1 h and then treated with or without 2 ng/ml PGDF or 10% FBS for 30 min. Levels of the indicated targets were measured by Western blotting. **(D)** Cells treated with 2 ng/ml PDGF for up to 60 min were IF stained using a YAP specific antibody; Scale bar, 50 μm. Quantified nuclear/cytoplasmic YAP fluorescence intensity is shown in **(E)**. Fluorescence was measured as indicated in *Materials and Methods* and expressed as nuclear/cytoplasmic ratio (mean ± SEM, *n* = 70–90 cells). As shown in the pictures, YAP staining was preferentially located in the nucleus in both control and PDGF-treated cells, and PDGF treatment did not alter YAP nuclear/cytoplasm ratios. Data in panels **A–E** are representative of three independent experiments.

we pre-treated imPaSC with the MEK inhibitor U0126 (10 μM) or the PI3K/AKT inhibitor LY294002 (20 μM) for 1 h, and then treated the cells with or without PGDF or 10% FBS for 30 min. As shown in **Figure 5C**, U0126 and LY294002 inhibited ERK1/2 and AKT activation, respectively in both PDGF- and serum treated imPaSC but did not alter levels of p-YAP. These data indicate that, at least at the time-point measured, YAP Ser127 phosphorylation elicited by PDGF is independent of ERK and AKT activation and is likely regulated by LATS1.

We next investigated whether PDGF-induced YAP Ser127 phosphorylation was associated with changes in YAP cellular localization or translocation of YAP from the nucleus to the cytoplasm. Surprisingly, we found that PDGF-induced YAP phosphorylation did not change YAP nuclear location, as determined by immunofluorescence staining (**Figure 5D**) and quantification of nuclear-to-cytoplasm YAP fluorescence intensity ratios (**Figure 5E**).

Yes-Associated Protein 1 siRNA Knockdown Reduces PDGF-Induced Proliferation and Blunts the Persistent Activation of AKT and ERK Induced by Long-Term Stimulation With PDGF

The data illustrated in **Figure 4** suggest that YAP downregulation diminishes PaSC proliferation. To examine the potential involvement of YAP in PDGF-induced PaSC proliferation, we measured ERK1/2 and AKT activation state and PaSC proliferation in YAP siRNA- vs. mock-transfected cells treated with PDGF for up to 48 h. We found that in mock-transfected cells (**Figure 6A**), PDGF induced YAP Ser127 phosphorylation and phosphorylation-dependent activation of ERK1/2, AKT and p70S6K, an effector protein kinase in the mTORC1 pathway that we found regulates cell growth in PaSC (Yang et al., 2016). These PDGF effects persisted for at least 48 h. Compared to mock-transfected cells, YAP siRNA treatment did not affect early activation
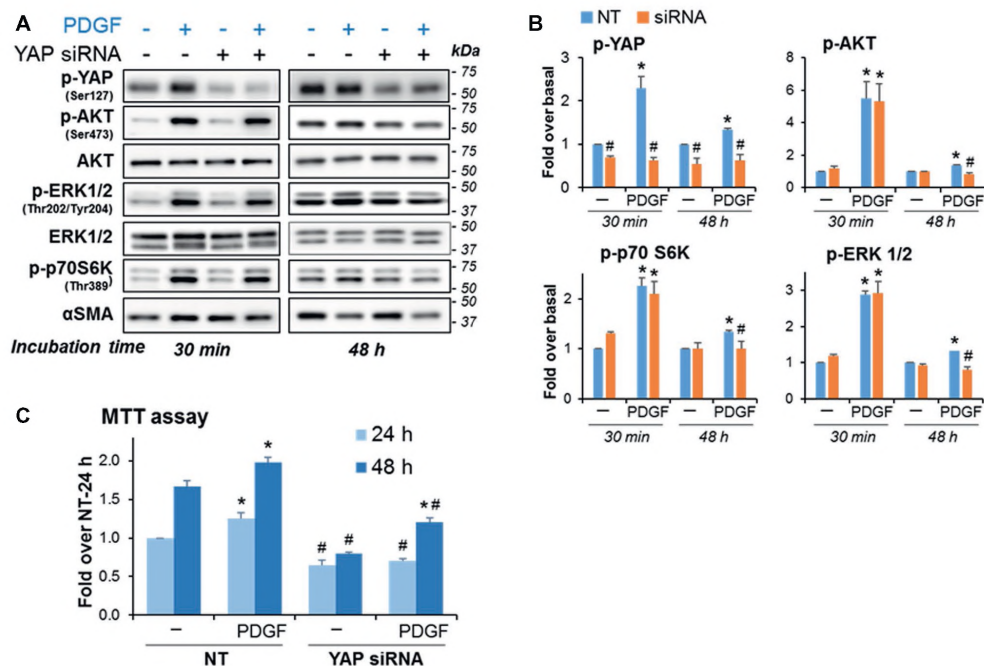
FIGURE 6 | YAP knockdown blunts the persistent activation of AKT and ERK induced by long-term stimulation with PDGF and reduces PDGF-induced proliferation in imPaSC. Mock and YAP-transfected cells were treated with 2 ng/ml PDGF for the indicated times. **(A)** Levels of phosphorylated and total AKT, ERK1/2 and p70S6K (a kinase in the mTOR pathway) were assessed by Western blotting. αSMA was tested as a marker of activation. **(B)** Graphs show optical density (OD) of the immunoblots depicted in panel **A** determined by densitometry. As indicated in the graphs, YAP knockdown did not affect PDGF-induced early activation of AKT, ERK1/2 and mTOR signaling but reduced the long-term (48 h) PDGF effects on growth signaling. **(C)** YAP siRNA treatment also reduced basal and PDGF-induced cell proliferation as indicated by MTT assay. Data in graphs are mean ± SEM; $n = 3$. $*p < 0.05$ vs. control (–); $^\#p < 0.05$ vs. NT.

of AKT and ERK (at 30 min) but blunted long-term effects (at 48 h) of PDGF (**Figures 6A,B**). Compared to mock-transfected cells, YAP siRNA knockdown also diminished PDGF-induced proliferation (**Figure 6C**) but did not completely block PDGF effects, supporting YAP-dependent and -independent pathways regulating cell growth in imPaSC.

Crosstalk Between Yes-Associated Protein 1 and Transforming Growth Factor Beta 1 Signaling in Cultured Pancreatic Stellate Cells

TGFβ1 is a potent activator of fibroinflammatory responses in PaSC (Apte et al., 1999; Xue et al., 2015). TGFβ1 effects on gene transcription are mediated *via* SMAD transcription factor signaling, and mounting evidence supports the existence of crosstalk between the Hippo pathway and SMAD signaling (Chen et al., 2019). For example, YAP and TAZ bind to SMAD2/3 within transcriptional complexes and regulate gene expression (Piersma et al., 2015), and YAP was reported to affect TGFβ1 signaling by upregulating the SMAD2/3 inhibitor SMAD7 (Qin et al., 2018).

Here, we first evaluate whether TGFβ1 modulates YAP levels and phosphorylation state in activated PaSC. We found that, unlike PDGF (**Figures 5, 6**), TGFβ1 (5 ng/ml) did not alter YAP protein levels or phosphorylation at Ser127 at any of the time-points examined (30 min, 24 h, and 48 h) (**Figure 7A**).

Like PDGF, TGFβ1 stimulation had no perceptible effect on YAP nuclear localization. In this respect, we found that 100% of αSMA-positive hPaSC exhibit nuclear YAP both before (**Figure 2D**) and after 60 min treatment with TGFβ1 (**Figure 7B**) and that TGFβ1 treatment did not modify the nuclear-to-cytoplasmic YAP immunofluorescence ratios observed in non-treated hPaSC (**Figure 7C**). These findings suggest that under our culture conditions, YAP cellular localization in activated PaSC is not controlled by YAP Ser127 phosphorylation.

We next studied whether siRNA-mediated YAP knockdown would alter TGFβ1-induced SMAD2/3 activation and fibrosing responses in imPaSC. After 24 h of transfection, imPaSC were treated with TGFβ1 (5 ng/ml) for up to 6 h and levels of phosphorylated or total SMAD2/3 proteins were measured in cell lysates by Western blotting. We found that TGFβ1 induces rapid SMAD2/3 phosphorylation in non-transfected cells that persists for at least 6 h (not shown). As expected, YAP knockdown (**Figure 8C**) did not affect TGFβ1-induced Smad2/3 phosphorylation in imPaSC (**Figures 8A,B**). However, YAP knockdown almost completely abolished TGFβ1-induced Ctgf, and significantly diminished interleukin 6 (IL6) expression in these cells (**Figure 8D**). Interestingly, YAP knockdown did not affect the marked upregulation of plasminogen activator inhibitor 1 (PAI-1) elicited by TGFβ1 (**Figure 8D**), implying that YAP and TGFβ1 cooperate in the transcription of distinct gene networks in PaSC.

FIGURE 7 | TGFβ1 does not affect does not affect YAP phosphorylation at Ser127 or YAP cellular localization in PaSC. **(A)** imPaSC were cultured in DMEM containing 10% FBS, starved in serum-free media for 12 h before experiment and then left untreated or treated with PDGF (2 ng/ml) or TGFβ1 (5 ng/ml). Immunoblots show protein levels of the indicated targets; β-actin was used as loading control. As shown in the pictures, PDGF induced sustained YAP phosphorylation at Ser127, whereas TGFβ1 had no effect. Similar results were found in primary PaSC obtained from mouse or human tissues (not shown). **(B)** hPaSC isolated from cadaveric pancreata (organ donors) or pancreatic tumor surgical resections (PDAC patients; see **Figure 2D**) were expanded in culture using DMEM/F12 medium containing 10% FBS until 70–90% confluency (as in **Figure 2D**) and then treated with 5 ng/ml TGFβ1 for 60 min. As observed in untreated cells (**Figure 2D**), YAP immunofluorescence was also mainly restricted to the nucleus in TGFβ1-treated cells. Data are representative of three independent experiments. Scale bar, 50 µm. **(C)** Graph shows relative YAP localization in untreated and TGFβ-treated cells obtained from donors or PDAC patients. Cellular YAP fluorescence is expressed as the nuclear/cytoplasmic ratio (mean ± SEM, n = 70–90 cells). As shown in the graph, TGFβ1 treatment had little effect on cellular localization of YAP.
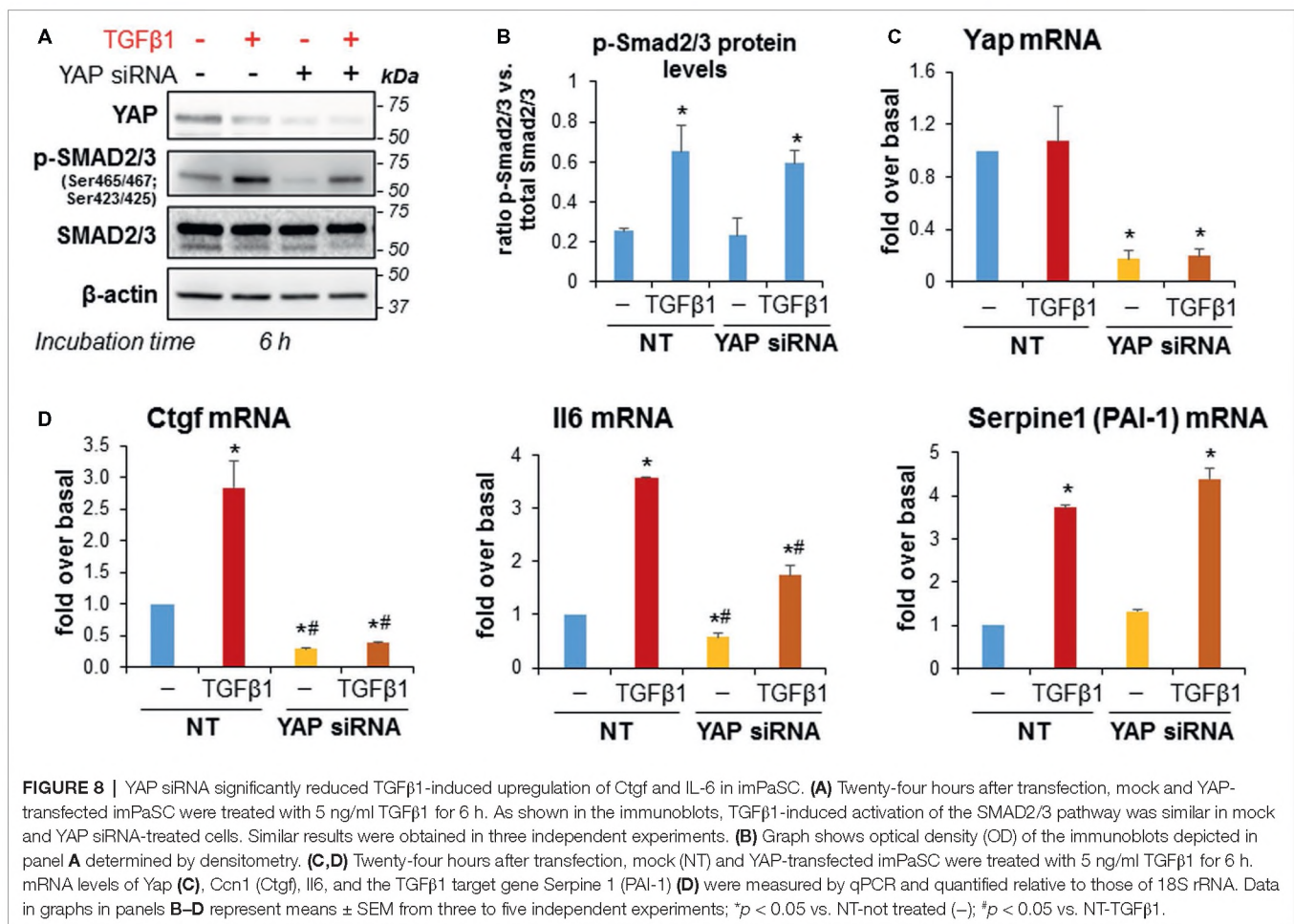
DISCUSSION

CP and PDAC are devastating pancreatic diseases characterized by high morbidity and mortality and limited treatment options (Garrido-Laguna and Hidalgo, 2015; Adamska et al., 2017; Kleeff et al., 2017). It is widely accepted that activated, myofibroblast-like PaSC modulate disease states and are major contributors to the extensive pancreatic desmoplasia and fibrosis observed in CP and PDAC (Apte et al., 2013). However, the mechanisms that govern PaSC activation, proliferation and fibroinflammatory responses during disease initiation and progression are not completely understood. Moreover, the contribution of key cellular pathways such as the Hippo/YAP pathway, that is involved in CP and PDAC progression (Murakami et al., 2017; Zhao et al., 2017), to the pathobiology of PaSC is poorly defined. This area of research is important because therapies directed to those specific pathways may have an impact on PaSC responses and PaSC modulation of the disease.

A previous study from this laboratory showed immunohistochemical evidence of YAP expression within activated, αSMA-positive PaSC in human CP and PDAC tumors,

and KC mice (Morvaridi et al., 2015). In this study, we found that YAP expression upregulates in the diseased pancreas in parallel with PaSC activation. Moreover, YAP expression in cultured PaSC is linked to the cell activation state. Activated PaSC obtained either from normal mouse or human pancreas, or from human or mouse PDAC tumor tissues exhibit preferential YAP nuclear staining, suggesting that YAP is transcriptionally active in these cells. Preferential YAP nuclear localization was a constant feature in cultured PaSC regardless of cell confluency (60–100%). These findings are consistent with previous studies demonstrating that YAP cellular localization is regulated by cell morphology and the F-actin cytoskeleton (Wada et al., 2011; Calvo et al., 2013). Cell spreading, a feature of myofibroblasts including PaSC, leads to YAP activation and translocation to the nucleus (Wada et al., 2011). Moreover, it was reported that incorporation of αSMA into stress fibers in mesenchymal cells promotes YAP nuclear translocation and YAP transcriptional activity (Talele et al., 2015).

Recent studies observed that treatment with BET inhibitors effectively reduced fibrosis and PDAC progression in mice, and implied that the activated state of PaSC was attenuated

FIGURE 8 | YAP siRNA significantly reduced TGFβ1-induced upregulation of Ctgf and IL-6 in imPaSC. **(A)** Twenty-four hours after transfection, mock and YAP-transfected imPaSC were treated with 5 ng/ml TGFβ1 for 6 h. As shown in the immunoblots, TGFβ1-induced activation of the SMAD2/3 pathway was similar in mock and YAP siRNA-treated cells. Similar results were obtained in three independent experiments. **(B)** Graph shows optical density (OD) of the immunoblots depicted in panel **A** determined by densitometry. **(C,D)** Twenty-four hours after transfection, mock (NT) and YAP-transfected imPaSC were treated with 5 ng/ml TGFβ1 for 6 h. mRNA levels of Yap **(C)**, Ccn1 (Ctgf), Il6, and the TGFβ1 target gene Serpine 1 (PAI-1) **(D)** were measured by qPCR and quantified relative to those of 18S rRNA. Data in graphs in panels **B–D** represent means ± SEM from three to five independent experiments; *$p < 0.05$ vs. NT-not treated (−); #$p < 0.05$ vs. NT-TGFβ1.

(Ding et al., 2015; Mazur et al., 2015). BRD4, a major BET protein, has also been implicated as a modulator of YAP/TAZ transcriptional activity at distinct promoters in cancer cells (Zanconato et al., 2018). Consistent with these reports, we found that treatment with the pan-specific BET protein inhibitor iBET151 reduced both mRNA and protein levels of YAP, and induced quiescence in PaSC, extending the mechanisms by which BET proteins regulate YAP/TAZ activities to the level of YAP/TAZ expression. Like BET inhibitors, we found that the p38 MAPK inhibitor SB 203580 also induced quiescence and reduced YAP expression in PaSC, further supporting a close association between YAP levels and PaSC activation state. Treatment with the mTOR inhibitor, KU63794, that decreased proliferation and ECM production in PaSC (Yang et al., 2016), also reduced YAP levels by 70% (data not shown). These findings support a key role of YAP in the activated PaSC phenotype. Further studies are needed to elucidate the mechanisms whereby p38 MAPK and mTOR pathways may intersect with BET proteins and other regulators of YAP/TAZ expression and activity.

Growth factors such as PDGF, IGF1, and TGFβ1 were identified as inducers of PaSC activation into proliferative myofibroblasts (Apte et al., 1999, 2013; Luttenberger et al., 2000; Schneider et al., 2001; Mews et al., 2002; Yang et al., 2016). This study addresses crosstalk between PDGF or TGFβ1 signaling

and YAP in PaSC. PaSC activation is associated with rapid and marked upregulation of PDGFRβ, and PDGF is a potent mitogen in PaSC. As expected, we found that PDGF induced sustained activation of AKT and ERK signaling. We also found that PDGF enhanced LATS Ser473 and YAP Ser127 phosphorylation. In other cell types, negative regulation by LATS protein kinases that phosphorylate YAP Ser127 typically restrict nuclear translocation and decrease co-transcriptional activity. Here, PDGF treatment dramatically enhanced YAP Ser127 phosphorylation but had no perceptible effect on preferential YAP nuclear localization in PaSC. These findings are consistent with a previous report demonstrating that pharmacological inhibition of PDGFRβ or PDGFRβ siRNA silencing decreased levels of YAP Ser127 and induced YAP translocation to the cytoplasm in cholangiocarcinoma cells (Smoot et al., 2018), suggesting a distinct role for PDGF signaling in regulating YAP activation. In this study, we found that YAP knockdown blunted the PDGF-induced persistent activation of AKT and ERK, and reduced PDGF-induced proliferation, further supporting a crosstalk between PDGF and YAP signaling.

TGFβ1 treatment on the other hand had no effect on the levels of total or Ser127-phosphorylated YAP. Further, whereas TGFβ1-induced Smad2/3 pathway activation was unaffected, and TGFβ1-induced of CTGF and IL-6 upregulation were markedly

blocked by YAP knockdown in PaSC. Thus, YAP modulates gene transcription elicited by TGFβ1/SMAD pathways in PaSC, as previously shown in other cell types (Zheng and Pan, 2019). These findings support YAP activity in PaSC as an important regulator of TGFβ1-induced fibroinflammatory responses in CP and PDAC.

Taken together, our data further substantiate the importance of nuclear YAP previously detected in PaSC in CP and PDAC stroma (Morvaridi et al., 2015). In particular, our novel findings clarify a key role for YAP in regulating PaSC activation state, proliferation, and fibroinflammatory responses conducive to CP and PDAC progression. These results highlight YAP signaling as an important therapeutic target to prevent or halt the expansion of desmoplasia in pancreatic disorders. Further studies are necessary to explore the complex crosstalk between distinct signaling systems including YAP, TGFβ1, and mitogenic signals regulating the activation state of PaSC in these disorders.

DATA AVAILABILITY STATEMENT

The datasets generated for this study are available on request to the corresponding author.

ETHICS STATEMENT

Animal studies were approved by the Institutional Animal Care and Use Committee at Cedars-Sinai Medical Center (Los Angeles, CA) and were in accordance with the NIH Guide for the Care and Use of Laboratory Animals. The use of human tissues was performed in accordance with regulations and IRB protocols approved by the Institutional Review Board at Cedars-Sinai Medical Center (Los Angeles, CA; IRB protocols Pro31101 and Pro32114).

AUTHOR CONTRIBUTIONS

CH, JY, H-YS, RW, MZ, and AL participated in the design and coordination of the study, performed experiments, data acquisition, analysis, and interpretations. CH, RW, SP, and AL participated in study concept and manuscript writing. LL and QX reviewed and approved the final manuscript. All authors read and approved the final manuscript.

FUNDING

ACKNOWLEDGMENTS

SUPPLEMENTARY MATERIAL

The Supplementary Material for this article can be found online at: https://www.frontiersin.org/articles/10.3389/fphys.2019.01467/full#supplementary-material

SUPPLEMENTARY FIGURE S1 | (A) Pancreas damage in mice during recurrent acute pancreatitis (RAP). C57BL/6 mice were subjected to two episodes of acute cerulein pancreatitis (days 1 and 3; 1 day apart). Each episode consisted of 7 hourly intraperitoneal injections of 50 μg/kg cerulein or saline as vehicle control. Tissues were collected 2 days after the second episode of pancreatitis (day 5; d5). Panels show representative H&E-stained pancreatic tissue sections from mice treated with saline (control; panels **a,b**) or cerulein (RAP-d5; panels **c,d**); five to six mice per group. Dotted boxes in panels **a,c** (scale bar, 200 μm) are shown at higher magnification (scale bar 50 μm) in panels **b,d**, respectively. As shown in the images, pancreas from control mice (panels **a,b**) exhibit a normal exocrine parenchyma composed of groups of acinar cells (acini) enriched in digestive enzymes (zymogen granules). Islets (endocrine cells) are also observed in the pictures. At day 5 after RAP (panels **c,d**), pancreatic tissues display acinar cell necrosis, loss of normal parenchyma, and stromal expansion enriched in immune cells and PaSC. As shown in **Figure 1C**, α-SMA-positive PaSC were found in RAP-5d but not in control tissues. **(B)** Pancreas histology in wild type and Kras mice. Representative IHC images showing αSMA staining (brown) in pancreas tissues of 3 month-old wild-type and Ptf1-Cre; LSL-Kras$^{G12D/+}$ (KC) mice. In wild-type mice, precancerous lesions (pancreatic intraepithelial neoplasia or PanIN) are not present and positive staining is found only in the wall of blood vessels (see arrow head). In KC mice, abundant αSMA-positive cells are found in the stroma surrounding PanINs, indicating activated PaSC.

SUPPLEMENTARY FIGURE S2 | (A) Immortalized mouse PaSC (imPaSC) were treated with the BET inhibitor, iBET151 for 72 h. **(B)** imPaSC were transfected with non-targeting negative control (**NT**, 10 nmol/L) or a targeted siRNA (**YAP**, 10 nmol/L), and proteins extracted 48 h later. Immunoblots show levels of full length (~35 kDa) and cleaved (~17 kDa) Caspase-3. GAPDH was used as loading control. Compared to controls, neither iBET151 nor YAP siRNA treatments increased levels of cleaved Caspase-3. Data are representative of three to four independent experiments.

REFERENCES

Adamska, A., Domenichini, A., and Falasca, M. (2017). Pancreatic ductal adenocarcinoma: current and evolving therapies. *Int. J. Mol. Sci.* 18:1338. doi: 10.3390/ijms18071338

Ansari, D., Ohlsson, H., Althini, C., Bauden, M., Zhou, Q., Hu, D., et al. (2019). The hippo signaling pathway in pancreatic cancer. *Anticancer Res.* 39, 3317–3321. doi: 10.21873/anticanres.13474

Apte, M. V., Haber, P. S., Darby, S. J., Rodgers, S. C., McCaughan, G. W., Korsten, M. A., et al. (1999). Pancreatic stellate cells are activated by

proinflammatory cytokines: implications for pancreatic fibrogenesis. *Gut* 44, 534–541.

Apte, M. V., Pirola, R. C., and Wilson, J. S. (2012). Pancreatic stellate cells: a starring role in normal and diseased pancreas. *Front. Physiol.* 3:344. doi: 10.3389/fphys.2012.00344

Apte, M. V., Wilson, J. S., Lugea, A., and Pandol, S. J. (2013). A starring role for stellate cells in the pancreatic cancer microenvironment. *Gastroenterology* 144, 1210–1219. doi: 10.1053/j.gastro.2012.11.037

Bachem, M. G., Schunemann, M., Ramadani, M., Siech, M., Beger, H., Buck, A., et al. (2005). Pancreatic carcinoma cells induce fibrosis by stimulating proliferation and matrix synthesis of stellate cells. *Gastroenterology* 128, 907–921. doi: 10.1053/j.gastro.2004.12.036

Biffi, G., Oni, T. E., Spielman, B., Hao, Y., Elyada, E., Park, Y., et al. (2019). IL1-induced JAK/STAT signaling is antagonized by TGFbeta to shape CAF heterogeneity in pancreatic ductal adenocarcinoma. *Cancer Discov.* 9, 282–301. doi: 10.1158/2159-8290.CD-18-0710

Calvo, F., Ege, N., Grande-Garcia, A., Hooper, S., Jenkins, R. P., Chaudhry, S. I., et al. (2013). Mechanotransduction and YAP-dependent matrix remodelling is required for the generation and maintenance of cancer-associated fibroblasts. *Nat. Cell Biol.* 15, 637–646. doi: 10.1038/ncb2756

Cebola, I., Rodriguez-Segui, S. A., Cho, C. H., Bessa, J., Rovira, M., Luengo, M., et al. (2015). TEAD and YAP regulate the enhancer network of human embryonic pancreatic progenitors. *Nat. Cell Biol.* 17, 615–626. doi: 10.1038/ncb3160

Chang, H. H., Moro, A., Takakura, K., Su, H. Y., Mo, A., Nakanishi, M., et al. (2017). Incidence of pancreatic cancer is dramatically increased by a high fat, high calorie diet in KrasG12D mice. *PLoS One* 12:e0184455. doi: 10.1371/journal.pone.0184455

Chen, Y. A., Lu, C. Y., Cheng, T. Y., Pan, S. H., Chen, H. F., and Chang, N. S. (2019). WW domain-containing proteins YAP and TAZ in the hippo pathway as key regulators in stemness maintenance, tissue homeostasis, and tumorigenesis. *Front. Oncol.* 9:60. doi: 10.3389/fonc.2019.00060

Dawson, D. W., Hertzer, K., Moro, A., Donald, G., Chang, H. H., Go, V. L., et al. (2013). High-fat, high-calorie diet promotes early pancreatic neoplasia in the conditional KrasG12D mouse model. *Cancer Prev. Res.* 6, 1064–1073. doi: 10.1158/1940-6207.CAPR-13-0065

Ding, N., Hah, N., Yu, R. T., Sherman, M. H., Benner, C., Leblanc, M., et al. (2015). BRD4 is a novel therapeutic target for liver fibrosis. *Proc. Natl. Acad. Sci. USA* 112, 15713–15718. doi: 10.1073/pnas.1522163112.

Dupont, S., Morsut, L., Aragona, M., Enzo, E., Giulitti, S., Cordenonsi, M., et al. (2011). Role of YAP/TAZ in mechanotransduction. *Nature* 474, 179–183. doi: 10.1038/nature10137

Eibl, G., and Rozengurt, E. (2019). KRAS, YAP, and obesity in pancreatic cancer: a signaling network with multiple loops. *Semin. Cancer Biol.* 54, 50–62. doi: 10.1016/j.semcancer.2017.10.007

Erkan, M., Adler, G., Apte, M. V., Bachem, M. G., Buchholz, M., Detlefsen, S., et al. (2012). StellaTUM: current consensus and discussion on pancreatic stellate cell research. *Gut* 61, 172–178. doi: 10.1136/gutjnl-2011-301220

Garrido-Laguna, I., and Hidalgo, M. (2015). Pancreatic cancer: from state-of-the-art treatments to promising novel therapies. *Nat. Rev. Clin. Oncol.* 12, 319–334. doi: 10.1038/nrclinonc.2015.53.

Gukovskaya, A. S., Gorelick, F. S., Groblewski, G. E., Mareninova, O. A., Lugea, A., Antonucci, L., et al. (2019). Recent insights into the pathogenic mechanism of pancreatitis: role of acinar cell organelle disorders. *Pancreas* 48, 459–470. doi: 10.1097/MPA.0000000000001298

Hao, F., Xu, Q., Zhao, Y., Stevens, J. V., Young, S. H., Sinnett-Smith, J., et al. (2017). Insulin receptor and GPCR crosstalk stimulates YAP *via* PI3K and PKD in pancreatic cancer cells. *Mol. Cancer Res.* 15, 929–941. doi: 10.1158/1541-7786.MCR-17-0023

Heldin, C. H. (2013). Targeting the PDGF signaling pathway in tumor treatment. *Cell Commun. Signal* 11:97. doi: 10.1186/1478-811X-11-97

Kapoor, A., Yao, W., Ying, H., Hua, S., Liewen, A., Wang, Q., et al. (2014). Yap1 activation enables bypass of oncogenic Kras addiction in pancreatic cancer. *Cell* 158, 185–197. doi: 10.1016/j.cell.2014.06.003.

Kirkegard, J., Mortensen, F. V., and Cronin-Fenton, D. (2017). Chronic pancreatitis and pancreatic cancer risk: a systematic review and meta-analysis. *Am. J. Gastroenterol.* 112, 1366–1372. doi: 10.1038/ajg.2017.218

Kleeff, J., Whitcomb, D. C., Shimosegawa, T., Esposito, I., Lerch, M. M., Gress, T., et al. (2017). Chronic pancreatitis. *Nat. Rev. Dis. Primers.* 3:17060. doi: 10.1038/nrdp.2017.60

Kordes, C., Brookmann, S., Haussinger, D., and Klonowski-Stumpe, H. (2005). Differential and synergistic effects of platelet-derived growth factor-BB and transforming growth factor-beta1 on activated pancreatic stellate cells. *Pancreas* 31, 156–167. doi: 10.1097/01.mpa.0000168222.05591.a0

Kumar, K., DeCant, B. T., Grippo, P. J., Hwang, R. F., Bentrem, D. J., Ebine, K., et al. (2017). BET inhibitors block pancreatic stellate cell collagen I production and attenuate fibrosis in vivo. *JCI Insight* 2:e88032. doi: 10.1172/jci.insight.88032

Lew, D., Afghani, E., and Pandol, S. (2017). Chronic pancreatitis: current status and challenges for prevention and treatment. *Dig. Dis. Sci.* 62, 1702–1712. doi: 10.1007/s10620-017-4602-2

Lugea, A., Nan, L., French, S. W., Bezerra, J. A., Gukovskaya, A. S., and Pandol, S. J. (2006). Pancreas recovery following cerulein-induced pancreatitis is impaired in plasminogen-deficient mice. *Gastroenterology* 131, 885–899. doi: 10.1053/j.gastro.2006.06.023

Lugea, A., Waldron, R. T., Mareninova, O. A., Shalbueva, N., Deng, N., Su, H. Y., et al. (2017). Human pancreatic acinar cells: proteomic characterization, physiologic responses, and organellar disorders in ex vivo pancreatitis. *Am. J. Pathol.* 187, 2726–2743. doi: 10.1016/j.ajpath.2017.08.017

Luttenberger, T., Schmid-Kotsas, A., Menke, A., Siech, M., Beger, H., Adler, G., et al. (2000). Platelet-derived growth factors stimulate proliferation and extracellular matrix synthesis of pancreatic stellate cells: implications in pathogenesis of pancreas fibrosis. *Lab. Investig.* 80, 47–55. doi: 10.1038/labinvest.3780007

Majumder, S., and Chari, S. T. (2016). Chronic pancreatitis. *Lancet* 387, 1957–1966. doi: 10.1016/S0140-6736(16)00097-0

Mannaerts, I., Leite, S. B., Verhulst, S., Claerhout, S., Eysackers, N., Thoen, L. F., et al. (2015). The hippo pathway effector YAP controls mouse hepatic stellate cell activation. *J. Hepatol.* 63, 679–688. doi: 10.1016/j.jhep.2015.04.011

Masamune, A., Satoh, M., Kikuta, K., Sakai, Y., Satoh, A., and Shimosegawa, T. (2003). Inhibition of p38 mitogen-activated protein kinase blocks activation of rat pancreatic stellate cells. *J. Pharmacol. Exp. Ther.* 304, 8–14. doi: 10.1124/jpet.102.040287

Mazur, P. K., Herner, A., Mello, S. S., Wirth, M., Hausmann, S., Sanchez-Rivera, F. J., et al. (2015). Combined inhibition of BET family proteins and histone deacetylases as a potential epigenetics-based therapy for pancreatic ductal adenocarcinoma. *Nat. Med.* 21, 1163–1171. doi: 10.1038/nm.3952

Mews, P., Phillips, P., Fahmy, R., Korsten, M., Pirola, R., Wilson, J., et al. (2002). Pancreatic stellate cells respond to inflammatory cytokines: potential role in chronic pancreatitis. *Gut* 50, 535–541. doi: 10.1136/gut.50.4.535

Morvaridi, S., Dhall, D., Greene, M. I., Pandol, S. J., and Wang, Q. (2015). Role of YAP and TAZ in pancreatic ductal adenocarcinoma and in stellate cells associated with cancer and chronic pancreatitis. *Sci. Rep.* 5:16759. doi: 10.1038/srep16759

Murakami, S., Shahbazian, D., Surana, R., Zhang, W., Chen, H., Graham, G. T., et al. (2017). Yes-associated protein mediates immune reprogramming in pancreatic ductal adenocarcinoma. *Oncogene* 36, 1232–1244. doi: 10.1038/onc.2016.288

Ohlund, D., Handly-Santana, A., Biffi, G., Elyada, E., Almeida, A. S., Ponz-Sarvise, M., et al. (2017). Distinct populations of inflammatory fibroblasts and myofibroblasts in pancreatic cancer. *J. Exp. Med.* 214, 579–596. doi: 10.1084/jem.20162024

Omary, M. B., Lugea, A., Lowe, A. W., and Pandol, S. J. (2007). The pancreatic stellate cell: a star on the rise in pancreatic diseases. *J. Clin. Invest.* 117, 50–59. doi: 10.1172/jci30082

Pandol, S., Gukovskaya, A., Edderkaoui, M., Dawson, D., Eibl, G., and Lugea, A. (2012). Epidemiology, risk factors, and the promotion of pancreatic cancer: role of the stellate cell. *J. Gastroenterol. Hepatol.* 27(Suppl. 2), 127–134. doi: 10.1111/j.1440-1746.2011.07013.x

Peery, A. F., Dellon, E. S., Lund, J., Crockett, S. D., McGowan, C. E., Bulsiewicz, W. J., et al. (2012). Burden of gastrointestinal disease in the United States: 2012 update. *Gastroenterology* 143, 1179–1187.e3. doi: 10.1053/j.gastro.2012.08.002

Piersma, B., Bank, R. A., and Boersema, M. (2015). Signaling in fibrosis: TGF-beta, WNT, and YAP/TAZ converge. *Front. Med.* 2:59. doi: 10.3389/fmed.2015.00059

Pothula, S. P., Xu, Z., Goldstein, D., Merrett, N., Pirola, R. C., Wilson, J. S., et al. (2017). Targeting the HGF/c-MET pathway: stromal remodelling in pancreatic cancer. *Oncotarget* 8, 76722–76739. doi: 10.18632/oncotarget.20822

Qin, Z., Xia, W., Fisher, G. J., Voorhees, J. J., and Quan, T. (2018). YAP/TAZ regulates TGF-beta/Smad3 signaling by induction of Smad7 *via* AP-1 in

human skin dermal fibroblasts. *Cell Commun. Signal* 16:18. doi: 10.1186/s12964-018-0232-3

Row, S., Liu, Y., Alimperti, S., Agarwal, S. K., and Andreadis, S. T. (2016). Cadherin-11 is a novel regulator of extracellular matrix synthesis and tissue mechanics. *J. Cell Sci.* 129, 2950–2961. doi: 10.1242/jcs.183772

Rozengurt, E., Sinnett-Smith, J., and Eibl, G. (2018). Yes-associated protein (YAP) in pancreatic cancer: at the epicenter of a targetable signaling network associated with patient survival. *Signal Transduct. Target. Ther.* 3:11. doi: 10.1038/s41392-017-0005-2

Schneider, E., Schmid-Kotsas, A., Zhao, J., Weidenbach, H., Schmid, R. M., Menke, A., et al. (2001). Identification of mediators stimulating proliferation and matrix synthesis of rat pancreatic stellate cells. *Am. J. Physiol. Cell Physiol.* 281, C532–C543. doi: 10.1152/ajpcell.2001.281.2.C532

Smoot, R. L., Werneburg, N. W., Sugihara, T., Hernandez, M. C., Yang, L., Mehner, C., et al. (2018). Platelet-derived growth factor regulates YAP transcriptional activity *via* Src family kinase dependent tyrosine phosphorylation. *J. Cell. Biochem.* 119, 824–836. doi: 10.1002/jcb.26246

Song, X., Qian, X., Shen, M., Jiang, R., Wagner, M. B., Ding, G., et al. (2015). Protein kinase C promotes cardiac fibrosis and heart failure by modulating galectin-3 expression. *Biochim. Biophys. Acta* 1853, 513–521. doi: 10.1016/j.bbamcr.2014.12.001

Su, H. Y., Waldron, R. T., Gong, R., Ramanujan, V. K., Pandol, S. J., and Lugea, A. (2016). The unfolded protein response plays a predominant homeostatic role in response to mitochondrial stress in pancreatic stellate cells. *PLoS One* 11:e0148999. doi: 10.1371/journal.pone.0148999

Talele, N. P., Fradette, J., Davies, J. E., Kapus, A., and Hinz, B. (2015). Expression of alpha-smooth muscle actin determines the fate of mesenchymal stromal cells. *Stem Cell Rep.* 4, 1016–1030. doi: 10.1016/j.stemcr.2015.05.004

Wada, K., Itoga, K., Okano, T., Yonemura, S., and Sasaki, H. (2011). Hippo pathway regulation by cell morphology and stress fibers. *Development* 138, 3907–3914. doi: 10.1242/dev.070987

Xue, J., Sharma, V., Hsieh, M. H., Chawla, A., Murali, R., Pandol, S. J., et al. (2015). Alternatively activated macrophages promote pancreatic fibrosis in chronic pancreatitis. *Nat. Commun.* 6:7158. doi: 10.1038/ncomms8158

Yang, D., and Forsmark, C. E. (2017). Chronic pancreatitis. *Curr. Opin. Gastroenterol.* 33, 396–403. doi: 10.1097/MOG.0000000000000377

Yang, J., Waldron, R. T., Su, H. Y., Moro, A., Chang, H. H., Eibl, G., et al. (2016). Insulin promotes proliferation and fibrosing responses in activated pancreatic stellate cells. *Am. J. Physiol. Gastrointest. Liver Physiol.* 311, G675–G687. doi: 10.1152/ajpgi.00251.2016

Yu, F. X., Zhao, B., Panupinthu, N., Jewell, J. L., Lian, I., Wang, L. H., et al. (2012). Regulation of the hippo-YAP pathway by G-protein-coupled receptor signaling. *Cell* 150, 780–791. doi: 10.1016/j.cell.2012.06.037

Zanconato, F., Battilana, G., Forcato, M., Filippi, L., Azzolin, L., Manfrin, A., et al. (2018). Transcriptional addiction in cancer cells is mediated by YAP/TAZ through BRD4. *Nat. Med.* 24, 1599–1610. doi: 10.1038/s41591-018-0158-8

Zhang, W., Nandakumar, N., Shi, Y., Manzano, M., Smith, A., Graham, G., et al. (2014). Downstream of mutant KRAS, the transcription regulator YAP is essential for neoplastic progression to pancreatic ductal adenocarcinoma. *Sci. Signal.* 7:ra42. doi: 10.1126/scisignal.2005049

Zhao, X., Wang, X., Fang, L., Lan, C., Zheng, X., Wang, Y., et al. (2017). A combinatorial strategy using YAP and pan-RAF inhibitors for treating KRAS-mutant pancreatic cancer. *Cancer Lett.* 402, 61–70. doi: 10.1016/j.canlet.2017.05.015

Zhao, B., Wei, X., Li, W., Udan, R. S., Yang, Q., Kim, J., et al. (2007). Inactivation of YAP oncoprotein by the hippo pathway is involved in cell contact inhibition and tissue growth control. *Genes Dev.* 21, 2747–2761. doi: 10.1101/gad.1602907

Zheng, Y., and Pan, D. (2019). The hippo signaling pathway in development and disease. *Dev. Cell* 50, 264–282. doi: 10.1016/j.devcel.2019.06.003

In Pursuit of the Parietal Cell – An Evolution of Scientific Methodology and Techniques

Vanessa Baratta[1], Jason Own[1], Chiara Di Renzo[2], Jenna Ollodart[1], John P. Geibel[1,3]* and Maria Barahona[1]

[1] Department of Surgery, Yale University School of Medicine, New Haven, CT, United States, [2] Department of Surgery, Oncology and Gastroenterology, Hepatobiliary Surgery and Liver Transplantation, Padua University, Padua, Italy, [3] Department of Cellular and Molecular Physiology, Yale University School of Medicine, New Haven, CT, United States

The stomach has unique embryologic and anatomic properties, making the study of the parietal cell technically challenging. Numerous individuals have devoted decades of research to unraveling the pathophysiological basis of this cell type. Here, we perform a scoping review of novel *in vitro* and *in vivo* methodology pertaining to the parietal cell. First, we evaluate early *in vitro* methods of parietal cell analysis. This section focuses on three major techniques: gastric gland isolation, parietal cell isolation, and parietal cell culture. We also discuss parietal cell physiology and pathophysiology. Second, we discuss more contemporary efforts involving confocal microscopy and gastric organoids, a new technique that holds much promise in unveiling the temporal-spatial dynamics of the cell. Finally, we will discuss findings from our laboratory where we identified an active gastric vacuolar H^+-ATPase as a putative mechanism for refractory GERD. Overall, this review aims to highlight the major milestones in understanding an elusive yet important cell. Though in no way comprehensive, we hope to provide a birds-eye view to the study of this unique cell type in the gastrointestinal tract.

Keywords: parietal cell, methodology, *in vitro* techniques, gastric gland isolation, *in vivo* confocal imaging

INTRODUCTION

The human stomach is composed of approximately one billion parietal or oxyntic cells (Naik et al., 1971). The stomach itself is lined by columnar epithelium and punctuated by various gastric glands where specialized cells reside. These specialized cell types that are regionally distributed based on the anatomic region. Broadly, the stomach has two functional units (Schubert, 2012). The larger, oxyntic region comprises the cardia, fundus, and corpus and accounts for 80% of the stomach, whereas the pyloric region comprises the remaining 20% via the pylorus and antrum (**Figure 1A**). As the name implies, the oxyntic portion of the stomach is where the oxyntic or parietal cell resides. A gastric gland is divided into the pit, isthmus, neck, and base and has at least five specialized cell types based on location (**Figure 1B**). In the oxyntic fundus or body, parietal cells are particularly abundant and secrete acid. Neighboring cells in the gland may include chief cells, enterochromaffin cells, D cells, and mucous cells.

A single parietal cell can concentrate hydrogen up to 4 million times, from pH 7.4 – 0.8 (Rabon et al., 1983). It undergoes a series of well-orchestrated events to generate HCl through the H^+, K^+ ATPase and the associated Cl^- and K^+ channels (Schubert, 2012). When stimulated, tubulovesicles

fuse with the membrane to form an extensive network of canaliculi, increasing the surface area of the parietal cell's apical membrane (Sachs, 2003; Sachs et al., 2007). Following stimulation, the H^+, K^+ ATPase appears in the microvilli. When stimulation ceases, the canaliculi break down and the tubulovesicles are restored, as the parietal cell transitions back to the non-secretory state. These changes have been captured at the ultrastructural level. **Figure 2** demonstrates BCECF-loading of parietal cells from our laboratory (**Figures 2A–C**, unpublished). Parietal cells not only govern gastric acid secretion, but also produce growth factors crucial for cell maturation. Our current knowledge of the parietal cell, however, has evolved from rudimentary beginnings.

In the early 1800's, people were fascinated by stomach digestion but were puzzled by the agent responsible for degrading food matter (Baron, 1979). Since food could not be broken down by common acids, it was postulated that the stomach possessed a certain "vital force" (Kousoulis et al., 2012). In 1824, William Beaumont studied the gastric contents of a gunshot wound victim through a gastric fistula, further proving that the stomach generated acidic contents (Baron, 1979), **Figure 3**. Over a century later, little remained known about the stomach. In 1968, the editors of Gastroenterology mused, "The major questions in the field…are still unanswered. We cannot formulate the reactions within the parietal cell which result in hydrogen ion production. We are unable to state the etiology of peptic ulcer" (Davenport, 1968).

Later that year, critical findings on the parietal cell began to unfold. Sachs studied hog gastric mucosa and first described the K^+-stimulated ATPase (Sachs et al., 1976). Subsequently, a wave of studies emerged to further characterize this transporter (Ganser and Forte, 1973; Lee et al., 1974; Rabon et al., 1982). In the latter half of the twentieth century, three *in vitro* techniques emerged, permitting investigative studies on the parietal cell: (1) Gastric gland isolation. (2) Parietal cell isolation. (3) Parietal cell cultures.

As we shine a spotlight on supporting gastrointestinal cell types, we hope to illuminate the efforts that have led to our current understanding of the parietal cell. **Figure 3** and **Table 1** may serve as visual guides during the narrative.

GASTRIC GLAND ISOLATION

Berglindh and Obrink (1976) developed a method for isolating gastric glands from the corpus of rabbit mucosa, as delineated in methodology of their 1976 paper. Briefly, after appropriate anesthetization, they harvested the stomach. Next, they stripped off the corpus mucosa, minced the tissue, and exposed it to collagenase. To demonstrate gland viability, they measured oxygen consumption and evaluated electrolyte content. Gastric gland cells were identified through staining and electron microscopy (Berglindh and Obrink, 1976).

With this technique, scientists were able to expose isolated gastric tissue to various secretagogues to assess gastric acid production. For example, the effects of histamine, acetylcholine (ACh) and gastrin were found by measuring the degree of

oxygen consumption in gastric glands. They also employed an aminopyrine (AP) uptake assay to indirectly measure HCl excretion (Sack and Spenney, 1982). The ratio of the accumulated ^{14}C-AP in the intra- versus extra glandular compartments served as an index of parietal cell function, quantified via a scintillation counter. AP is a weak base with a pKa of 5.0. In an unprotonated state, the weak base freely diffuses across membranes. In a protonated state, the aminopyrine remains in a particular compartment. Impurities in the base and variations in centrifugation falsely lowered aminopyrine ratios and underestimated the parietal cell activity (Sack and Spenney, 1982). Nevertheless, the technique was an invaluable tool to quantify gastric acid secretion.

Overall, gastric gland isolation was an important scientific technique with advantages and disadvantages (**Table 1**). Gastric gland isolation was beneficial in that the tight junctions and polarity of the cells were unperturbed. As a result, scientists could study cell-cell interactions. However, the presence of collagenase affected the transport proteins and limited studies on signal transduction pathways. In addition, isolated glands contained non-parietal cells, preventing experimentation on individual parietal cells. These limitations paved the way for parietal cell isolation.

PARIETAL CELL ISOLATION

The parietal cell is particularly challenging to isolate, due to its thick connective tissue. As a result, a combination of mechanical and chemical digestants was used to isolate the cells. Susceptibility of the gastric tissue to separation is species-dependent (Walder and Lunseth, 1963). For example, collagenase fully disperses all gastric cells in dogs and guinea pigs yet has poorer dissociating power in rabbits and rats. Pronase and EDTA are alternative agents for cellular separation. Early attempts to isolate parietal cells involved excessive damage to the cells (Walder and Lunseth, 1963; Blum et al., 1971; Romrell et al., 1975).

The first landmark study in parietal cell isolation was that performed by Soll (1978) on canine stomachs (Soll, 1978). His technique was unique in that he (a) completely isolated the mucosa from the submucosa and (b) introduced a calcium chelation step to facilitate disruption of cell junctions thereby minimizing exposure to chemical digestants.

In the first part of the experiment, the mucosa of the oxyntic part of the stomach was stripped from the submucosa and incubated in collagenase, EDTA, and collagenase again. The mucosal cells were then serially centrifuged and resuspended before being passed through a nylon mesh.

In the second part of the experiment, the parietal cell population was purified with a Beckman elutriator rotor. The rotor separated cells by counter-flow centrifugation based on varying sedimentation velocities. Parietal cell yields were obtained up to 85%.

Another method of parietal cell isolation was the Percoll method. In this technique, polyvinyl pyrrolidone-coated colloidal silica particles (Percoll, Pharmacia Fine Chemicals, Uppsala,

FIGURE 1 | Schematic representations of the stomach **(A)** and oxyntic gland **(B)**. **(A)** The stomach is divided into two functional regions, the oxyntic region (composed of the cardia, fundus, and corpus) and the pyloric region (composed of the antrum and pylorus). **(B)** A representative oxyntic gland from the oxyntic region of the stomach features a gastric pit, isthmus, neck, and base. A variety of stomach cell types exist, including parietal cells, enterochromaffin cells, and mucous cells.

FIGURE 2 | Images of the human gastric gland **(A)**. Phase contrast of the human gland at $40\times$ Magnification **(B)**. pH sensitive dye BCECF-selective loading in parietal cells **(C)**. Pseudo color image of the parietal cells following stimulation with a secretagogue. All images acquired with a Olympus OM2 microscope.

Sweden), were mixed with isolated cells to a specified density (Pretlow and Pretlow, 2014). Afterward, the cells underwent 15 min of 190 G centrifugation in a swinging bucket. The surface layer consists of parietal cells, while the bottom layer consisted of non-parietal cells.

Overall, isolated cells are advantageous, because they are easy to manipulate in the absence of a connective tissue diffusion barrier. However, the *in vitro* technique has numerous limitations (**Table 1**). In the isolation process, the cell loses its polarity and its capacity to secrete HCl. In fact, many scientists preferred studying gastric glands as they were the smallest functional unit of the stomach. In addition, parietal cell isolation is time consuming and can result in cell clumping. The repeated centrifugation process concentrates the number of parietal cells but does not obtain a pure parietal cell population. To overcome some of these limitations, investigators focused on culturing cells.

PARIETAL CELL CULTURES

A working parietal cell culture was long sought after though difficult to attain (Chew, 1994). Even after serial centrifugation to enrich the cell pool, parietal cells dwindled with cell passages. Scientists initially hypothesized that parietal cells dedifferentiated over time. It later became apparent that the more rapidly dividing mucous cells out-populated the parietal cells.

Chew et al. (1989) were able to obtain a nearly 100% parietal cell yield by combining centrifugation and density gradient techniques. When they placed highly enriched parietal cells in culture lacking serum, the parietal cells persisted. The cells were also responsive to known secretagogues, thus exhibiting the parietal phenotype. For the parietal cells to survive, they were placed in a unique basement membrane extract called Matrigel. The cells required high water quality with a specific resistivity and
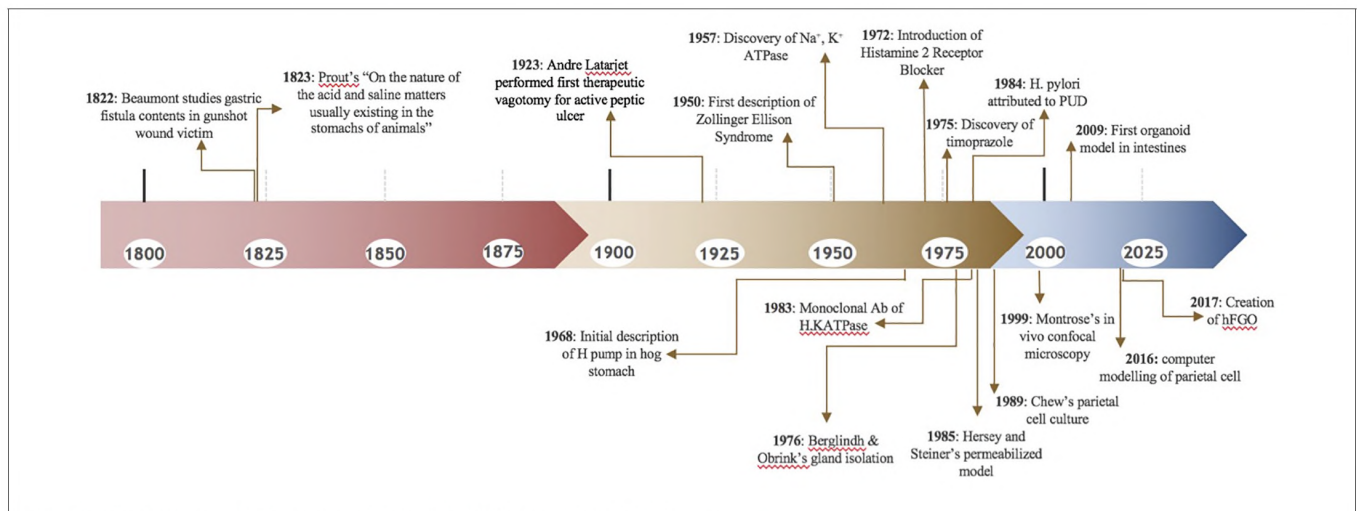
FIGURE 3 | Key Events and Studies Involving the Parietal Cell and Gastric Acid Production.

TABLE 1 | Pros and cons of parietal cell methodology.

Technique	Pros	Cons
Gastric gland isolation	– Able to study smallest functional unit of stomach	– Indirect method of measuring H^+ secretion
		– Collagenase affected transport proteins
		– Also contains non–parietal cells
Parietal cell isolation	– Easy to manipulate pH, ion composition w/o diffusion barrier	– Time consuming
	– Study on a single cell type	– Inconsistent parietal cell yields
		– Chemical digestants damage the cell
		– Isolated parietal cells behaves differently
Parietal cell cultures	– Can attain high yields of parietal cells	– Loss of parietal cells over time
	– Study on a single cell type	– Unable to see cell–cell interactions
Permeabilized gastric gland models	– Allows for assessment of signal transduction in the Parietal cell	– Digitoxin: cells lose secretagogue sensitivity
		– Alpha toxin: only smaller proteins were permeable
In vivo confocal microscopy	– Allows for real–time pH monitoring during acid secretion	– Not accurate for pH < 2
	– Evaluates effects *in vivo*	
Gastric gland dissection	– Can monitor effects of various drugs on H^+, K^+ ATPase through changes in intracellular pH, Ca, Cl	– Restricted to *in vitro* analysis
	– Can selectively inactivate sodium and potassium dependent transporters by exposing it to 0–Na and 0–K solutions	
Gastric organoids	– A near physiological three–dimensional model	– Difficult to maintain high population parietal cells
	– More accurate representation of *in vivo* system	– Lack of immune cells, neurons, vascularization
	– Can sustain *H. pylori* microinjections	

inclusion of antibiotics and antimycotics (Pretlow and Pretlow, 2014). Issues with the parietal cell culture included inevitable loss of cell numbers, around 10% per day. In addition, the presence of the parietal cell was verified only indirectly through its response to known secretagogues and the accumulation of aminopyrine.

In the wake of parietal cell cultures, Forte and colleagues applied high-pressure freezing (HPF) techniques to capture ultrastructural changes during acid secretion (Sawaguchi et al., 2002). Cultured parietal cells were mounted on aluminum plates and frozen at high pressures to prevent crystal formation. Ice in the frozen specimen was substituted with an organic solvent, gradually warmed to 20°C, embedded in Epon, and cut into thin sections. The nucleus and cytoskeletal were better preserved with HPF than conventional chemical

fixation. In addition, the tubulovesicle changes were captured by pre-exposure to histamine. The presence of the cell membrane in parietal cell cultures made it difficult for investigators to evaluate signal transduction pathways. Scientists sought to introduce protein fragments into the cytoplasm to evaluate downstream effects. To facilitate this, permeable parietal cell models emerged (Yao and Forte, 2003).

PERMEABILIZED MODELS

One of the earlier permeabilized models using the detergent digitoxin was introduced by Hersey and Steiner (1985). Digitoxin permeabilized the parietal cell by creating pores

in the membrane to permit protein entry. A downside was that the cell was no longer sensitive to secretagogue stimulation. Subsequently, Thibideau introduced the alpha toxin permeabilized model (Thibodeau et al., 1994). Alpha-toxin was isolated from *Staphylococcus aureus* to create pores in the parietal cell membrane. Here, the parietal cell was still receptive to secretagogues while maintaining permeability. A downside was that the alpha-toxin generated narrow pore sizes, so only small nucleotides could pass through. Gentler detergents like Beta-escin were introduced that permitted entry of larger molecules without disrupting the parietal cell (Akagi et al., 1999). Overall, these three *in vitro* methods – gastric gland isolation, parietal cell isolation, and parietal cell cultures with permeabilization – paved the way for newer techniques to emerge.

IN VIVO CONFOCAL MICROSCOPY

The stomach's ability to resist damage from its own highly acidic fluid has been a topic of interest. Through *in vivo* confocal imaging on an everted rat stomach, Montrose and colleagues quantified pH changes at the gel-mucous gastric surface (Chu et al., 1999). First, they used a surgical exteriorization technique. The stomach was exteriorized, opened along the greater curvature, and everted to expose the mucosa. Baseline luminal pH measurements of the gastric contents were recorded. The everted stomach was secured to the abdominal wall with sutures and the rat was placed prone on the microscope stage. The stomach tissue was maintained at physiological temperatures and continuously perfused with solutions of varying pH's.

To measure pH changes in real time, they used a fluorescent extracellular dye, Cl-NERF in the perfusate. They excited the dye with an argon laser and calculated fluorescence intensity ratios of the emissions (Chu et al., 1999). As an internal reference, Lucifer yellow was added to the perfusate and Cl-NERF/Lucifer ratios were converted to various pH's at the level of the gastric surface. As hypothesized, when the gastric mucosa was perfused with acidic solutions, the gastric surface pH was relatively alkaline. When the rats were injected with pentagastrin, the pH of the perfusate decreased, while the pH at the gastric surface remained alkaline. These studies confirmed that the gel-mucous stomach layer provides a self-protective mechanism from the acidic contents it secretes. With confocal microscopy, high resolution images were obtained at various depths of a tissue specimen without sectioning and processing. Overall, this technology has permitted significant advances in the understanding of stomach physiology.

PARIETAL CELL PHYSIOLOGY

Parietal cells carry the H, K ATPase in cytoplasmic tubulovesicles that are eventually shuttled to the apical membrane through various routes of activation. Three primary pathways, the neurocrine, paracrine, and endocrine, are involved in inducing parietal cell acid secretion (Schubert, 2012). With regards to the neurocrine pathway, the neurotransmitter ACh is responsible for acid secretion. Ach directly activates the parietal cell by attaching to the muscularinic M3 receptor. This activation triggers downstream phospholipase C's conversion of phosphatidylinositol bisphosphate (PIP2) into inositol trisphosphate (IP3), leading to release of intracellular calcium stores and activation of calmodulin kinases that activate acid secretion (**Figure 4A**).
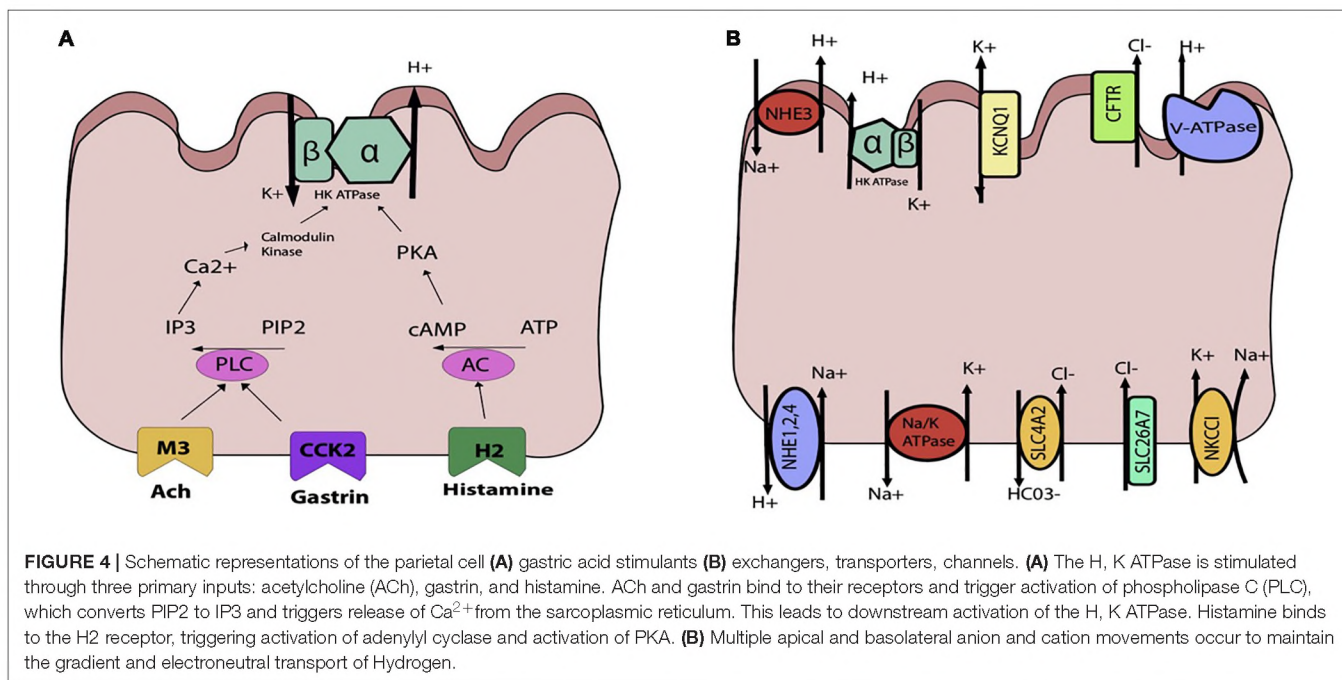
In the endocrine activation pathway, antral endocrine G cells secrete gastrin which directly binds to type B cholecystokinin receptors, triggering the same pathway generating increased intracellular calcium as that of ACh. Indirectly, gastrin also stimulates histamine secretion from ECL cells.

In the paracrine pathway, enterochromaffin cell releases histamine, which separately activate acid secretion. By binding to H2-specific receptors on the parietal cell, histamine triggers a signal transduction pathway through activation of adenylyl cyclase, which increases intracellular cAMP that serves. Indirectly, histamine acts through H_3 receptors which suppress somatostatin secretion, thereby abolishing any inhibition of acid secretion by somatostatin.

Overall, there are multiple interactions amongst ACh, gastrin, and histamine and their associated pathways to regulate acid secretion. While these are the three main mediators of acid production, a variety of other stimulants have been identified, including gastrin-releasing peptide, nitric oxide in specific amounts, pituitary adenylate cyclase activating polypeptide, ghrelin, atrial natriuretic peptide, and even coffee (Schubert, 2012).

As the parietal cell is activated by one or more pathways previously described, the hydronium ion is generated and HCl secreted. In order to maintain the H^+, K^+ ATPase pump, a careful interplay of channels, exchangers, and transporters is required (**Figure 4B**). On the apical side is the H^+, K^+ ATPase, which is a dimeric protein and member of the P-Type family of ATPases. The alpha subunit spans the membrane 10 times, whereas the beta subunit spans once. This transporter is typically stored in tubulovesicular elements (TVE) that fuse with the apical membrane under parietal cell stimulation to deliver the transporter machinery to the membrane (Schubert, 2012). To maintain the potassium gradient, the apical KCNQ1 channel is nearby (Heitzmann and Warth, 2007). Other apical K^+ channels include Kir 2.1 and Kir 4.1 (Forte, 2004). The bicarbonate that is generated from the hydrogen that is extruded by the H^+, K^+ ATPase is generated along with H^+ from the intracellular carbonic anhydrase reaction exits the cell through the SCL4A2. For each hydrogen that is secreted, bicarb leaves the cell basolaterally. To maintain electroneutral acid secretion, chloride is also apically secreted along with hydrogen, generating HCl. On the apical side, the CFTR allows for chloride entry into the gastric lumen (Sidani et al., 2007). Basolaterally, chloride enters the cell through SLC4A2, SLC26A7, and NKCC1 (Kosiek et al., 2007). Overall, various cations and anions are involved in transcellular movement to maintain the H^+, K^+ ATPase pump. Though calcium is not directly involved in transcellular movement, its release from the sarcoplasmic reticulum is essential for parietal cell stimulation. The identification of the calcium sensing receptor (CaSR) on the surface of freshly isolated rat gastric tissue
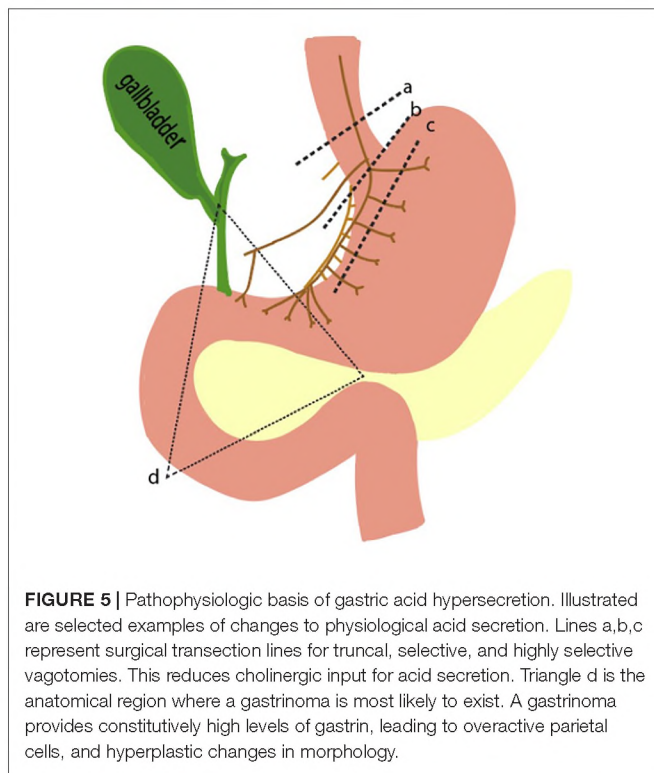
FIGURE 4 | Schematic representations of the parietal cell **(A)** gastric acid stimulants **(B)** exchangers, transporters, channels. **(A)** The H, K ATPase is stimulated through three primary inputs: acetylcholine (ACh), gastrin, and histamine. ACh and gastrin bind to their receptors and trigger activation of phospholipase C (PLC), which converts PIP2 to IP3 and triggers release of Ca^{2+} from the sarcoplasmic reticulum. This leads to downstream activation of the H, K ATPase. Histamine binds to the H2 receptor, triggering activation of adenylyl cyclase and activation of PKA. **(B)** Multiple apical and basolateral anion and cation movements occur to maintain the gradient and electroneutral transport of Hydrogen.

has also been associated with an increase in intracellular calcium release and parietal cell activation (Dufner et al., 2005).

PARIETAL CELL PATHOPHYSIOLOGY

A spectrum of diseases emerges when any of the well-regulated pathways in parietal cell function go awry. There may be disorders of increased and decreased gastric acid secretion. On one end of the spectrum, gastric hypersecretion can result from various pathologic disease states, ranging from gastrinoma to peptic ulcer disease. On the other end, achlorhydria or the absence of HCl, can result from autoimmune disease states or from surgical interventions like vagotomies. As explained previously, three main inputs – gastrin, ACh, and histamine – are known to stimulate the parietal cell. Thus, perturbations of this inputs result in altered gastric acid secretion (**Figure 5**).

Pathophysiological elevations in gastrin can occur in patients with gastrinomas, a type of neuroendocrine tumor that can arise sporadically or as part of the familial syndrome, MEN1 (Kitagawa and Dempsey, 2005). The state of having elevated gastric acid secretion due to a gastrinoma is Zollinger Ellison syndrome, which manifests as intractable ulcers, weight loss, and abdominal pain (Isenberg et al., 1973; De Angelis et al., 2018). Surgery is the mainstay of treatment, though preoperative and intraoperative identification of the small gastrinomas can be difficult. Over 90% of tumors are found in the gastrinoma triangle, an anatomical zone defined by the junction of the pancreatic neck and body, the junction of the second to third parts of the duodenum, and the junction of the cystic and common bile duct (**Figure 5**).

Acetylcholine is the other main stimulator of parietal cell secretion, which has been a primary target for surgically reducing acid hypersecretion. Shown in **Figure 5** are the three different

FIGURE 5 | Pathophysiologic basis of gastric acid hypersecretion. Illustrated are selected examples of changes to physiological acid secretion. Lines a,b,c represent surgical transection lines for truncal, selective, and highly selective vagotomies. This reduces cholinergic input for acid secretion. Triangle d is the anatomical region where a gastrinoma is most likely to exist. A gastrinoma provides constitutively high levels of gastrin, leading to overactive parietal cells, and hyperplastic changes in morphology.

types of vagotomies that can be performed: truncal vagotomy (a), selective vagotomy (b), and highly selective vagotomy (c). The more selective vagotomies leave parts of the vagus nerve, which helps facilitate gastric emptying problems associated with the truncal vagotomy. Due to the advent of proton pump inhibitors, the need for surgical vagotomies has declined.

One of the most common disease states linked to altered gastric acid homeostasis is peptic ulcer disease. Peptic ulcers are focal lesions in either the stomach or duodenum that can emerge for a variety of reasons, most commonly *Helicobacter pylori*. *H. pylori* is a spiral shaped bacterium that can protect itself from the damaging effect of nearby HCl through its local production of urease, which converts urea into ammonium and bicarbonate (Kitagawa and Dempsey, 2005). Various mechanisms by which *H. pylori* causes damage has been studied and is discussed at length in other reviews (Camilo et al., 2017; Kamboj et al., 2017. As it pertains to acid hypersecretion, *H. pylori* inhibits the antral D cells that produce somatostatin, thereby leading to hypergastrinemia and acid overproduction. Therapy for *H. pylori* include a combined course of antibiotics as well as proton pump inhibitors (PPI, Yang et al., 2014; Strand et al., 2017).

AN EXPLANATION OF PPI FAILURE

A better understanding of stomach physiology has led to major advances in the treatment of gastric disease. Characterization of the H^+, K^+ ATPase resulted in the development of proton pump inhibitors that irreversibly inhibit the transporter. However, many patients still suffer from acid hypersecretion. Using the ammonium prepulse technique, our lab identified the vacuolar ATPase as a constitutively active H^+-ATPase that is not susceptible to proton pump inhibitors (Kitay et al., 2018). In this experiment, we performed gastric gland dissection to isolate tissue. We then loaded parietal cells in the gastric tissue with acid and flushed them with solutions that were free of sodium and potassium in order to eliminate activity of the endogenous H^+, K^+ ATPase and the sodium hydrogen exchanger (NHE). We then exposed cells to omeprazole and identified persistent efflux of hydrogen, as measured by intracellular pH (pH_i). The subsequent recovery of pH_i was attributable to H^+-ATPase, the only remaining pathway for the extrusions of protons. In addition, we discovered that the activity of the H^+-ATPase was upregulated when exposed to calcium (Kitay et al., 2018; **Figure 4B**).

GASTRIC ORGANOIDS

Organoids are three-dimensional, stem cell-derived cell models first developed in murine intestines. In 2009, Sato placed intestinal stem cells into an extracellular matrix enriched with intestine-specific niche factors. They obtained cells that differentiated into intestinal cell types ranging from goblet to Paneth cells (Sato et al., 2009). The first gastric organoids were developed as an extension of the intestinal organoid protocol (Barker et al., 2010). Adult stem cells from murine antral glands were embedded into extracellular matrices and exposed to stomach-specific niche factors (Barker et al., 2010). Gastric organoid cells differentiated into chief, neck, pit and enteroendocrine cells. The one cell type that was elusive was the parietal cell. Though present in the initial culture, the parietal cells decreased with multiple passages.

To counteract this problem, scientists used pluripotent stem cells (PSCs). Noguchi cultured corpus organoids from mouse ESCs, which generated all three germ layers (Noguchi et al., 2015). The embryoid bodies from primordium spheroids were embedded into matrix and allowed to differentiate over 60 days with exposure to selected niche factors. These gastric organoids developed functional parietal cells. McCracken and colleagues then exposed human PSC-derived foregut progenitors to beta catenin to create human, fundic-type gastric organoids (hFGOs) (McCracken et al., 2017). From here, they exposed the hFGOs to a variety of putative parietal cell agonists and measured expression of ATP4A and ATP4B, known parietal cell markers (McCracken et al., 2017). Interestingly, mature, terminal parietal cells have dedifferentiating capacity; Notch activation in parietal cells can be de-differentiated into stem cells (Kim and Shivdasani, 2011). Other transgenic mice that have been engineered to overexpress Noggin, led to the development of dedifferentiated cells at the cost of the parietal cell lineage (Tetreault and Katz, 2012). What is most notable in transgenic studies on parietal cells is that genetic alterations more frequently lead to parietal cell loss than parietal cell gain. Overall, the embryonic properties of parietal cells remains under investigation.

Overall, organoids unite the positive aspects of both *in vitro* and *in vivo* systems in that they allow for easy experimental manipulation, while maintaining the cellular diversity of native tissue (Engevik et al., 2018). Nevertheless, it is still difficult to maintain organoids with high populations of parietal cells. New studies are evaluating the effects of *H. pylori* microinjections into gastric organoids. It is important that gastric organoids maintain parietal cells over time.

COMPUTER MODELING OF THE PARIETAL CELL

Another new concept in the understanding of the parietal cell is computer modeling using Berkeley Madonna Software (Crothers et al., 2016). The software is a mathematical modeling package and a differential equations solver. Crothers et al. (2016) created a dynamic model of the parietal cell based on known features of Na^+, K^+ATPase, AE2, and the H^+, K^+ ATPase. It quantitatively represents the activity of all parietal cells located within 1 cm^2 of adult mammalian tissue. Voltage measurements from classical studies in a resting and stimulated parietal cell were entered into the software to recapitulate a model of the cell. The model adequately predicted flux and potential differences but also provided novel insight into the role of canalicular potassium in parietal cell secretion.

DISCUSSION

Clearly, we have made significant strides in the understanding of the parietal cell. Historically, the study of the parietal cell plagued the most ambitious and astute researcher. Since the stomach consists of a variety of cell types, it was particularly challenging to isolate the parietal cell. In this chronological review, we described

some of the various methodological milestones that helped shape our current understanding of the parietal cell.

The parietal cell is a small component of the alimentary tract, yet immense research has been devoted to the topic. This phenomenon may be twofold. First, dysfunctional parietal cells lead to human disease with a large socioeconomic burden, which has galvanized research efforts (Banic et al., 2011). With the discovery of proton pump inhibitors, gastroesophageal reflux disease is now manageable. Second, the parietal cell has historically been challenging to study. The stomach has multiple cell types that are affected by autocrine, endocrine, and paracrine

pathways. It is therefore difficult to dissect the underlying physiological roles. With time, scientists have built upon one another to find novel ways to study this otherwise elusive cell.

AUTHOR CONTRIBUTIONS

VB involved in conception, design, and writing and editing of the manuscript. JOw, CD, JOl, and MB involved in writing and editing of the manuscript. JG involved in conception, design, and editing of the manuscript.

REFERENCES

Akagi, K., Nagao, T., and Urushidani, T. (1999). Responsiveness of beta-escin-permeabilized rabbit gastric gland model: effects of functional peptide fragments. *Am. J. Physiol.* 277, G736–G744. doi: 10.1152/ajpgi.1999.277.3.G736

Banic, M., Malfertheiner, P., Babic, Z., Ostojic, R., Kujundzic, M., Fatovic-Ferencic, S., et al. (2011). Historical impact to drive research in peptic ulcer disease. *Dig. Dis.* 29, 444–453. doi: 10.1159/000331512

Barker, N., Huch, M., Kujala, P., Van De Wetering, M., Snippert, H. J., Van Es, J. H., et al. (2010). Lgr5(+ve) stem cells drive self-renewal in the stomach and build long-lived gastric units in vitro. *Cell Stem Cell* 6, 25–36. doi: 10.1016/j.stem.2009.11.013

Baron, J. H. (1979). The discovery of gastric acid. *Gastroenterology* 76, 1056–1064.

Berglindh, T., and Obrink, K. J. (1976). A method for preparing isolated glands from the rabbit gastric mucosa. *Acta Physiol. Scand.* 96, 150–159. doi: 10.1111/j.1748-1716.1976.tb10184.x

Blum, A. L., Shah, G. T., Wiebelhaus, V. D., Brennan, F. T., Helander, H. F., Ceballos, R., et al. (1971). Pronase method for isolation of viable cells from *Necturus* gastric mucosa. *Gastroenterology* 61, 189–200. doi: 10.1016/s0016-5085(19)33595-4

Camilo, V., Sugiyama, T., and Touati, E. (2017). Pathogenesis of *Helicobacter pylori* infection. *Helicobacter* 22(Suppl.3), 7–9.

Chew, C. S. (1994). Parietal cell culture: new models and directions. *Annu. Rev. Physiol.* 56, 445–461. doi: 10.1146/annurev.physiol.56.1.445

Chew, C. S., Ljungstrom, M., Smolka, A., and Brown, M. R. (1989). Primary culture of secretagogue-responsive parietal cells from rabbit gastric mucosa. *Am. J. Physiol.* 256, G254–G263.

Chu, S., Tanaka, S., Kaunitz, J. D., and Montrose, M. H. (1999). Dynamic regulation of gastric surface pH by luminal pH. *J. Clin. Invest.* 103, 605–612. doi: 10.1172/jci5217

Crothers, J. M. Jr., Forte, J. G., and Machen, T. E. (2016). Computer modeling of gastric parietal cell: significance of canalicular space, gland lumen, and variable canalicular [K+]. *Am. J. Physiol. Gastrointest. Liver Physiol.* 310, G671–G681.

Davenport, H. (1968). The mechanisms of acid secretion. *Gastroenterology* 54, 701–702.

De Angelis, C., Cortegoso Valdivia, P., Venezia, L., Bruno, M., and Pellicano, R. (2018). Diagnosis and management of Zollinger-Ellison syndrome in 2018. *Minerva Endocrinol.* 43, 212–220.

Dufner, M. M., Kirchhoff, P., Remy, C., Hafner, P., Muller, M. K., Cheng, S. X., et al. (2005). The calcium-sensing receptor acts as a modulator of gastric acid secretion in freshly isolated human gastric glands. *Am. J. Physiol. Gastrointest. Liver Physiol.* 289, G1084–G1090.

Engevik, K. A., Matthis, A. L., Montrose, M. H., and Aihara, E. (2018). Organoids as a Model to Study Infectious Disease. *Methods Mol. Biol.* 1734, 71–81. doi: 10.1007/978-1-4939-7604-1_8

Forte, J. G. (2004). K+ channels in the secretory membrane of the parietal cell. focus on "Gastric parietal cell secretory membrane contains PKA- and acid-activated Kir2.1 K+ channels". *Am. J. Physiol. Cell Physiol.* 286, C495–C506.

Ganser, A. L., and Forte, J. G. (1973). K + -stimulated ATPase in purified microsomes of bullfrog oxyntic cells. *Biochim. Biophys Acta* 307, 169–180. doi: 10.1016/0005-2736(73)90035-7

Heitzmann, D., and Warth, R. (2007). No potassium, no acid: K+ channels and gastric acid secretion. *Physiology* 22, 335–341. doi: 10.1152/physiol.00016.2007

Hersey, S. J., and Steiner, L. (1985). Acid formation by permeable gastric glands: enhancement by prestimulation. *Am. J. Physiol.* 248, G561–G568.

Isenberg, J. I., Walsh, J. H., and Grossman, M. I. (1973). Zollinger-Ellison syndrome. *Gastroenterology* 65, 140–165.

Kamboj, A. K., Cotter, T. G., and Oxentenko, A. S. (2017). *Helicobacter pylori*: the Past, Present, and Future in Management. *Mayo Clin. Proc.* 92, 599–604. doi: 10.1016/j.mayocp.2016.11.017

Kim, T.-H., and Shivdasani, R. A. (2011). Notch signaling in stomach epithelial stem cell homeostasis. *J. Exp. Med.* 208, 677–688. doi: 10.1084/jem.20101737

Kitagawa, Y., and Dempsey, D. (2005). "Stomach," in *Schwartz's Principles of Surgery*, eds F. C. Brunicardi, and I. S. Seymour, (New York, NY: McGraw-Hill), 1035–1045.

Kitay, A. M., Schneebacher, M. T., Schmitt, A., Heschl, K., Kopic, S., Alfadda, T., et al. (2018). Modulations in extracellular calcium lead to H(+)-ATPase-dependent acid secretion: a clarification of PPI failure. *Am. J. Physiol. Gastrointest. Liver Physiol.* 315, G36–G42. doi: 10.1152/ajpgi.00132.2017

Kosiek, O., Busque, S. M., Foller, M., Shcheynikov, N., Kirchhoff, P., Bleich, M., et al. (2007). SLC26A7 can function as a chloride-loading mechanism in parietal cells. *Pflugers Arch.* 454, 989–998. doi: 10.1007/s00424-007-0254-y

Kousoulis, A. A., Tsoucalas, G., Armenis, I., Marineli, F., Karamanou, M., and Androutsos, G. (2012). From the "hungry acid" to pepsinogen: a journey through time in quest for the stomach's secretion. *Ann. Gastroenterol.* 25, 119–122.

Lee, J., Simpson, G., and Scholes, P. (1974). An ATPase from dog gastric mucosa: changes of outer pH in suspensions of membrane vesicles accompanying ATP hydrolysis. *Biochem. Biophys. Res. Commun.* 60, 825–832. doi: 10.1016/0006-291x(74)90315-5

McCracken, K. W., Aihara, E., Martin, B., Crawford, C. M., Broda, T., Treguier, J., et al. (2017). Wnt/beta-catenin promotes gastric fundus specification in mice and humans. *Nature* 541, 182–187. doi: 10.1038/nature21021

Naik, S. R., Bajaj, S. C., Goyal, R. K., Gupta, D. N., and Chuttani, H. K. (1971). Parietal cell mass in healthy human stomach. *Gastroenterology* 61, 682–685. doi: 10.1016/s0016-5085(19)33431-6

Noguchi, T. K., Ninomiya, N., Sekine, M., Komazaki, S., Wang, P. C., Asashima, M., et al. (2015). Generation of stomach tissue from mouse embryonic stem cells. *Nat. Cell Biol.* 17, 984–993. doi: 10.1038/ncb3200

Pretlow, T. G., and Pretlow, T. P. (2014). *Cell Separation : Methods and Selected Applications.* Cambridge, CA: Academic press.

Rabon, E., Cuppoletti, J., Malinowska, D., Smolka, A., Helander, H. F., Mendlein, J., et al. (1983). Proton secretion by the gastric parietal cell. *J. Exp. Biol.* 106, 119–133.

Rabon, E. C., Mcfall, T. L., and Sachs, G. (1982). The gastric [H,K]ATPase:H+/ATP stoichiometry. *J. Biol. Chem.* 257, 6296–6299.

Romrell, L. J., Coppe, M. R., Munro, D. R., and Ito, S. (1975). Isolation and separation of highly enriched fractions of viable mouse gastric parietal cells by velocity sedimentation. *J. Cell Biol.* 65, 428–438. doi: 10.1083/jcb.65.2.428

Sachs, G. (2003). Physiology of the parietal cell and therapeutic implications. *Pharmacotherapy* 23, 68s–73s. doi: 10.1592/phco.23.13.68s.31931

Sachs, G., Chang, H. H., Rabon, E., Schackman, R., Lewin, M., and Saccomani, G. (1976). A nonelectrogenic H+ pump in plasma membranes of hog stomach. *J. Biol. Chem.* 251, 7690–7698.

Sachs, G., Shin, J. M., Vagin, O., Lambrecht, N., Yakubov, I., and Munson, K. (2007). The gastric H,K ATPase as a drug target: past, present, and future. *J. Clin. Gastroenterol.* 41(Suppl. 2), S226–S242.

Sack, J., and Spenney, J. G. (1982). Aminopyrine accumulation by mammalian gastric glands: an analysis of the technique. *Am. J. Physiol.* 243, G313–G319.

Sato, T., Vries, R. G., Snippert, H. J., Van De Wetering, M., Barker, N., Stange, D. E., et al. (2009). Single Lgr5 stem cells build crypt-villus structures in vitro without a mesenchymal niche. *Nature* 459, 262–265. doi: 10.1038/nature07935

Sawaguchi, A., Mcdonald, K. L., Karvar, S., and Forte, J. G. (2002). A new approach for high-pressure freezing of primary culture cells: the fine structure and stimulation-associated transformation of cultured rabbit gastric parietal cells. *J. Microsc.* 208, 158–166. doi: 10.1046/j.1365-2818.2002.01085.x

Schubert, M. (2012). "Regulation of gastric acid secretion," in . *Physiology of the Gastrointestinal Tract*, ed. J. R. Leonard, (Amsterdam: Elsevier Science & Technology).

Sidani, S. M., Kirchhoff, P., Socrates, T., Stelter, L., Ferreira, E., Caputo, C., et al. (2007). DeltaF508 mutation results in impaired gastric acid secretion. *J. Biol. Chem.* 282, 6068–6074. doi: 10.1074/jbc.m608427200

Soll, A. H. (1978). The actions of secretagogues on oxygen uptake by isolated mammalian parietal cells. *J. Clin. Invest.* 61, 370–380. doi: 10.1172/jci108947

Strand, D. S., Kim, D., and Peura, D. A. (2017). 25 Years of Proton Pump Inhibitors: a Comprehensive Review. *Gut Liver* 11, 27–37. doi: 10.5009/gnl15502

Tetreault, M. P., and Katz, J. P. (2012). "Transgenic Animal Models of Gastrointestinal Function," in *Physiology of the Gastrointestinal Tract*, ed. J. R. Leonard, (Amsterdam: Elsevier Science & Technology).

Thibodeau, A., Yao, X., and Forte, J. G. (1994). Acid secretion in alpha-toxin-permeabilized gastric glands. *Biochem. Cell Biol.* 72, 26–35. doi: 10.1139/o94-005

Walder, A. I., and Lunseth, J. B. (1963). A technique for separation of the cells of the gastric mucosa. *Proc. Soc. Exp. Biol. Med.* 112, 494–496. doi: 10.3181/00379727-112-28086

Yang, J. C., Lu, C. W., and Lin, C. J. (2014). Treatment of *Helicobacter pylori* infection: current status and future concepts. *World J. Gastroenterol.* 20, 5283–5293. doi: 10.3748/wjg.v20.i18.5283

Yao, X., and Forte, J. G. (2003). Cell biology of acid secretion by the parietal cell. *Annu. Rev. Physiol.* 65, 103–131. doi: 10.1146/annurev.physiol.65.072302.114200

Intestinal Epithelial Cells Respond to Chronic Inflammation and Dysbiosis by Synthesizing H_2O_2

Juan F. Burgueño[1†], Julia Fritsch[1,2†], Ana M. Santander[1], Nivis Brito[1], Irina Fernández[1], Judith Pignac-Kobinger[1], Gregory E. Conner[3] and Maria T. Abreu[1,2*]

[1] Division of Gastroenterology, Department of Medicine, Leonard M. Miller School of Medicine, University of Miami, Miami, FL, United States, [2] Department of Microbiology and Immunology, Leonard M. Miller School of Medicine, University of Miami, Miami, FL, United States, [3] Department of Cell Biology, Leonard M. Miller School of Medicine, University of Miami, Miami, FL, United States

The microbes in the gastrointestinal tract are separated from the host by a single layer of intestinal epithelial cells (IECs) that plays pivotal roles in maintaining homeostasis by absorbing nutrients and providing a physical and immunological barrier to potential pathogens. Preservation of homeostasis requires the crosstalk between the epithelium and the microbial environment. One epithelial-driven innate immune mechanism that participates in host-microbe communication involves the release of reactive oxygen species (ROS), such as hydrogen peroxide (H_2O_2), toward the lumen. Phagocytes produce high amounts of ROS which is critical for microbicidal functions; the functional contribution of epithelial ROS, however, has been hindered by the lack of methodologies to reliably quantify extracellular release of ROS. Here, we used a modified Amplex Red assay to investigate the inflammatory and microbial regulation of IEC-generated H_2O_2 and the potential role of Duox2, a NADPH oxidase that is an important source of H_2O_2. We found that colonoids respond to interferon-γ and flagellin by enhancing production of H_2O_2 in a Duox2-mediated fashion. To extend these findings, we analyzed *ex vivo* production of H_2O_2 by IECs after acute and chronic inflammation, as well as after exposure to dysbiotic microbiota. While acute inflammation did not induce a significant increase in epithelial-driven H_2O_2, chronic inflammation caused IECs to release higher levels of H_2O_2. Furthermore, colonization of germ-free mice with dysbiotic microbiota from mice or patients with IBD resulted in increased H_2O_2 production compared with healthy controls. Collectively, these data suggest that IECs are capable of H_2O_2 production during chronic inflammation and dysbiotic states. Our results provide insight into luminal production of H_2O_2 by IECs as a read-out of innate defense by the mucosa.

Keywords: colitis, intestinal inflammation, inflammatory bowel disease, microbiome, host-microbe interactions

INTRODUCTION

The gut epithelial barrier consists of a single layer of IECs that separates the largest compartment of the host's immune system from an environment with a high microbial and antigenic load (Mowat and Agace, 2014; Sender et al., 2016). This epithelial monolayer acts as a physical, chemical, and immune barrier, minimizing the contact between the host and the microbiota and therefore maintaining homeostasis. While epithelial-dependent immune functions, such as the secretion of mucus, the production of antimicrobial peptides, and the transportation of immunoglobulin A, have been widely investigated, the functions of IEC-generated ROS as signaling intermediates in host defense are still not well understood due to the lack of reliable methodologies to measure extracellular release of ROS.

Reactive oxygen species are reduced metabolites of oxygen that can oxidize other molecules and have microbicidal or signaling functions depending on their concentration in the microenvironment (Mittal et al., 2014). High levels of ROS produced by neutrophils and other phagocytes play important microbicidal functions during an oxidative burst. Under such conditions, ROS are likely to act as microbicidal agents in conjunction with MPO, which uses H$_2$O$_2$ to oxidize chloride forming the antimicrobial hypochlorous acid (Klebanoff et al., 2013). On the other hand, in steady-state conditions, low amounts of ROS released by non-phagocytic cells activate both host and microbial signaling pathways by altering the phosphotyrosine signaling network and inducing certain transcription factors (Holmstrom and Finkel, 2014). ROS are generated either as byproducts of mitochondrial oxidative phosphorylation or through NADPH oxidases, including Nox 1 through 5 as well as Duox 1 and 2 (Mittal et al., 2014; Aviello and Knaus, 2017). In the gut epithelium, the two major NADPH oxidases are Nox1 and Duox2 (Grasberger et al., 2015; Aviello and Knaus, 2018). Duox2 generates H$_2$O$_2$, whereas Nox1 produces superoxide (O$_2^-$), which can in turn be converted into H$_2$O$_2$ by superoxide dismutase (Dikalov and Harrison, 2014). Given its stability and diffusibility, H$_2$O$_2$ produced by epithelial NADPH oxidases can diffuse to the extracellular milieu and act as a messenger to communicate with neighboring host and microbial cells (Aviello and Knaus, 2017). Indeed, IEC-generated ROS participate in mucosal healing processes by inactivating diverse phosphatases that regulate cell migration (Swanson et al., 2011; Leoni et al., 2013; Moll et al., 2018). Furthermore, ROS interact with microbes, modifying bacterial proteins involved in signal transduction, virulence, motility, and invasiveness, ultimately restraining colonization of the mucosa (Botteaux et al., 2009; Corcionivoschi et al., 2012; Grasberger et al., 2013; Hayes et al., 2015).

Inflammatory bowel diseases are characterized by dysbiosis, disproportionate immune responses against the microbiota, and high levels of ROS (McKenzie et al., 1996; Gitter et al., 2001; Hussain et al., 2003; Itzkowitz and Yio, 2004; Tamboli et al., 2004; Luceri et al., 2019). Even though the high oxidative stress in IBD patients is likely due to the oxidative burst of infiltrating neutrophils, epithelial Nox1 and Duox2 are overexpressed in IBD patient biopsies (MacFie et al., 2014; Chu et al., 2017).

Furthermore, Duox2 is an early upregulated gene in very early onset (VEO) IBD and loss of function mutations in both Nox1 and Duox2 have been associated with such disease (Haberman et al., 2014; Hayes et al., 2015; Parlato et al., 2017). Although it is still unclear whether the upregulation of epithelial NADPH oxidases in IBD perpetuates inflammation, some models have proposed a role for Nox1 and Duox2 in facilitating dysbiosis by providing anaerobic substrates for facultative anaerobes to bloom (Winter et al., 2013; Zhu et al., 2019). However, the fact that Duox2 is upregulated after humanization of germ-free mice with human dysbiotic microflora and prevents microbes from invading the mucosa suggests that epithelial ROS may be necessary to control dysbiosis and promote epithelial repair (Grasberger et al., 2013, 2015).

Given that ROS mediate the communication between the epithelial barrier and the mucosa-associated microbiota and have also been associated with dysbiosis and inflammation, we sought to characterize the extracellular release of H$_2$O$_2$ by IECs in these settings. To this end, we measured the oxidation of 10-Acetyl-3,7-dihydroxyphenoxazine (Amplex Red) into resorufin in the presence of HRP and H$_2$O$_2$ in IECs. This method, which is highly sensitive, allowed for real time measurement of H$_2$O$_2$ produced by IEC in the nanomolar range (Zhou et al., 1997). To overcome the technical difficulties posed by carboxylesterases, which are expressed in IECs and oxidize Amplex Red (AR) in an HRP-independent way, we supplemented our reaction buffers with the serine protease inhibitor PMSF, as previously described in other cell types from liver and kidney (Miwa et al., 2016). Here, we demonstrate that upon inflammatory and microbial challenge, primary IECs in culture release H$_2$O$_2$ to the extracellular milieu in a Duox2-mediated mechanism. Furthermore, we report that freshly isolated IECs synthesize H$_2$O$_2$ in response to chronic inflammation and dysbiosis. Our findings support a key role for Duox2 in mediating mucosal responses to dysbiosis.

MATERIALS AND METHODS

Human Tissue and Stool Acquisition

The acquisition and use of human data, biopsies, and stool samples were approved by the University of Miami, Miller School of Medicine Institutional Review Board. At the time the patient samples were collected, a complete history and assessment of disease was completed (**Supplementary Table 1**). Colonoscopic biopsies were obtained from 6 non-inflamed IBD patients and processed the same day for organoid culture. Stool from IBD patients in remission and HS was aliquoted in an anaerobic chamber (Coy) the same day of collection and stored in −80°C.

Animals

C57Bl/6 and Nox1 total knock-out (Nox1-KO; Nox1^{TM1Kkr}) mice were purchased from Jackson Laboratory. Epithelial DuoxA1/A2-KO mice, which are functionally deficient in Duox1 and Duox2, were obtained by crossing the DuoxA1/A2-floxed mice generated at Dr. Kaunitz's laboratory (UCLA) with villin-cre (Tg(Vil1-cre)997Gum) mice purchased from Jackson Laboratory. Even though these mice are double knock-out for Duox

isoenzymes, they are widely accepted as a model to investigate the role of Duox2 in the colon given that the expression of Duox1 in the gut is exceedingly low (Grasberger et al., 2015; Aviello and Knaus, 2018; van der Vliet et al., 2018). Villin-TLR4 mice, which express a transgene that renders TLR4 constitutively active under the villin promoter, were generated as previously described (Shang et al., 2008). Germ-free adult C57Bl/6 mice were bred and housed at the University of Miami Gnotobiotic Facility in Class Biologically Clean flexible film isolators and transferred to Biocontainment Unit (BCU) cage system after microbial transfer. All mice were generated on a C57Bl/6 background, housed in either specific pathogen-free or germ-free conditions with a controlled temperature of 20 ± 2°C, and allowed free access to food and water, either regular or autoclaved for specific pathogen-free and germ-free mice, respectively. All experiments were performed with the approval of the Institutional Animal Care and Use Committee (IACUC) at the University of Miami (Protocols 17-196 and 18-169). The University of Miami is internationally accredited by the Association for Assessment and Accreditation of Laboratory Animal Care (AAALAC).

Experimental Design, Colitis Induction, and Collection Samples

Mice between 8 to 16 weeks of age, of both sexes, were randomly assigned cages and then adapted for at least 5 days prior to starting experiments. In order to induce colitis, 3% of DSS (40-50 kDa; Affymetrix/USB, ThermoFisher Scientific) was added to the drinking water for either 2, 4, or 6 consecutive days and replaced every other day. To minimize variability in our determinations, all mice were euthanized on the same day (**Figure 3B**). The AOM-DSS model of colitis-associated cancer (CAC) was utilized in order to investigate chronic inflammation and tumorigenesis. AOM (7.4 mg/kg; Sigma-Aldrich) was injected intraperitoneally 1 week before beginning a 5-day cycle of 3% DSS. After the first cycle of DSS, the mice were allowed to recover for 2 weeks before subsequently starting a second 5-day cycle of 3% DSS. Mice were euthanized on day 56 (**Figure 3E**). The weight loss for each mouse was assessed daily during the DSS cycles and the first week of recovery for the CAC model as previously described to evaluate the severity of colitis. Mice losing more than 30% of initial body weight or displaying severe bloody diarrhea with lack of exploratory behavior were immediately euthanized. No animals died or met the endpoint criteria prior to the end of the study.

Mice were euthanized by cervical dislocation under isoflurane (Piramal Critical Care) anesthesia. Subsequently, the colon was removed, flushed, cut along the mesenteric border, and pinned flat on a Sylgard TM-coated Petri dish. One longitudinal section of the colon was prepared for histology by rolling it into a Swiss roll and fixing it in 4% paraformaldehyde. The rest of the colon was utilized for either IEC isolation, MPO determination, or preparation of mucosa-associated microbiota homogenates.

Microbial Engraftment

Mucosa-associated microbiota homogenates were prepared from C57Bl/6J or villin-TLR4 mice by homogenizing flushed colons in Hank's balanced salt solution (HBSS) using a BeadBlasterTM24 (Benchmark) in a vinyl anaerobic chamber (Coy). One mL of HBSS was used for every 50 mg of colon. To prepare the human stool samples, frozen stool was mixed with sterile HBSS (1:10 ratio of stool weight:HBSS) and filtered with a 40 μm strainer in an anaerobic chamber. GF mice were then orally gavaged with 200 uL of either the resulting mucosa-associated microbiota or stool slurry and housed in separate iso-cages depending on the donor microbiome (C57Bl/6J vs. vilin-TLR4; HS vs. IBD). After a 3-week engraftment (**Figures 4A**, **5A**), mice were euthanized as indicated above. The colon of these mice was used for same histopathological, enzymatic, and transcriptomic determinations.

DNA Extraction and 16S Sequencing

Total bacterial DNA was extracted, quantified, and sequenced at the University of Minnesota Genomic Center (UMGC) as previously described (Gohl et al., 2016). Briefly, DNA was extracted using PowerSoil/fecal DNA Isolation Kit (MoBio Laboratories) and the 16S-V4 region was amplified using Meta_V4_515F and Meta_V4_806R primers, and KAPAHiFidelity Hot Start Polymerase PCR. After a first amplification, the products were diluted 1:100, 5 uL of which were used for the second round of amplification. Various different combinations of forward and reverse indexing primers were used for the second PCR. For sequencing, pooled samples were denatured with NaOH, diluted to 8 pM in Illumina's HT1 buffer, spiked with 15% PhiX, and denatured at 96°C for 2 min. A MiSeq600 cycle v3 kit was used to sequence the DNA, and Nextera adapter sequences were used for post-run trimming.

Microbiome Data Analysis

The paired-end sequences were obtained as forward and reverse demultiplexed fastq files from the Illumina MiSeq. CosmosID bioinformatics software package (CosmosID Inc.) was used to identify bacterial species, quantify the relative abundance, calculate alpha diversity, and generate a principal component analysis. Briefly, CosmosID pipeline uses a high-performance data-mining k-mer algorithm that rapidly disambiguates millions of short sequencing reads into the discrete genomes engendering the particular sequences. This pipeline has two separable comparators that include a pre-computation phase that matches a k-mer to a uniquely identified reference database and a per-sample computation that statistically scores the entire read to verify the identification and to avoid false positive identifications. For the pre-computation phase, the input is microbial genome databases, and the output is phylogeny trees and variable length k-mer fingerprints (biomarkers) that uniquely identify nodes generating branches and leaves of the tree. While the second per-sample computation phase searches 100s of millions of short sequence reads or contigs from a draft assembly against fingerprint sets. Finally, to obtain fine-grain taxonomic and relative abundance estimates for the microbial datasets, the resulting statistics are analyzed.

Isolation of IECs and Colonoid Preparation

In order to isolate IECs, the murine colonic sections and human biopsies were shaken at 150 rpm for 45 min at room temperature in a chelation buffer prepared with 10 mM EDTA in HBSS. The residual EDTA was then gently washed with HBSS, and the crypts were released by gentle agitation for 30 min. The remaining longitudinal tissue was removed and snap frozen for future MPO experiments. The released crypts were either used to generate colonoids, utilized for the direct measurement of H_2O_2, or lysed in Trizol (ThermoFisher) for qPCR. To generate colonoids, the IECs were pelleted and resuspended in ice-cold Cultrex reduced growth factor basement membrane, type R1 (R&D systems). For 2 days, mouse colonoids were grown in 50% conditioned medium containing wnt3a, R-spondin-3, noggin, and 20% fetal bovine serum (WRNC medium) (Miyoshi and Stappenbeck, 2013) supplemented with 5 μM Chir99021 (Cayman Chemical), 2.5 μM Thiazovivin (Cayman Chemical), and 100 μg/mL Primocin (Invivogen). Human colonoids were grown in a mixture of Human Intesticult Organoid Growth Medium (STEMCELL Technologies) and WRNC medium (1:3 ratio) and supplemented with 5 μM Chir99021, 2.5 μM Thiazovivin, 0.5 μM A83-01 (Cayman Chemical), 10 μM SB202190 (Cayman Chemical), 100 μg/mL Primocin, and 1x gentamicin-amphotericin B (ThermoFisher). After 2 days, colonoids were switched to a growth factor-restricted, less reactive medium containing DMEM/F12, 10% R-spondin-2 (Bell et al., 2008) and 10% noggin-conditioned media (Heijmans et al., 2014), 10% fetal bovine serum, mouse epidermal growth factor (50 ng/mL; Life Technologies), Primocin (100 μg/mL) and Chir00921 (5 μM) (RENC medium). Colonoids stimulated on day 6 for 24 h with or without 100 ng/mL interferon (IFN)γ (Biolegend) or 100 ng/mL ultrapure *Salmonella typhimurium* flagellin (Invivogen) in RENC were utilized for H_2O_2 measurement.

Real-Time Measurement of Hydrogen Peroxide Production

Intestinal epithelial cells or colonoids seeded in 96 well plates were incubated in Dulbecco's PBS (DPBS) solution containing $Ca2^+$, $Mg2^+$, 0.1 U/mL HRP (Sigma Aldrich), 30 μM 10-Acetyl-3,7-dihydroxyphenoxazine (Biotium), and 100 μM PMSF (Sigma-Aldrich). The real-time formation of fluorescent resorufin (Ex 530 nm/Em 590 nm) was read at 60 s intervals for 10 min at 37°C in a Synergy H1 fluorometer (BioTek). In order to assess the amount of H_2O_2 produced by NADPH oxidases, DMSO (vehicle; EMD Millipore) or 10 μM of the NADPH oxidases inhibitor DPI (Cayman Chemical) were added after the first 10 min of kinetic reading. The reaction was then run for another 20 min at 60 s intervals. Immediately after H_2O_2 measurement, MTT (ATCC) assay was performed (per manufacturer's instructions) to normalize H_2O_2 production to the amount of viable cells. All samples were assayed in triplicates. The amount of H_2O_2 was determined using a standard curve of H_2O_2 prepared fresh for each experiment. Data are expressed as the rate of H_2O_2 release over the last 8 min for non-DPI experiments or 18 min for experiments using DPI.

Myeloperoxidase Activity

Snap-frozen longitudinal colon sections were homogenized in 50 mM phosphate buffer containing 13.7 mM of hexadecyltrimethylammonium bromide (Sigma Aldrich) by means of a GentleMACS dissociator (Miltenyi Biotec). MPO activity of the supernatants was determined by measuring their ability to oxidize *o*-dianisidine (Sigma Aldrich) in the presence of H_2O_2 and interpolating their values to those of a known MPO standard. The MPO activity was finally normalized to the initial weight of each sample.

Quantitative PCR Analysis

RNA from colonoids or IECs lysed in Trizol was isolated using phenol-chloroform extraction (Chomczynski and Sacchi, 1987). 50 and 500 ng RNA, respectively, were retrotranscribed using PrimeScript RT reagent Kit (Takara Bio Inc.), and the resulting cDNA was amplified on a LightCycler 480 II instrument (Roche Applied Science) in the presence of selected primers (**Supplementary Table 2**) using the SYBR Premix Ex Taq (Takara). mRNA expression levels were calculated by means of the $\Delta\Delta Ct$ method (Livak and Schmittgen, 2001) and normalized to the geometric mean of the housekeeping genes β-actin and glucuronidase-β.

Statistical Analysis

Results are presented as mean values and standard deviation (SD). Except for the microbiome data, all of the other data analysis and plots were performed using Prism8 (GraphPad Software, Inc.) and compared using Student's *t*-test, one-way ANOVA, or two-way ANOVA, as indicated. For the microbiome analysis, MicrobiomeAnalyst was used to perform non-parametric multivariate ANOVA (PEMANOVA) to assess the statistical significance of the principal component analysis (Dhariwal et al., 2017). A *P* value of < 0.05 was considered to be significant. All datasets can be found in **Supplementary Data Sheet 1**.

RESULTS

Accurate Measurement of Epithelial H_2O_2 Release Requires the Inhibition of Carboxylesterases

Cultured cells and tissues, such as liver and kidney, contain carboxylesterases that oxidize AR to resorufin even in the absence of HRP (Miwa et al., 2016). Given that IECs express carboxylesterases (Jones et al., 2013), we first sought to determine whether these enzymes impact the oxidation of AR distorting the measurement of epithelial-released H_2O_2. In order to inhibit carboxylesterase-mediated oxidation, freshly isolated IECs from mouse colon were incubated with PMSF and used to determine the formation of resorufin. In the absence of PMSF, colonic IECs induced a high rate of oxidation of AR that was significantly reduced upon addition of PMSF to the reaction buffer (untreated = 149.5 (SD 32.9) vs. PMSF = 9.44 (SD 3.5) pmol/min/MTT unit, *P* < 0.0001; **Figures 1A,B**),

FIGURE 1 | Carboxylesterase activity can obscure measurement of H_2O_2 released by IECs. IECs were assayed for their ability to oxidize AR in the presence or absence of PMSF *ex vivo* and *in vitro*. **(A)** Representative experiment showing real-time oxidation kinetics of AR in freshly isolated IECs with or without PMSF. Samples were run in triplicate. RFU, relative fluorescence units. **(B)** AR oxidation rate by freshly isolated IECs in the presence or absence of PMSF. PMSF vs. untreated, ***$P < 0.001$ as determined by two-tailed Student's *t*-test ($n = 6$–8 mice). **(C)** Real-time oxidation kinetics of AR in cultured colonoids. **(D)** AR oxidation rate by cultured colonoids in response to inflammatory and microbial stimuli in the presence or absence of PMSF. IFNγ vs. control, **$P < 0.01$; Flagellin vs. control, *$P < 0.05$ as determined by one-way ANOVA followed by Dunnett's *post hoc* test ($n = 6$ colonoid cultures). Two-way ANOVA additionally identified a significant overall effect for PMSF, $P < 0.001$ ($n = 4$–6 colonoid cultures).

demonstrating that carboxylesterases affect the quantification of H_2O_2 production when using this method. Indeed, the high rate of oxidation of AR in the absence of PMSF was in fact HRP-independent, as similar rate values were obtained without the addition of HRP (data not shown). This was also seen in IECs from other sections of the gastrointestinal tract, including the duodenum, jejunum, and ileum, indicating that the distortion of H_2O_2 measurements by carboxylesterases is not only limited to the colon (**Supplementary Figure 1A**). Indeed, we found that inhibition of carboxylesterases revealed significant differences in the production of ROS between duodenum, jejunum, and colon (**Supplementary Figure 1A**).

To determine whether carboxylesterases also obscure differences in H_2O_2 production upon microbial and inflammatory challenge *in vitro*, we treated organoid cultures from mouse colonic IECs (colonoids) with IFNγ and flagellin, and measured oxidation of AR with or without PMSF. Similar to freshly isolated IECs, untreated colonoids caused a high oxidation of AR in the absence of PMSF

that was dramatically reduced with the addition of PMSF (**Figure 1C**). Moreover, inhibition of carboxylesterase activity with PMSF revealed that mouse colonic IECs respond to stimulation with IFNγ and flagellin by releasing H_2O_2 to the extracellular milieu (ctrl = 6.3 (SD 2.3) vs. IFNγ = 18.08 (SD 4.8) vs. flagellin = 15.19 (SD 5.6) pmol/min/MTT unit; $P < 0.01$ for IFNγ and $P < 0.05$ for flagellin; **Figure 1D**). These differences were not observed in colonoids incubated without PMSF (**Figure 1D**). We additionally characterized the basal production of H_2O_2 in human colonoids isolated from biopsies of IBD patients in remission and in human epithelial cell lines. While incubation of PMSF was necessary to quantify the actual production of H_2O_2 in steady-state conditions in human colonoids, human IEC lines HT-29 and SW480 did not require neutralization of carboxylesterase activity (**Supplementary Figures 1B,C**). Human colonoids were also assayed for their responses to IFNγ and flagellin. Whereas we did not observe a consistent increase in H_2O_2 upon stimulation with IFNγ, flagellin did cause a higher

production of epithelial H_2O_2 (ctrl = 7.57 (SD 4.08) vs. flagellin = 11.66 (SD 5.91) pmol/min/MMT unit; $P < 0.05$; **Supplementary Figure 1D**), demonstrating that human colonoids also respond to microbial stimuli by producing ROS. Taken together, these results suggest that the presence of carboxylesterases in primary IECs masks the actual release of ROS in steady-state and in response to microbial and proinflammatory stimuli.

Duox2 Mediates Epithelial H_2O_2 Production in Response to Proinflammatory and Bacterial Stimuli
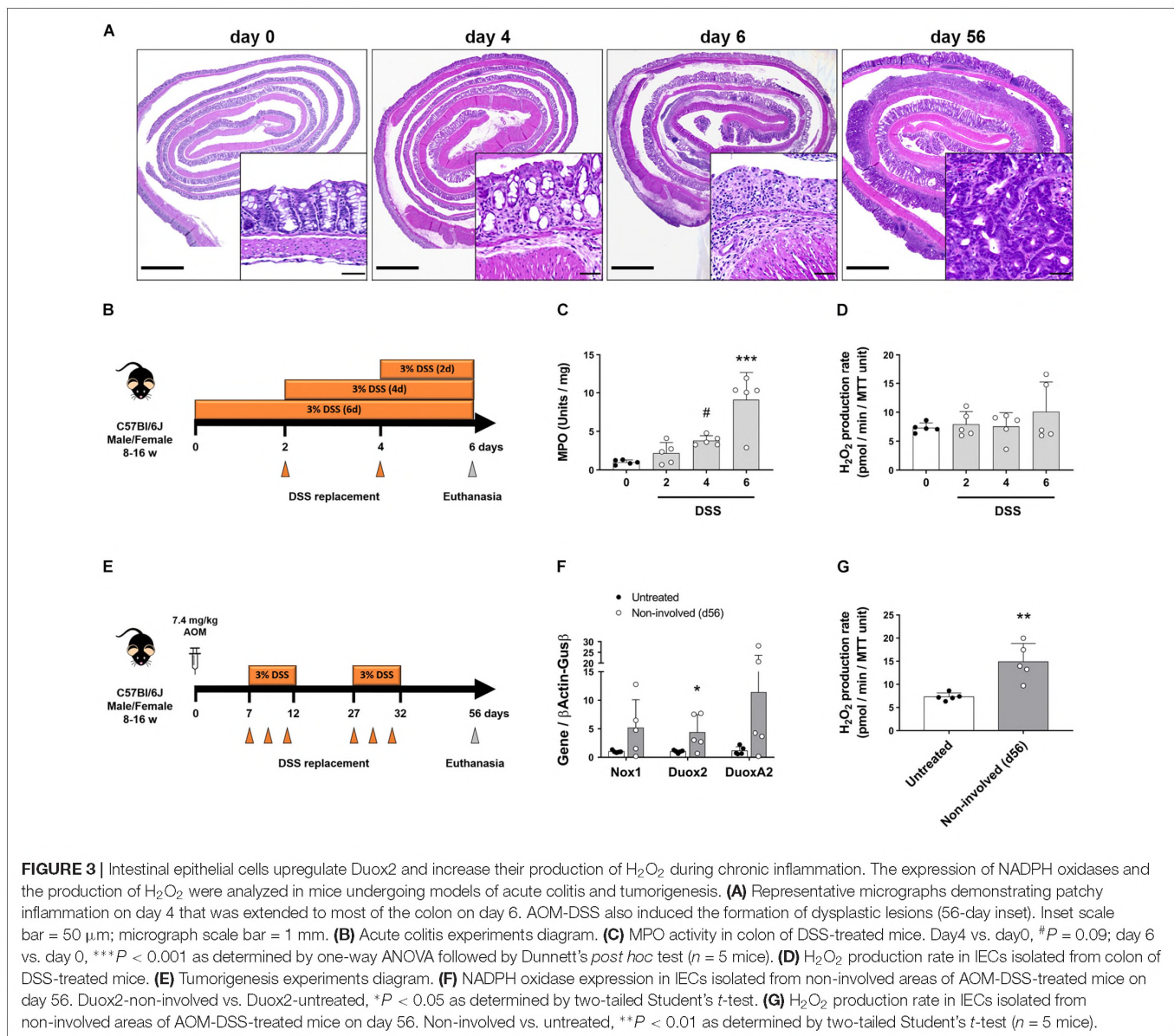
Previous work has demonstrated that human airway epithelial cells produce H_2O_2 in response to IFNγ and flagellin in a NADPH oxidase-dependent manner (Gattas et al., 2009). Furthermore, increased mucosal abundance of Enterobacteriaceae in the gut has been associated with

a higher expression of the NADPH oxidases Duox2 and DuoxA2 (Grasberger et al., 2015). Given that many species of enterobacteria are flagellated, we asked whether the structural component of flagella, flagellin, and IFNγ induced these enzymes in IECs to produce H_2O_2 and whether our modified assay could accurately quantify the resulting H_2O_2 production. Colonoids in culture were incubated overnight with IFNγ or flagellin, and the conversion of AR to resorufin was measured in the presence of PMSF. To test the dependence of H_2O_2 production on NADPH oxidases, we added the inhibitor DPI to colonoid cultures. Our results demonstrate that incubation with IFNγ and flagellin elicited an increase in the production of H_2O_2 in colonoids that was totally inhibited by treatment with DPI but not by its vehicle, DMSO (**Figures 2A–C**). These results suggest that colonoids respond to proinflammatory stimuli and bacterial motifs by producing ROS in a NADPH oxidase-mediated fashion. Furthermore, these results validate the specificity of this modified AR assay in measuring IEC-released H_2O_2.
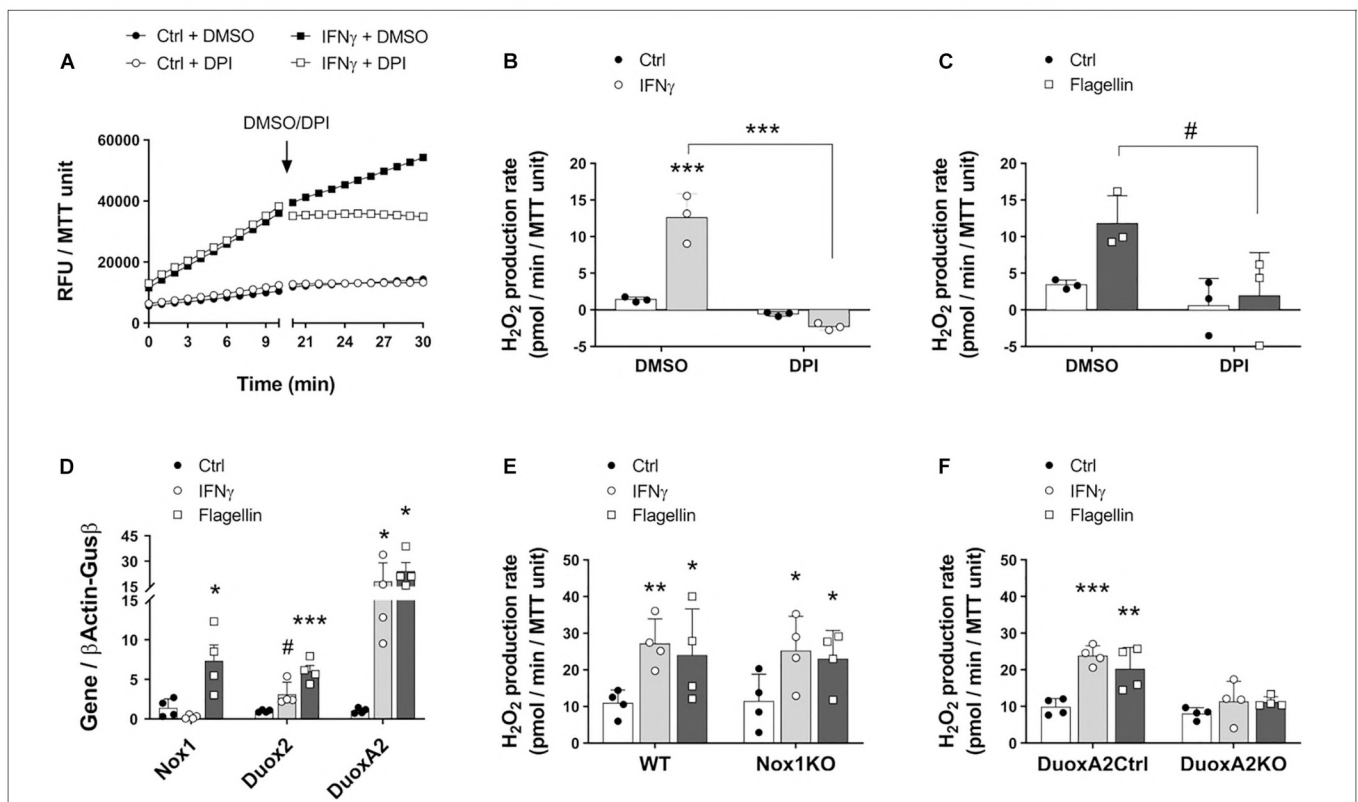
FIGURE 2 | Intestinal epithelial cells in culture respond to inflammatory and microbial stimuli by inducing the synthesis of H_2O_2 via Duox2. The involvement of NADPH oxidases Nox1 and Duox2 in epithelial responses to IFNγ and flagellin was determined in cultured colonoids. **(A)** Representative experiment showing real-time production of H_2O_2 in response to IFNγ before and after the addition of the NADPH oxidase inhibitor DPI or its vehicle, DMSO. **(B)** H_2O_2 production rate in response to IFNγ and in the presence of DPI/DMSO. IFNγ-DMSO vs. IFNγ-DPI, ***$P < 0.001$ as determined by two-way ANOVA followed by Tukey's *post hoc* test ($n = 3$ colonoid cultures). **(C)** H_2O_2 production rate in response to flagellin and in the presence of DPI/DMSO. Flagellin-DMSO vs. Flagellin-DPI, #$P = 0.063$ as determined by two-way ANOVA followed by Tukey's *post hoc* test ($n = 3$ colonoid cultures). **(D)** NADPH oxidase expression in cultured IECs stimulated with IFNγ or flagellin. Nox1-flagellin vs. Nox1-control, *$P < 0.05$; Duox2-IFNγ vs. Duox2-control, #$P = 0.085$; Duox2-flagellin vs. Duox2-control, ***$P < 0.001$; DuoxA2-IFNγ vs. DuoxA2-control, *$P < 0.05$; DuoxA2-flagellin vs. DuoxA2-control, *$P < 0.05$ as determined by two-way ANOVA followed by Tukey's *post hoc* test ($n = 4$ colonoid cultures). **(E)** Nox1 involvement in IEC responses to IFNγ and flagellin. WT-IFNγ vs. WT-control, **$P < 0.01$; WT-flagellin vs. WT-control, *$P < 0.05$; Nox1-KO-IFNγ vs. Nox1-KO-control, *$P < 0.05$; Nox1-KO-flagellin vs. Nox1-KO-control, *$P < 0.05$ as determined by two-way ANOVA followed by Tukey's *post hoc* test ($n = 4$ colonoid cultures). **(F)** Duox2 involvement in IEC responses to IFNγ and flagellin. DuoxA2 control-IFNγ vs. DuoxA2 control-control, ***$P < 0.001$; DuoxA2 control-flagellin vs. DuoxA2 control-control, **$P < 0.01$ as determined by two-way ANOVA followed by Tukey's *post hoc* test ($n = 4$ colonoid cultures).

FIGURE 3 | Intestinal epithelial cells upregulate Duox2 and increase their production of H$_2$O$_2$ during chronic inflammation. The expression of NADPH oxidases and the production of H$_2$O$_2$ were analyzed in mice undergoing models of acute colitis and tumorigenesis. **(A)** Representative micrographs demonstrating patchy inflammation on day 4 that was extended to most of the colon on day 6. AOM-DSS also induced the formation of dysplastic lesions (56-day inset). Inset scale bar = 50 μm; micrograph scale bar = 1 mm. **(B)** Acute colitis experiments diagram. **(C)** MPO activity in colon of DSS-treated mice. Day4 vs. day0, #P = 0.09; day 6 vs. day 0, ***P < 0.001 as determined by one-way ANOVA followed by Dunnett's *post hoc* test (n = 5 mice). **(D)** H$_2$O$_2$ production rate in IECs isolated from colon of DSS-treated mice. **(E)** Tumorigenesis experiments diagram. **(F)** NADPH oxidase expression in IECs isolated from non-involved areas of AOM-DSS-treated mice on day 56. Duox2-non-involved vs. Duox2-untreated, *P < 0.05 as determined by two-tailed Student's *t*-test. **(G)** H$_2$O$_2$ production rate in IECs isolated from non-involved areas of AOM-DSS-treated mice on day 56. Non-involved vs. untreated, **P < 0.01 as determined by two-tailed Student's *t*-test (n = 5 mice).

Nox1 and Duox2 are the two main inducible NADPH oxidases in the intestinal epithelium (Grasberger et al., 2015; Aviello and Knaus, 2018). To interrogate whether these enzymes are associated with the redox responses that we observed toward IFNγ and flagellin, we stimulated wild type colonoids with these molecules and analyzed the expression of Nox1, Duox2, and the Duox2 maturation factor DuoxA2. Stimulation with the proinflammatory cytokine IFNγ slightly upregulated Duox2 (ctrl = 1.01 (SD 0.16) vs. IFNγ = 3.12 (SD 0.76) folds, P = 0.085) and significantly increased the expression of DuoxA2 transcripts (ctrl = 1.04 (SD 0.34) vs. IFNγ = 18.15 (SD 10.83) folds, P < 0.05; **Figure 2D**). Moreover, the bacterial ligand flagellin significantly upregulated Nox1 (ctrl = 1.4 (SD 1.14) vs. flagellin = 7.34 (SD 2.01) folds, P < 0.05), Duox2 (ctrl = 1.01 (SD 0.16) vs. flagellin = 6.04 (SD 1.46) folds, P < 0.001) and DuoxA2 (ctrl = 1.04 (SD 0.34) vs. flagellin = 24.13 (SD

10.07) folds, P < 0.05; **Figure 2D**). These findings suggest that both Nox1 and Duox2 might participate in enhancing the release of epithelial H$_2$O$_2$ upon proinflammatory challenges. To further determine whether Nox1 and Duox2 drive these responses, we prepared colonoids from Nox1-KO mice, epithelial DuoxA2-KO mice and their corresponding wild type littermates and incubated them with IFNγ or flagellin. We observed that Nox1- and Duox2-deficient colonoids displayed a similar basal production of H$_2$O$_2$ compared to their matched control colonoids. However, while Nox1-KO colonoids responded to IFNγ and flagellin by significantly increasing H$_2$O$_2$ production (ctrl = 11.41 (SD 7.43) vs. IFNγ = 25.13 (SD 9.49) vs. flagellin = 22.92 (SD 7.85) pmol/min/MTT unit, P < 0.05 for both molecules; **Figure 2E**), DuoxA2-KO colonoids failed to respond to these stimuli (ctrl = 8.08 (SD 1.56) vs. IFNγ = 11.35 (SD 5.49) vs. flagellin = 11.19 (SD 1.45) pmol/min/MTT unit;

FIGURE 4 | Dysbiosis induces upregulation of Duox2 and enhances the epithelial release of H_2O_2. Germ-free mice were colonized with the mucosa-associated microbiota of WT or dysbiotic (villin-TLR4) mice and their epithelial responses were analyzed after a 3-week engraftment. **(A)** Engraftment experiments diagram. **(B)** Representative micrographs showing no signs of inflammation and no major morphological differences between WT- and dysbiotic-microbiota recipient mice. Inset scale bar = 50 μm; micrograph scale bar = 1 mm. **(C)** MPO activity in colon from engrafted mice. **(D)** NADPH oxidase expression in IECs isolated from engrafted mice. Duox2-dysbiotic vs. Duox2-WT, $*P < 0.05$ as determined by two-tailed Student's t-test ($n = 3$ mice). **(E)** H_2O_2 production rate in IECs isolated from engrafted mice. Dysbiotic vs. WT, $**P < 0.01$ as determined by two-tailed Student's t-test ($n = 3$ mice).
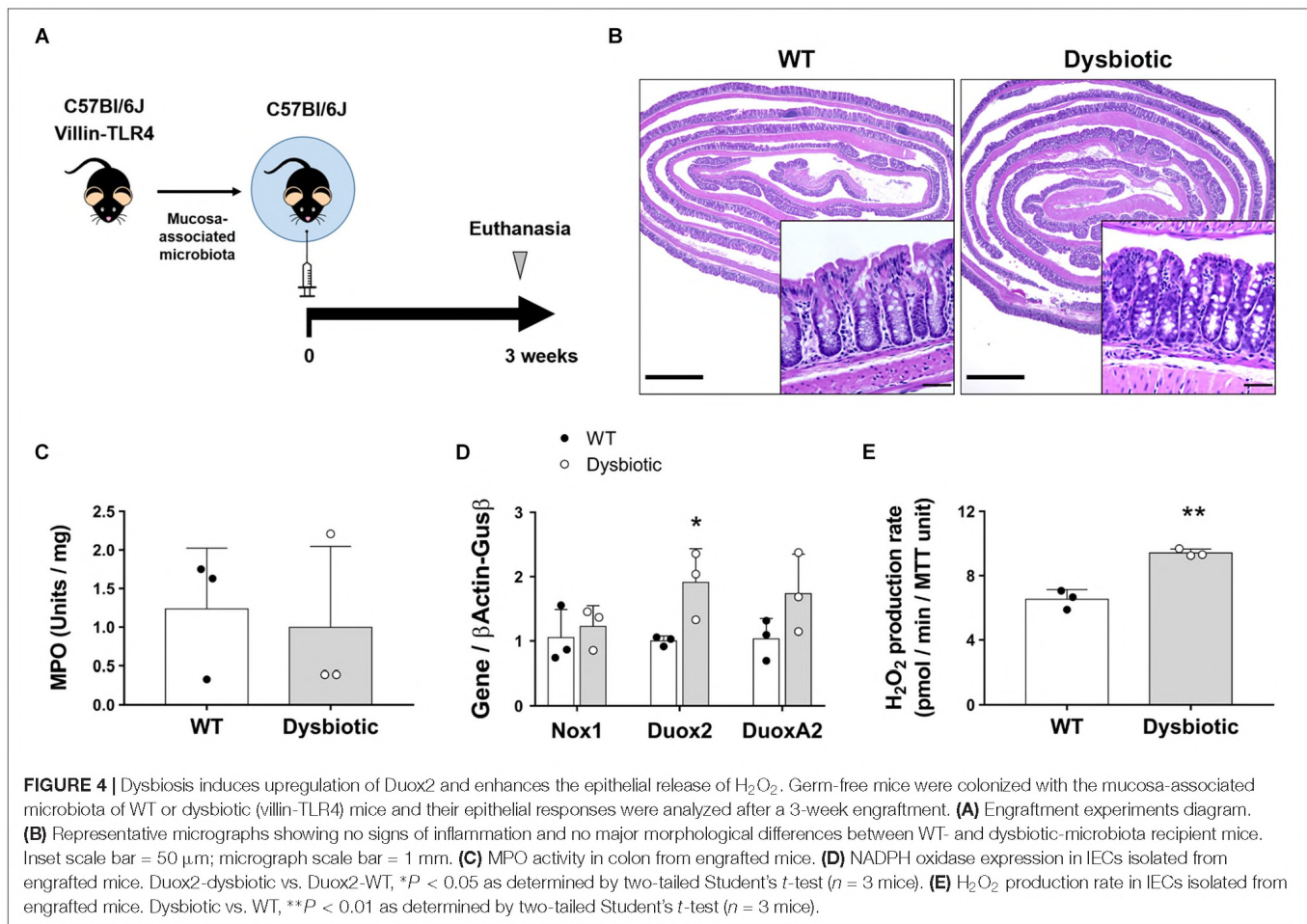
Figure 2F). These results demonstrate that the increase in the epithelial production of ROS in response to proinflammatory and microbial stimuli is mediated by Duox2.
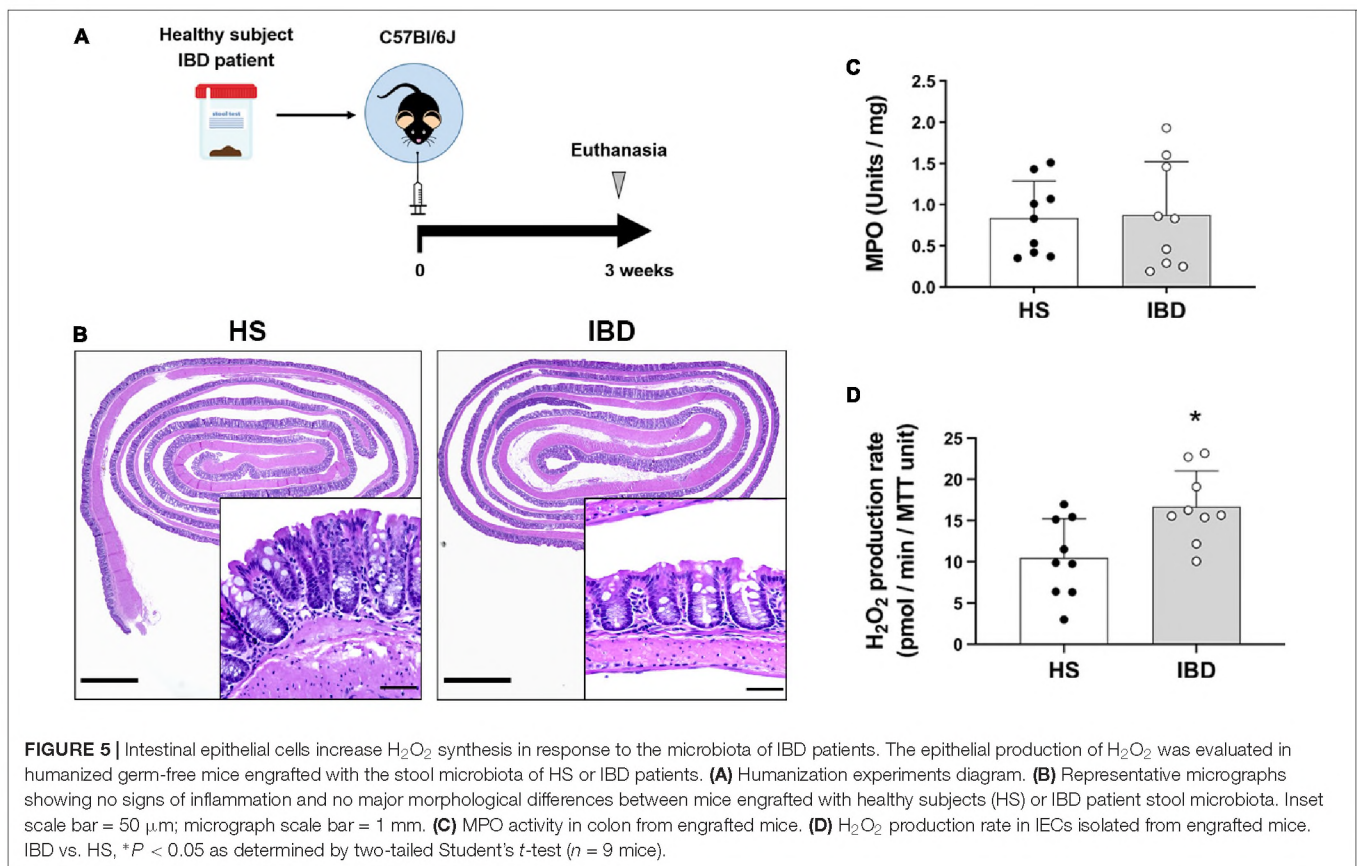
Chronic but Not Acute Inflammation Results in Intestinal Epithelial Production of H_2O_2

Various studies have implicated Duox2 in intestinal inflammation and as an early signal in VEO-IBD (Haberman et al., 2015; Sommer and Backhed, 2015). However, the functional consequences of Duox2 overexpression has not been addressed. To determine whether increased epithelial-driven H_2O_2 production is an early event in intestinal inflammation, we treated mice for various lengths of time with DSS and interrogated the timing of H_2O_2 release in response to inflammation (**Figure 3B**). We confirmed that DSS induced inflammation on days 4 and 6 by histology and using an MPO assay. Histological sections on day 4 were characterized by discrete areas of crypt destruction, edema and immune cell infiltration of the mucosa and submucosa, which became extensive and involved most of the colon by day 6 (**Figure 3A**). Accordingly, while on day 4 we saw a trend of increased MPO activity, there was a significant increase in MPO on day 6 (day

0 = 1.01 (SD 0.3) vs. day 4 = 3.81 (SD 0.63) vs. day 6 = 9.1 (SD 3.54), $P = 0.089$ and $P < 0.0001$, respectively; **Figure 3C**). In spite of acute inflammation, we did not find that isolated IECs increased production of H_2O_2 (**Figure 3D**). This was corroborated by a lack of induction of NADPH oxidases at the mRNA level (**Supplementary Figures 2A–C**). These data demonstrate that the intestinal epithelium does not contribute to an oxidative environment during acute inflammation.

We next asked whether chronic inflammation or neoplasia changed the potential of IECs to release H_2O_2. To address this question, we challenged mice with AOM-DSS (**Figure 3E**) and isolated IECs from specific segments of the mucosa – either from dysplastic tumors or surrounding non-involved (non-dysplastic and non-inflamed) mucosa. Our modified AR assay measured significantly higher levels of H_2O_2 in freshly isolated IECs from polypoid tumors compared with surrounding IECs (**Supplementary Figure 2D**), corroborating previous findings that tumorigenic cells have a higher redox activity than steady-state cells (Schieber and Chandel, 2014). Following AOM-DSS, IECs isolated from non-involved areas expressed significantly higher levels of Duox2 transcripts when compared to IECs in untreated mice (untreated = 1.03 (SD 0.24) vs. non-involved = 4.35 (SD 3.13), $P < 0.05$; **Figure 3F**). This upregulation in NADPH oxidases translated into a significantly

FIGURE 5 | Intestinal epithelial cells increase H$_2$O$_2$ synthesis in response to the microbiota of IBD patients. The epithelial production of H$_2$O$_2$ was evaluated in humanized germ-free mice engrafted with the stool microbiota of HS or IBD patients. **(A)** Humanization experiments diagram. **(B)** Representative micrographs showing no signs of inflammation and no major morphological differences between mice engrafted with healthy subjects (HS) or IBD patient stool microbiota. Inset scale bar = 50 μm; micrograph scale bar = 1 mm. **(C)** MPO activity in colon from engrafted mice. **(D)** H$_2$O$_2$ production rate in IECs isolated from engrafted mice. IBD vs. HS, *P < 0.05 as determined by two-tailed Student's t-test (n = 9 mice).

increased production of H$_2$O$_2$ (untreated = 7.33 (SD 0.83) vs. non-involved = 14.89 (SD 3.97), P < 0.01; **Figure 3G**). Taken together, these data demonstrate that animal models of colitis-associated neoplasia have increased epithelial production of H$_2$O$_2$ along with increased expression of NADPH oxidases. Even though all the AOM-DSS-treated mice had higher H$_2$O$_2$ levels in IECs from non-involved areas, MPO activity was not significantly different between non-involved areas of AOM-DSS-treated and untreated mice (**Supplementary Figure 2E**). These data suggest that IECs produce H$_2$O$_2$ in the setting of chronic injury even in the absence of inflammation.

Intestinal Epithelial Cells Upregulate Duox2 and Release H$_2$O$_2$ in Response to Dysbiosis

Dysbiosis is an indirect consequence of both acute and chronic inflammation and has been shown to upregulate Duox2 (Grasberger et al., 2015; Fritsch and Abreu, 2019). However, whether this translates into a functional increase in the synthesis of ROS by IECs has not been directly demonstrated. We hypothesized that the overexpression of Duox2 during dysbiosis is associated with an increased epithelial H$_2$O$_2$ production. To investigate dysbiosis as a stimulus for H$_2$O$_2$, we used dysbiotic mucosa-associated microbiota from our transgenic villin-TLR4 mice (Shang et al., 2008; Dheer et al., 2016). We transferred mucosa-associated microbiota

from a pool of WT or villin-TLR4 donor mice to WT GF recipient mice (**Figure 4A**). After a 3-week engraftment, the microbial populations were analyzed for the stability of engraftment, and the IECs from recipient mice were analyzed for the expression of NADPH oxidases as well as H$_2$O$_2$ production. 16s rRNA sequencing of donor and recipient mucosa-associated microbiota samples revealed a stable transfer of more than 80% of the phylum, class, order, and genus-level taxa (**Supplementary Table 3**) that resulted in a similar overall clustering pattern between the donors and their corresponding recipients (**Supplementary Figure 3A**). The GF mice that received dysbiotic mucosa had a decreased Shannon alpha diversity, an indicator of dysbiosis (**Supplementary Figure 3B**). Transference of mucosa-associated microbiota did not cause inflammation, as demonstrated by the normal histology of the colon in all recipient mice (**Figure 4B**) and the low values of MPO activity (**Figure 4C**).

At a transcriptional level, we found that transfer of mucosa-associated microbiota led to similar expression levels of Nox1 in IECs regardless of donor type. Conversely, the microbiota of the dysbiotic mice elicited an increased expression of Duox2 when compared to WT microbiota in colonic IECs of recipient mice (WT recipient = 1.0 (SD 0.08) vs. dysbiotic recipient = 1.91 (SD 0.53) folds, P < 0.05; **Figure 4D**). Consistent with these findings, IECs isolated from dysbiotic microbiota-recipient mice had a higher production of H$_2$O$_2$ when compared to WT microbiota-recipient mice (WT recipient = 6.53 (SD 0.6) vs. dysbiotic

recipient $= 9.42$ (SD 0.24) pmol/min/MTT unit, $P < 0.01$; **Figure 4E**). These findings indicate that, in the absence of inflammation, IECs respond to dysbiosis by upregulating Duox2 and by subsequently inducing the production of H_2O_2.

We next asked whether engraftment of GF mice with dysbiotic human microbiota increased epithelial production of H_2O_2. We humanized GF mice with stool of either healthy subjects (HS) or IBD patients with no signs of inflammation (**Figure 5A**) and studied epithelial responses to human dysbiosis. 16s rRNA sequencing revealed that, compared to HS donors, IBD donors had a higher proportion of facultative anaerobes, particularly Proteobacteria and Actinobacteria (**Supplementary Figure 4A**). Engraftment of human microbiota did not induce inflammation, as determined by histological examination and MPO activity (**Figures 5B,C**). Previous work has shown that humanization of GF mice with the dysbiotic microbiota from IBD patients induces an increase in Duox2 expression in IECs (Grasberger et al., 2015). We found that IBD dysbiosis induced IECs to increase their production of H_2O_2 compared to HS microbiota (HS $= 10.49$ (SD 4.75) vs. IBD $= 16.68$ (SD 4.36), $P < 0.05$; **Figure 5D**). One healthy subject (HS2) with no known disease had dysbiotic microbiota with a decreased proportion of Firmicutes and an increased proportion of facultative anaerobes (Actinobacteria) that was accompanied by a higher, although not significant, production of H_2O_2 compared to the other healthy donors (HS1 $= 8.15$ (SD 6.28) vs. HS2 $= 14.63$ (SD 2.81) vs. HS3 $= 8.68$ (SD 1.99); **Supplementary Figure 4B**). Our data demonstrate that dysbiosis can lead to increased local production of H_2O_2 even in the absence of histologic or biochemical inflammation. These data suggest that dysbiosis can be a first step toward abnormal immune activation in the gut and that IECs may play an active role in this process.

DISCUSSION

To maintain gut homeostasis, IECs recognize microbial motifs and metabolites and respond by producing peptides and other molecules that interact with microbes. One form of bidirectional epithelial-microbial interaction involves the synthesis and release of ROS. However, the short half-life of these molecules and the inadequacy of common methodologies to measure epithelial H_2O_2 at low nanomolar ranges hinders the ability to study ROS as signaling intermediates. Here, we took advantage of a modified AR assay to demonstrate that, *in vitro*, inflammatory and microbial stimuli induce the epithelial release of H_2O_2 in a Duox2-dependent manner. Furthermore, we report that IECs release H_2O_2 into the extracellular milieu in animal models of chronic inflammation and dysbiosis. To our knowledge, this is the first report that shows a direct production of epithelial H_2O_2 in response to murine and IBD-driven dysbiosis, supporting the idea that epithelial ROS is a potential mechanism of host-microbe crosstalk in the intestine. Moreover, our results suggest that Duox2 plays a key role in mediating the production of H_2O_2 in response to dysbiotic microbiota and chronic inflammation.

Non-phagocytic cells, including IECs, produce ROS at low nanomolar concentrations. The only common method that

determines extracellular ROS at the nanomolar level measures the oxidation of AR into resorufin in the presence of HRP and H_2O_2 (Dikalov and Harrison, 2014). Even though this method is highly specific and sensitive, it is hindered by the presence of carboxylesterases, which oxidize AR to resorufin in an HRP- and H_2O_2-independent manner. While it is known that these esterases distort H_2O_2 determination in other cell types from liver and kidney (Miwa et al., 2016), it is not known whether they impact the measurement of H_2O_2 in IECs. Our findings demonstrate that modification of the AR assay with PMSF is necessary to quantify H_2O_2 released by primary IECs isolated from duodenum, jejunum, ileum, or colon, which are known to express several types of carboxylesterases (Jones et al., 2013). We were able to validate the specificity of H_2O_2 release by demonstrating increased production with inflammatory mediators and using a pan-NADPH oxidase inhibitor, DPI, to inhibit epithelial H_2O_2 production. In addition, the production of H_2O_2 was markedly increased in IECs isolated from tumors, which are known to have high redox activity (Schieber and Chandel, 2014). In contrast to primary IECs, the human IEC lines we tested did not require the inhibition of esterases for the measurement of H_2O_2 in steady-state conditions. This observation supports why previous studies were able to determine the H_2O_2 release of IEC lines in response to enteric bacteria without modifying the AR assay (Corcionivoschi et al., 2012; MacFie et al., 2014; Alvarez et al., 2016). However, the use of 3D primary cultures is likely to gradually displace cell lines given their increased genetic stability and their functional similarity to normal IECs *in vivo*. Our data strongly support that this modified AR assay provides a valuable tool to precisely quantify the amounts of H_2O_2 released by primary IECs, both *ex vivo* and *in vitro*. This method will contribute to improved understanding of the host-microbe interactions mediated through the release of ROS.

IECs are in constant interaction with the microbiota and *lamina propria* cells. Here, we challenged IECs *in vitro* and *in vivo* with stimuli coming from the host (IFNγ/inflammation) and the microbiota (flagellin/dysbiosis) and found a release of epithelial H_2O_2 at nanomolar concentrations. At these levels, H_2O_2 is likely to participate in host and microbial signaling transduction by altering the phosphotyrosine signaling network and inducing redox-sensitive transcription factors (Kumar et al., 1992; Xanthoudakis and Curran, 1992; Glineur et al., 2000; Leslie et al., 2003; Aviello and Knaus, 2018). For example, in the host, increased levels of H_2O_2 have been shown to either enhance inflammation (Chu et al., 2017) or mediate mucosal healing by promoting stem cell proliferation and IEC migration (Buchon et al., 2009; Leoni et al., 2013; Pircalabioru et al., 2016). In bacteria, H_2O_2 can have bacteriostatic effects and alter bacterial enzymes involved in the synthesis of virulence factors, reducing the bacterial fitness advantage (Ha et al., 2005; Corcionivoschi et al., 2012; Grasberger et al., 2013; Hayes et al., 2015; Alvarez et al., 2016). Gaining insight into the type of IEC that drives epithelial H_2O_2 and its location could potentially provide clarification of the cellular targets and downstream implications of H_2O_2. Given that Duox2 is expressed in the tips of the crypt (MacFie et al., 2014; Sommer and Backhed, 2015),

we believe that the IECs driving this dysbiosis-induced H_2O_2 production are either absorptive enterocytes or goblet cells. These are the most exposed IECs to the microbiota due to their location in the crypt. Conversely, Nox1, which is expressed in the lower two-thirds of the colon crypts, did not play a major role in mediating dysbiosis-induced H_2O_2 production (Geiszt et al., 2003; Moll et al., 2018). Therefore, Duox2-mediated ROS is probably more involved in regulating the microbiota opposed to having host inflammatory effects.

In the intestinal epithelium, Duox2 is upregulated by microbial stimuli, including dysbiotic flora and segmented filamentous bacteria (Haberman et al., 2014; Grasberger et al., 2015). Here, we demonstrate that the upregulation of NADPH oxidases in response to inflammatory and microbial stimuli translates into a Duox2-dependent epithelial increase in the production of H_2O_2. Indeed, Duox2-deficient colonoids failed to increase H_2O_2 synthesis in response to both types of stimuli. Our findings also suggest that the upregulation of Duox2 and subsequent functional increase in H_2O_2 requires chronic inflammation or chronic exposure to dysbiotic microbiota. Even though there was apparent inflammation on days 4 and 6, we did not see an increase in epithelial H_2O_2 production. By contrast, after chronic inflammation, non-involved areas without inflammation had an increase in the production of H_2O_2. Taken together, these observations suggest that there is another driver of Duox2-mediated H_2O_2 production in IECs that is not acute inflammation. Our results support that one such driver could be dysbiosis, which is a known inducer of Duox2 expression (Grasberger et al., 2015). Indeed, we saw that not only murine and IBD dysbiosis but also dysbiosis from a HS enhanced the production of epithelial H_2O_2. Since time-course studies in the DSS model of colitis have demonstrated that dysbiosis occurs later on day 8, the lack of a significant increase in H_2O_2 production during acute inflammation at day 6 would be expected if dysbiosis were the main driver (Schwab et al., 2014).

The importance of maintaining ROS in homeostasis is exemplified by the fact that IBD patients either have loss of function mutations or an upregulation of Duox2 (Haberman et al., 2014; MacFie et al., 2014; Hayes et al., 2015; Levine et al., 2016; Chu et al., 2017; Parlato et al., 2017). The fact that missense mutations in Duox2 in VEO-IBD patients results in an increased invasiveness of bacteria suggests that the upregulation of this enzyme during inflammation is an attempt to contain dysbiosis (Hayes et al., 2015). Since dysbiosis is intimately linked to IBD (Day and Lopez, 2015; Nagao-Kitamoto et al., 2016; Fritsch and Abreu, 2019; Zhu et al., 2019), it is possible that dysbiosis enhances inflammation through the induction of epithelial ROS. Inflammation subsequently exacerbates dysbiosis by providing ROS-generated substrates for facultative anaerobes to bloom

generating a feed-forward inflammatory loop. Our results provide the methodology to tease apart epithelial production of H_2O_2 and its role in a feed forward inflammatory cycle seen in IBD and IBD-associated neoplasia.

DATA AVAILABILITY STATEMENT

All datasets generated for this study are included in the article/**Supplementary Material**.

ETHICS STATEMENT

The studies involving human participants were reviewed and approved by the University of Miami, Leonard Miller M. School of Medicine, Institutional Review Board. The patients/participants provided their written informed consent to participate in this study. The animal study was reviewed and approved by the Institutional Animal Care and Use Committee (IACUC) at the University of Miami.

AUTHOR CONTRIBUTIONS

JB, JF, GC, and MA conceived the study, designed the experiments, and wrote the manuscript. JB, JF, and AS performed the experiments. IF and NB bred, genotyped, and maintained the mice colony, as well as managed the germ free facility. JP-K coordinated patient samples and data. JB and JF analyzed the data. All authors have read the manuscript and approved its contents.

FUNDING

SUPPLEMENTARY MATERIAL

The Supplementary Material for this article can be found online at: https://www.frontiersin.org/articles/10.3389/fphys.2019.01484/full#supplementary-material

REFERENCES

Alvarez, L. A., Kovacic, L., Rodriguez, J., Gosemann, J. H., Kubica, M., Pircalabioru, G. G., et al. (2016). NADPH oxidase-derived H_2O_2 subverts pathogen signaling by oxidative phosphotyrosine conversion to PB-DOPA. *Proc. Natl. Acad. Sci. U.S.A.* 113, 10406–10411. doi: 10.1073/pnas.1605443113

Aviello, G., and Knaus, U. G. (2017). ROS in gastrointestinal inflammation: rescue or sabotage? *Br. J. Pharmacol.* 174, 1704–1718. doi: 10.1111/bph.13428

Aviello, G., and Knaus, U. G. (2018). NADPH oxidases and ROS signaling in the gastrointestinal tract. *Mucosal Immunol.* 2018, 1011–1023. doi: 10.1038/s41385-018-0021-8

Bell, S. M., Schreiner, C. M., Wert, S. E., Mucenski, M. L., Scott, W. J., and Whitsett, J. A. (2008). R-spondin 2 is required for normal laryngeal-tracheal, lung and limb morphogenesis. *Development* 135, 1049–1058. doi: 10.1242/dev.013359

Botteaux, A., Hoste, C., Dumont, J. E., Van Sande, J., and Allaoui, A. (2009). Potential role of noxes in the protection of mucosae: H(2)O(2) as a bacterial repellent. *Microbes Infect.* 11, 537–544. doi: 10.1016/j.micinf.2009.02.009

Buchon, N., Broderick, N. A., Chakrabarti, S., and Lemaitre, B. (2009). Invasive and indigenous microbiota impact intestinal stem cell activity through multiple pathways in *Drosophila*. *Genes Dev.* 23, 2333–2344. doi: 10.1101/gad.1827009

Chomczynski, P., and Sacchi, N. (1987). Single-step method of RNA isolation by acid guanidinium thiocyanate-phenol-chloroform extraction. *Anal. Biochem.* 162, 156–159. doi: 10.1006/abio.1987.9999

Chu, F. F., Esworthy, R. S., Doroshow, J. H., Helmut, G., Agnes, D., Thomas, L. L., et al. (2017). Deficiency in Duox2 activity alleviates ileitis in GPx1- and GPx2-knockout mice without affecting apoptosis incidence in the crypt epithelium. *Redox Biol.* 2017, 144–156. doi: 10.1016/j.redox.2016.11.001

Corcionivoschi, N., Alvarez, L. A., Sharp, T. H., Strengert, M., Alemka, A., Mantell, J., et al. (2012). Mucosal reactive oxygen species decrease virulence by disrupting *Campylobacter jejuni* phosphotyrosine signaling. *Cell Host Microbe* 12, 47–59. doi: 10.1016/j.chom.2012.05.018

Day, A. S., and Lopez, R. N. (2015). Exclusive enteral nutrition in children with Crohn's disease. *World J. Gastroenterol.* 2015, 6809–6816. doi: 10.3748/wjg.v21.i22.6809

Dhariwal, A., Chong, J., Habib, S., King, I. L., Agellon, L. B., and Xia, J. (2017). Microbiomeanalyst: a web-based tool for comprehensive statistical, visual and meta-analysis of microbiome data. *Nucleic Acids Res.* 45, W180–W188. doi: 10.1093/nar/gkx295

Dheer, R., Santaolalla, R., Davies, J. M., Lang, J. K., Phillips, M. C., Pastorini, C., et al. (2016). Intestinal epithelial toll-like receptor 4 signaling affects epithelial function and colonic microbiota and promotes a risk for transmissible colitis. *Infect. Immun.* 84, 798–810. doi: 10.1128/IAI.01374-15

Dikalov, S. I., and Harrison, D. G. (2014). Methods for detection of mitochondrial and cellular reactive oxygen species. *Antioxid. Redox Signal.* 20, 372–382. doi: 10.1089/ars.2012.4886

Fritsch, J., and Abreu, M. T. (2019). The microbiota and the immune response: what is the chicken and what is the egg? *Gastrointest. Endosc. Clin. N. Am.* 29, 381–393. doi: 10.1016/j.giec.2019.02.005

Gattas, M. V., Forteza, R., Fragoso, M. A., Fregien, N., Salas, P., Salathe, M., et al. (2009). Oxidative epithelial host defense is regulated by infectious and inflammatory stimuli. *Free Radic. Biol. Med.* 47, 1450–1458. doi: 10.1016/j.freeradbiomed.2009.08.017

Geiszt, M., Lekstrom, K., Brenner, S., Hewitt, S. M., Dana, R., Malech, H. L., et al. (2003). NAD(P)H oxidase 1, a product of differentiated colon epithelial cells, can partially replace glycoprotein 91phox in the regulated production of superoxide by phagocytes. *J. Immunol.* 2003, 299–306. doi: 10.4049/jimmunol.171.1.299

Gitter, A. H., Wullstein, F., Fromm, M., and Schulzke, J. D. (2001). Epithelial barrier defects in ulcerative colitis: characterization and quantification by electrophysiological imaging. *Gastroenterology* 121, 1320–1328. doi: 10.1053/gast.2001.29694

Glineur, C., Davioud-Charvet, E., and Vandenbunder, B. (2000). The conserved redox-sensitive cysteine residue of the DNA-binding region in the c-Rel protein is involved in the regulation of the phosphorylation of the protein. *Biochem. J.* 352(Pt 2), 583–591. doi: 10.1042/bj3520583

Gohl, D. M., Vangay, P., Garbe, J., MacLean, A., Hauge, A., Becker, A., et al. (2016). Systematic improvement of amplicon marker gene methods for increased accuracy in microbiome studies. *Nat. Biotechnol.* 34, 942–949. doi: 10.1038/nbt.3601

Grasberger, H., El-Zaatari, M., Dang, D. T., and Merchant, J. L. (2013). Dual oxidases control release of hydrogen peroxide by the gastric epithelium to prevent *Helicobacter felis* infection and inflammation in mice. *Gastroenterology* 145, 1045–1054. doi: 10.1053/j.gastro.2013.07.011

Grasberger, H., Gao, J., Nagao-Kitamoto, H., Kitamoto, S., Zhang, M., Kamada, N., et al. (2015). Increased expression of DUOX2 is an epithelial response to mucosal dysbiosis required for immune homeostasis in mouse intestine. *Gastroenterology* 149, 1849–1859. doi: 10.1053/j.gastro.2015.07.062

Ha, E. M., Oh, C. T., Bae, Y. S., and Lee, W. J. (2005). A direct role for dual oxidase in *Drosophila* gut immunity. *Science* 310, 847–850. doi: 10.1126/science.1117311

Haberman, Y., Tickle, T. L., Dexheimer, P. J., Kim, M. O., Tang, D., Karns, R., et al. (2014). Pediatric Crohn disease patients exhibit specific ileal transcriptome and microbiome signature. *J. Clin. Investig.* 124, 3617–3633. doi: 10.1172/JCI75436

Haberman, Y., Tickle, T. L., Dexheimer, P. J., Kim, M. O., Tang, D., Karns, R., et al. (2015). Corrigendum. Pediatric Crohn disease patients exhibit specific ileal transcriptome and microbiome signature. *J. Clin. Investig.* 125:1363. doi: 10.1172/jci79657

Hayes, P., Dhillon, S., O'Neill, K., Thoeni, C., Hui, K. Y., Elkadri, A., et al. (2015). Defects in NADPH oxidase genes NOX1 and DUOX2 in very early onset inflammatory bowel disease. *Cell. Mol. Gastroenterol. Hepatol.* 1, 489–502. doi: 10.1016/j.jcmgh.2015.06.005

Heijmans, J., Wielenga, M. C., Rosekrans, S. L., van Lidth de Jeude, J. F., Roelofs, J., G1roothuis, P., et al. (2014). Oestrogens promote tumorigenesis in a mouse model for colitis-associated cancer. *Gut* 63, 310–316. doi: 10.1136/gutjnl-2012-304216

Holmstrom, K. M., and Finkel, T. (2014). Cellular mechanisms and physiological consequences of redox-dependent signalling. *Nat. Rev. Mol. Cell Biol.* 15, 411–421. doi: 10.1038/nrm3801

Hussain, S. P., Hofseth, L. J., and Harris, C. C. (2003). Radical causes of cancer. *Nat. Rev. Cancer* 3, 276–285. doi: 10.1038/nrc1046

Itzkowitz, S. H., and Yio, X. (2004). Inflammation and cancer IV. Colorectal cancer in inflammatory bowel disease: the role of inflammation. *Am. J. Physiol. Gastrointest. Liver Physiol.* 287, G7–G17.

Jones, R. D., Taylor, A. M., Tong, E. Y., and Repa, J. J. (2013). Carboxylesterases are uniquely expressed among tissues and regulated by nuclear hormone receptors in the mouse. *Drug Metab. Dispos.* 41, 40–49. doi: 10.1124/dmd.112.048397

Klebanoff, S. J., Kettle, A. J., Rosen, H., Winterbourn, C. C., and Nauseef, W. M. (2013). Myeloperoxidase: a front-line defender against phagocytosed microorganisms. *J. Leukoc. Biol.* 93, 185–198. doi: 10.1189/jlb.0712349

Kumar, S., Rabson, A. B., and Gelinas, C. (1992). The RxxRxRxxC motif conserved in all Rel/kappa B proteins is essential for the DNA-binding activity and redox regulation of the v-Rel oncoprotein. *Mol. Cell. Biol.* 12, 3094–3106. doi: 10.1128/mcb.12.7.3094

Leoni, G., Alam, A., Neumann, P. A., Lambeth, J. D., Cheng, G., McCoy, J., et al. (2013). Annexin A1, formyl peptide receptor, and NOX1 orchestrate epithelial repair. *J. Clin. Investig.* 123, 443–454. doi: 10.1172/JCI65831

Leslie, N. R., Bennett, D., Lindsay, Y. E., Stewart, H., Gray, A., and Downes, C. P. (2003). Redox regulation of PI 3-kinase signalling via inactivation of PTEN. *EMBO J.* 22, 5501–5510. doi: 10.1093/emboj/cdg513

Levine, A. P., Pontikos, N., Schiff, E. R., Lovat, L. B., Barrett, J. C., Grasberger, H., et al. (2016). Genetic complexity of Crohn's disease in two large ashkenazi jewish families. *Gastroenterology* 151, 698–709. doi: 10.1053/j.gastro.2016.06.040

Livak, K. J., and Schmittgen, T. D. (2001). Analysis of relative gene expression data using real-time quantitative PCR and the 2(-Delta Delta C(T)) Method. *Methods* 25, 402–408. doi: 10.1006/meth.2001.1262

Luceri, C., Bigagli, E., Agostiniani, S., Giudici, F., Zambonin, D., Scaringi, S., et al. (2019). Analysis of oxidative stress-related markers in Crohn's disease patients at surgery and correlations with clinical findings. *Antioxidants* 8:E378. doi: 10.3390/antiox8090378

MacFie, T. S., Poulsom, R., Parker, A., Warnes, G., Boitsova, T., Nijhuis, A., et al. (2014). DUOX2 and DUOXA2 form the predominant enzyme system capable of producing the reactive oxygen species H$_2$O$_2$ in active ulcerative colitis and are modulated by 5-aminosalicylic acid. *Inflamm. Bowel Dis.* 20, 514–524. doi: 10.1097/01.MIB.0000442012.45038.0e

McKenzie, S. J., Baker, M. S., Buffinton, G. D., and Doe, W. F. (1996). Evidence of oxidant-induced injury to epithelial cells during inflammatory bowel disease. *J. Clin. Investig.* 98, 136–141. doi: 10.1172/jci118757

Mittal, M., Siddiqui, M. R., Tran, K., Reddy, S. P., and Malik, A. B. (2014). Reactive oxygen species in inflammation and tissue injury. *Antioxid. Redox Signal.* 20, 1126–1167. doi: 10.1089/ars.2012.5149

Miwa, S., Treumann, A., Bell, A., Vistoli, G., Nelson, G., Hay, S., et al. (2016). Carboxylesterase converts amplex red to resorufin: implications for mitochondrial H$_2$O$_2$ release assays. *Free Radic. Biol. Med.* 90, 173–183. doi: 10.1016/j.freeradbiomed.2015.11.011

Miyoshi, H., and Stappenbeck, T. S. (2013). In vitro expansion and genetic modification of gastrointestinal stem cells in spheroid culture. *Nat. Protoc.* 8, 2471–2482. doi: 10.1038/nprot.2013.153

Moll, F., Walter, M., Rezende, F., Helfinger, V., Vasconez, E., De Oliveira, T., et al. (2018). NoxO1 controls proliferation of colon epithelial cells. *Front. Immunol.* 2018:973. doi: 10.3389/fimmu.2018.00973

Mowat, A. M., and Agace, W. W. (2014). Regional specialization within the intestinal immune system. *Nat. Rev. Immunol.* 14, 667–685. doi: 10.1038/nri3738

Nagao-Kitamoto, H., Shreiner, A. B., Gillilland, M. G., Kitamoto, S., Ishii, C., Hirayama, A., et al. (2016). Functional characterization of inflammatory bowel disease-associated gut dysbiosis in gnotobiotic mice. *Cell. Mol. Gastroenterol. Hepatol.* 2, 468–481. doi: 10.1016/j.jcmgh.2016.02.003

Parlato, M., Charbit-Henrion, F., Hayes, P., Tiberti, A., Aloi, M., Cucchiara, S., et al. (2017). First identification of biallelic inherited DUOX2 inactivating mutations as a cause of very early onset inflammatory bowel disease. *Gastroenterology* 153, 609.e3–611.e3.

Pircalabioru, G., Aviello, G., Kubica, M., Zhdanov, A., Paclet, M. H., Brennan, L., et al. (2016). Defensive mutualism rescues NADPH oxidase inactivation in gut infection. *Cell Host Microbe* 19, 651–663. doi: 10.1016/j.chom.2016.04.007

Schieber, M., and Chandel, N. S. (2014). ROS function in redox signaling and oxidative stress. *Curr. Biol.* 24, R453–R462. doi: 10.1016/j.cub.2014.03.034

Schwab, C., Berry, D., Rauch, I., Rennisch, I., Ramesmayer, J., Hainzl, E., et al. (2014). Longitudinal study of murine microbiota activity and interactions with the host during acute inflammation and recovery. *ISME J.* 8, 1101–1114. doi: 10.1038/ismej.2013.223

Sender, R., Fuchs, S., and Milo, R. (2016). Revised estimates for the number of human and bacteria cells in the body. *PLoS Biol.* 14:e1002533. doi: 10.1371/journal.pbio.1002533

Shang, L., Fukata, M., Thirunarayanan, N., Martin, A. P., Arnaboldi, P., Maussang, D., et al. (2008). Toll-like receptor signaling in small intestinal epithelium promotes B-cell recruitment and IgA production in lamina propria. *Gastroenterology* 135, 529–538. doi: 10.1053/j.gastro.2008.04.020

Sommer, F., and Backhed, F. (2015). The gut microbiota engages different signaling pathways to induce Duox2 expression in the ileum and colon epithelium. *Mucosal Immunol.* 8, 372–379. doi: 10.1038/mi.2014.74

Swanson, P. A. II, Kumar, A., Samarin, S., Vijay-Kumar, M., Kundu, K., Murthy, N., et al. (2011). Enteric commensal bacteria potentiate epithelial restitution via reactive oxygen species-mediated inactivation of focal adhesion kinase phosphatases. *Proc. Natl. Acad. Sci. U.S.A.* 108, 8803–8808. doi: 10.1073/pnas.1010042108

Tamboli, C. P., Neut, C., Desreumaux, P., and Colombel, J. F. (2004). Dysbiosis in inflammatory bowel disease. *Gut* 53, 1–4. doi: 10.1136/gut.53.1.1

van der Vliet, A., Danyal, K., and Heppner, D. E. (2018). Dual oxidase: a novel therapeutic target in allergic disease. *Br. J. Pharmacol.* 175, 1401–1418. doi: 10.1111/bph.14158

Winter, S. E., Winter, M. G., Xavier, M. N., Thiennimitr, P., Poon, V., Keestra, A. M., et al. (2013). Host-derived nitrate boosts growth of *E. coli* in the inflamed gut. *Science* 339, 708–711. doi: 10.1126/science.1232467

Xanthoudakis, S., and Curran, T. (1992). Identification and characterization of Ref-1, a nuclear protein that facilitates AP-1 DNA-binding activity. *EMBO J.* 11, 653–665. doi: 10.1002/j.1460-2075.1992.tb05097.x

Zhou, M., Diwu, Z., Panchuk-Voloshina, N., and Haugland, R. P. (1997). A stable nonfluorescent derivative of resorufin for the fluorometric determination of trace hydrogen peroxide: applications in detecting the activity of phagocyte NADPH oxidase and other oxidases. *Anal. Biochem.* 253, 162–168. doi: 10.1006/abio.1997.2391

Zhu, W., Miyata, N., Winter, M. G., Arenales, A., Hughes, E. R., Spiga, L., et al. (2019). Editing of the gut microbiota reduces carcinogenesis in mouse models of colitis-associated colorectal cancer. *J. Exp. Med.* 216, 2378–2393. doi: 10.1084/jem.20181939

Distinct Cell Types With the Bitter Receptor Tas2r126 in Different Compartments of the Stomach

Patricia Widmayer[1]*, Vanessa Partsch[1], Jonas Pospiech[1], Soumya Kusumakshi[2], Ulrich Boehm[2] and Heinz Breer[1]

[1] Institute of Physiology, University of Hohenheim, Stuttgart, Germany, [2] Experimental Pharmacology, Center for Molecular Signaling, School of Medicine, Saarland University, Homburg, Germany

Cells expressing bitter taste receptors (T2Rs or Tas2rs) in extraoral tissues are considered to be chemosensory cells mediating protective responses to potentially harmful or even antiinflammatory or antimicrobial compounds. In a previous study the activity of the *Tas2R143/Tas2R135/Tas2r126* cluster promoter in the stomach was monitored using a Cre-reporter mouse line. Reporter gene expression and *Tas2r126* mRNA were found in brush cells located at the distal wall of the gastric groove. In this study, we explored whether brush cells and epithelial cells of the stomach in fact contain the Tas2r126 receptor protein. Using immunohistochemistry, we demonstrate the presence of Tas2r126 immunoreactivity in different cell populations in the glandular stomach, in a subset of brush cells at the gastric groove and in unique glandular units as well as in certain enteroendocrine cells. In brush cells at the gastric groove, a strong immunofluorescence signal for the Tas2r126 receptor was observed at the most apical region of the cells, i.e., the microvillar tuft. In addition, we found a high density of Tas2r126-positive brush cells in the unique glandular units. These invaginations are located distally to the groove, open directly into the furrow and are enwrapped by smoothelin-immunoreactive muscles. In the corpus, Tas2r126 immunoreactivity was found in histamine-producing ECL cells and in ghrelin-producing X/A-like cells, the main enteroendcrine cells of this compartment. In the antrum, Tas2r126 labeling was observed in serotonin-storing EC cells and ghrelin cells, both representing only minor populations of enteroendocrine cells in this compartment. In conclusion, our data provide evidence for the presence of the Tas2r126 receptor protein in distinct cell types in the epithelium lining the mouse stomach which render the stomach responsive to agonists for bitter receptors.

Keywords: T2R, Tas2r, bitter sensing, brush cell, gastric groove, glandular units, enteroendocrine cells

INTRODUCTION

Bitter compounds, such as secondary plant substances, strongly influence food intake (Fraenkel, 1959) as well as metabolic processes (Dotson et al., 2008; Vegezzi et al., 2014; Avau et al., 2015). In addition, several studies have shown their antiinflammatory or antimicrobial effects (Kaji et al., 2009; Prandi et al., 2013, 2018; Hariri et al., 2017) as well as their effect on hormone release in the gastrointestinal (GI) tract (Chen et al., 2006; Rozengurt et al., 2006; Jeon et al., 2008, 2011; Janssen et al., 2011; Kim et al., 2014). As a prerequisite for the induction of these characteristic effects, it is assumed that cells exist, which can sense such compounds and are positioned in distinct compartments of the GI tract.

Recognition of bitter compounds is based on a large family of G protein coupled receptors, the Tas2r receptors (Adler et al., 2000; Chandrashekar et al., 2000; Matsunami et al., 2000). The mouse genome comprises 35 genes encoding distinct Tas2R receptor types (Shi et al., 2003; Hayakawa et al., 2014; Li and Zhang, 2014). Meanwhile, there are several reports indicating that genes encoding receptors for bitter compounds are not only expressed in taste cells, but also in solitary cells interspersed in the epithelium lining the GI tract (see for review: Rozengurt, 2006; Sternini et al., 2008; Behrens and Meyerhof, 2011; Xie et al., 2018). However, very little is known about the expression of bitter receptors in the stomach. The current information is mainly based on PCR analyses (Wu et al., 2002, 2005; Vegezzi et al., 2014; Prandi et al., 2018); only recently immunohistochemical evidence was presented for the presence of TAS2R10 receptor protein in parietal and chief cells of human stomach (Liszt et al., 2017).

In a previous study, the activity of a promoter that controls the gene cluster *Tas2R143/Tas2R135/Tas2r126* was visualized by fluorescent marker protein (EGFP) expression in a transgenic reporter mouse line and revealed EGFP-labeled cells in the epithelium of the stomach (Liu et al., 2017). These were mostly located at the boundary between fundus and corpus and found to express DCLK1, a marker for brush cells, which are also called tuft, caveolated, multivesicular, or fibrillovesicular cells (Luciano and Reale, 1992). In fact, ~15% of all DCLK1-positive brush cells were EGFP-positive; furthermore, in isolated brush cells only mRNA for the receptor gene *Tas2r126* was found (Liu et al., 2017). However, it remained elusive whether these cells indeed comprise the Tas2r126 receptor protein. Based on previous studies, brush cells at the gastric groove, a tissue fold at the boundary between fundus and corpus, are considered to be putative taste-like chemosensory cells (Höfer et al., 1996; Eberle et al., 2013). These cells are arranged in a palisade-like manner and express elements of the canonical taste signaling cascade, including gustducin (Höfer et al., 1996; Hass et al., 2007), PLCβ2 (Eberle et al., 2013) and TRPM5 (Kaske et al., 2007) as well as receptors for nutrients (Hass et al., 2010; Janssen et al., 2012; Eberle et al., 2014; Widmayer et al., 2015, 2019). Situated at a strategic position between the storage compartment fundus and the digestive compartment corpus, brush cells supposedly act as sensor cells monitoring the

constituents of the luminal content and consequently influencing the regulation of gastric processes, such gastric motility, secretion and hormone release. Based on the results of RNA-seq analysis by Liu et al. (2017), we set out to analyze whether the Tas2r126 receptor protein is in fact present in gastric cells, to determine their localization in the stomach epithelium and to characterize the cell types which express the receptor Tas2r126.

MATERIALS AND METHODS

Mice

Studies were performed with adult C57/BL6J and TRPM5-IRES-Cre/eR26-τGFP (Kusumakshi et al., 2015) mice. Animals were fed *ad libitum* with standard laboratory chow and had free access to water. For tissue preparations, animals were killed with carbon dioxide.

Tissue Preparation

For immunohistochemistry and Western blotting, tongues and stomachs were removed and washed in ice-cold PBS (0.85% NaCl, 1.4 mM KH_2PO_4, 8 mM Na_2HPO_4, pH 7.4). For immersion fixation of the stomach, the fundus was cut off, the stomach opened along the greater curvature and washed with ice-cold PBS. For plane sectioning, the opened stomach was mounted on a piece of rubber and fixed with needles (Eberle et al., 2013). For longitudinal sectioning, a transverse strip of the entire stomach wall including the fundus, cardia, corpus and antrum was excised.

All tissues were fixed using 4% paraformaldehyde (in 150 mM phosphate buffer, pH 7.4) for 2 h. After fixation, tissues were cryoprotected by incubation in 25% sucrose overnight at 4°C. Then, tissues were embedded in Tissue Freezing Medium (Leica Microsystems, Bensheim, Germany) and quickly frozen on liquid nitrogen-cooled metal covers.

Western Blotting

Total protein was extracted from pooled posterior papillae. 30 μg of the homogenate were loaded onto a 12.5% SDS-PAGE gel and transferred to a nitrocellulose membrane. The immunoblot was blocked with 6% milk powder in PBS buffer containing 0.1% Tween 20 (TBST) for 1 h and then probed with a rabbit anti-Tas2r126 antiserum (SAB signaling antibody, #44656, Baltimore, United States; rabbits were immunized with a synthesized peptide derived from human TAS2R41, the ortholog of mouse Tas2r126, predicting a species reactivity for human, mouse and rat) diluted 1:200 in 5% BSA in TBST overnight at 4°C. After washing in TBST, the blot was incubated with a goat anti-rabbit horseradish peroxidase (HRP)-conjugated IgG antiserum (Sigma-Aldrich), diluted 1:10000 in blocking solution and developed using the Amersham ECL Select kit (Thermo Fisher Scientific). The membrane was scanned using a C-DiGit blot scanner (LI-COR Biotechnology, Bad Homburg, Germany).

Immunohistochemistry

Each tissue was serially cut into 6–8 μm thick sections. Cryosections were mounted onto Superfrost Plus microscope slides (Menzel-Gläser, Braunschweig, Germany) using a CM3050S cryostat (Leica Microsystems), air-dried for 1 h and stored at −20°C until use. For immunohistochemistry, cryosections underwent citrate-antigen-retrieval. Frozen sections were incubated in a sodium citrate buffer (10 mM sodium citrate, 0.05% Tween 20, pH 6.0) for 45 min at 4°C. Afterward, sections were immersed in the same sodium citrate buffer for 1 min at 100°C. Then slides were rinsed in PBS for 10 min and blocked in 0.3% Triton X-100 in PBS containing 10% normal donkey serum (NDS; Dianova, Hamburg, Germany) for 1 h at room temperature. After three changes of PBS, slides were incubated with the primary antisera overnight at 4°C. Antibodies were diluted in 0.3% Triton X-100 in PBS containing 10% NDS and used in the following dilutions: chicken anti-GFP [1:400; ab13970, Abcam, Cambridge, United Kingdom; van der Heijden et al. (2016)], rabbit anti-TRPM5 serum73 [1:600; purified antibody (AB-321); described in Kaske et al. (2007)], goat anti-COX-2 [1:200; sc-1747, Santa Cruz, Dallas, TX, United States; Widmayer et al. (2019)], rabbit anti-smoothelin [1:200, sc-28562, Santa Cruz; Frick et al. (2017)], goat anti-chromogranin A [1:200; sc-1488, Santa Cruz; Gerbe et al. (2011)], goat anti-HDC [1:20, sc-34458, Santa Cruz; Frick et al. (2017)], goat anti-ghrelin [1:800, sc-10368, Santa Cruz; Caminos et al. (2003)], goat anti-5-HT [1:3000; ab66047, Abcam, Cambridge, United Kingdom; Lund et al. (2018)], and goat anti-somatostatin [1:800, sc-7819, Santa Cruz; Frick et al. (2017)]. After washing in PBS, primary antisera were visualized using donkey anti-goat IgG (H + L) Alexa Fluor 488, Invitrogen (1:500; Fisher Scientific, Goteborg, Sweden), donkey anti-rabbit IgG (H + L) Alexa Fluor 568, Invitrogen (1:500; Fisher Scientific), and donkey anti-goat AMCA (1:200; Jackson, ImmunoResearch), diluted in PBS with 0.3% Triton X-100 containing 10% NDS for 2 h at room temperature. After a further three washes with PBS, tissue sections were counterstained with DAPI (1.0 μg/mL, Sigma-Aldrich) 1:1000. After incubation for 3 min at room temperature, sections were rinsed with double-distilled water and mounted in MOWIOL (10% polyvinyl alcohol 4-88 (Sigma-Aldrich), 20% glycerol in 1x PBS). No immunoreactivity was observed when the primary antisera were omitted.

Cell Counting

Digital microscopic images of longitudinal sections were acquired at 40× magnification. For cell counts in the corpus and antrum, a continuous epithelial area of 2000 μm × 250 μm was defined starting at the edge of the proximal stomach and transitional junction from corpus to antrum, respectively. Counts were then expressed as cells per 0.5 mm². To determine brush cell numbers in large invaginations, images of three consecutive longitudinal sections through the proximal stomach were acquired. Then, the average cell counts of immunopositive cells were determined. Cells were quantified as percentage of DAPI-labeled nuclei of immunoreactive cells. To assess the proportion of Tas2r126-expressing cells among enteroendocrine

cells, the number of immunoreactive cells on 3–5 consecutive sections within an area of 355 μm × 265 μm was counted. The percentage and number of positive cells were expressed as a mean ± SD.

RESULTS

Visualization and Characterization of Tas2r126-Immunoreactive Cells

Previous experimental evidence for *Tas2r126* expression in the stomach is based on EGFP-positive epithelial cells in a Cre-reporter mouse line and RNA-seq analysis of isolated EGFP-positive cells (Liu et al., 2017). In order to analyze whether the receptor protein is in fact present in epithelial cells lining the stomach, we used an antiserum against Tas2r126 in immunological approaches. For this, we employed a commercially available antiserum raised against human TAS2R41 sharing an overall amino acid sequence identity of 69% to the mouse Tas2r126. The TAS2R41 epitope is localized in the region of the extracellular loop 2 and transmembrane domain 5 that shares a high number of identical and conserved amino acid residues with the mouse one-to-one ortholog (**Figure 1A**). To evaluate a potential cross-reactivity with related stomach-specific bitter receptors (Prandi et al., 2018), the relevant sequence motifs were compared. The alignment shows a high degree of diversity (**Figure 1B**) indicating that cross-reactivity is unlikely. Since no blocking peptide was provided by the supplier to prove the epitope specificity of the antiserum, we experimentally validated its specificity by performing Western blot analyses with preparations of posterior taste papillae. The result is depicted in **Figure 1C** and demonstrates that the antiserum recognized a protein at the expected size. We then probed tissue sections through the posterior region of the murine tongue with the Tas2r126 antiserum. As shown in **Figure 1D**, distinct cells in taste buds were specifically labeled; in contrast, sections incubated only with the secondary antibody were devoid of any staining (**Figure 1E**). Subsequently, tissue sections from the mouse stomach were analyzed. As depicted in **Figure 1F**, the epithelium of the aglandular fundus was devoid of any labeled cells. Instead, Tas2r126-immunolabeled cells were restricted to the glandular compartment of the stomach. Omission of the primary antiserum on an adjacent section shows the absence of any staining (**Figure 1G**). Particularly striking was the high density of labeled cells opposite of the limiting ridge, which surrounds the entire fundus/corpus border of the stomach as well as the esophageal orifice (Wattel and Geuze, 1978; Luciano and Reale, 1992). Beneath the limiting ridge large clusters of Tas2r126-positive cells were visible (**Figure 1H**). This clustering of the antiserum-labeled cells at the so-called gastric groove is reminiscent of the pattern of EGFP-positive cells in the Cre-reporter mouse line (Liu et al., 2017). In addition, we also found Tas2r126-immunopositive cells in the mucosal glands of the corpus (**Figure 1F**), where the labeled cells were mainly located in the basal half of the epithelium.

Upon closer inspection of the labeled cells at the gastric groove a variety of staining patterns emerged. While in some
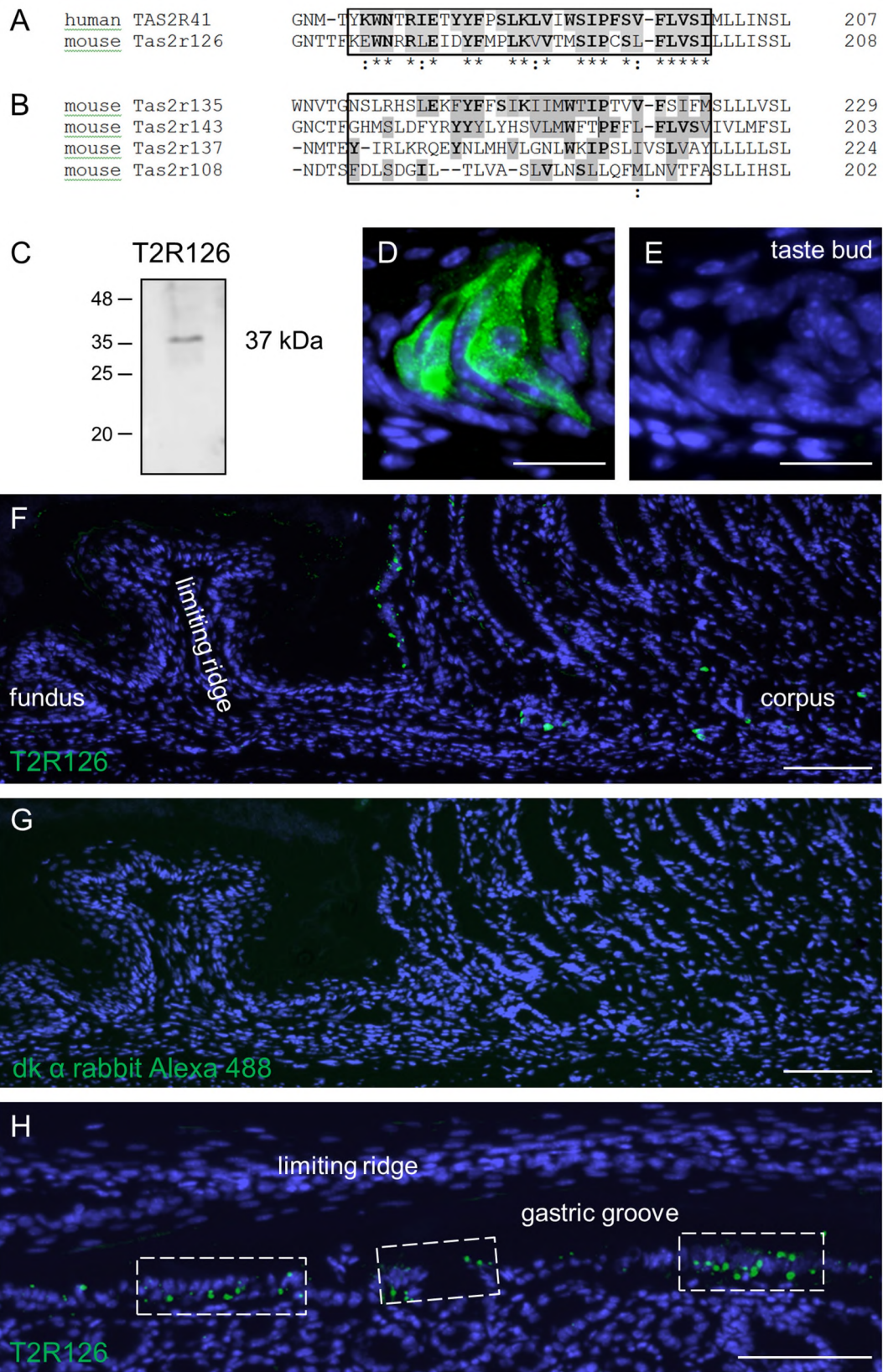
FIGURE 1 | Continued

FIGURE 1 | Sequence alignments and expression of the bitter receptor Tas2r126 assessed by Western Blot analyses and immunohistochemistry in mouse tongue and stomach. **(A)** Comparison of the sequence region for the one-to-one orthologs, human TAS2R41 and mouse Tas2r126, showing the sequence region used for the antiserum generation. Identical amino acids are highlighted in gray with bold letters, conservative replacements shaded in gray and divergent residues in white. The epitope alignment is marked in the box and indicates a considerable degree of sequence identity and similarity between TAS2R41 and Tas2r126.
(B) Comparison of the corresponding sequence region of Tas2r subtypes which originate from the same phylogenetic clade and which are expressed in the stomach. There is a high degree of sequence diversity within the epitope region (boxed area) compared to TAS2R41, thus cross-reactivity with Tas2r subtypes other than Tas2r126 seems unlikely. Alignments were performed with the program Clustal Omega, EMBL-EBI. **(C)** Western blot analysis of whole cell lysates from posterior taste papillae revealed that the Tas2r126 antiserum recognized a band with an apparent molecular weight of ∼37 kDa corresponding with the expected size of 36.2 kDa. **(D)** In posterior taste buds the antiserum specifically labeled gustatory cells. **(E)** A consecutive section of the papilla probed with only the secondary antibody showed no labeling. **(F)** Immunohistochemistry on tissue sections through the whole stomach, longitudinally opened along the greater curvature, to analyze the aglandular and glandular gastric regions. In the fundus, no immunopositive cells were detected, whereas opposite the limiting ridge multiple Tas2r126-positive cells were labeled. In the corpus mucosa Tas2r126-immunoreactive cells were visible in the basal half of the invaginations. **(G)** A minus primary antiserum control of a consecutive section did not show any staining. **(H)** Analysis of a perpendicular section through the gastric ridge region showing multiple Tas2r126-positive cells in clusters. Scale bars **(D,E)**, 20 μm, **(F–H)**, 100 μm.
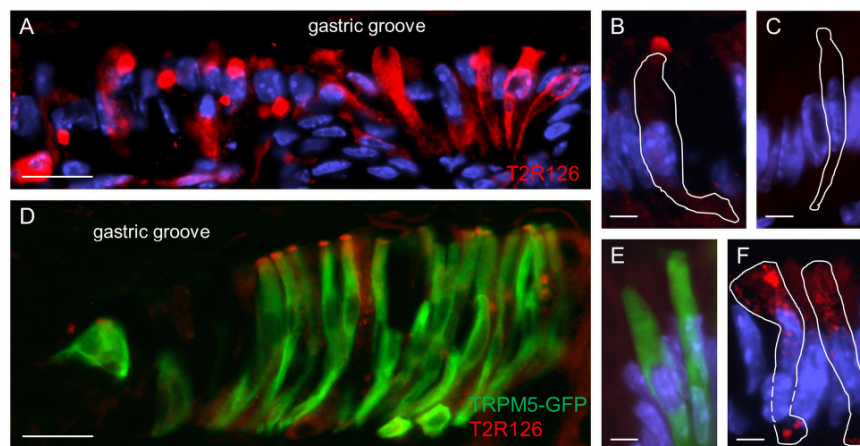
FIGURE 2 | Expression of Tas2r126 in cells of the epithelial band at the gastric groove circumscribing the stomach. **(A)** Cells in the epithelial band displayed different staining characteristics. While in some cells the entire cell body was labeled, other cells showed a more punctate staining. **(B)** Several cells were characterized by a strong immunoreactivity at the most apical part; apparently the apical microvillar tuft of brush cells. **(C)** Omission of the primary antiserum served as negative control. **(D)** The identity as brush cells was confirmed analyzing TRPM5-IRES-Cre/eR26-τGFP mice; the τGFP immunostaining (green) is colocalized with Tas2r126 immunoreactivity (red) in a subset of brush cells. **(E)** Omission of the Tas2r126 antiserum resulted only in τGFP immunostaining (green). **(F)** Some columnar cells with a wide microvillar apex were also stained. Beneath the apical cell membrane, punctate staining was visible. Scale bars **(A,D)**, 20 μm, **(B,C,E,F)**, 5 μm.

cases the entire cell body was labeled, in other cases only a punctate staining was observed (**Figure 2A**). For some of the cells strong immunoreactivity was selectively visible at the apical region; the tuft-like labeling suggests that these cells are brush cells (**Figure 2B**). To test this hypothesis, we used TRPM5 as a brush cell marker and a transgenic mouse line allowing us to visualize TRPM5-expressing cells due to their endogenous GFP fluorescence (Kusumakshi et al., 2015). The results of double labeling experiments visualizing GFP and Tas2r126 immunoreactivity are depicted in **Figure 2D**. As can be seen, several of the TRPM5-positive cells showed a strong immunoreactivity for Tas2r126 at the apical region, probably at the microvilli. This result indicates that some of the Tas2r126-positive cells at the gastric groove are in fact brush cells. However, only a subset of the brush cells was Tas2r126-immunoreactive consistent with the observations by Liu et al. (2017). Additionally, some columnar cells also showed Tas2r126 immunoreactivity. These cells are characterized by a wide microvillar apex (**Figure 2F**). Controls omitting the Tas2r126 antiserum on sections from wildtype and transgenic

mice resulted in negative staining (**Figure 2C**) and GFP-specific labeling (**Figure 2E**), respectively, thus indicating the specificity of the used antiserum.

Tas2r126-Positive Cells in Large Invaginations at the Bottom of the Gastric Groove

Upon inspection of sections through the proximal edge of the corpus, we identified large invaginations that comprised a large number of brush cells (**Figure 3A**) and often also contained a high density of Tas2r126-labeled cells (**Figure 3B**). The invaginations are located in a narrow region, distally adjacent to the gastric groove at both the smaller and the greater curvature; this region corresponds to the so-called cardiac zone according to Wattel and Geuze (1978). This structure, called first gland, is considered to be a unique anatomical entity (O'Neil et al., 2017). The invaginations are often branched, almost ovoid or sometimes round in shape and have different sizes (small: 40 μm × 40 μm; large: 100 μm × 60 μm up to 240 μm × 160 μm). Those
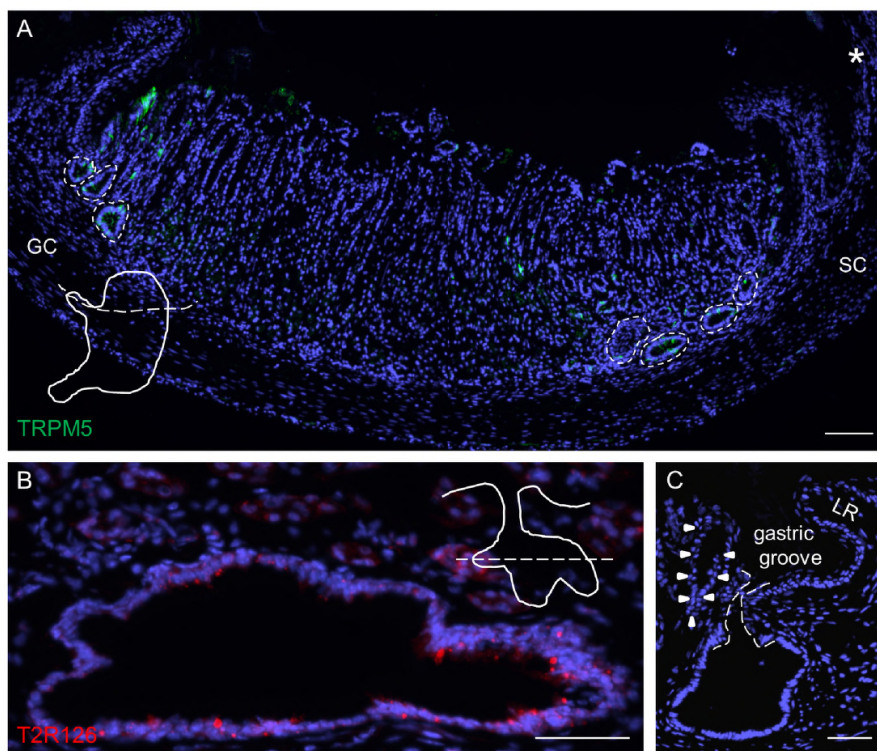
FIGURE 3 | Analyses of Tas2r126-expressing cells in unique glandular units at the smaller and greater curvature adjacent to the gastric groove. **(A)** Distribution of large invaginations on stomach sections at the level of the esophagus orifice (asterisk). TRPM5 was used as marker for brush cells. In order to prepare the sections the stomach was cut along the dotted line as illustrated. **(B)** Large invaginations were often branched and fused into oval structures with a large lumen; the lining epithelium comprised numerous cells with Tas2r126 immunoreactivity (red). An example area at the smaller curvature is shown. The schematic drawing indicates the cutting level (dotted line). **(C)** Invaginations associated with the first gland (marked by arrow heads) which are located very close to the bottom of the gastric groove have an open connection to the gastric lumen. The connecting channel of the invagination is encircled by the dotted line. GC, greater curvature, SC, smaller curvature, LR, limiting ridge. Scale bars **(A)**, 100 μm, **(B,C)**, 50 μm.
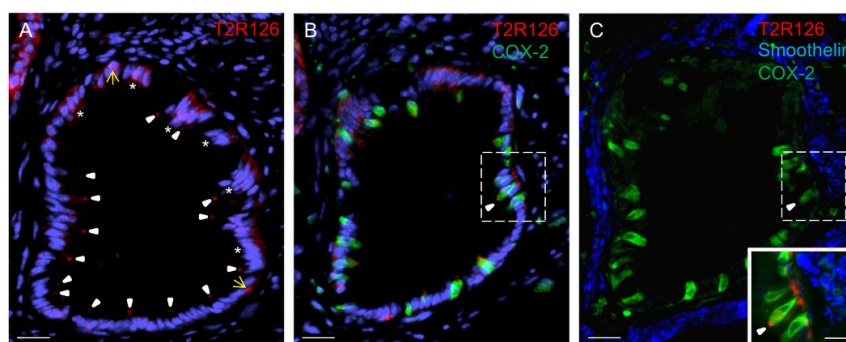
FIGURE 4 | Cells with Tas2r126 immunoreactivity in glandular units at the bottom of the gastric groove enwrapped by smooth muscles **(A)** In these invaginations Tas2r126 labeling was found at the apex of brush cells (arrowhead) and basally located round cells (yellow arrow); furthermore groups of columnar cells (*) were labeled. **(B)** Brush cells with Tas2r126 immunoreactivity (red) contain the rate limiting enzyme for the synthesis of prostaglandin COX-2 (green). **(C)** A consecutive section was probed with a smoothelin antiserum (blue); the labeled structures surround the invagination so that smooth muscle cells are located next to the COX-2 positive brush cells (green). Inset: An overlay of the marked regions in **(B,C)** indicates that brush cells (green) with Tas2r126 immunoreactivity (red) are adjacent to smooth muscle cells (blue). Scale bars **(A–C)**, 20 μm, (inset), 10 μm.

invaginations adjacent to the gastric groove open directly into this furrow (**Figure 3C**).

Within these invaginations, we detected Tas2r126 labeling at the apex of brush cells, at the base of round cells and some columnar cells (**Figure 4A**). Quantification indicated that within the epithelium of these structures 57 ± 5.9% of all brush cells were also positive for Tas2r126 ($n = 3$ mice); whereas at the limiting ridge only ∼15% of the brush cells were found to express

Tas2r126 (Liu et al., 2017). At the bottom of the gastric groove, the invaginations merged into the thick *lamina muscularis mucosae* that further extends deep into the limiting ridge (Luciano and Reale, 1992). To explore whether the Tas2r126-expressing brush cells might come in close contact with muscle fibers in this region, we performed immunolabeling for Tas2r126, COX-2 and smoothelin. **Figure 4B** shows the distribution of Tas2r126-expressing brush cells within an invagination, which is enwrapped by muscle fibers (**Figure 4C**). At higher magnification it becomes apparent that some Tas2r126-immunoreactive brush cells are indeed located in close vicinity to smooth muscle cells (**Figure 4C**, inset).

Characterization of Tas2r126-Positive Cells in Mucosal Glands

Analyzing corpus and antrum for Tas2r126-immunoreactive cells revealed that labeled cells were present in both compartments, albeit at quite different densities (**Figure 5A**). Whereas 60 ± 9.6 labeled cells per 0.5 mm^2 were counted in the corpus ($n = 3$ mice), the antrum only contained 17.3 ± 3.5 cells per 0.5 mm^2 ($n = 3$ mice). Based on the localization of the cells at the lower half of the invaginations the Tas2r126-immunoreactive cells in the corpus and antrum glands may be enteroendocrine cells (EECs). To test this hypothesis, double labeling experiments were performed using the antiserum against Tas2r126 in combination with an antiserum against CgA, a general marker for EECs. The results depicted in **Figure 5B** indicate that among the CgA-positive cells several were immunoreactive for Tas2r126; in fact, this applied to $52 \pm 8.4\%$ of the CgA cells ($n = 3$ mice). In order to further characterize the molecular phenotype of the Tas2r126-expressing EECs in the corpus, we used an antiserum against HDC, the key enzyme involved in synthesis of histamine, as well as antisera against ghrelin, serotonin, and somatostatin. In the corpus glands, subpopulations of Tas2r126-positive cells were labeled with antisera against HDC and ghrelin, respectively (**Figures 5C,D**). The analyses of numerous preparations revealed that the proportion of EEC cells, which were positive for Tas2r126, decreased from proximal to distal. In antral glands, only $21 \pm 9.3\%$ of CgA-positive cells were positive for Tas2r126 ($n = 3$ mice) (**Figure 6A**); subsets were found to be co-labeled for serotonin (5-HT) or for ghrelin (**Figures 6B,C**). In both compartments, Tas2r126-immunoreactive somatostatin-producing D cells were only rarely seen (data not shown).

DISCUSSION

In the present study, we have identified distinct cell types in the gastric epithelium expressing a bitter receptor protein; thus, confirming and extending the results of previous studies, which demonstrated the presence of mRNA for bitter receptors in epithelial cells of the stomach (Wu et al., 2002; Vegezzi et al., 2014; Liu et al., 2017; Prandi et al., 2018). Expression of the Tas2r126 receptor in distinct cell types enables the stomach to sense certain bitter compounds and elicit adequate responses. Based on the results of PCR experiments one may assume that additional types of bitter taste receptors are present

in the stomach. In fact, a recent study identified a set of distinct Tas2r receptor types that was expressed in the stomach (Prandi et al., 2018). In view of possible implications it will be of great interest to further explore whether individual combinations of receptor types may be expressed in distinct cell types or in cells at certain positions. This would allow defined responses to various bitter compounds and may explain diverse effects of bitter compounds on stomach functions, such as gastric emptying (Glendinning et al., 2008), antral contractility, stimulation of ghrelin release (Janssen et al., 2011, 2012; Wang et al., 2019) and induction of gastric acid secretion (Liszt et al., 2017, 2018).

The presence of Tas2r126 protein in distinct epithelial cells of the stomach is consistent with a functional role of Tas2r126 agonists in regulating gastric processes. Deorphanization studies of mouse Tas2r by heterologous expression using a large variety of compounds revealed that the receptor type Tas2r126 has an intermediate molecular receptive range; compounds which activate Tas2r126 all share a phenyl ring and include arbutin and salicin (Lossow et al., 2016). Interestingly, arbutin is considered to have antimicrobial effects (Ma et al., 2019) and salicin to have antiinflammatory effects (Li et al., 2015). Thus, cells equipped with a functional Tas2r126 receptor might be involved in gastro-protective processes.

The presence of the bitter receptor Tas2r126 in a subset of brush cells, which are arranged in a continuous band beneath the limiting ridge as demonstrated in this study and by Liu et al. (2017), is particularly interesting in view of previous findings demonstrating that brush cells at the gastric ridge comprise receptor types for short chain fatty acids (Eberle et al., 2014) as well as for long chain fatty acids (Widmayer et al., 2015, 2019). An obvious question in this context is whether the bitter receptor-expressing brush cells also contain short and/or long chain fatty acid receptors or whether they constitute separate populations. Brush cells with a broad receptor expression profile may operate as multisensory cells capable to respond to a variety of chemical constituents in the luminal content, whereas distinct sets of bush cells with different chemosensory properties could point to region-specific functions. Moreover, it is unclear whether all brush cells at the gastric ridge have the enzymatic capacity to produce the candidate messenger compounds, such as nitric oxide, prostaglandins and acetylcholine (Kugler et al., 1994; Eberle et al., 2013; Widmayer et al., 2019) which could operate as paracrine mediators between brush cells and adjacent effector cells. The high proportion of brush cells with Tas2r126 immunoreactivity in the large invaginations at the proximal edge of the corpus is a striking observation. Although the functional implication is unknown, it is interesting to note that these invaginations constitute, together with the so-called first gland, a unique glandular unit enriched in brush and mucus cells, which are considered to be a source of the mucin MUC4 (O'Neil et al., 2017).

The arrangement of Tas2r126 cells at the border between the reservoir compartment fundus and the digestive compartment corpus with secretory epithelial cells might point to an involvement of brush cells in defense mechanisms by controlling the activity of secretory cells. Interestingly, this zone is separating
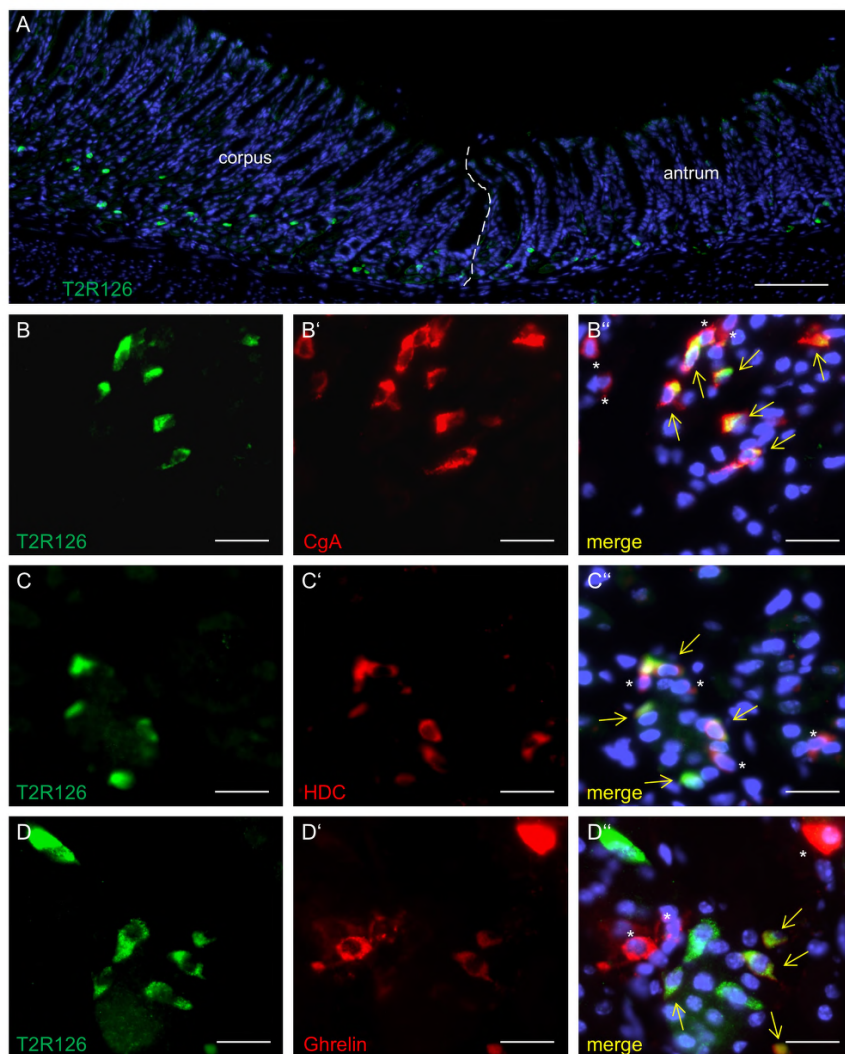
FIGURE 5 | Molecular phenotypes of cells with Tas2r126 immunoreactivity in the glandular regions corpus and antrum. **(A)** On sections of the transition region between the corpus and antrum it was apparent that the antrum mucosa contained only very few Tas2r126-positive cells compared to the corpus mucosa. **(B–D)** Double immunohistochemical analyses of the corpus mucosa. **(B)** Labeling for Tas2r126 (green) and CgA (red) indicates that several CgA-positive cells were also positive for Tas2r126. **(C)** Visualization of histamine-producing cells (red) by an antiserum for histidine decarboxylase (HDC) revealed that several were also immunopositive for Tas2r126 (green). **(D)** A subset of X/A-like cells, identified by ghrelin (red), was also immunoreactive for Tas2r126 (green). Yellow arrows point to co-labeled cells (merge). Asterisks mark hormone-producing cells devoid of Tas2r126 staining. Scale bars **(A)**, 100 μm, **(B–D)**, 10 μm.

the luminal content of the two compartments as well as in controlling the transfer from the aglandular fundus into the glandular part of the stomach. The ingested food stored in the fundus is probably separated by an adequate mucus barrier generated by the numerous mucus-containing glands (Lee et al., 1982) and columnar cells secreting the TFF1 (unpublished results); the activity of both may be controlled by the sensing of brush cells. In this context, it is conceivable that ingested secondary plant compounds, such as arbutin, which is present in various berries and activate the Tas2r126 receptor, might induce such effects.

Stimulation of Tas2r126 in brush cells thus might result in the activation of the canonical downstream components of the taste signal transduction (Wong et al., 1996; Rössler et al., 1998;

Liu and Liman, 2003), since all functional elements of the canonical taste signaling cascade are expressed in the stomach, including gustducin, PLCβ2, TRPM5 (Höfer et al., 1996; Hass et al., 2007; Kaske et al., 2007; Eberle et al., 2013). According to the proposed mechanism, it is conceivable that an activation of bitter receptors in brush cells will lead to the dissociation of the βγ-dimer from the α-subunit gustducin and an activation of PLCβ2 that in turn generates IP_3 that opens IP_3R channels to release calcium. Elevated calcium levels then may activate TRPM5 channels leading to a calcium influx and consequently the release of signaling molecules. Such paracrine messengers may in turn induce the secretion of mucins, TFF1 or antimicrobial peptides from the surrounding epithelial cells. In fact, studies by Lee et al. (2014, 2017) demonstrated that in the
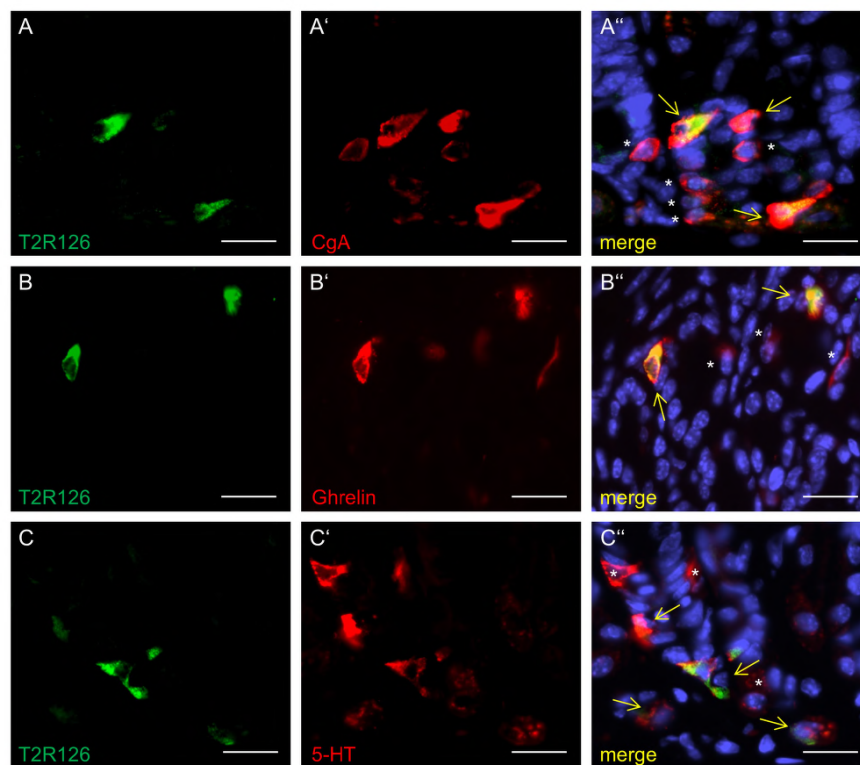
FIGURE 6 | Distinct enteroendocrine cell types in the mouse antrum express Tas2r126. **(A)** Numerous CgA-positive EECs (red) were found to be immunoreactive for Tas2r126 (green). **(B)** Cells which were double labeled for Tas2r126 (green) and ghrelin (red) were also found in the antrum. **(C)** Dual immunostaining showed the presence of Tas2r126 immunoreactivity (green) in serotonin-producing EC cells, identified by 5-HT (red). Yellow arrows point to co-labeled cells (merge). Asterisks mark hormone-producing cells devoid of Tas2r126 staining. Scale bars **(A–C)**, 10 μm.

airways bitter agonist-induced activation of brush cells leads to a secretion of β-defensin 1.

Some of the invaginations close to the gastric groove open into the furrow and are enwrapped by smooth muscles (Wattel and Geuze, 1978). The close vicinity of brush cells and smooth muscle cells may suggest some paracrine influence of brush cells on the contraction state of muscles. The interaction between brush cells and smooth muscles could for example be involved in tightly closing the stomach opening (Montedonico et al., 1999) and in guiding ingested food into the fundus. Furthermore, for brush cells in the small intestine it has recently been shown that they trigger IL-25-mediated type 2 immune responses upon a parasite and bacterial infection (Gerbe et al., 2016; Howitt et al., 2016; von Moltke et al., 2016; Nadjsombati et al., 2018). It is currently unknown whether brush cells in the stomach are also involved in the regulation of local immune circuits. Based on the afore mentioned examples, Tas2r126-expressing brush cells might be considered as sentinel cells of the stomach, however, the mechanisms associated with their proposed protective role still awaits elucidation.

In this report, we provide evidence that a subpopulation of ghrelin-producing X/A-like cells and histamine-storing ECL cells in the corpus contain the Tas2r126 receptor. This observation is in line with transcriptome analysis of sorted ghrelin cells demonstrating enrichment of *Tas2r126* RNA when compared to

non-fluoresent cells (Engelstoft et al., 2013). Ghrelin cells are typically closed type cells which are assumed to be activated via the blood stream. However, it has recently been shown that salicin, a potent activator of the Tas2r126 receptor, affects the secretion of ghrelin as well as gastric emptying and food intake (Janssen et al., 2011). Conversely, the bitter compounds denatonium benzoate (DB) or phenylthiocarbamide (PTU) evoked opposite effects (Janssen et al., 2011). These differences support the notion that additional Tas2R receptor types are active in the stomach, possibly in different subpopulations of cells. In histamine- and ghrelin-producing cells the stimulation with Tas2r126 agonists may elicit an elevation of intracellular calcium and thus trigger the release of hormones. Indeed, recent studies showed that certain bitter agonists stimulate the secretion of ghrelin from human and mouse cells (Janssen et al., 2011; Wang et al., 2019). Activation of ghrelin cells via bitter receptors may involve gustatory α-subunits, since both gustducin and transducin were found to be expressed in subpopulations of mouse ghrelin cells and the lack of gustducin affected acyl ghrelin (Janssen et al., 2012).

In conclusion, distinct cell types with the receptor Tas2r126 are located at characteristic positions in the stomach and may operate as a specialized surveillance system monitoring the luminal content for defined constituents. Moreover, these cells might convey the sensed information via paracrine

signaling onto gastric effector systems, adapting the motor and secretory activities according to the changing composition of the luminal content.

DATA AVAILABILITY STATEMENT

All data generated or analyzed during this study are included in this published article.

ETHICS STATEMENT

The animal study was reviewed and approved by the institutional and national guidelines for the care and use of laboratory animals according to the Society of Laboratory Animals (GV-SOLAS) were followed. The work was approved by the Committee on the Ethics of Animal Experiments at the Regierungspräsidium Stuttgart (V318/14 Phy) and the University of Hohenheim Animal Welfare Officer (T125/14 Phy, T126/14 Phy). All experiments complied with the Principles of Animal Care, publication no. 85-23, revised 1985, of the National Institutes of Health and with the current laws of Germany.

AUTHOR CONTRIBUTIONS

ACKNOWLEDGMENTS

REFERENCES

Adler, E., Hoon, M. A., Mueller, K. L., Chandrashekar, J., Ryba, N. J. P., and Zuker, C. S. (2000). A novel family of mammalian taste receptors. *Cell* 100, 693–702. doi: 10.1016/S0092-8674(00)80705-9

Avau, B., Bauters, D., Steensels, S., Vancleef, L., Laermans, J., Lesuisse, J., et al. (2015). The gustatory signaling pathway and bitter taste receptors affect the development of obesity and adipocyte metabolism in mice. *PLoS One* 10:e0145538. doi: 10.1371/journal.pone.0145538

Behrens, M., and Meyerhof, W. (2011). Gustatory and extragustatory functions of mammalian taste receptors. *Physiol. Behav.* 105, 4–13. doi: 10.1016/j.physbeh.2011.02.010

Caminos, J. E., Nogueiras, R., Blanco, M., Seoane, L. M., Bravo, S., Alvarez, C. V., et al. (2003). Cellular distribution and regulation of ghrelin messenger ribonucleic acid in the rat pituitary gland. *Endocrinology* 144, 5089–5097. doi: 10.1210/en.2003-0529

Chandrashekar, J., Mueller, K. L., Hoon, M. A., Adler, E., Feng, L., Guo, W., et al. (2000). T2Rs function as bitter taste receptors. *Cell* 100, 703–711. doi: 10.1016/S0092-8674(00)80706-0

Chen, M. C., Wu, S. V., Reeve, J. R., and Rozengurt, E. (2006). Bitter stimuli induce Ca2+ signaling and CCK release in enteroendocrine STC-1 cells: role of L-type voltage-sensitive Ca2+ channels. *Am. J. Physiol. Physiol.* 291, C726–C739. doi: 10.1152/ajpcell.00003.2006

Dotson, C. D., Zhang, L., Xu, H., Shin, Y.-K., Vigues, S., Ott, S. H., et al. (2008). Bitter taste receptors influence glucose homeostasis. *PLoS One* 3:e3974. doi: 10.1371/journal.pone.0003974

Eberle, J. A.-M., Richter, P., Widmayer, P., Chubanov, V., Gudermann, T., and Breer, H. (2013). Band-like arrangement of taste-like sensory cells at the gastric groove: evidence for paracrine communication. *Front. Physiol.* 4:58. doi: 10.3389/fphys.2013.00058

Eberle, J. A.-M., Widmayer, P., and Breer, H. (2014). Receptors for short-chain fatty acids in brush cells at the "gastric groove". *Front. Physiol.* 5:152. doi: 10.3389/fphys.2014.00152

Engelstoft, M. S., Park, W. M., Sakata, I., Kristensen, L. V., Husted, A. S., Osborne-Lawrence, S., et al. (2013). Seven transmembrane G protein-coupled receptor repertoire of gastric ghrelin cells. *Mol. Metab.* 2, 376–392. doi: 10.1016/j.molmet.2013.08.006

Fraenkel, G. S. (1959). The raison d'Être of secondary plant substances. *Science* 129, 1466–1470. doi: 10.1126/science.129.3361.1466

Frick, C., Martin, H. L., Bruder, J., Lang, K., and Breer, H. (2017). Topographic distribution pattern of morphologically different G cells in the murine antral mucosa. *Eur. J. Histochem.* 61:2810. doi: 10.4081/ejh.2017.2810

Gerbe, F., Sidot, E., Smyth, D. J., Ohmoto, M., Matsumoto, I., Dardalhon, V., et al. (2016). Intestinal epithelial tuft cells initiate type 2 mucosal immunity to helminth parasites. *Nature* 529, 226. doi: 10.1038/nature16527

Gerbe, F., van Es, J. H., Makrini, L., Brulin, B., Mellitzer, G., Robine, S., et al. (2011). Distinct ATOH1 and Neurog3 requirements define tuft cells as a new secretory cell type in the intestinal epithelium. *J. Cell Biol.* 192, 767–780. doi: 10.1083/jcb.201010127

Glendinning, J. I., Yiin, Y.-M., Ackroff, K., and Sclafani, A. (2008). Intragastric infusion of denatonium conditions flavor aversions and delays gastric emptying in rodents. *Physiol. Behav.* 93, 757–765. doi: 10.1016/j.physbeh.2007.11.029

Hariri, B. M., McMahon, D. B., Chen, B., Adappa, N. D., Palmer, J. N., Kennedy, D. W., et al. (2017). Plant flavones enhance antimicrobial activity of respiratory epithelial cell secretions against *Pseudomonas aeruginosa. PLoS One* 12:e0185203. doi: 10.1371/journal.pone.0185203

Hass, N., Schwarzenbacher, K., and Breer, H. (2007). A cluster of gustducin-expressing cells in the mouse stomach associated with two distinct populations of enteroendocrine cells. *Histochem. Cell Biol.* 128, 457–471. doi: 10.1007/s00418-007-0325-3

Hass, N., Schwarzenbacher, K., and Breer, H. (2010). T1R3 is expressed in brush cells and ghrelin-producing cells of murine stomach. *Cell Tissue Res.* 339, 493–504. doi: 10.1007/s00441-009-0907-6

Hayakawa, T., Suzuki-Hashido, N., Matsui, A., and Go, Y. (2014). Frequent expansions of the bitter taste receptor gene repertoire during evolution of mammals in the euarchontoglires clade. *Mol. Biol. Evol.* 31, 2018–2031. doi: 10.1093/molbev/msu144

Höfer, D., Püschel, B., and Drenckhahn, D. (1996). Taste receptor-like cells in the rat gut identified by expression of alpha-gustducin. *Proc. Natl. Acad. Sci. U.S.A.* 93, 6631–6634. doi: 10.1073/pnas.93.13.6631

Howitt, M. R., Lavoie, S., Michaud, M., Blum, A. M., Tran, S. V., Weinstock, J. V., et al. (2016). Tuft cells, taste-chemosensory cells, orchestrate parasite type 2 immunity in the gut. *Science* 351, 1329–1333. doi: 10.1126/science.aaf1648

Janssen, S., Laermans, J., Iwakura, H., Tack, J., and Depoortere, I. (2012). Sensing of fatty acids for octanoylation of ghrelin involves a gustatory G-protein. *PLoS One* 7:e40168. doi: 10.1371/journal.pone.0040168

Janssen, S., Laermans, J., Verhulst, P.-J., Thijs, T., Tack, J., and Depoortere, I. (2011). Bitter taste receptors and α-gustducin regulate the secretion of ghrelin with functional effects on food intake and gastric emptying. *Proc. Natl. Acad. Sci. U.S.A.* 108, 2094–2099. doi: 10.1073/pnas.1011508108

Jeon, T.-I., Seo, Y.-K., and Osborne, T. F. (2011). Gut bitter taste receptor signalling induces ABCB1 through a mechanism involving CCK. *Biochem. J.* 438, 33–37. doi: 10.1042/BJ20110009

Jeon, T.-I., Zhu, B., Larson, J. L., and Osborne, T. F. (2008). SREBP-2 regulates gut peptide secretion through intestinal bitter taste receptor signaling in mice. *J. Clin. Invest.* 118, 3693–3700. doi: 10.1172/JCI36461

Kaji, I., Karaki, S., Fukami, Y., Terasaki, M., and Kuwahara, A. (2009). Secretory effects of a luminal bitter tastant and expressions of bitter taste receptors, T2Rs, in the human and rat large intestine. *Am. J. Physiol. Liver Physiol.* 296, G971–G981. doi: 10.1152/ajpgi.90514.2008

Kaske, S., Krasteva, G., König, P., Kummer, W., Hofmann, T., Gudermann, T., et al. (2007). TRPM5, a taste-signaling transient receptor potential ion-channel, is a ubiquitous signaling component in chemosensory cells. *BMC Neurosci.* 8:49. doi: 10.1186/1471-2202-8-49

Kim, K.-S., Egan, J. M., and Jang, H.-J. (2014). Denatonium induces secretion of glucagon-like peptide-1 through activation of bitter taste receptor pathways. *Diabetologia* 57, 2117–2125. doi: 10.1007/s00125-014-3326-5

Kugler, P., Höfer, D., Mayer, B., and Drenckhahn, D. (1994). Nitric oxide synthase and NADP-linked glucose-6-phosphate dehydrogenase are co-localized in brush cells of rat stomach and pancreas. *J. Histochem. Cytochem.* 42, 1317–1321. doi: 10.1177/42.10.7523487

Kusumakshi, S., Voigt, A., Hübner, S., Hermans-Borgmeyer, I., Ortalli, A., Pyrski, M., et al. (2015). A binary genetic approach to characterize TRPM5 Cells in mice. *Chem. Senses* 40, 413–425. doi: 10.1093/chemse/bjv023

Lee, E. R., Trasler, J., Dwivedi, S., and Leblond, C. P. (1982). Division of the mouse gastric mucosa into zymogenic and mucous regions on the basis of gland features. *Am. J. Anat.* 164, 187–207. doi: 10.1002/aja.1001640302

Lee, R. J., Hariri, B. M., McMahon, D. B., Chen, B., Doghramji, L., Adappa, N. D., et al. (2017). Bacterial d-amino acids suppress sinonasal innate immunity through sweet taste receptors in solitary chemosensory cells. *Sci. Signal.* 10:eaam7703. doi: 10.1126/scisignal.aam7703

Lee, R. J., Kofonow, J. M., Rosen, P. L., Siebert, A. P., Chen, B., Doghramji, L., et al. (2014). Bitter and sweet taste receptors regulate human upper respiratory innate immunity. *J. Clin. Invest.* 124, 1393–1405. doi: 10.1172/JCI72094

Li, D., and Zhang, J. (2014). Diet shapes the evolution of the vertebrate bitter taste receptor gene repertoire. *Mol. Biol. Evol.* 31, 303–309. doi: 10.1093/molbev/mst219

Li, Y., Wu, Q., Deng, Y., Lv, H., Qiu, J., Chi, G., et al. (2015). D(-)-Salicin inhibits the LPS-induced inflammation in RAW264.7 cells and mouse models. *Int. Immunopharmacol.* 26, 286–294. doi: 10.1016/j.intimp.2015.04.016

Liszt, K. I., Hans, J., Ley, J. P., Köck, E., and Somoza, V. (2018). Characterization of bitter compounds via modulation of proton secretion in human gastric parietal cells in culture. *J. Agric. Food Chem.* 66, 2295–2300. doi: 10.1021/acs.jafc.7b01051

Liszt, K. I., Ley, J. P., Lieder, B., Behrens, M., Stöger, V., Reiner, A., et al. (2017). Caffeine induces gastric acid secretion via bitter taste signaling in gastric parietal cells. *Proc. Natl. Acad. Sci. U.S.A.* 114, E6260–E6269. doi: 10.1073/pnas.1703728114

Liu, D., and Liman, E. R. (2003). Intracellular Ca2+ and the phospholipid PIP2 regulate the taste transduction ion channel TRPM5. *Proc. Natl. Acad. Sci. U.S.A.* 100, 15160–15165. doi: 10.1073/pnas.2334159100

Liu, S., Lu, S., Xu, R., Atzberger, A., Günther, S., Wettschureck, N., et al. (2017). Members of bitter taste receptor cluster Tas2r143/Tas2r135/Tas2r126 are expressed in the epithelium of murine airways and other non-gustatory tissues. *Front. Physiol.* 8:849. doi: 10.3389/fphys.2017.00849

Lossow, K., Hübner, S., Roudnitzky, N., Slack, J. P., Pollastro, F., Behrens, M., et al. (2016). Comprehensive analysis of mouse bitter taste receptors reveals different molecular receptive ranges for orthologous receptors in mice and humans. *J. Biol. Chem.* 291, 15358–15377. doi: 10.1074/jbc.M116.718544

Luciano, L., and Reale, E. (1992). The "Limiting Ridge" of the rat stomach. *Arch. Histol. Cytol.* 55(Suppl.), 131–138. doi: 10.1679/aohc.55.Suppl-131

Lund, M. L., Egerod, K. L., Engelstoft, M. S., Dmytriyeva, O., Theodorsson, E., Patel, B. A., et al. (2018). Enterochromaffin 5-HT cells - A major target for GLP-1 and gut microbial metabolites. *Mol. Metab.* 11, 70–83. doi: 10.1016/j.molmet.2018.03.004

Ma, C., He, N., Zhao, Y., Xia, D., Wei, J., and Kang, W. (2019). Antimicrobial mechanism of hydroquinone. *Appl. Biochem. Biotechnol.* 189, 1291–1303. doi: 10.1007/s12010-019-03067-1

Matsunami, H., Montmayeur, J.-P., and Buck, L. B. (2000). A family of candidate taste receptors in human and mouse. *Nature* 404, 601–604. doi: 10.1038/35007072

Montedonico, S., Diez-Pardo, J. A., and Tovar, J. A. (1999). Gastroesophageal reflux after combined lower esophageal sphincter and diaphragmatic crural sling inactivation in the rat. *Dig. Dis. Sci.* 44, 2283–2289. doi: 10.1023/A:1026665022685

Nadjsombati, M. S., McGinty, J. W., Lyons-Cohen, M. R., Jaffe, J. B., DiPeso, L., Schneider, C., et al. (2018). Detection of succinate by intestinal tuft cells triggers a Type 2 innate immune circuit. *Immunity* 49, 33.e–41.e. doi: 10.1016/j.immuni.2018.06.016

O'Neil, A., Petersen, C. P., Choi, E., Engevik, A. C., and Goldenring, J. R. (2017). Unique cellular lineage composition of the first gland of the mouse gastric corpus. *J. Histochem. Cytochem.* 65, 47–58. doi: 10.1369/0022155416678182

Prandi, S., Bromke, M., Hübner, S., Voigt, A., Boehm, U., Meyerhof, W., et al. (2013). A subset of mouse colonic goblet cells expresses the bitter taste receptor Tas2r131. *PLoS One* 8:e82820. doi: 10.1371/journal.pone.0082820

Prandi, S., Voigt, A., Meyerhof, W., and Behrens, M. (2018). Expression profiling of Tas2r genes reveals a complex pattern along the mouse GI tract and the presence of Tas2r131 in a subset of intestinal Paneth cells. *Cell. Mol. Life Sci.* 75, 49–65. doi: 10.1007/s00018-017-2621-y

Rössler, P., Kroner, C., Freitag, J., Noè, J., and Breer, H. (1998). Identification of a phospholipase C beta subtype in rat taste cells. *Eur. J. Cell Biol.* 77, 253–261. doi: 10.1016/s0171-9335(98)80114-3

Rozengurt, E. (2006). Taste receptors in the gastrointestinal tract. I. Bitter taste receptors and α-gustducin in the mammalian gut. *Am. J. Physiol. Liver Physiol.* 291, G171–G177. doi: 10.1152/ajpgi.00073.2006

Rozengurt, N., Wu, S. V., Chen, M. C., Huang, C., Sternini, C., and Rozengurt, E. (2006). Colocalization of the α-subunit of gustducin with PYY and GLP-1 in L cells of human colon. *Am. J. Physiol. Liver Physiol.* 291, G792–G802. doi: 10.1152/ajpgi.00074.2006

Shi, P., Zhang, J., Yang, H., and Zhang, Y. (2003). Adaptive diversification of bitter taste receptor genes in mammalian evolution. *Mol. Biol. Evol.* 20, 805–814. doi: 10.1093/molbev/msg083

Sternini, C., Anselmi, L., and Rozengurt, E. (2008). Enteroendocrine cells: a site of "taste" in gastrointestinal chemosensing. *Curr. Opin. Endocrinol. Diabetes. Obes.* 15, 73–78. doi: 10.1097/MED.0b013e3282f43a73

van der Heijden, M., Zimberlin, C. D., Nicholson, A. M., Colak, S., Kemp, R., Meijer, S. L., et al. (2016). Bcl-2 is a critical mediator of intestinal transformation. *Nat. Commun.* 7:10916. doi: 10.1038/ncomms10916

Vegezzi, G., Anselmi, L., Huynh, J., Barocelli, E., Rozengurt, E., Raybould, H., et al. (2014). Diet-induced regulation of bitter taste receptor subtypes in the mouse gastrointestinal tract. *PLoS One* 9:e107732. doi: 10.1371/journal.pone.0107732

von Moltke, J., Ji, M., Liang, H.-E., and Locksley, R. M. (2016). Tuft-cell-derived IL-25 regulates an intestinal ILC2-epithelial response circuit. *Nature* 529, 221–225. doi: 10.1038/nature16161

Wang, Q., Liszt, K. I., Deloose, E., Canovai, E., Thijs, T., Farré, R., et al. (2019). Obesity alters adrenergic and chemosensory signaling pathways that regulate ghrelin secretion in the human gut. *FASEB J.* 33, 4907–4920. doi: 10.1096/fj.201801661RR

Wattel, W., and Geuze, J. J. (1978). The cells of the rat gastric groove and cardia. *Cell Tissue Res.* 186, 375–391. doi: 10.1007/BF00224928

Widmayer, P., Goldschmid, H., Henkel, H., Küper, M., Königsrainer, A., and Breer, H. (2015). High fat feeding affects the number of GPR120 cells and enteroendocrine cells in the mouse stomach. *Front. Physiol.* 6:53. doi: 10.3389/fphys.2015.00053

Widmayer, P., Hischer, L., Hennemann, K., Kusumakshi, S., Boehm, U., and Breer, H. (2019). Long-chain fatty acid-induced intracellular signaling in GPR120-

expressing brush cells at the limiting ridge of the murine stomach. *Cell Tissue Res.* 376, 71–81. doi: 10.1007/s00441-018-2972-1

Wong, G. T., Gannon, K. S., and Margolskee, R. F. (1996). Transduction of bitter and sweet taste by gustducin. *Nature* 381, 796–800. doi: 10.1038/381 796a0

Wu, S. V., Chen, M. C., and Rozengurt, E. (2005). Genomic organization, expression, and function of bitter taste receptors (T2R) in mouse and rat. *Physiol. Genom.* 22, 139–149. doi: 10.1152/physiolgenomics.00030.2005

Wu, S. V., Rozengurt, N., Yang, M., Young, S. H., Sinnett-Smith, J., and Rozengurt, E. (2002). Expression of bitter taste receptors of the T2R family in the gastrointestinal tract and enteroendocrine STC-1 cells. *Proc. Natl. Acad. Sci. U.S.A.* 99, 2392–2397. doi: 10.1073/pnas.042617699

Xie, C., Wang, X., Young, R. L., Horowitz, M., Rayner, C. K., and Wu, T. (2018). Role of intestinal bitter sensing in enteroendocrine hormone secretion

and metabolic control. *Front. Endocrinol.* 9:576. doi: 10.3389/fendo.2018.00576

Protonation of Piezo1 Impairs Cell-Matrix Interactions of Pancreatic Stellate Cells

Anna Kuntze[1†], Ole Goetsch[1†], Benedikt Fels[2], Karolina Najder[1], Andreas Unger[1], Marianne Wilhelmi[1], Sarah Sargin[1], Sandra Schimmelpfennig[1], Ilka Neumann[1], Albrecht Schwab[1] and Zoltan Pethő[1*]

[1] Institute of Physiology II, University of Münster, Münster, Germany, [2] Institute of Physiology, University of Lübeck, Lübeck, Germany

Pancreatic ductal adenocarcinoma (PDAC) is characterized by an acidic and fibrotic stroma. The extracellular matrix (ECM) causing the fibrosis is primarily formed by pancreatic stellate cells (PSCs). The effects of the altered biomechanics and pH landscape in the pathogenesis of PDAC, however, are poorly understood. Mechanotransduction in cells has been linked to the function of mechanosensitive ion channels such as Piezo1. Here, we tested whether this channel plays crucial roles in transducing mechanical signals in the acidic PDAC microenvironment. We performed immunofluorescence, Ca^{2+} influx and intracellular pH measurements in PSCs and complemented them by live-cell imaging migration experiments in order to assess the function of Piezo1 channels in PSCs. We evaluated whether Piezo1 responds to changes of extracellular and/or intracellular pH in the pathophysiological range (pH 6.6 and pH 6.9, respectively). We validated our results using Piezo1-transfected HEK293 cells as a model system. Indeed, acidification of the intracellular space severely inhibits Piezo1-mediated Ca^{2+} influx into PSCs. In addition, stimulation of Piezo1 channels with its activator Yoda1 accelerates migration of PSCs on a two-dimensional ECM as well as in a 3D setting. Furthermore, Yoda1-activated PSCs transmit more force to the surrounding ECM under physiological pH, as revealed by measuring the dislocation of microbeads embedded in the surrounding matrix. This is paralleled by an enhanced phosphorylation of myosin light chain isoform 9 after Piezo1 stimulation. Intriguingly, upon acidification, Piezo1 activation leads to the initiation of cell death and disruption of PSC spheroids. In summary, stimulating Piezo1 activates PSCs by inducing Ca^{2+} influx which in turn alters the cytoskeletal architecture. This results in increased cellular motility and ECM traction, which can be useful for the cells to invade the surroundings and to detach from the tissue. However, in the presence of an acidic extracellular pH, although net Ca^{2+} influx is reduced, Piezo1 activation leads to severe cell stress also limiting cellular viability. In conclusion, our results indicate a strong interdependence between environmental pH, the mechanical output of PSCs and stromal mechanics, which promotes early local invasion of PDAC cells.

Keywords: piezo1, pancreatic stellate cells, pancreatic cancer, fibrosis, pH homeostasis, cell migration

INTRODUCTION

Pancreatic ductal adenocarcinoma (PDAC) is the most common primary malignant tumor of the exocrine pancreas, and credits for an abysmal prognosis among all forms of cancer. PDAC is characterized by a collagen-rich desmoplastic stroma that compresses the tumor, which thereby reaches hydrostatic pressure levels of up to 100 mmHg (DuFort et al., 2016). In addition, the desmoplastic PDAC microenvironment is markedly acidic reaching even below pH 6.5 (Cruz-Monserrate et al., 2014; Pedersen et al., 2017). Over time the acidic extracellular pH (pH$_e$) can also lead to an acidification of the tightly regulated intracellular pH (pH$_i$) (Riemann et al., 2013). Consequently cellular migration is affected and cell death pathways are initiated in most eukaryotic cells (Martin et al., 2011; Justus et al., 2013; Schwab and Stock, 2014).

In PDAC, the desmoplastic stroma is mainly produced by pancreatic stellate cells (PSCs) (Xue et al., 2018). Activated PSCs have a myofibroblast-like phenotype with expression of markers such as α-smooth muscle actin (αSMA). They are involved in fibrotic remodeling of the extracellular matrix (ECM). In PDAC this leads to the formation of a characteristic tumor niche that insulates tumor cells from the immune system and from the effect of chemotherapeutic drugs (Lonardo et al., 2012). Moreover, PSCs invade the surrounding tissues together with PDAC cells, thus actively facilitating PDAC metastasis (Liu et al., 2019).

Although not studied as extensively as in PDAC cells, it has become clear that Ca^{2+} signaling plays an important role in PSC physiology and pathophysiology (Ferdek and Jakubowska, 2017; Storck et al., 2017). Ca^{2+} signals can be elicited through multiple mediators, e.g., bradykinin, angiotensin, ATP as well as environmental pressure (Hennigs et al., 2011; Won et al., 2011; Fels et al., 2016). Ion channels that have been studied to mediate Ca^{2+} influx in PSCs are manifold, ranging from CRAC channel, P2X$_7$ receptor to a wide array of TRP channels (TRPV4, TRPM7, TRPC1, TRPC3, TRPC6) (Haanes et al., 2012; Fels et al., 2016; Jakubowska et al., 2016; Nielsen et al., 2017; Storck et al., 2017).

Recent evidence implies that activation of Piezo1—a mechanosensitive cation channel that mediates preferentially Ca^{2+} influx upon mechanical stress—is essential for the formation of the fibrotic pancreatic stroma in chronic pancreatitis (Romac et al., 2018). In concordance with this finding, our previous work shows that PSCs express a large amount of Piezo1 mRNA (Fels et al., 2016). Activation of Piezo1 in PSCs would lead to Ca^{2+} influx which in turn prompts a myriad of cellular responses in cancer (Fels et al., 2018; Pethő et al., 2019). These responses include phosphorylation of regulatory myosin light chains (MYLs) and activation of calmodulin-dependent cellular pathways that eventually coordinate gene expression, secretion of extracellular matrix,

cellular contractility and migration, proliferation and cell death (Tsai et al., 2015; Gryshchenko et al., 2016).

Ca^{2+} influx will also lead to the downstream activation of calcium-activated K$^+$ channels (e.g., K$_{Ca}$3.1) which in turn feeds back on Piezo1 channels by their impact on the cell membrane potential (Storck et al., 2017; Pethő et al., 2019). In PDAC the characteristic mechanical properties of the desmoplastic microenvironment are expected to lead to continuous Piezo1 activation and hence, to sustained Ca^{2+} influx. The Ca^{2+} signals could be interpreted by the cells as a stiffness-derived survival signal in case of moderate, controlled Ca^{2+} influx. Another possibility could be that the cells get overloaded by an excessive or prolonged Ca^{2+} signal and enter cell death pathways (Harr and Distelhorst, 2010).

The open probability of Piezo1 can be allosterically enhanced by the small-molecular agonist Yoda1 (Syeda et al., 2015), which is known to induce Ca^{2+} influx in transformed fibroblasts and myofibroblasts (Blythe et al., 2019; Chubinskiy-Nadezhdin et al., 2019). In contrast, Piezo1 can be inhibited by rendering it in an inactive conformation by extracellular acidification below pH 6.9, as demonstrated by a thorough patch clamp study (Bae et al., 2015). While Piezo1 is inherently mechanosensitive even in artificial lipid bilayers (Syeda et al., 2016), it is widely accepted that channel function is fine-tuned in live cells by intracellular tethers such as the actin-myosin cytoskeleton as well as by extracellular tethers such as the ECM (Ranade et al., 2015; Nourse and Pathak, 2017).

We hypothesize that Piezo1-mediated mechanosensation in PSCs is heavily dependent on the pH microenvironment and is fine-tuned by its interaction with intra- and extracellular tethers. In this study, we tested, whether Piezo1 is still active in the presence of an acidic pH$_i$ and/or pH$_e$, conditions that resemble the acidic tumor core. As validation, we inspected the pH-dependence of Piezo1-mediated Ca^{2+} influx in Piezo1-transfected HEK293 cells. Lastly, we investigated Piezo1-cytoskeleton and Piezo1-ECM interactions in PSCs in 2D and 3D systems and whether they are impacted by environmental pH.

MATERIALS AND METHODS

Animal Experiments

Animal experiments were carried out with the approval of the local ethics committee for animal care (*Landesamt für Natur, Umwelt und Verbraucherschutz Nordrhein-Westfalen,* permit number 84-02.05.50.15.010).

Murine PSC Isolation and Culture

PSCs were isolated from healthy wild-type C57BL/6J mice aged 8–12 weeks as described previously (Fels et al., 2016). Briefly, murine pancreata were isolated, and then enzymatically digested with 0.1% collagenase P (Sigma-Aldrich, Merck KGaA, Darmstadt, Germany) for 25 min at 37°C. After centrifugation, the homogenized tissue was resuspended in cell culture medium (DMEM/Ham F12 1:1, supplemented with 10% FCS and 1% penicillin/streptomycin) and seeded onto FCS-coated tissue culture dishes for 2 h. Afterwards, non-adherent cells were forcefully washed off the tissue culture plate, resulting in a

homogeneous PSC culture. PSCs were used for experiments after two passages.

Plasmids and Transfection

The pRK9 plasmid containing Piezo1-IRES-GFP (size 13,701 bp) was kindly provided by Prof. Gary R. Lewin's laboratory. The IRES promoter allows GFP to be transcribed only when Piezo1 has been transcribed, too. To create a suitable control plasmid, we removed the Piezo1 and IRES coding DNA from the plasmid. For this, we applied the restriction enzymes NotI and MscI (New England Biolabs, Ipswitch, MA, USA) to the Piezo1-IRES-GFP plasmid for 1 h at 37°C according to the manufacturer's instructions. Thus, the resulting plasmid was a structurally analogous control plasmid (size 5,411 bp) coding GFP but not the Piezo1 or IRES. Plasmid fragments were separated by gel electrophoresis on 1% agarose gel, then excised and purified using the QIAquick Gel Extraction Kit (Qiagen, Hilden, Germany). Following purification, DNA ends were blunted using the Klenow DNA Polymerase I, and finally, the $3'$ and $5'$ ends were ligated using T4 DNA ligase following the manufacturer's manual (New England Biolabs, Ipswitch, MA, USA).

A total of 25,000 HEK293 cells were seeded in glass-bottom dishes (Cell E&G, San Diego, USA) and after overnight incubation in 10% FCS-supplemented DMEM at 37°C, cells were transiently transfected with either the pRK9 Piezo1-IRES-GFP (HEK$^{Piezo1+}$) or the pRK9-GFP control plasmid (HEK^{GFP+}) using 1 μg plasmid DNA and 40 μl Lipofectamine$^{®}$ 3000 (Sigma-Aldrich, Merck KGaA, Darmstadt, Germany) in Opti-MEM reduced serum media (Thermo Fisher Scientific, Inc., Waltham, MA, USA). Twenty-four to forty-eight hours after transfection, HEK$^{Piezo1+}$ and HEK^{GFP+} cells could be identified in the GFP channel of the fluorescence microscope (Visitron Systems, Puhheim, Germany) and subsequently used for Mn^{2+} quench experiments.

Immunocytochemistry

For immunocytochemistry, 30,000 PSCs were plated onto collagen I (Corning, New York, NY, USA) coated glass coverslips and cultured for 48 h. Following incubation, PSCs were treated with 5 μM Yoda1 (Tocris Bioscience, Bristol, UK) or solvent (0.2% DMSO) for 1 h. To monitor the effects of blebbistatin, cells were additionally treated with 5 μM blebbistatin (Sigma-Aldrich, Merck KGaA, Darmstadt, Germany) for 15 min.

For visualizing Piezo1 membrane expression, live cell staining was performed as described previously by our group (Waschk et al., 2011; Storck et al., 2017). First, cells were blocked with Ringer's solution (122.5 mM NaCl, 5.4 mM KCl, 1.2 mM CaCl$_2$, 0.8 mM MgCl$_2$, 5.5 mM d-glucose and 10.0 mM HEPES, titrated to pH 7.4) supplemented with 1% bovine serum albumin (Sigma-Aldrich, Merck KGaA, Darmstadt, Germany) for 1 h on ice. This was followed by staining with the primary antibody against mPiezo1 (Proteintech, Manchester, UK, #15939-1-AP, 1:200) for 2 h at 4°C. This antibody recognizes an extracellular epitope of the channel protein so that cell permeabilization was not necessary. After washing five times, coverslips were fixed in 3.5% paraformaldehyde for 20 min at 4°C. Afterwards, Alexa 488-conjugated secondary antibody (Invitrogen, Carlsbad, CA, USA,

1:500) was applied for 1 h at room temperature. Finally, after washing 3 times with PBS, 0.1% DAPI (Sigma-Aldrich, Merck KGaA, Darmstadt, Germany) was applied in DAKO mounting solution (DAKO Deutschland GmbH, Hamburg, Germany) and coverslips were mounted onto slides.

For other immunofluorescence assays, fixation was performed on ice using 3.5% paraformaldehyde for 1 h, followed by washing with PBS 3 times. Cells were subsequently permeabilized using 0.25% Triton-X-100 in PBS, then blocked using 10% goat serum for 1 h at room temperature. Primary antibodies against αSMA (Sigma-Aldrich, Merck KGaA, Darmstadt, Germany, #A2547, 1:200), phosphorylated myosin light chain 9 (P-MYL-9; Invitrogen, Carlsbad, CA, USA, 1:100), and non-muscle myosin IIa (NMIIA) (Novus Biologicals, Littleton, CO, USA, 1:100) were applied overnight at 4°C. After washing three times with PBS, Alexa 488-conjugated secondary antibodies against mouse (Invitrogen, Carlsbad, CA, USA, 1:500) and rabbit (Invitrogen, Carlsbad, CA, USA, 1:500) were applied for 1 h at room temperature. Lastly, after washing three times with PBS, 0.1% DAPI was applied in DAKO mounting solution and coverslips were mounted onto slides.

Fluorescent images were acquired using a Zeiss Axiovert 200 inverted fluorescence microscope (Zeiss, Oberkochen, Germany) at 40× or 100× magnification. Quantification of Piezo1 channel density was performed manually by counting bright spots representing channels in 10 rectangular regions of 7.6 μm × 7.6 μm per cell and subtracting the mean number of spots in equivalent extracellular regions. For P-MYL9 and NMIIA immunocytochemistry fluorescence ratios of P-MYL9/NMIIA were assessed in an unpaired manner, as both primary antibodies originate from the same species (rabbit). First, the total cellular P-MYL9 and NMIIA intensities of 30 cells were measured using similar exposure and illumination settings. Afterwards, the amount of P-MYL9 was normalized to the total NMIIA of a randomly assigned cell. To evaluate the effects of blebbistatin, a scoring system was used to measure the stress fibers, the dendrite-like processes and cellular concavities (**Figure 1**).

Western Blot

Western blots of Piezo1, GAPDH, MYL2, and phospho-MYL2 (P-MYL2) were performed as described previously (Bulk et al., 2017). Total protein of PSCs was extracted using radioimmunoprecipitation assay (RIPA) buffer [50 mmol/l Tris, 150 mmol/l NaCl, 0.1% SDS, 0.5% sodium deoxycholate, 1% NP-40, and 1% Complete Mini protease inhibitor (Roche, Mannheim, Germany)]. Protein concentration of the samples was determined with Pierce^{TM} BCA Protein Assay Kit (Thermo Fisher Scientific, Inc., Waltham, MA, USA). Fifteen microgram of denatured total cellular protein was applied to each lane of a 15% polyacrylamide gel for electrophoresis at 80 mV. After overnight transfer to PVDF membranes at 4°C, we blocked the membrane with PBS containing 5% skim milk for 1 h, then incubated the blots with primary antibodies against mPiezo1 (Proteintech, Manchester, UK, #15939-1-AP, 1:100), P-MYL2 (1:500, MYL-Ser19 mouse mAb, #3675 Cell Signaling Technology, Danvers, Ma, USA), or MYL2 (1:500, MYL2 rabbit Ab, #3672 Cell Signaling Technology, Danvers, Ma, USA), and

FIGURE 1 | Blebbistatin scoring system. Scores ranging from 1 to 3 were given for individual pancreatic stellate cells (PSCs) based on three criteria (membrane concavities, stress fibers, and dendritic-like processes), which are characteristic morphological alterations observed in blebbistatin-treated PSCs. The representative images show αSMA immunocytochemistry of PSCs. The membrane concavities are highlighted with orange arrows.

for housekeeping control GAPDH (1:2,000, GAPDH mouse mAb, #ab125247, Abcam, Cambridge, UK) overnight at 4°C. After washing three times with PBS, we applied HRP-conjugated goat-anti rabbit (1:10,000, Goat Anti-Rabbit IgG H&L, #ab6721, Abcam, Cambridge, UK) in case of Piezo1 and P-MYL2; and goat anti mouse secondary antibody (1:10,000, Goat Anti-Mouse IgG H&L, #ab6708, Abcam, Cambridge, UK) in case of MYL2. Chemiluminescence was detected using a commercial detection system (Chemidoc MP, Bio-Rad, Hercules, CA, USA), and band intensities were evaluated with ImageJ.

Calcium Influx Measurement

We applied the Mn^{2+} quench technique to monitor calcium influx into the cells (Merritt et al., 1989; Fels et al., 2016; Nielsen et al., 2017). Mn^{2+} largely mimics Ca^{2+} as it enters cells via similar pathways. In contrast to Ca^{2+} ions, Mn^{2+} ions quench the fluorescence emission of the calcium sensitive dye Fura-2. These experiments are performed at the Ca^{2+} insensitive, isosbestic excitation wavelength of Fura-2. The Mn^{2+}-induced drop of the Fura-2 fluorescence is largely proportional to the transmembrane influx of Ca^{2+}.

After staining the cells with the Ca^{2+}-sensing dye Fura-2-AM (#F1221, Thermo Fisher Scientific, Inc., Waltham, MA,

USA; $6 \mu M$) for 20 min at 37°C in HEPES buffered Ringer's solution, cells were visualized using a ionic imaging setup consisting of a fluorescence microscope, a high-speed shutter and a polychromator (Visitron Systems, Puchheim, Germany). The proper isosbestic excitation wavelength, at which the emission is Ca^{2+} independent, was determined using the Ca^{2+} ionophore ionomycin (not shown). Thereafter, measurements were conducted at an excitation wavelength of 357 nm and fluorescence emission was recorded at 510 nm. Images were acquired in 10 s intervals. The experimental protocol started with an initial 3 min incubation in Ringer's solution. This was followed by another 3 min incubation in a Ca^{2+}-containing, Mn^{2+} supplemented Ringer's solution for the experiments depicted in **Figures 2C, 5A**. For all other measurements we used a Ca^{2+}-free, Mn^{2+} supplemented Ringer's solution (Mn^{2+} Ringer's). The Mn^{2+} concentration in Mn^{2+} Ringer's was $400 \mu M$ in case of PSCs and 1 mM in case of HEK293 cells. Also, in HEK293 cells, GFP caused negligible interference with the Fura-2 signals (not shown).

Data analysis was performed by measuring fluorescence intensities over the whole cell area and correcting it for background fluorescence. The extracted fluorescence intensities F were normalized to the initial fluorescence intensities F_0

FIGURE 2 | Piezo1 is functionally expressed in PCSs. **(A)** Representative Western blots of Piezo1 compared to GAPDH in PSCs, wild-type HEK293 cells (HEK^{WT}) and HEK293 cells transfected with control plasmid (HEK^{GFP+}) or Piezo1 (HEK$^{Piezo1+}$) ($N = 3$). **(B)** Piezo1 immunocytochemistry of non-permabilized PSCs shows homogeneous channel distribution in the cell membrane. **(C)** Representative Mn^{2+}-induced Fura-2 quench traces of PSCs in the presence of 20 μM Yoda1 or equivalent amount of the solvent, 0.075% DMSO (Ctrl). The scatter plots on the right show the respective values of Mn^{2+} quench slopes, the Mn^{2+} entry rate. The black lines indicate mean $\pm$ SEM. ($n = 72$, $N = 3$ for each condition). **(D)** Representative GFP image of Piezo1-transfected HEK293 cells. Only GFP$^+$ cells were evaluated in the Mn^{2+} quench experiments. The bar chart on the right shows the evaluation of GFP signal intensities after control plasmid (HEK^{GFP+}) and Piezo1 (HEK$^{Piezo1+}$) transfection compared to untransfected HEK293 cells with intensities <100. **(E)** HEK293 cell derived Mn^{2+} quench traces in the presence of the solvent 0.025% DMSO or 5 μM Yoda1 in case of HEK^{GFP+} ($n = 82$; $n = 50$, respectively, $N = 3$) or HEK$^{Piezo1+}$ cells ($n = 106$; $n = 60$, respectively, $N = 3$). The scatter plots indicate Mn^{2+} entry rates of individual cells for each condition. The black lines indicate mean $\pm$ SEM. *$p < 0.05$.

determined under control conditions in the presence of Ringer's solution (F/F$_0$). For each cell, slopes of linear regression (ΔF/F$_0$/min) were calculated before and after Mn^{2+} application during intervals of 30 s. Subsequently, the slope after Mn^{2+} application was subtracted by the slope in the presence of Ringer's solution to correct for potential photobleaching. Lastly, for easier interpretation, the inverse value of the Mn^{2+} quench was determined which directly correlates with Ca^{2+} influx.

Determination of the Intracellular pH

We assessed the intracellular pH (pH$_i$) of HEK293 cells using the fluorescent pH indicator BCECF-AM. Prior to the experiment, HCO$_3^-$-buffered cell culture medium was exchanged for the HEPES-buffered Ringer's solution for 15 min to equilibrate pH$_i$ at 37°C. BCECF staining was performed using 1 μM BCECF-AM for 3 min in Ringer's solution (pH 7.4) at 37°C. Afterwards, cells were washed and continuously superfused with Ringer's solution for 3 min, followed by 3 min superfusion of acidified Ringer's

solution (pH 6.6) or Ringer's solution supplemented with 30 mM sodium propionate (Sigma-Aldrich, Merck KGaA, Darmstadt, Germany). To maintain osmolarity the latter replaced 30 mM NaCl. Lastly, for calibration purposes, cells were permeabilized for protons using 1 μM nigericin (Sigma-Aldrich, Merck KGaA, Darmstadt, Germany) and superfused with a modified Ringer's solution (KCl 125 mM, MgCl$_2$ 1 mM, CaCl$_2$ 1 mM, and HEPES 20 mM) titrated to pH 7.5 and pH 6.5. Data were acquired with the same ionic imaging setup used for Ca^{2+} influx measurements measuring with dual excitation wavelengths of 440 and 490 nm and emission wavelength of 510 nm.

During data analysis, fluorescence intensities were measured over the whole cell area and corrected for background fluorescence. Subsequently, the 440 nm$_{ex}$/490 nm$_{ex}$ fluorescence intensity ratios were calculated. As BCECF fluorescence ratio follows a linear trend between pH 6.5 and pH 7.5, two-point calibration was performed using linear regression.

Cell Migration and Spheroid Traction Experiments

Migration of PSCs was monitored using time-lapse video microscopy as described previously (Schwab et al., 2005; Fels et al., 2016). PSCs in cell culture medium were seeded in pre-coated 12.5 cm^2 dishes, Here, the coating matrix mimics the desmoplastic stroma and contained the following: 40 μg/ml laminin (Sigma-Aldrich, Merck KGaA, Darmstadt, Germany), 40 μg/ml fibronectin (Sigma-Aldrich, Merck KGaA, Darmstadt, Germany), 800 μg/ml collagen I (Corning, New York, NY, USA), 12 μg/ml collagen III (Corning, New York, NY, USA), and 5.4 μg/ml collagen IV (BD Biosciences, Heidelberg, Germany). Cell migration was recorded in temperature-controlled chambers (37°C) with CMOS cameras for 12 h at 5 min intervals using the MicroCamLab 3.1 software (Bresser, Rhede, Germany). Quantitative analysis of single cell migration was based on the segmentation of PSC contours using the Amira software suite (Thermo Fisher Scientific, Inc., Waltham, MA, USA). From the segmented cell contours, cell velocity (μm/min) and translocation were calculated as described before (Dieterich et al., 2008). Migration velocity was defined as the displacement of the cell centroid as a function of time. Mean translocation represents the net distance covered during the entire experiment.

For spheroid formation, 5,000 PSCs were inserted into a hanging drop of 40 μL containing 0.31% methylcellulose (Sigma-Aldrich, Merck KGaA, Darmstadt, Germany) in cell culture medium. Spheroids formed spontaneously within 48 h. They were transferred into a modified matrix suitable for spheroid embedding containing 75 μg/ml laminin, 75 μg/ml fibronectin, 4.3 mg/ml collagen I, 27 μg/ml collagen III, and 12 μg/ml collagen IV. The matrix also contained 1 × 1,010 microbeads per ml (FluoSpheres 1 μm, Invitrogen, Carlsbad, CA, USA) to monitor matrix traction. Eighty microliter of matrix containing a spheroid was allowed to polymerize in 12.5 cm^2 tissue culture dishes for 2 h at 37°C in 5% CO$_2$, and subsequently 3 mL cell culture medium was added to the dishes supplemented with 50 ng/ml platelet-derived growth factor (PDGF). The experiments started after an equilibration period of another 2 h at 37°C in a 5% CO$_2$/air atmosphere.

The fate of PSC spheroids in the three-dimensional matrix was monitored using time-lapse video microscopy for a total of 48 h, similarly to the single cell migration assay described above. As a readout of spheroid invasion, the equatorial cross-sectional area of a given spheroid after 24 h was divided by the initial spheroid area at $t = 0$ h. The number of cells detached from the spheroid after 24 h was counted. Spheroids apply a remarkable amount of traction toward the matrix, as visible in **Video 1**. The traction of the matrix was evaluated by quantifying the movement of 10 beads within a maximal radius of 500 μm neighboring the spheroid during a 12 h period. The mean velocity of the beads (μm/h) is a surrogate of the traction of the spheroid toward the surrounding matrix.

Spheroid Histology and Confocal Reflectance Imaging

PSC spheroids were incubated for 24 h at pH 7.4 and pH 6.6 in the presence of 20 μM Yoda1 or vehicle (0.1%

DMSO), respectively. Afterwards, the collagen matrix containing spheroids was scraped off the dishes using a scalpel. Spheroids in the collagen matrix were fixed in 4% paraformaldehyde, 15% saturated picric acid in 100 mM phosphate buffer overnight at 4°C, dehydrated via ascending ethanol series, and embedded in paraffin. For histology, thin sections (5–7 μm) were cut with a rotary microtome (Leica RM 2135), rehydrated, and a routine hematoxylin and eosin stain (HE) was performed. The hematoxylin stains cell nuclei in a blue color, whereas eosin stains the ECM as well as the cytoplasm pink.

To evaluate the consistence of PSC spheroids, first, total cross-sectional area of spheroids was measured in multiple sections of each spheroid. Afterwards, by thresholding according to Li (Li and Tam, 1998), the acellular area within each spheroid could be measured in ImageJ. Spheroid fragmentation was calculated by dividing the acellular spheroid area by total spheroid area.

Assessment of Cellular Viability

MTT assays were performed with matrix-embedded PSC spheroids cultured at pH 7.4 and pH 6.6 with 20 μM Yoda1 or vehicle (0.1% DMSO), respectively, for 24 h. First, spheroids were transferred to a 96-well plate, medium was exchanged for one containing 0.5 mg/ml MTT reagent (Sigma-Aldrich, Merck KGaA, Darmstadt, Germany). Spheroids were incubated at 37°C in 5% CO$_2$ for 2 h. Then medium was discarded and 100 μL DMSO were added in order to dissolve formazan crystals. Absorbance was measured at 546 nm and corrected for absorbance at 650 nm using a multi-well spectrophotometer (Beckman Coulter, Brea, CA, USA). MTT reduction was normalized to absorbance of spheroids cultured at pH 7.4 with vehicle.

Annexin V staining was performed with trypsin-digested PSC spheroids according to manufacturer's instructions. Briefly, PSC spheroids were extracted from the collagen gels manually, washed with PBS and then inserted into tubes containing 0.25% Trypsin-EDTA solution (Sigma-Aldrich, Merck KGaA, Darmstadt, Germany) and shaken at 250 rpm at 37°C for 10 min. After centrifugation at 200 g for 5 min, cells were resuspended in Annexin V binding buffer (Mybiosource, San Diego, CA, USA) and stained with Annexin V conjugated with Alexa 555 (A35108, Invitrogen, Carlsbad, CA, USA, 1:20) at RT for 15 min. Lastly, cells were washed with Annexin V binding buffer and visualized using a fluorescence microscope at 10× magnification in the red fluorescence channel and DIC (Zeiss Axio Observer, Zeiss, Oberkochen, Germany). Annexin V positivity was evaluated by manual thresholding in ImageJ for 3 visual fields per spheroid. Annexin V positive cells were counted and summed for all visual fields and divided by the total number of cells counted in the respective DIC images.

Statistics

Data are presented as mean values ± S.E.M and following test for normality unpaired Student's t-tests or one-way ANOVA were performed with Tukey's *post-hoc* test where applicable using Graphpad Prism 7. Statistical significance was assumed when $p < 0.05$.

RESULTS

Piezo1 Channels Are Expressed in Pancreatic Stellate Cells

We performed Western blot to investigate Piezo1 expression in whole-cell lysates of cell populations investigated in our study: namely in untransfected HEK293 cells, in HEK293 cells transiently transfected with control plasmid or Piezo1 and in PSCs (**Figure 2A**). We found that Piezo1 is abundantly expressed in PSCs, whereas overall Piezo1 was scarcely expressed in both untransfected and transiently transfected HEK293 cells. To visualize membrane expression of Piezo1 in PSCs, we labeled the channel using immunocytochemistry (**Figure 2B**). Piezo1 is expressed homogeneously in the cell membrane at a density of 0.52 ± 0.08 channels/μm^2 ($n = 300$ regions of 30 cells, $N = 3$ experiments). Moreover, to assess functionality of the channels, we measured Piezo1-mediated Ca^{2+} influx using the Mn^{2+} quench technique in the presence or absence of the Piezo1 agonist, Yoda1. Here, we found that 20 μM Yoda1 almost doubles Ca^{2+} influx into PSCs, from 0.29 ± 0.02 to 0.52 ± 0.03 $\Delta F/F_0$/min ($p < 0.0001$, $N = 3$ experiments with $n = 72$ PSCs) (**Figure 2C**).

To validate the specificity of the Yoda1-induced Mn^{2+} quench assay, we compared Ca^{2+} influx into untransfected HEK293 cells with that into HEK293 cells transfected with a control plasmid or with Piezo1 (**Figure 2E**). As overall Piezo1 expression in the transiently transfected HEK293 cell population is low, we only measured Mn^{2+} quench in transfected GFP$^+$ HEK293 cells (**Figure 2D**). GFP intensities of GFP$^+$ control (1,724 $\pm$ 79, $n = 523$) and Piezo1 transfection (2,266 $\pm$ 61, $n = 816$) were proportionately increased compared to wild-type HEK293 autofluorescence with intensities <100 (**Figure 2D**). Untransfected and control transfected HEK293 cells exhibit the same ($p = 0.97$) Yoda1-induced Mn^{2+} quench rate: 0.27 ± 0.02 $\Delta F/F_0$/min ($n = 50$, $N = 3$) and 0.28 ± 0.02 $\Delta F/F_0$/min ($n = 82$, $N = 3$), respectively (**Figure 2E**). In contrast, Piezo1-transfection leads to a 2-fold higher Mn^{2+} quench rate in HEK293 cells (0.55 ± 0.02 $\Delta F/F_0$/min, $n = 106$, $N = 3$). Interestingly and in line with the Western blot results shown in **Figure 2A**, we needed a considerably higher Mn^{2+} concentration for HEK293 cells than for PSCs to elicit comparable quench rates. Piezo1-mediated Ca^{2+} influx is distinctly amplified using 5 μM Yoda1 (0.81 ± 0.03 $\Delta F/F_0$/min, $n = 60$, $N = 3$) compared to solvent (0.025% DMSO) superfusion (**Figure 2E**). Collectively, these results provide evidence that PSCs express Piezo1 channels and that their function can be assessed with the Mn^{2+} quench technique.

Piezo1 Channels Facilitate Pancreatic Stellate Cell Migration and Cell-ECM Interaction

Aiming for a readout of the physiological functions of Piezo1 in PSCs, we investigated whether cellular migration is altered by the Piezo1 activator Yoda1. Indeed, 5 μM Yoda1 stimulate the migration of PSCs seeded on a matrix resembling the desmoplastic matrix found in the PDAC stroma (**Figure 3A**).

Velocity and translocation rise from 0.25 ± 0.01 μm/min and 20.4 ± 2.2 μm ($n = 83$, $N = 3$) under control conditions (0.075% DMSO) to 0.29 ± 0.01 μm/min ($p = 0.0002$) and 41.2 ± 4.3 μm ($p = 0.0089$, $n = 52$, $N = 3$), respectively. The fact that the increase of translocation is more pronounced than that of the velocity indicates a Yoda1-mediated increase in directionality (**Figure 3B**). Further increasing the concentration of Yoda1 to 15 μM lessens the stimulatory effect on PSC migration (velocity 0.27 ± 0.01 μm/min, $p = 0.04$; translocation 32.5 ± 3.6 μm, $p = 0.62$; $n = 47$, $N = 3$ experiments). In the presence of 50 μM Yoda1, PSCs are no longer accelerated (velocity 0.22 ± 0.01 and translocation 17.0 ± 1.4 μm; $n = 36$, $N = 3$) when compared to equivalent vehicle-treated PSCs (0.25 % DMSO; velocity 0.25 ± 0.02 μm/min, $p = 0.09$; translocation 18.6 ± 1.9 μm, $p = 0.48$; $n = 45$, $N = 3$; **Figure 3B**).

We next tested whether the Piezo1 activator Yoda1 also affects the migratory behavior of PSCs in a more physiological three-dimensional environment (**Figure 3C**). To this end we monitored the emigration of PSCs from a spheroid placed in a 3D desmoplastic collagen matrix. The normalized equatorial cross sectional area of PSC spheroids after 24 h increases similarly under control conditions (0.1% DMSO; by 3.5 ± 0.2-fold, $n = 51$ spheroids; $N = 8$) and in the presence of 20 μM Yoda1 (by 3.0 ± 0.2-fold, $n = 54$ spheroids, $N = 8$; $p = 0.06$). However, 20 μM Yoda1 lead to the detachment of more cells from the spheroid (11.0 ± 1.3 cells, $n = 45$ spheroids; $N = 3$) compared to control cells (6.5 ± 0.7 cells, $n = 40$ spheroids; $N = 3$) (**Figure 3C**).

When monitoring PSC emigration from spheroids with live-cell imaging, it was conspicuous that the surrounding matrix was pulled toward the spheroids. We quantified this phenomenon by tracking the movement of microbeads incorporated into the matrix (**Figure 3D**). As judged from the bead movement, spheroids pull on the matrix more vigorously in the presence of 20 μM Yoda1 (11.0 ± 0.4 μm/h, $n = 105$ beads, $N = 3$) compared to DMSO-treated spheroids (9.5 ± 0.4 μm/h, $n = 90$ beads, $N = 3$) (**Video 1**).

Both Intra- and Extracellular Acidification Impair Piezo1 Activity

In order to assess how extracellular and/or intracellular acidification affect Piezo1 function, Piezo1-transfected HEK293 cells were treated with pH 6.6 Ringer's solution ($n = 64$, $N = 3$) and/or with 30 mM sodium propionate ($n = 68$, $N = 3$), respectively (**Figure 4A**). Our pH$_i$ measurements indicate that 30 mM sodium propionate acidify HEK293 cells from pH$_i$ 7.24 to pH$_i$ 6.77 (ΔpH$_i$ = -0.47 $\pm$ 0.01) within 1 min. pH$_i$ then reaches a steady state. In contrast, pH$_i$ acidification occurs much more slowly upon treatment with pH 6.6 Ringer's solution, as pH$_i$ only drops by 0.1 ± 0.002/min. Thus, when assessing Piezo1 function by means of the Mn^{2+} quench technique at $t = 1$ min after the start of the acidification stimulus, we can clearly distinguish between the effect of an intracellular or extracellular acidification.

Acidification of pH$_e$ decreases Ca^{2+} influx into Piezo1-transfected HEK293 cells (**Figure 4B**). The Mn^{2+} quench rate falls from 0.55 ± 0.02 under control conditions (pH$_e$7.4) to

FIGURE 3 | Yoda1-elicited responses in PSCs. **(A)** Trajectories of individual PSCs migrating on a 2D substrate in the absence or presence of 5 μM Yoda1. Trajectories are normalized to common starting points. The radii of the orange circles show the mean translocation in both cases. **(B)** Mean velocity and translocation, respectively, were calculated from the trajectories for a 6-h time span. Five micrometer and 15 μM Yoda1 treatments were compared to 0.075% DMSO (Ctrl), whereas 50 μM Yoda was compared to 0.25% DMSO (Ctrl high DMSO). **(C)** Phase contrast images of spheroids at time points 0 and 24 h show matrix invasion of the vehicle-treated (Ctrl) and 20 μM Yoda1-treated spheroids. The left plot shows spheroid area after 24 h normalized to the initial area at 0 h (Ctrl: $n = 54$, $N = 8$; Yoda1 $n = 51$, $N = 8$). The right plot indicates the number of cells detached from the spheroids (Ctrl: $n = 45$, $N = 8$; Yoda1 $n = 39$, $N = 8$). **(D)** Phase contrast image of 50 ng/ml PDGF-treated PSC spheroid boundary shows microbead traction toward the spheroid (pink lines, see also **Video 1**). Black lines on the scatter plot show mean ± SEM. *$p < 0.05$.
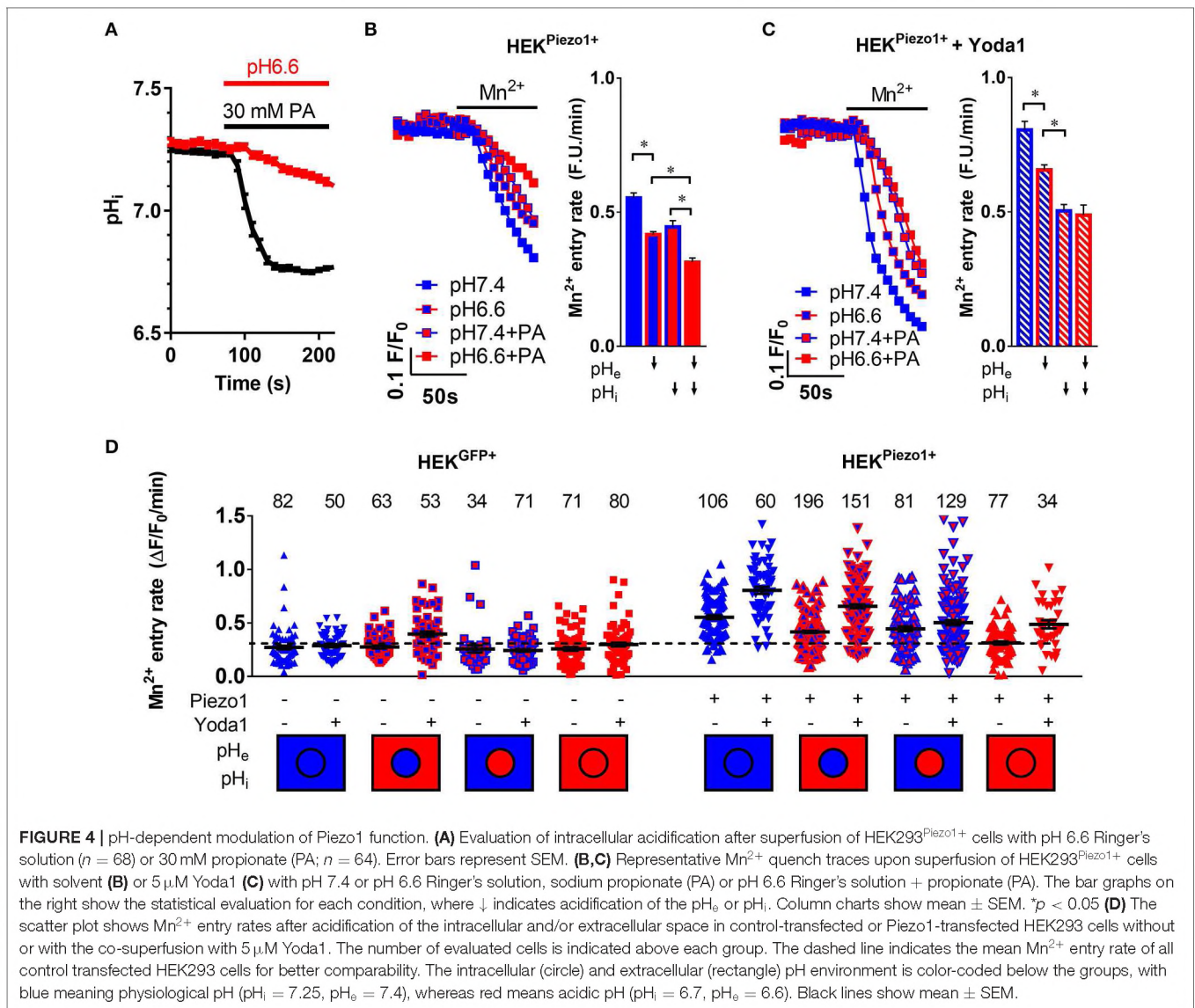
0.42 ± 0.01 $\Delta F/F_0$/min ($n = 196$, $N = 5$; $p < 0.0001$). The acidification of pH_i by sodium propionate elicits a similar effect: 0.45 ± 0.02 $\Delta F/F_0$/min ($n = 81$, $N = 3$; $p < 0.0001$). These effects are additive in Piezo1-transfected HEK293 cells, so that the most pronounced inhibition of Ca^{2+} influx occurs upon dual acidification of the intra- and extracellular space by co-applying pH 6.6 Ringer's solution with 30 mM sodium propionate: 0.31 ± 0.01 $\Delta F/F_0$/min, $n = 77$, $N = 3$; $p < 0.0001$). This combined acidification diminishes the Mn^{2+} quench to a rate that is only 20% higher than that of control plasmid-transfected HEK293 cells (**Figure 4D**).

When Piezo1-transfected HEK293 cells are treated with 5 μM Yoda1, pH_e acidification (0.66 ± 0.02 $\Delta F/F_0$/min, $n = 151$, $N = 4$) as well as pH_i acidification (0.5 ± 0.02 $\Delta F/F_0$/min, $n = 129$, $N = 4$) still impair Ca^{2+} influx (**Figure 4C**). Interestingly, in case of Yoda1 stimulation, intracellular acidification is more effective in inhibiting Ca^{2+} influx than extracellular acidification ($p < 0.0001$), and there appears to be no additional effect of dual acidification (0.48 ± 0.04 $\Delta F/F_0$/min, $n = 34, N = 2$).

Piezo1 Function in PSCs Is Affected by the Cytoskeleton

As it is not known whether Piezo1 is functionally coupled to cytoskeletal tethers in PSCs, we aimed to investigate this by disrupting the actomyosin architecture using the myosin-inhibitor blebbistatin. Upon pre-incubating PSCs with 5 μM blebbistatin for only 15 min, 5 μM of the Piezo1 activator Yoda1 leads to an increase of only 28% in Mn^{2+} quench (0.37 ± 0.02 $\Delta F/F_0$/min, $n = 175$, $N = 3$) (**Figure 5A**). This effect is not due to decreased membrane recruitment of the channel. Immunofluorescence staining of Piezo1 in the plasma membrane showed that the channel density after 5 μM blebbistatin treatment (0.47 ± 0.01 channels/μm) does not differ from that of untreated PSCs ($p = 0.91$, **Figure 5B**). Blebbistatin also causes substantial morphological changes in PSCs, that we evaluated by the criteria shown in **Figure 1**. Compared to control incubation with 0.1% DMSO (membrane concavities: 1.3 ± 0.1; stress fibers: 2.7 ± 0.1; dendrite-like protrusions: 1.3 ± 0.1; $n = 30$, from $N = 3$), PSCs treated with blebbistatin have more membrane concavities (2.7 ± 0.1) and denrite-like protrusions

FIGURE 4 | pH-dependent modulation of Piezo1 function. **(A)** Evaluation of intracellular acidification after superfusion of HEK293$^{Piezo1+}$ cells with pH 6.6 Ringer's solution ($n = 68$) or 30 mM propionate (PA; $n = 64$). Error bars represent SEM. **(B,C)** Representative Mn^{2+} quench traces upon superfusion of HEK293$^{Piezo1+}$ cells with solvent **(B)** or 5 μM Yoda1 **(C)** with pH 7.4 or pH 6.6 Ringer's solution, sodium propionate (PA) or pH 6.6 Ringer's solution + propionate (PA). The bar graphs on the right show the statistical evaluation for each condition, where ↓ indicates acidification of the pH$_e$ or pH$_i$. Column charts show mean ± SEM. *$p < 0.05$ **(D)** The scatter plot shows Mn^{2+} entry rates after acidification of the intracellular and/or extracellular space in control-transfected or Piezo1-transfected HEK293 cells without or with the co-superfusion with 5 μM Yoda1. The number of evaluated cells is indicated above each group. The dashed line indicates the mean Mn^{2+} entry rate of all control transfected HEK293 cells for better comparability. The intracellular (circle) and extracellular (rectangle) pH environment is color-coded below the groups, with blue meaning physiological pH (pH$_i$ = 7.25, pH$_e$ = 7.4), whereas red means acidic pH (pH$_i$ = 6.7, pH$_e$ = 6.6). Black lines show mean ± SEM.

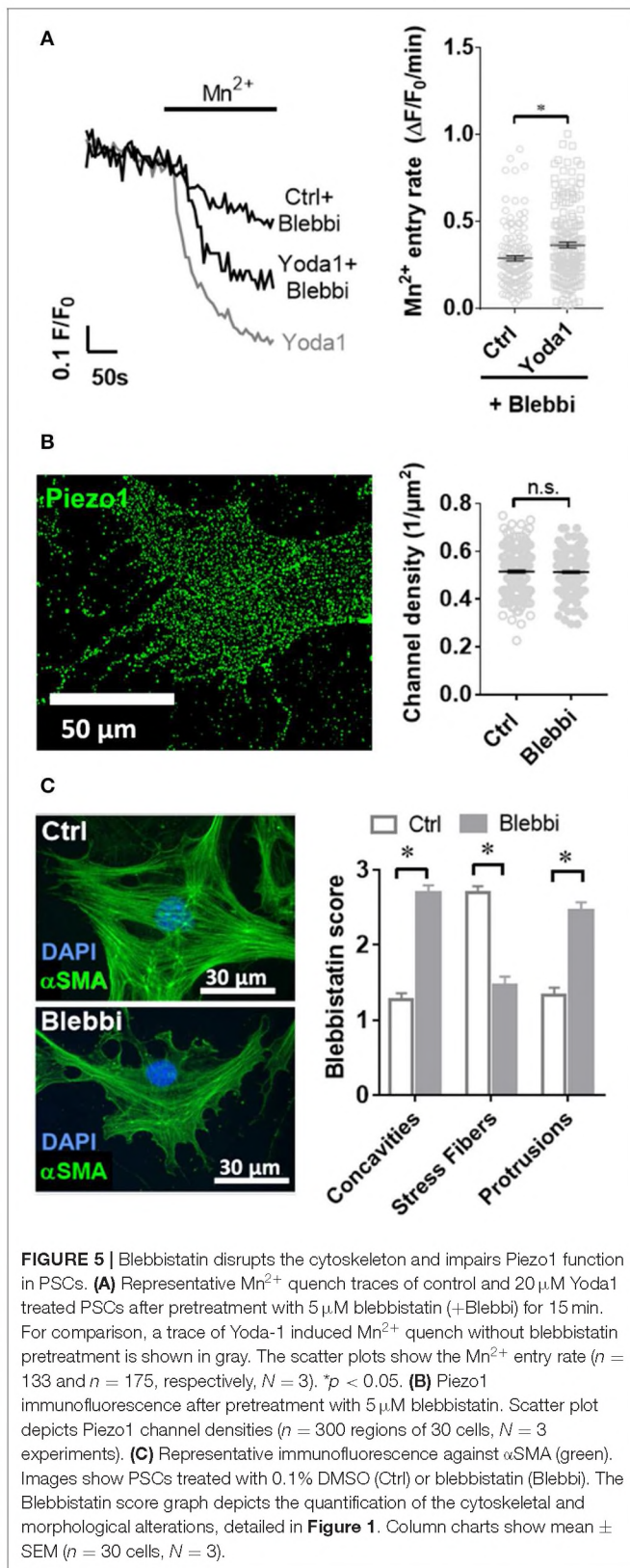(2.5 ± 0.1), but less stress fibers (1.5 ± 0.1; $n = 30$, $N = 3$) (**Figure 5C**).

To elucidate whether Piezo1 modulates cellular contractility, we measured the phosphorylation status of the regulatory myosin light chain MYL9, which is known to have a regulatory role in smooth muscle cells (**Figure 6A**). We performed immunocytochemistry experiments and normalized the staining of P-MYL9 to that of the non-muscle myosin NMIIA. The treatment with 5 μM Yoda1 increased the ratio of P-MYL9/NMIIA from 0.90 ± 0.03 (vehicle-treated cells) to 1.31 ± 0.04 ($n = 90$, $N = 3$ for both conditions; $p < 0.0001$). For comparison, we also measured the phosphorylation status of MYL2, another regulatory myosin light chain that exerts its main function in cardiac muscle. The Western blot analysis comparing the amount of P-MYL2 to MYL2 in PSC cell lysates shows that the phosphorylation of MYL2 is not significantly different in Yoda1-treated cells (1.4 ± 0.4, $n = 5$, $N = 5$ control lysates vs.

3.2 ± 1.2, $n = 4$, $N = 4$ lysates from Yoda1-treated PSCs; $N = 5$ each; $p = 0.17$) (**Figure 6B**).

Acidic pH Disrupts PSC Spheroid Integrity

To get a better understanding of how PSC physiology is affected in the acidic tumor core, we inspected how changes in intra- and extracellular pH affect Piezo1-elicited responses of PSCs. Our results show that Mn^{2+} entry rate in case of pH$_e$ acidification alone (0.23 ± 0.02 $\Delta F/F_0$/min, $n = 57$, $N = 5$) remains analogous to the control pH 7.4 Ringer's perfusion (0.24 ± 0.02 $\Delta F/F_0$/min, $n = 48$, $N = 5$; $p = 0.99$) (**Figure 7A**). On the contrary, intracellular acidification decreases Mn^{2+} entry by 40% (0.14 ± 0.01 $\Delta F/F_0$/min, $n = 45$, $N = 5$; $p = 0.003$) similarly to combined intra- and extracellular acidification (0.16 ± 0.01 $\Delta F/F_0$/min, $n = 46$, $N = 5$; $p = 0.03$). Thus, Ca^{2+} influx and thereby Piezo1 function appears to be predominantly inhibited by an intracellular acidification of PSCs.

FIGURE 5 | Blebbistatin disrupts the cytoskeleton and impairs Piezo1 function in PSCs. **(A)** Representative Mn^{2+} quench traces of control and $20\,\mu M$ Yoda1 treated PSCs after pretreatment with $5\,\mu M$ blebbistatin ($+$Blebbi) for 15 min. For comparison, a trace of Yoda-1 induced Mn^{2+} quench without blebbistatin pretreatment is shown in gray. The scatter plots show the Mn^{2+} entry rate ($n = 133$ and $n = 175$, respectively, $N = 3$). *$p < 0.05$. **(B)** Piezo1 immunofluorescence after pretreatment with $5\,\mu M$ blebbistatin. Scatter plot depicts Piezo1 channel densities ($n = 300$ regions of 30 cells, $N = 3$ experiments). **(C)** Representative immunofluorescence against αSMA (green). Images show PSCs treated with 0.1% DMSO (Ctrl) or blebbistatin (Blebbi). The Blebbistatin score graph depicts the quantification of the cytoskeletal and morphological alterations, detailed in **Figure 1**. Column charts show mean $\pm$ SEM ($n = 30$ cells, $N = 3$).

As PSCs require Ca^{2+} to exert ECM traction, we expected that inhibited Ca^{2+} influx in acidic conditions would impair bead
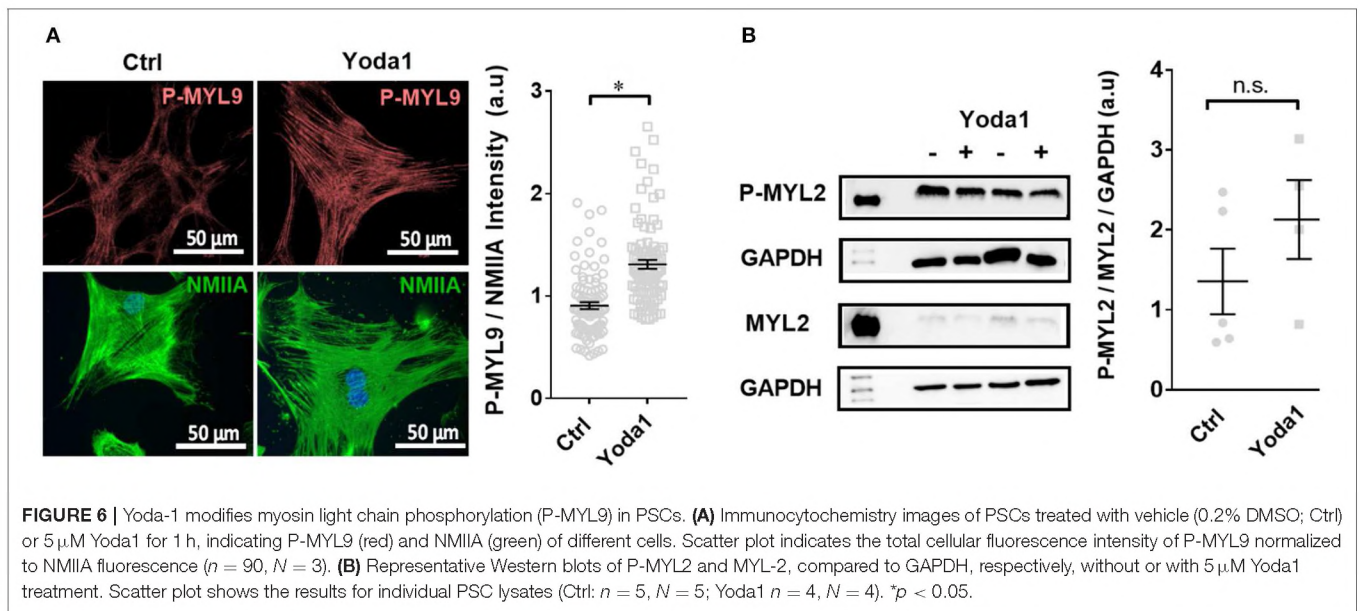
traction in PSC spheroids (**Figure 7B**). Interestingly, it turned out bead displacement toward PSC spheroids at $pH_e6.6$ ($9.5 \pm 0.4\,\mu m/h$, $n = 57$, $N = 5$) is comparable to the displacement at $pH_e7.4$ ($11.0 \pm 0.4\,\mu m/h$, $n = 108$, $N = 5$). Even more intriguingly, in the presence of $20\,\mu M$ Yoda1 at $pH_e6.6$, bead displacement is decreased by 40% ($5.8 \pm 0.3\,\mu m/h$, $n = 37$, $N = 5$). To obtain knowledge regarding the mechanism of these phenomena, we investigated the composition of spheroids at different conditions by hematoxylin and eosin staining (**Figure 7D**). Spheroids treated with $20\,\mu M$ Yoda1 at $pH_e6.6$ are largely fragmented (19.3 ± 1.5 % spheroid cross sectional area, $n = 52$ sections, $N = 3$ spheroids) compared to $pH_e6.6$ alone (6.1 ± 0.5 % area, $n = 35$, $N = 3$, $p < 0.0001$) (**Figure 7C**). In contrast, at $pH_e7.4$ there is no difference between vehicle (5.1 ± 0.4 % area, $n = 58$, $N = 3$) and $20\,\mu M$ Yoda1 treatment (4.5 ± 0.4% area, $n = 42$, $N = 3$, $p = 0.99$). Lastly, we investigated the cellular viability in order to find out whether spheroid fragmentation is due to impaired cell metabolism and viability. MTT reduction normalized to control spheroids cultured at $pH_e7.4$ (1.00 ± 0.07, $n = n = 6$, $N = 3$) is almost halved at $pH_e6.6$ in the presence of $20\,\mu M$ Yoda1 (0.52 ± 0.05, $n = 6$, $N = 3$, $p = 0.03$) (**Figure 7E**). For comparison, MTT reduction in the presence of $20\,\mu M$ Yoda1 at $pH_e7.4$ (1.19 ± 0.07, $n = 6$, $N = 3$, $p = 0.56$) and $pH_e6.6$ cultured spheroids with vehicle treatment (0.82 ± 0.12, $n = 6$, $N = 3$, $p = 0.6$) is not different. However, loss of MTT reduction can also be attributed to decreased proliferation and decreased cell metabolism and is not a specific readout for cell viability in general. Therefore, we also performed Annexin V staining to detect apoptosis (**Figure 7F**). Here, cells derived from spheroids that were treated with Yoda1 and pH 6.6 have approximately twice as many Annexin V positive cells ($31.0\% \pm 4.4$, $n = 6$, $N = 3$) than under control conditions ($16.3\% \pm 2.3$, $n = 6$, $N = 3$, $p = 0.0046$).

DISCUSSION

Research from recent years has shown that activated myofibroblast-like cells such as pancreatic stellate cells, could serve as potential therapeutic targets in fibrotic conditions. PDAC is characterized by a massive fibrosis produced by PSCs (Robinson et al., 2016) which causes a markedly increased tissue pressure and an acidosis inside the desmoplastic tumor tissue. Our study demonstrates that Piezo1 is a prominent transduction channel involved in adapting the behavior of PSCs to the ambient microenvironmental conditions. Our study focused in particular on the impact of the intra- and extracellular pH for Piezo1 and PSC function.

According to the "force through lipid" model the intrinsically mechanosensitive Piezo1 recognizes changes of tension of the neighboring phospholipid bilayer (Teng et al., 2015). In contrast, the "force through tether" model postulates the necessity of associated proteins e.g., laminin or collagens to translate the force applied to the cell membrane (Lewis and Grandl, 2015; Gaub and Muller, 2017). Our findings support the "force through tether" model, as disruption of the cytoskeleton through blebbistatin inhibited Yoda1-induced activation of Piezo1 (**Figure 5A**).

FIGURE 6 | Yoda-1 modifies myosin light chain phosphorylation (P-MYL9) in PSCs. **(A)** Immunocytochemistry images of PSCs treated with vehicle (0.2% DMSO; Ctrl) or 5 μM Yoda1 for 1 h, indicating P-MYL9 (red) and NMIIA (green) of different cells. Scatter plot indicates the total cellular fluorescence intensity of P-MYL9 normalized to NMIIA fluorescence ($n = 90$, $N = 3$). **(B)** Representative Western blots of P-MYL2 and MYL-2, compared to GAPDH, respectively, without or with 5 μM Yoda1 treatment. Scatter plot shows the results for individual PSC lysates (Ctrl: $n = 5$, $N = 5$; Yoda1 $n = 4$, $N = 4$). *$p < 0.05$.

Upon blebbistatin-mediated inhibition of the myosin ATPase, morphological changes in the cytoskeleton of PSCs are also striking. Similar morphological changes were observed in hepatic stellate cells, who also showed decreased cell contraction in the presence of blebbistatin (Liu et al., 2010). Moreover, blebbistatin-treated PSCs are less sensitive to Yoda1 which then no longer induces Ca^{2+} influx into the cells. A reason for that could have been that the overall Piezo1 density decreases upon blebbistatin treatment. However, our immunocytochemistry data declines this possibility. Thus, our results are consistent with the notion that in PSCs, Piezo1 exhibits its downstream effects through its direct or indirect interaction with the cytoskeleton.
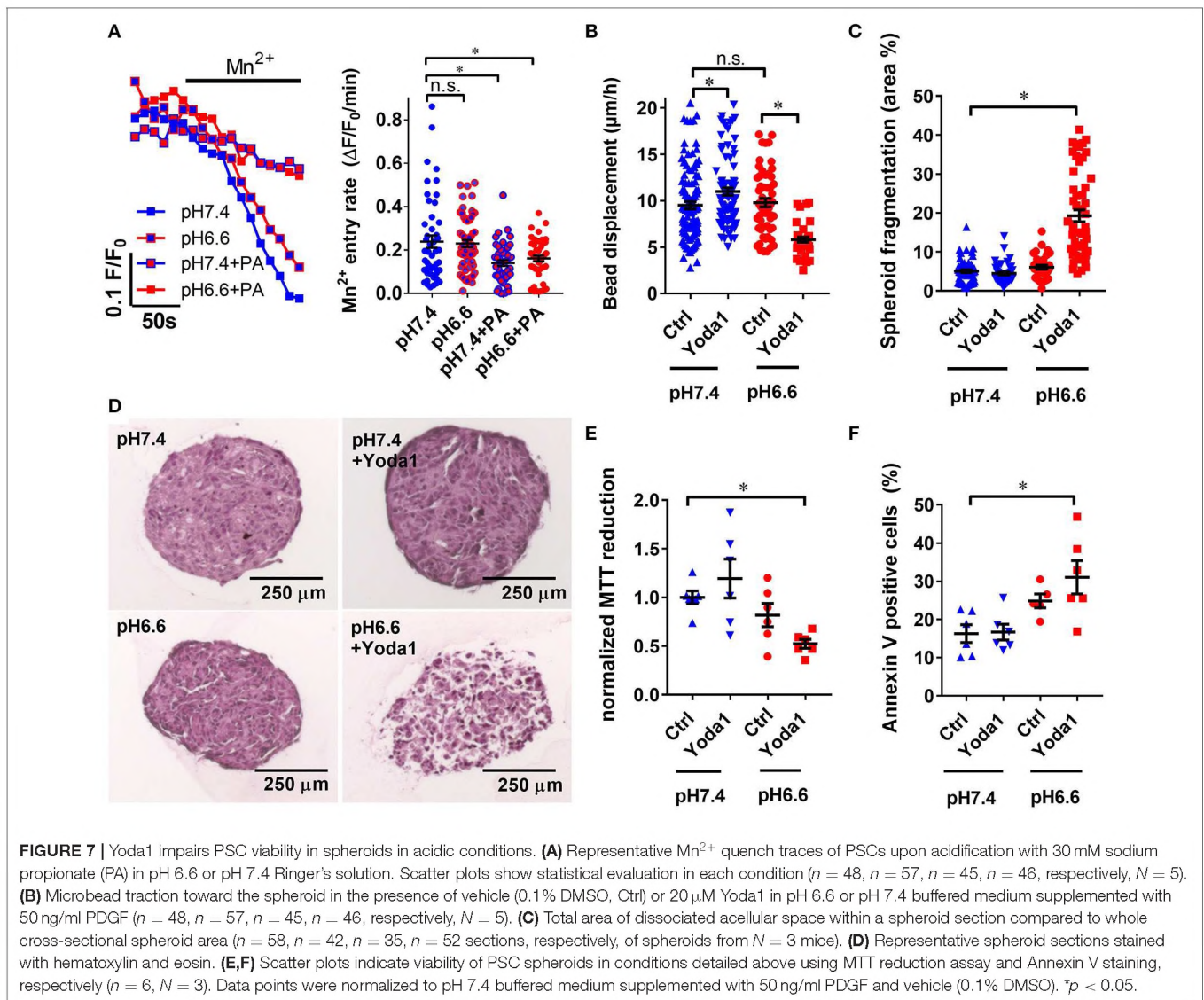
Employing the Piezo1 activator Yoda1, we showed a dose-dependent change in the motility of PSCs plated on a two-dimensional matrix, with enhanced cell migration at lower concentrations and inhibition at high concentrations (**Figure 3**). In contrast, a recent study focused on transformed fibroblasts (Chubinskiy-Nadezhdin et al., 2019) found that similar concentrations of Yoda1 inhibit collective cell migration in wound healing in a dose-dependent manner. Those experiments investigated directed collective cell migration toward the mechano-chemical gradient in wound healing assay. In our 2D setting we investigated the spontaneous undirected cell migration. Thus, the discrepancies may indicate that Piezo1 has a differential role in the distinct forms of cell migration. Furthermore, we did not see a difference in the overall matrix invasion of the 3D spheroid, which is characterized by a collective and directed cell migration from the spheroid core. However, the number of detached cells increased. In another 3D system investigating lymphatic valve formation, Piezo1 also plays an eminent role in the protrusion of valve leaflets, which is associated with collective cell migration (Nonomura et al., 2018). These findings reinforce our hypothesis that Piezo1 acts differently in different cell migration settings and may direct cells to detach from cell aggregates.

The effects seen by using Yoda1 in cell migration studies can be credited to downstream effects of Piezo1-induced Ca^{2+} influx such as those on the contractile apparatus of PSCs. Ca^{2+} influx leads to phosphorylation of myosin light chains such as MYL9 and activation of the myosin II ATPase. This in turn causes retraction of the trailing edge of cells and mediates the polarity of the leading front edge, which are essential for proper cell migration (Vicente-Manzanares et al., 2009). TRPV4, another mechanosensitive ion channel has also been shown to be involved in the retraction of the trailing part of migrating HEK293 cells (Mrkonjic et al., 2015). Also, cell migration is supported by the concomitant activation of Ca^{2+} activated ion channels such as $K_{Ca}3.1$ which trigger a localized volume loss at the rear part of migrating cells (Schwab et al., 2012).

We showed that Piezo1 activation leads to a boosted phosphorylation state of the regulatory myosin light chain P-MYL9, thus further strengthening the cell cortex (**Figure 6**). Even though MYL phosphorylation is impacted by Piezo1, MYL and ion channel function are not interchangeable. First, elevation of $[Ca^{2+}]_i$ through ion channels has many cytoskeleton-independent consequences as reviewed by Gryshchenko et al. (Gryshchenko et al., 2016). Also, interfering with myosins can lead to secondary signaling alterations. This is indicated by the fact that $Myo9b^{-/-}$ dendritic cells have not only impaired migratory capacity but also an altered dendritic cell-T cell interaction (Xu et al., 2014).

We did not observe any changes in total cellular MYL2 phosphorylation in Western blot, which is in line with our work on endothelial cells (Prystopiuk et al., 2018). This phenomenon argues for localized phosphorylation of myosin light chains in the cell cortical area. A beautiful example of such a localized signaling complex has been described in the recent work of Ellefsen et al. where they have shown that traction forces generated by myosin II evoke Piezo1-dependent localized Ca^{2+} flickers (Ellefsen et al., 2019).

FIGURE 7 | Yoda1 impairs PSC viability in spheroids in acidic conditions. **(A)** Representative Mn^{2+} quench traces of PSCs upon acidification with 30 mM sodium propionate (PA) in pH 6.6 or pH 7.4 Ringer's solution. Scatter plots show statistical evaluation in each condition ($n = 48$, $n = 57$, $n = 45$, $n = 46$, respectively, $N = 5$). **(B)** Microbead traction toward the spheroid in the presence of vehicle (0.1% DMSO, Ctrl) or 20 μM Yoda1 in pH 6.6 or pH 7.4 buffered medium supplemented with 50 ng/ml PDGF ($n = 48$, $n = 57$, $n = 45$, $n = 46$, respectively, $N = 5$). **(C)** Total area of dissociated acellular space within a spheroid section compared to whole cross-sectional spheroid area ($n = 58$, $n = 42$, $n = 35$, $n = 52$ sections, respectively, of spheroids from $N = 3$ mice). **(D)** Representative spheroid sections stained with hematoxylin and eosin. **(E,F)** Scatter plots indicate viability of PSC spheroids in conditions detailed above using MTT reduction assay and Annexin V staining, respectively ($n = 6$, $N = 3$). Data points were normalized to pH 7.4 buffered medium supplemented with 50 ng/ml PDGF and vehicle (0.1% DMSO). *$p < 0.05$.

Another Ca^{2+} signaling mediator that may be affected after Piezo1-induced Ca^{2+} influx is bradykinin, which is implicated to have key physiological functions in PSCs through the bradykinin receptor 2 (Won et al., 2011; Gryshchenko et al., 2016). This is further supported by the fact that bradykinin in return potentiates Piezo2 currents (Borbiro and Rohacs, 2017). These findings imply that after initial PSC activation by bradykinin, Piezo channel function may be potentiated in PSCs and cause an enhanced Ca^{2+} influx.

Tumor tissue is not only characterized by an increased matrix elasticity, but also by a marked interstitial acidosis. Our experiments showed in a large sample of cells that Piezo1 is modified through extracellular and intracellular acidosis in a partly additive manner (**Figures 4B,C**). Our observation, that an intracellular acidification with propionate leads to a stronger inhibition of Mn^{2+} quench, is very well in line with the thorough patch-clamp based study of Bae et al., where protonation of Piezo1 was shown to stabilize the channel in an inactivated

state (Bae et al., 2015). Another possibility is that the short chain fatty acid propionate directly interacts with the channel and/or modifies the biophysical properties of the cell membrane. As fatty acids have been described to fine-tune the function of Piezo1 (Romero et al., 2019), this may indeed contribute to the effects seen by our propionate treatment. On the other hand, the inhibitory effect of a propionate-induced intracellular acidification might have been underestimated. Exposing cells to 30 mM propionate causes a substantial cell swelling which could increase membrane tension and thereby constitute a trigger for Piezo1 activation.

In prolonged extracellular acidosis, the pH_i of stromal cells becomes acidic as well. Under these conditions Piezo1 is likely to not fully function, as demonstrated by our experiments with HEK293 cells (**Figures 4B,C**) and PSCs (**Figure 7A**). This indeed seems to have an important protective function for the cells. When acid-primed PSCs are treated with the Piezo1 activator Yoda1, there is less traction applied to the matrix indicated

by the decreased bead displacement (**Figure 7B**). Also, MTT reduction becomes decreased (**Figure 7D**). Both findings point to a severe loss of spheroid integrity. This loss can be accredited to Ca^{2+} overload and a subsequent induction of cell death which is also supported by the fragmentation of the spheroid (**Figure 7C**). The decreased viability of Yoda-1 treated acid-stressed spheroids is confirmed by increased Annexin V positivity of cells derived from the spheroid (**Figure 7E**). Besides apoptosis, a supplementary explanation for the loss of spheroid integrity could be that due to the acidic environment PSCs lose attachment from neighboring cells in a similar manner as we observed previously in melanoma cells (Hofschroer et al., 2017). Along these lines, the fragmentation of the spheroids can be explained by prolonged cell contraction and acidosis-induced loss of cell-to-cell contact.

In conclusion, our study shows that Piezo1 in PSCs is in close cooperation with the cytoskeleton and is sensitive to changes in extra- and intracellular pH. Although the desmoplastic tissue of PDAC exerts a massive mechanical stress onto the cells, the marked tissue acidosis in the tumor core renders Piezo1 less responsive, thus less active in PSCs and cells do not undergo cell death. Because of this protective effect, PSCs may survive to migrate into the well-perfused invasive border of the tumor, where Piezo1 is fully responding to mechanical cues due to the lack of protonation-caused inhibition.

DATA AVAILABILITY STATEMENT

The datasets generated for this study are available on request to the corresponding author.

ETHICS STATEMENT

The animal study was reviewed and approved by Landesamt für Natur, Umwelt und Verbraucherschutz Nordrhein-Westfalen, permit number 84-02.05.50.15.010.

AUTHOR CONTRIBUTIONS

AK was involved in all experiments regarding PSCs, focusing on cell migration, immunofluorescence and Mn^{2+} quench experiments under the guidance of BF, who was involved in interpreting the results and data analysis. OG performed all Mn^{2+} quench and pH measurements with HEK293 cells. SSa created and validated the control plasmid. SSc and IN performed Western blots and analyzed cell migration experiments. AU and MW performed histological analyses of PSC spheroids. AS supervised the project interpreted the data and edited the manuscript with the help of KN. ZP coordinated the project and drafted the manuscript. All authors approved the final version of the manuscript.

SUPPLEMENTARY MATERIAL

The Supplementary Material for this article can be found online at: https://www.frontiersin.org/articles/10.3389/fphys.2020.00089/full#supplementary-material

Video 1 | Extracellular matrix traction by pancreatic stellate cell spheroids.

REFERENCES

Bae, C., Sachs, F., and Gottlieb, P. A. (2015). Protonation of the human PIEZO1 ion channel stabilizes inactivation. *J. Biol. Chem.* 290, 5167–5173. doi: 10.1074/jbc.M114.604033

Blythe, N. M., Stylianidis, V., Ludlow, M. J., Gilbert, H. T. J., Evans, E. L., Cuthbertson, K., et al. (2019). Stimulation of cardiac fibroblast Piezo1 channels opposes myofibroblast differentiation and induces IL-6 secretion via Ca^{2+}-mediated p38 MAP kinase activation. *bioRxiv*. 603456. doi: 10.1101/603456

Borbiro, I., and Rohacs, T. (2017). Regulation of piezo channels by cellular signaling pathways. *Curr. Top. Membr.* 79, 245–261. doi: 10.1016/bs.ctm.2016.10.002

Bulk, E., Kramko, N., Liashkovich, I., Glaser, F., Schillers, H., Schnittler, H. J., et al. (2017). KCa3.1 channel inhibition leads to an ICAM-1 dependent increase of cell-cell adhesion between A549 lung cancer and HMEC-1 endothelial cells. *Oncotarget* 8, 112268–112282. doi: 10.18632/oncotarget.22735

Chubinskiy-Nadezhdin, V. I., Vasileva, V. Y., Vassilieva, I. O., Sudarikova, A. V., Morachevskaya, E. A., and Negulyaev, Y. A. (2019). Agonist-induced Piezo1 activation suppresses migration of transformed fibroblasts. *Biochem. Biophys. Res. Commun.* 514, 173–179. doi: 10.1016/j.bbrc.2019.04.139

Cruz-Monserrate, Z., Roland, C. L., Deng, D., Arumugam, T., Moshnikova, A., Andreev, O. A., et al. (2014). Targeting pancreatic ductal adenocarcinoma acidic microenvironment. *Sci. Rep.* 4:4410. doi: 10.1038/srep 04410

Dieterich, P., Klages, R., Preuss, R., and Schwab, A. (2008). Anomalous dynamics of cell migration. *Proc. Natl. Acad. Sci. U.S.A.* 105, 459–463. doi: 10.1073/pnas.0707603105

DuFort, C. C., DelGiorno, K. E., Carlson, M. A., Osgood, R. J., Zhao, C., Huang, Z., et al. (2016). Interstitial pressure in pancreatic ductal adenocarcinoma is dominated by a gel-fluid phase. *Biophys. J.* 110, 2106–2119. doi: 10.1016/j.bpj.2016.03.040

Ellefsen, K. L., Holt, J. R., Chang, A. C., Nourse, J. L., Arulmoli, J., Mekhdjian, A. H., et al. (2019). Myosin-II mediated traction forces evoke localized Piezo1-dependent Ca(2+) flickers. *Commun. Biol.* 2:298. doi: 10.1038/s42003-019-0514-3

Fels, B., Bulk, E., Pethő, Z., and Schwab, A. (2018). The role of TRP channels in the metastatic cascade. *Pharmaceuticals.* 11:48. doi: 10.3390/ph11020048

Fels, B., Nielsen, N., and Schwab, A. (2016). Role of TRPC1 channels in pressure-mediated activation of murine pancreatic stellate cells. *Eur. Biophys. J.* 45, 657–670. doi: 10.1007/s00249-016-1176-4

Ferdek, P. E., and Jakubowska, M. A. (2017). Biology of pancreatic stellate cells-more than just pancreatic cancer. *Pflugers Arch.* 469, 1039–1050. doi: 10.1007/s00424-017-1968-0

Gaub, B. M., and Muller, D. J. (2017). Mechanical stimulation of piezo1 receptors depends on extracellular matrix proteins and directionality of force. *Nano Lett.* 17, 2064–2072. doi: 10.1021/acs.nanolett.7b00177

Gryshchenko, O., Gerasimenko, J. V., Gerasimenko, O. V., and Petersen, O. H. (2016). Calcium signalling in pancreatic stellate cells: mechanisms and potential roles. *Cell Calcium* 59, 140–144. doi: 10.1016/j.ceca.2016. 02.003

Haanes, K. A., Schwab, A., and Novak, I. (2012). The P2X7 receptor supports both life and death in fibrogenic pancreatic stellate cells. *PLoS ONE* 7:e51164. doi: 10.1371/journal.pone.0051164

Harr, M. W., and Distelhorst, C. W. (2010). Apoptosis and autophagy: decoding calcium signals that mediate life or death. *Cold Spring Harb. Perspect. Biol.* 2:a005579. doi: 10.1101/cshperspect.a0 05579

Hennigs, J. K., Seiz, O., Spiro, J., Berna, M. J., Baumann, H. J., Klose, H., et al. (2011). Molecular basis of P2-receptor-mediated calcium signaling in activated pancreatic stellate cells. *Pancreas* 40, 740–746. doi: 10.1097/MPA.0b013e31821b5b68

Hofschroer, V., Koch, K. A., Ludwig, F. T., Friedl, P., Oberleithner, H., Stock, C., et al. (2017). Extracellular protonation modulates cell-cell interaction mechanics and tissue invasion in human melanoma cells. *Sci. Rep.* 7:42369. doi: 10.1038/srep 42369

Jakubowska, M. A., Ferdek, P. E., Gerasimenko, O. V., Gerasimenko, J. V., and Petersen, O. H. (2016). Nitric oxide signals are interlinked with calcium signals in normal pancreatic stellate cells upon oxidative stress and inflammation. *Open Biol.* 6:160149. doi: 10.1098/rsob.160149

Justus, C. R., Dong, L., and Yang, L. V. (2013). Acidic tumor microenvironment and pH-sensing G protein-coupled receptors. *Front. Physiol.* 4:354. doi: 10.3389/fphys.2013.00354

Lewis, A. H., and Grandl, J. (2015). Mechanical sensitivity of Piezo1 ion channels can be tuned by cellular membrane tension. *Elife* 4:e12088. doi: 10.7554/eLife.120 88.010

Li, C. H., and Tam, P. K. S. (1998). An iterative algorithm for minimum cross entropy thresholding. *Pattern Recogn. Lett.* 19, 771–776. doi: 10.1016/S0167-8655(98)00057-9

Liu, S. L., Cao, S. G., Li, Y., Sun, B., Chen, D., Wang, D. S., et al. (2019). Pancreatic stellate cells facilitate pancreatic cancer cell viability and invasion. *Oncol. Lett.* 17, 2057–2062. doi: 10.3892/ol.201 8.9816

Liu, Z., van Grunsven, L. A., Van Rossen, E., Schroyen, B., Timmermans, J. P., Geerts, A., et al. (2010). Blebbistatin inhibits contraction and accelerates migration in mouse hepatic stellate cells. *Br. J. Pharmacol.* 159, 304–315. doi: 10.1111/j.1476-5381.2009.00477.x

Lonardo, E., Frias-Aldeguer, J., Hermann, P. C., and Heeschen, C. (2012). Pancreatic stellate cells form a niche for cancer stem cells and promote their self-renewal and invasiveness. *Cell Cycle* 11, 1282–1290. doi: 10.4161/cc.19679

Martin, C., Pedersen, S. F., Schwab, A., and Stock, C. (2011). Intracellular pH gradients in migrating cells. *Am. J. Physiol. Cell. Physiol.* 300, C490–495. doi: 10.1152/ajpcell.002 80.2010

Merritt, J. E., Jacob, R., and Hallam, T. J. (1989). Use of manganese to discriminate between calcium influx and mobilization from internal stores in stimulated human neutrophils. *J. Biol. Chem.* 264, 1522–1527.

Mrkonjic, S., Garcia-Elias, A., Pardo-Pastor, C., Bazellieres, E., Trepat, X., Vriens, J., et al. (2015). TRPV4 participates in the establishment of trailing adhesions and directional persistence of migrating cells. *Pflugers Arch.* 467, 2107–2119. doi: 10.1007/s00424-014-1679-8

Nielsen, N., Kondratska, K., Ruck, T., Hild, B., Kovalenko, I., Schimmelpfennig, S., et al. (2017). TRPC6 channels modulate the response of pancreatic stellate cells to hypoxia. *Pflugers Arch.* 469, 1567–1577. doi: 10.1007/s00424-017-2057-0

Nonomura, K., Lukacs, V., Sweet, D. T., Goddard, L. M., Kanie, A., Whitwam, T., et al. (2018). Mechanically activated ion channel PIEZO1 is required for

lymphatic valve formation. *Proc. Natl. Acad. Sci. U.S.A.* 115, 12817–12822. doi: 10.1073/pnas.1817070115

Nourse, J. L., and Pathak, M. M. (2017). How cells channel their stress: interplay between Piezo1 and the cytoskeleton. *Semin. Cell. Dev. Biol.* 71, 3–12. doi: 10.1016/j.semcdb.2017. 06.018

Pedersen, S. F., Novak, I., Alves, F., Schwab, A., and Pardo, L. A. (2017). Alternating pH landscapes shape epithelial cancer initiation and progression: focus on pancreatic cancer. *Bioessays* 39:1600253. doi: 10.1002/bies.201600253

Pethő, Z., Najder, K., Bulk, E., and Schwab, A. (2019). Mechanosensitive ion channels push cancer progression. *Cell Calcium* 80, 79–90. doi: 10.1016/j.ceca.2019. 03.007

Prystopiuk, V., Fels, B., Simon, C. S., Liashkovich, I., Pasrednik, D., Kronlage, C., et al. (2018). A two-phase response of endothelial cells to hydrostatic pressure. *J. Cell Sci.* 131:jcs206920. doi: 10.1242/jcs.206920

Ranade, S. S., Syeda, R., and Patapoutian, A. (2015). Mechanically activated ion channels. *Neuron* 87, 1162–1179. doi: 10.1016/j.neuron.2015.08.032

Riemann, A., Ihling, A., Schneider, B., Gekle, M., and Thews, O. (2013). Impact of extracellular acidosis on intracellular pH control and cell signaling in tumor cells. *Adv. Exp. Med. Biol.* 789, 221–228. doi: 10.1007/978-1-4614-7411-1_30

Robinson, B. K., Cortes, E., Rice, A. J., Sarper, M., and Del Rio Hernandez, A. (2016). Quantitative analysis of 3D extracellular matrix remodelling by pancreatic stellate cells. *Biol. Open* 5, 875–882. doi: 10.1242/bio.0 17632

Romac, J. M., Shahid, R. A., Swain, S. M., Vigna, S. R., and Liddle, R. A. (2018). Piezo1 is a mechanically activated ion channel and mediates pressure induced pancreatitis. *Nat. Commun.* 9:1715. doi: 10.1038/s41467-018-04194-9

Romero, L. O., Massey, A. E., Mata-Daboin, A. D., Sierra-Valdez, F. J., Chauhan, S. C., Cordero-Morales, J. F., et al. (2019). Dietary fatty acids fine-tune Piezo1 mechanical response. *Nat. Commun.* 10:1200. doi: 10.1038/s41467-019-09055-7

Schwab, A., Fabian, A., Hanley, P. J., and Stock, C. (2012). Role of ion channels and transporters in cell migration. *Physiol. Rev.* 92, 1865–1913. doi: 10.1152/physrev.0001 8.2011

Schwab, A., Rossmann, H., Klein, M., Dieterich, P., Gassner, B., Neff, C., et al. (2005). Functional role of Na+-HCO3- cotransport in migration of transformed renal epithelial cells. *J. Physiol.* 568(Pt 2), 445–458. doi: 10.1113/jphysiol.2005.092957

Schwab, A., and Stock, C. (2014). Ion channels and transporters in tumour cell migration and invasion. *Philos. Trans. R. Soc. Lond. B Biol. Sci.* 369:20130102. doi: 10.1098/rstb.2013.0102

Storck, H., Hild, B., Schimmelpfennig, S., Sargin, S., Nielsen, N., Zaccagnino, A., et al. (2017). Ion channels in control of pancreatic stellate cell migration. *Oncotarget* 8, 769–784. doi: 10.18632/oncotarget. 13647

Syeda, R., Florendo, M. N., Cox, C. D., Kefauver, J. M., Santos, J. S., Martinac, B., et al. (2016). Piezo1 channels are inherently mechanosensitive. *Cell. Rep.* 17, 1739–1746. doi: 10.1016/j.celrep.2016. 10.033

Syeda, R., Xu, J., Dubin, A. E., Coste, B., Mathur, J., Huynh, T., et al. (2015). Chemical activation of the mechanotransduction channel Piezo1. *Elife* 4:e07369. doi: 10.7554/eLife.07369.008

Teng, J., Loukin, S., Anishkin, A., and Kung, C. (2015). The force-from-lipid (FFL) principle of mechanosensitivity, at large and in elements. *Pflugers Arch.* 467, 27–37. doi: 10.1007/s00424-014-1530-2

Tsai, F. C., Kuo, G. H., Chang, S. W., and Tsai, P. J. (2015). Ca^{2+} signaling in cytoskeletal reorganization, cell migration, and cancer metastasis. *Biomed. Res. Int.* 2015:409245. doi: 10.1155/2015/4 09245

Vicente-Manzanares, M., Ma, X., Adelstein, R. S., and Horwitz, A. R. (2009). Non-muscle myosin II takes centre stage in cell adhesion and migration. *Nat. Rev. Mol. Cell Biol.* 10, 778–790. doi: 10.1038/nrm2786

Waschk, D. E., Fabian, A., Budde, T., and Schwab, A. (2011). Dual-color quantum dot detection of a heterotetrameric potassium channel (hKCa3.1). *Am. J. Physiol. Cell Physiol.* 300, C843–849. doi: 10.1152/ajpcell.000 53.2010

Won, J. H., Zhang, Y., Ji, B., Logsdon, C. D., and Yule, D. I. (2011). Phenotypic changes in mouse pancreatic stellate cell Ca^{2+} signaling events following activation in culture and in a disease model of pancreatitis. *Mol. Biol. Cell* 22, 421–436. doi: 10.1091/mbc.e10-10-0807

Xu, Y., Pektor, S., Balkow, S., Hemkemeyer, S. A., Liu, Z., Grobe, K., et al. (2014). Dendritic cell motility and T cell activation requires regulation of Rho-cofilin signaling by the Rho-GTPase activating protein myosin IXb. *J. Immunol.* 192, 3559–3568. doi: 10.4049/jimmunol.13 00695

Xue, R., Jia, K., Wang, J., Yang, L., Wang, Y., Gao, L., et al. (2018). A rising star in pancreatic diseases: pancreatic stellate cells. *Front. Physiol.* 9:754. doi: 10.3389/fphys.2018.00754

Tuft Cell Formation Reflects Epithelial Plasticity in Pancreatic Injury: Implications for Modeling Human Pancreatitis

Kathleen E. DelGiorno[1*†], Razia F. Naeem[1†], Linjing Fang[2], Chi-Yeh Chung[1‡], Cynthia Ramos[1], Natalie Luhtala[3], Carolyn O'Connor[4], Tony Hunter[3], Uri Manor[2] and Geoffrey M. Wahl[1*]

[1] Gene Expression Laboratory, Salk Institute for Biological Studies, La Jolla, CA, United States, [2] Waitt Advanced Biophotonics Center, Salk Institute for Biological Studies, La Jolla, CA, United States, [3] Molecular and Cell Biology Laboratory, Salk Institute for Biological Studies, La Jolla, CA, United States, [4] Flow Cytometry Core, Salk Institute for Biological Studies, La Jolla, CA, United States

Chronic pancreatitis, a known risk factor for the development of pancreatic ductal adenocarcinoma (PDA), is a serious, widespread medical condition characterized by inflammation, fibrosis, and acinar to ductal metaplasia (ADM). ADM is a cell type transdifferentiation event where pancreatic acinar cells become ductal-like under conditions of injury or oncogenic mutation. Here, we show that chronic pancreatitis and ADM in genetically wild type mice results in the formation of a significant population of chemosensory tuft cells. Transcriptomic analyses of pancreatitis tuft cells identify expression of inflammatory mediators, consistent with a role for tuft cells in injury progression and/or resolution. Though similar to tuft cell populations in other organs and disease systems, we identified a number of key differences that suggest context-specific tuft cell functions. We evaluated seven different mouse strains for tuft cell formation in response to chronic injury and identified significant heterogeneity reflecting varying proclivity for epithelial plasticity between strains. These results have interesting implications in the role of epithelial plasticity and heterogeneity in pancreatitis and highlight the importance of mouse strain selection when modeling human disease.

Keywords: tuft cells, Dclk1, pancreatitis, metaplasia, mouse models

INTRODUCTION

Pancreatitis, the third leading cause of gastrointestinal-related hospitalizations, is a serious medical condition characterized by inflammation of the exocrine pancreas. Major risk factors include gallstones and alcohol abuse; however, pancreatitis can also result from use of certain medications, autoimmune diseases, infection, trauma, metabolic disorders, surgery, or mutations in genes associated with digestive enzymes (such as *Prss1*) (Whitcomb, 2013). Pancreatitis presents in either an acute or chronic form. Acute pancreatitis is a painful, short-term condition with sudden onset that typically resolves within a few days following treatment, but can be fatal in severe cases associated with multi-organ failure (Murtaugh and Keefe, 2015; Yang and Forsmark, 2017). By contrast, chronic pancreatitis is largely asymptomatic, occurs gradually, and is typically diagnosed

only after the presentation of complications. In its chronic form, pancreatitis is characterized by persistent inflammation, fibrosis, and acinar cell metaplasia and results in permanent pancreatic damage (Murtaugh and Keefe, 2015). Repeated episodes of acute pancreatitis can progress to chronic pancreatitis. While both forms carry a risk of mortality, they can also lead to other serious conditions. For example, chronic pancreatitis is a known risk factor for pancreatic ductal adenocarcinoma (PDA), currently the third-most common cause of cancer-related death in the United States (Pinho et al., 2014; Siegel et al., 2019).

The exocrine compartment of a healthy pancreas is comprised largely of acinar cells, which produce and secrete digestive enzymes and ductal cells, which transport these enzymes to the duodenum. Under conditions of chronic injury or oncogenic mutation, differentiated acinar cells undergo metaplasia, or a morphological remodeling, to form ductal-like cells expressing developmental factors, thought to represent a facultative progenitor population (Storz, 2017). This acinar to ductal metaplasia (ADM) is a reversible process thought to play a role in tissue healing and regeneration after injury (Storz, 2017). In the presence of persistent oncogenic $Kras^{G12D}$ expression, however, metaplastic cells are no longer able to re-differentiate to acinar cells, and instead progress to pancreatic intraepithelial neoplasias (PanINs) and PDA (Storz, 2017).

We previously showed that $Kras^{G12D}$-induced ADM is characterized by substantial cellular heterogeneity, including a significant population of tuft cells (Delgiorno et al., 2014). Tuft cells are solitary chemosensory cells found in the hollow organs of the respiratory and digestive tracts and can be identified by their large microvilli and deep actin rootlets in the supranuclear cytoplasm (Sato, 2007). Tuft cell formation has been identified in response to tissue injury and tumorigenesis in a number of organs including the colon, lung, and stomach (Filippenko, 1981; Gerbe et al., 2011; Saqui-Salces et al., 2011). Tuft cells are associated with human pancreatitis, but have not previously been identified in genetically wild-type mouse models of pancreatic injury (Delgiorno et al., 2014).

Despite the discovery of this striking cell type in 1956, little functional data existed until recently (Jarvi and Keyrilainen, 1956; Rhodin and Dalhamn, 1956). Several groups have independently shown that intestinal tuft cells sense and repel parasite infection through the expression of succinate receptor 1 and secretion of cytokine IL-25 (Gerbe et al., 2011; Howitt et al., 2016; von Moltke et al., 2016; Lei et al., 2018; Nadjsombati et al., 2018; Schneider et al., 2018). Further, thymic tuft cells have been shown to play a role in the development and polarization of thymic invariant natural killer T cells (Bornstein et al., 2018; Miller et al., 2018). While these data demonstrate a role for tuft cells in mediating inflammation, their role in tissue injury represents a substantial knowledge gap.

In contrast to the intestines and thymus, the murine pancreas is normally devoid of tuft cells. Rather, pancreatic tuft cells emerge in response to expression of tumor-initiating mutations (Bailey et al., 2014; Delgiorno et al., 2014). Despite this unexpected discovery, we previously lacked the genetic tools and mouse models to properly study tuft cell function in the pancreas. This led tuft cell function to be predicted largely on

the basis of transcriptomic and protein expression studies done in the intestines. For example, in intestines, high expression of the tubulin kinase Dclk1 is largely restricted to tuft cells (Gerbe et al., 2011). In the pancreas, however, Westphalen et al. (2016) have shown by lineage tracing with BAC transgenic Dclk1-CreERT mice that Dclk1 labeling is not tuft cell-restricted as it also labels acinar and ductal cells. This is consistent with acinar cell plasticity and the reliance of the pancreas on metaplasia to heal. Intermediate cell types that exhibit acinar and ductal characteristics are generated during metaplasia and preclude the use of a single marker for tuft cell identification.

Here, we demonstrate that tuft cell formation occurs during ADM in response to chronic injury in multiple strains of genetically wild type mice. We characterize this pancreatitis tuft cell population using a combination of histology, fluorescence and electron microscopy, and molecular strategies. Transcriptomic characterization of pancreatitis tuft cells reveals both similarities and differences to those found in other organs and disease systems. Our data demonstrate that tuft cell formation is a normal part of pancreatic injury and suggest a role in recovery. Interestingly, we found tuft cell formation and loss of acinar identity to be strain-specific. We have found that a proportion of human pancreatitis cases are characterized by tuft cell formation (Delgiorno et al., 2014). Therefore, these data highlight the importance of using the appropriate mouse strain and conditions to more accurately model the human condition.

MATERIALS AND METHODS

Animal Strains

Mice were housed in accordance with NIH guidelines in Association for Assessment and Accreditation of Laboratory Animal Care (AAALAC)-accredited facilities at the Salk Institute for Biological Studies. The Institutional Animal Care and Use Committee at the Salk Institute approved all animal studies. C57BL/6J mice were either purchased from The Jackson Laboratory or bred in-house. Eight-weeks-old DBA/2, Swiss Webster, BALB/c, and FVB mice were purchased from Charles River Laboratories. CD-1 mice were either purchased from Charles River Laboratories or bred in-house. Eight-weeks-old 129S6 mice were purchased from Taconic Biosciences. $PtflaCre^{ERTM/+}$ and $Rosa^{YFP}$ strains have been previously described and were purchased from The Jackson Laboratory (Pan et al., 2013). FLARE25 ($Il25^{F25/F25}$) mice (C57Bl/6J strain) were generously provided by the Locksley (University of California at San Francisco, CA, United States) and von Moltke (University of Washington, WA, United States) laboratories and were bred to the CD-1 mouse strain (von Moltke et al., 2016). F1 mice were used for experiments.

Pancreatitis Induction

Pancreatitis was induced by intraperitoneal (IP) injection of caerulein (Bachem). One cycle includes twice daily treatment, 5 days a week at 125 μg/kg with 2 days recovery. Mice in **Supplementary Figure S3** were treated with 62.5 μg/kg, 125 μg/kg, or 250 μg/kg caerulein.

Lineage Tracing

Lineage tracing was conducted using the $Ptf1aCre^{ERTM/+}$; $Rosa^{YFP}$ mouse model, as previously described (Pan et al., 2013; Delgiorno et al., 2014). Mice were bred into the CD-1 mouse strain; F4 mice were used. In this model, tamoxifen treatment induces Cre activity, which then initiates expression of yellow fluorescent protein (YFP) specifically in $Ptf1a$ + acinar cells. Acinar cells were labeled in $Ptf1aCre^{ERTM/+}$; $Rosa^{YFP}$ mice with five daily doses of 5 mg tamoxifen (Sigma, 5 days/week for 2 weeks) delivered in corn oil (Sigma) by oral gavage. Pancreatitis was then induced with four cycles of 250 μg/kg caerulein.

Histological Staining and Quantification

Tissues were fixed overnight in zinc-containing neutral-buffered formalin (Fisher Scientific), embedded in paraffin, cut in 5 μm sections, mounted, and stained. Sections were deparaffinized in xylene, rehydrated in a series of ethanol, and then washed in PBST and PBS. Endogenous peroxidase activity was blocked with a 1:50 solution of 30% H_2O_2: PBS followed by microwave antigen retrieval in 100 mM sodium citrate, pH 6.0. Sections were blocked with 1% bovine serum albumin (BSA) and 5% goat or rabbit serum in 10 mM Tris (pH 7.4), 100 mM $MgCl_2$, and 0.5% Tween-20 for 1 h at room temperature, followed by an avidin/biotin blocking kit (Thermo Fisher Scientific) per the manufacturer's instructions. Primary antibodies were diluted in blocking solution and incubated overnight. Information on primary antibodies is provided in **Supplementary Table S1**. Slides were then washed, incubated in streptavidin-conjugated secondary antibodies (for rabbit or mouse antibodies, Abcam, for rat or goat antibodies, Vector) and developed with DAB substrate (Vector). Hematoxylin and eosin (H&E) staining was done to assess tissue morphology. All slides were scanned and imaged on an Olympus VS-120 Virtual Slide Scanning microscope. For quantification of histology, ten 20× fields per scanned slide were scored in a blinded fashion using the ImageJ/FIJI plugin immunohistochemistry (IHC) image analysis toolbox (Shu et al., 2013). A statistical color detection model was trained based on multiple regions of interest (ROIs) manually and selected from desired color pixel regions from sample images for each strain using the IHC Toolbox plugin. Each image was color deconvolved using its corresponding trained model within the plugin and a new RGB image containing only the isolated color was automatically generated. The hematoxylin counter stain was deconvolved in a similar manner. Using ImageJ/FIJI, the desired color-isolated image and the counter stain-isolated image was binarized and staining area of the two was measured by counting the number of pixels of foreground (Schindelin et al., 2012). The percentage of signal was determined by dividing the stain area by the sum of the stain area and the counter stain.

Fluorescence Microscopy

Immunofluorescence on paraffin-embedded tissues followed the IHC protocol until the blocking step. Instead, tissues were blocked with 5% normal donkey serum and 1% BSA in 10 mM PBS for 1 h at room temperature. Tissue sections were stained with primary antibodies in 10 mM PBS supplemented with 1%

BSA and 0.1% Triton X-100 overnight (**Supplementary Table S1**). Sections were then washed 3 × 15 min in PBS with 1% Triton X-100, incubated in Alexa Fluor secondary antibodies and/or phalloidin (Invitrogen), washed again for 3 × 5 min, rinsed with distilled water, and mounted with Prolong Gold containing Dapi (Invitrogen). Immunofluorescence on OCT-embedded sections was conducted as previously described (Delgiorno et al., 2014). Tissues were imaged on a Zeiss 710 confocal microscope, a Zeiss 880 Airyscan Super-Resolution microscope or an Olympus VS-120 Virtual Slide Scanning microscope.

Multiplex Immunofluorescence

Co-expression of amylase and pan-cytokeratin (antibodies, **Supplementary Table S1**) was determined using a Perkin Elmer Opal 4-color Manual IHC Kit (NEL810001KT) per the manufacturer's instructions.

Transmission Electron Microscopy

Tissues were fixed in a solution of 2% paraformaldehyde, 2.5% glutaraldehyde, and 2 mM $CaCl_2$ in 0.15 M sodium cacodylate buffer (pH 7.4) for 2 h at room temperature. They were then post-fixed in 1% osmium tetroxide for 40 min and 1.5% potassium ferricyanide in sodium cacodylate buffer for 1 h at 4°C in the dark. Tissues were stained en block in 1% aqueous uranyl acetate (4°C in the dark), dehydrated in a series of graded ethanol, and embedded in Eponate12 resin (Ted Pella). Ultra-thin sections (70 nm) were obtained using a diamond knife (Diatome) in an ultramicrotome (Leica EM UC7) and placed on copper grids (300 mesh). Sections were imaged on a Zeiss Libra 120 TEM operated at 120 kV.

All images (IHC, IF, and EM) were digitally enhanced to edit the color, brightness, and contrast levels using Zen (Carl Zeiss) and/or Photoshop (Adobe) software.

Tuft Cell Preparation and Cell Sorting

Pancreatitis tuft cells were isolated from wild-type CD-1 mice treated with four cycles of 250 μg/kg caerulein (allowed to recover for 0–2 days). The pancreas was quickly dissected, minced in 5 ml of DMEM with FBS and allowed to incubate for 2 min. Supernatant and fat were removed and pancreatic tissue was then incubated in 10 ml DMEM supplemented with 1 mg/ml collagenase I (Sigma), 1 mg/ml soybean trypsin inhibitor (Gibco), 1 mg/ml hyaluronidase (Sigma), and 250 μl of DNAse I, shaking gently at 37°C for a maximum of 30 min. Digestion was monitored and tissue was further digested mechanically by pipetting. Digested tissue was passed through a 100 μm filter, washed with fluorescence activated cell sorting (FACS) buffer (PBS, 1 mM EDTA, 0.5% BSA), and incubated with ACK lysing buffer (Gibco) to remove red blood cells before staining for FACS.

Single cell suspensions were incubated on ice with mouse Fc receptor block (BD Biosciences, 1:200) followed by antigen-specific antibodies in FACS buffer. DAPI (molecular probes, 1:1000) and Annexin V (Biolegend, Pacific Blue conjugate at 1:200) were used to exclude dead and dying cells. Cells were labeled with Cd45 (Alexa Fluor 488), EpCAM (Alexa Fluor 647), and Siglec F (PE) (Biolegend, 1:200) antibodies. Fluorescence

minus one (FMO) staining controls were included for gating populations of interest. Cells were FACS purified at the Salk Institute's Flow Cytometry core facility on a BD Biosciences Influx cell sorter (100-μm size nozzle, 1 × PBS sheath buffer with sheath pressure set to 20 PSI). Cells were sorted in 1-drop Single Cell sort mode for counting accuracy; these were deposited directly into lysis buffer composed of DNase/RNase-free water, (%) Triton X-100, and Ribolock (Thermo Fisher Scientific) in a 96 well plate.

RNA-seq Library Generation, High-Throughput Sequencing, and Analysis

Low input bulk RNA sequencing (RNA-seq) on pancreatitis tuft cells was performed using the Smart-Seq2 protocol as previously described (Picelli et al., 2014). In brief, five biological replicates, each with 100 tuft cells from an individual mouse, were sorted directly into 2 μl of Smart-Seq2 lysis buffer. Full-length cDNA was generated and size distribution was checked with Agilent TapeStation 4200 to ensure RNA quality. cDNA were then amplified with 18–22 PCR cycles, tagmentated, and amplified again with 10 PCR cycles using a Nextera XT kit (Illumina FC-131-1096). The sequencing library was purified with AMPure XP beads. 50 bp single-end sequencing was performed with Illumina HiSeq 2500. Sequencing reads were quality checked with FastQC and mapped to the mouse genome (mm9) using Hisat2 (Kim et al., 2015). Transcript assembly and quantification were performed by Stringtie and Ballgown (Pertea et al., 2016). Gene expression distribution between samples was checked to ensure similar transcriptome quality. Genes that have RPKM variance across samples <1 were first removed to exclude non-expressed genes. The RPKM values were then Log2 transformed and quantile normalized with the R package preprocessCore. Differential expression analysis between tuft and non-tuft epithelial cells was performed with empirical Bayes shrinkage and moderated t-test using the Limma package and p-values were converted into false discovery rates (FDR) using the Benjamini-Hochberg procedure (Ritchie et al., 2015). Heat map plotting and clustering (with Euclidean distance and complete linkage) was performed with heatmap.2 in R. The differential expression score was calculated as: $-\text{Log}_{10}$ (FDR) × Log_2 (fold change), which factors in both statistical confidence and the effect size. Gene ontology network analyses of differentially expressed genes were performed with ClueGO plug-in of Cytoscape (Bindea et al., 2009).

RT-qPCR

RT-qPCR was performed using Power SYBR Green PCR Master Mix (Applied Biosystems) on the ABI 7900 detection system (Applied Biosystems). Relative expression values were determined using the standard curve method. RT-qPCR was performed on bulk tuft cells and non-tuft epithelial cells from CD-1 mice with pancreatitis (100 cells per group) after the amplification step of the SmartSeq2 protocol (Picelli et al., 2014).

Results were normalized to the housekeeping gene Rplp0. Primer sequences can be found in **Supplementary Table S2**.

RESULTS

Chronic Pancreatic Injury Induces Tuft Cell Formation

Tuft cell formation is characteristic of a portion of human pancreatitis cases and has also been shown in multiple mouse models of tissue injury in several gastrointestinal organs (Saqui-Salces et al., 2011; Delgiorno et al., 2014). We and others have shown that tuft cells form in the pancreas in response to genetic modifications, such as oncogenic $Kras^{G12D}$ or TGFα, Sox17, or IL-1β overexpression (Bailey et al., 2014; Delgiorno et al., 2014; Westphalen et al., 2016). Importantly, studies of the generality of tuft cell formation in genetically wild type mice have yet to be reported. Therefore, we conducted a multiparameter analysis of caerulein-induced mouse pancreatitis.

Caerulein is a cholecystokinin ortholog that induces endoplasmic reticulum (ER) stress in pancreatic acinar cells, resulting in cell death, inflammation, and edema (Sah et al., 2014). Previously, we evaluated tuft cell formation in response to caerulein using mixed background mice and 2 weeks (two cycles) of treatment and were unable to detect a robust response (Delgiorno et al., 2014). To more thoroughly evaluate the potential for tuft cell genesis, we varied treatment dose and timing in outbred CD-1 mice. We found that prolonged caerulein treatment resulted in acinar cell loss and an increase in ADM, stromal deposition, and mucin expression (**Supplementary Figure S1**). By IHC, we identified robust up-regulation of Dclk1 + cells with tuft cell morphology after four cycles of caerulein treatment (**Figures 1A–C**). Interestingly, this response was enhanced with increasing caerulein dosage and length of time of treatment (data not shown). We confirmed tuft cell identity using co-immunofluorescence for additional tuft cell markers and F-actin marker phalloidin, which labels the deep actin rootlets and striking microvilli characteristic of this cell type (**Figures 1D–G**; Delgiorno et al., 2014). This analysis revealed that cells with high Dclk1 expression are tuft cells (100%+, 130/130 cells, 3 mice) (**Figure 1D**). We further confirmed tuft cell genesis with markers phospho-EGFR, a receptor tyrosine kinase (100%+, 128/128 cells, 3 mice), transient receptor potential cation channel, subfamily M, member 5 (Trpm5) a chemosensory cell marker (100%+, 110/110 cells, 3 mice), and Cox1, a prostaglandin synthase (95%+, 218/230, 3 mice) (**Figures 1E–G**; Bezencon et al., 2008; Gerbe et al., 2011; Delgiorno et al., 2014). Pancreatitis-induced tuft cells (Cox1+) express tuft cell master regulator Pou2f3 (97%+, 189/195 cells, 4 mice), and consistent with $Kras^{G12D}$-induced tuft cells, are not proliferative, (0% Ki67+, 150/150 cells, 3 mice) (**Figures 1H,I**; Delgiorno et al., 2014; Gerbe et al., 2016). Taken together, these data reveal tuft cell genesis in response to chronic, long-term injury in the outbred CD-1 mouse strain.

Next, we used transmission electron microscopy (TEM) to explore the ultrastructure of pancreatitis-induced tuft cells. We
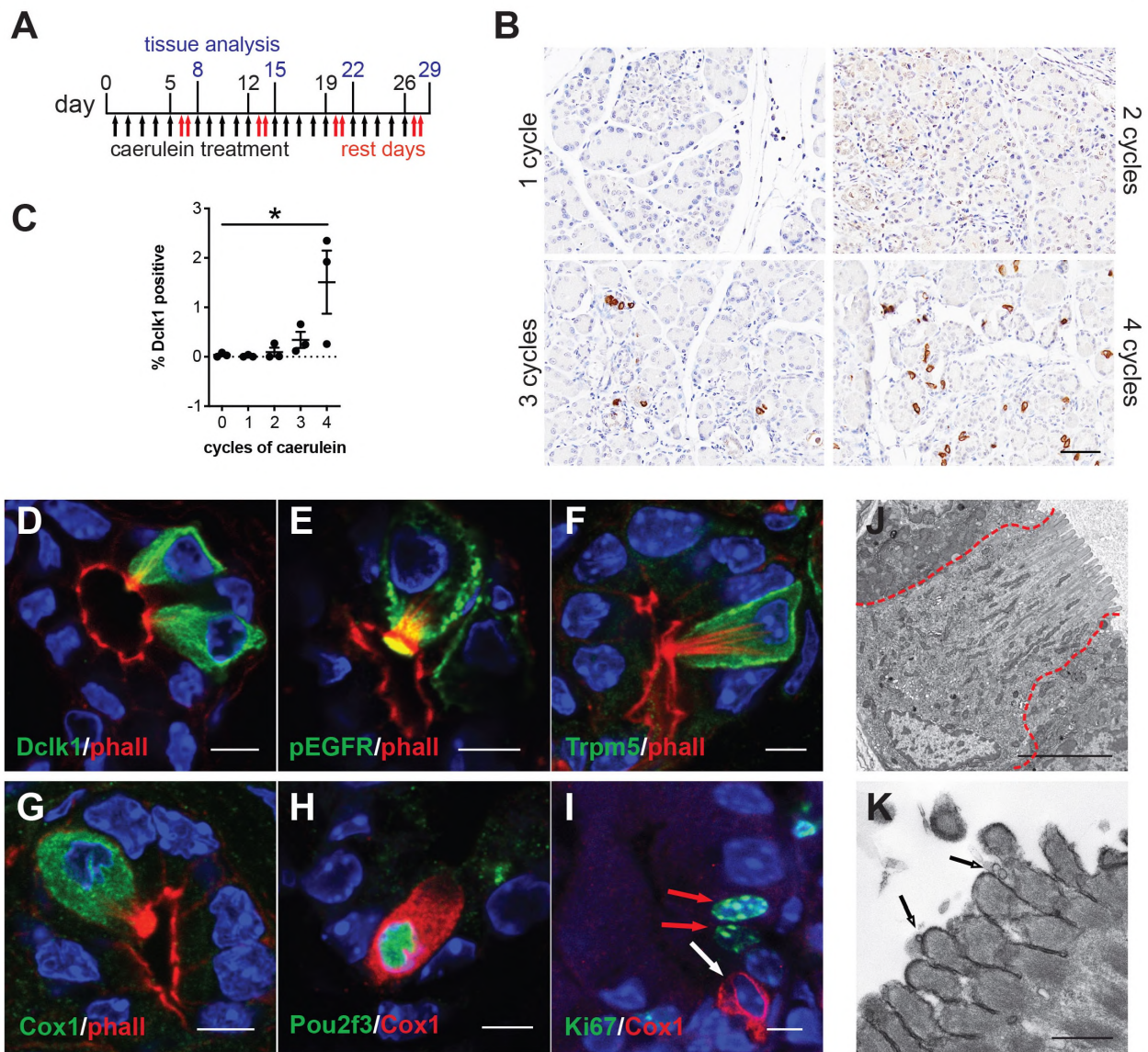
FIGURE 1 | Chronic injury induces tuft cell formation in the pancreata of wild type mice. **(A)** Schematic of caerulein treatment for pancreatitis induction in wild type mice. **(B)** Immunohistochemistry (IHC) demonstrating an increase in Dclk1 expression (brown) in the injured pancreas over time and quantified in **(C)** (n = 3 mice per condition). Scale bar, 50 μm. **(D)** Co-immunofluorescence (Co-IF) for tuft cell marker phalloidin (red, labels the microvilli and actin rootlets of tuft cells) and Dclk1, **(E)** phospho-EGFR, **(F)** Trpm5, or **(G)** Cox1 (green). **(H)** Co-IF for tuft cell marker Cox1 (red) and Pou2f3 or **(I)** Ki67 (green). Red arrows, Ki67 + nuclei, white arrow, Ki67- tuft cell. Scale bars, 5 μm. **(J)** Electron microscopy confirming tuft cell formation in pancreatitis, and **(K)** demonstrating the presence of vesicles at the tips of the microvilli (arrows). Scale bars, 5 μm and 500 nm, respectively.

induced pancreatic injury and tuft cell formation with four cycles of caerulein. We then confirmed tuft cell formation by the presence of cells with characteristic microvilli, actin rootlets, and abundant intracellular vesicles and mitochondria (**Figure 1J**). Closer examination revealed membrane-bound electron lucent vesicles, which appear to be budding from the tips of the microvilli, consistent with injury-induced tuft cells being a secretory cell type (**Figure 1K**). Collectively, these data identify *de novo*, spontaneous tuft cell formation in chemically induced pancreatic injury. The data further suggest a potential secretory role for pancreatic tuft cells in inflammation.

To further evaluate this role, we conducted RNA sequencing (RNA-seq).

Transcriptomic Analysis of Pancreatitis Tuft Cells

To provide a comprehensive, agnostic, molecular assessment of the potential role(s) for tuft cells in pancreatic injury, we used RNA-seq and bioinformatic analyses. To accomplish this, we induced pancreatitis with caerulein, collected tuft cells by FACS, and then conducted RNA-seq. Siglec f is a cell surface lectin

that is typically used to detect eosinophils, but expression is also evident in intestinal tuft cells (Gerbe et al., 2016). Using co-immunofluorescence with phalloidin, we found that Siglec f also labels pancreatitis-induced tuft cells in wild type CD-1 mice (98.6%+, 276/280 cells, n = 3 mice) (**Figure 2A**).

As tuft cells are rare in pancreatitis, we employed a small cell number sequencing approach. We used FACS to isolate 100 Cd45-neg; EpCAM+; Siglec f+ tuft cells and an equivalent number of Cd45-neg; EpCAM+; Siglec f-neg non-tuft epithelial cells from five mice with pancreatitis (**Supplementary Figure S2A**). Tuft cells constituted approximately 0.80% of the epithelium (range 0.2–1.7%). We then isolated bulk RNA, prepared cDNA, and amplified it using SmartSeq2 methodology (Picelli et al., 2014). RNA-seq identified 1010 genes as differentially expressed between tuft cells and non-tuft epithelial cells in pancreatitis (**Figure 2B**; FDR < 0.05 and average fold change >4). Tuft cell isolation and enrichment was confirmed in the Siglec f+ population by high expression of tuft cell markers such as *Dclk1*, *Pou2f3*, and *Trpm5* (**Figure 2C**), and low-to-no expression of acinar cell markers, such as amylase genes, or islet cell markers, such as chromogranin A and somatostatin (**Supplementary Figures S2B,C**). Similar to tuft cells characterized in other organs, pancreatitis-associated tuft cells express a number of genes associated with bacterial or viral infection (**Supplementary Figure S3**). In contrast to intestinal tuft cells, *Sucnr1* was not expressed (Nadjsombati et al., 2018). Interestingly, network analysis of genes differentially up-regulated in tuft cells identified a number of immune cell signaling pathways, consistent with a role in inflammation (**Figure 2D** and **Supplementary Figure S3**). These data are consistent with a sentinel cell role for pancreatitis tuft cells in innate immunity.

Pancreatitis Tuft Cells Express Cytokine IL-25

Interleukin 25 (IL-25, also called IL-17E) is a member of the IL-17 cytokine superfamily that has been demonstrated to both induce and enhance the helper T cell 2 (Th2) immune response while inhibiting Th1 and Th17-driven immunity. Expression has been shown in many different cell types, tissues, and systems, among which are tuft cells (Bezencon et al., 2008; von Moltke et al., 2016). Within the small intestine, tuft cell-derived IL-25 is required for the "weep and sweep" response that rids the host of helminth infection (Gerbe et al., 2016; Howitt et al., 2016; von Moltke et al., 2016). Given the established role for this cytokine as a tuft cell effector, we used several orthogonal methods to determine if IL-25 is expressed in pancreatitis tuft cells. By RNA-seq, we found *Il25* expression to be significantly higher in tuft cells than non-tuft epithelial cells (**Figure 3A**), which was confirmed by RT-qPCR (**Figure 3B**). To further confirm IL-25 expression, we induced chronic injury in IL-25 reporter mice (Flare25, flox and reporter of *Il25*; *Il25$^{F25/F25}$*). By co-immunofluorescence with phalloidin, we found that 100% of tuft cells analyzed (101/101 cells, n = 5 mice) were positive for red fluorescent protein (RFP) and IL-25 expression (**Figure 3C**). These data suggest a potential role for tuft cell-derived IL-25 in pancreatitis.
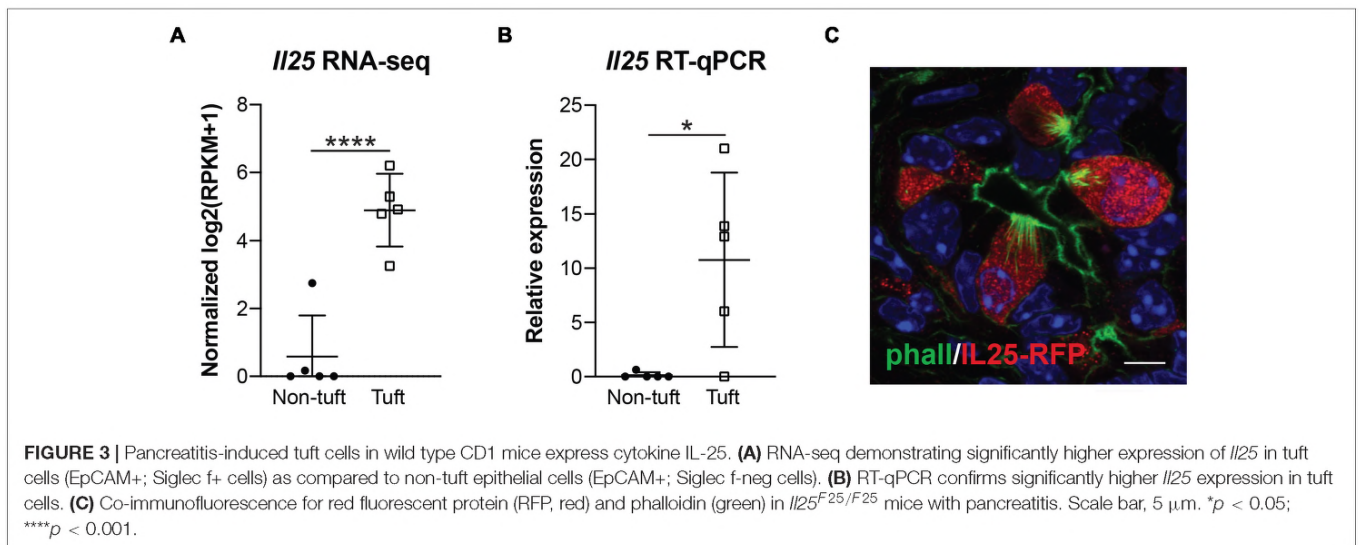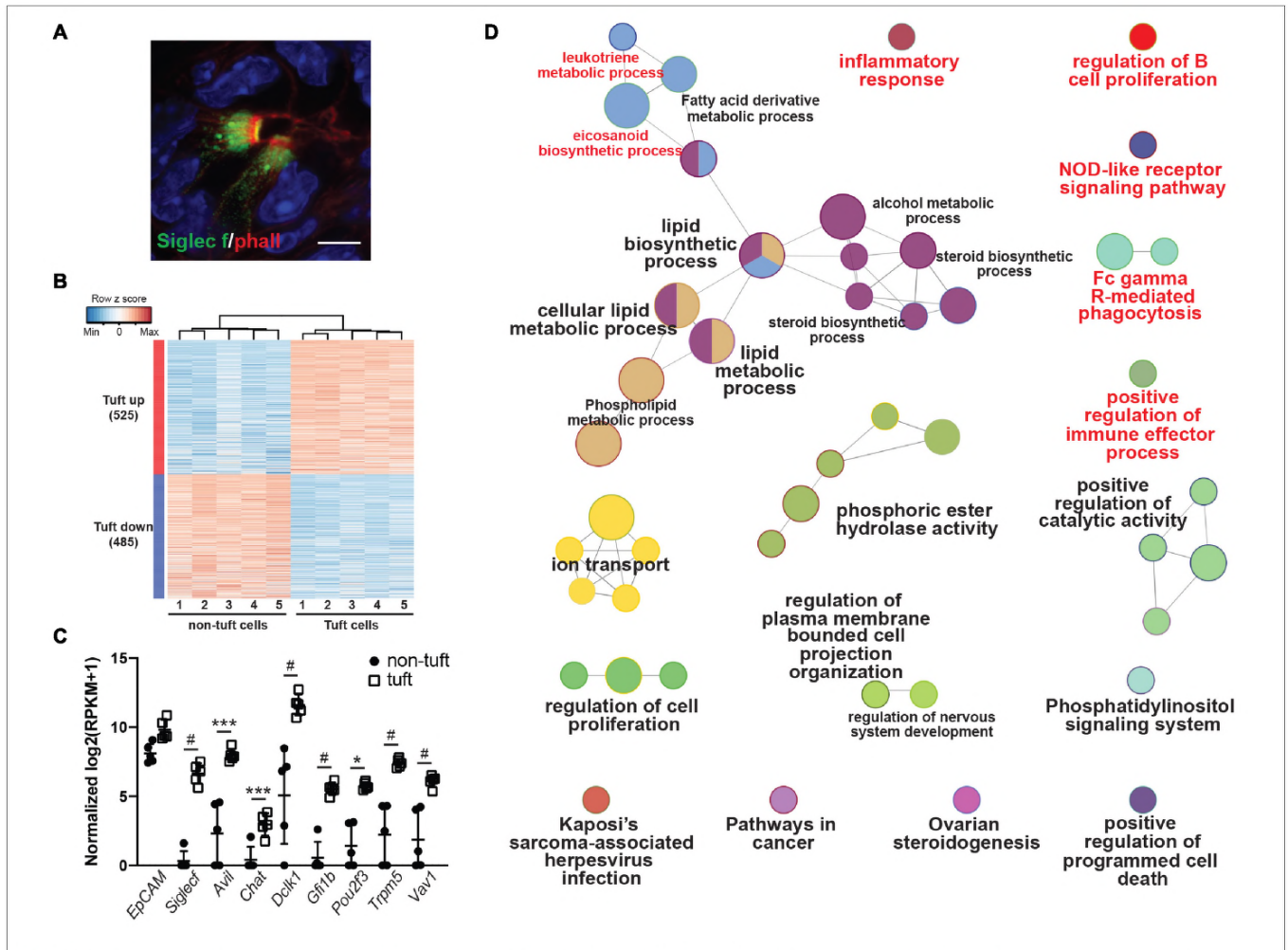
Pancreatitis Tuft Cells Result From Acinar to Ductal Metaplasia

Previously, we used lineage tracing to show that the majority of *Kras^{G12D}*-induced pancreatic tuft cells result from acinar-to-ductal metaplasia (ADM, 68.7%) (Delgiorno et al., 2014). To determine if pancreatitis tuft cells transdifferentiate from the acinar cell epithelium in response to injury, we conducted lineage tracing using *Ptf1aCre$^{ERTM/}$+;Rosa^{YFP}* mice crossed into the CD-1 background. In this model, tamoxifen treatment induces Cre activity and expression of YFP, specifically in *Ptf1a*+ adult acinar cells (Pan et al., 2013). Adult mice were given tamoxifen followed by four cycles of caerulein treatment to induce pancreatitis and tuft cell formation (**Figure 4A**). To identify tuft cells, we conducted co-immunofluorescence with phalloidin and observed YFP expression in 97.6% of tuft cells analyzed (203/208 cells, n = 2 mice), signifying that injury-induced pancreatitis tuft cells can arise from acinar cells (**Figure 4B**). The other 2.4% of tuft cells may not have expressed YFP due to incomplete recombination, reporter methylation, or additional cell(s) of origin (ductal cells, etc.). Interestingly, although significantly lower than in non-tuft epithelial cells, a number of acinar cell genes were detected in our Siglec f+ tuft cell population by RNA-seq (**Supplementary Figure S2B**), perhaps reflecting their acinar cell of origin.
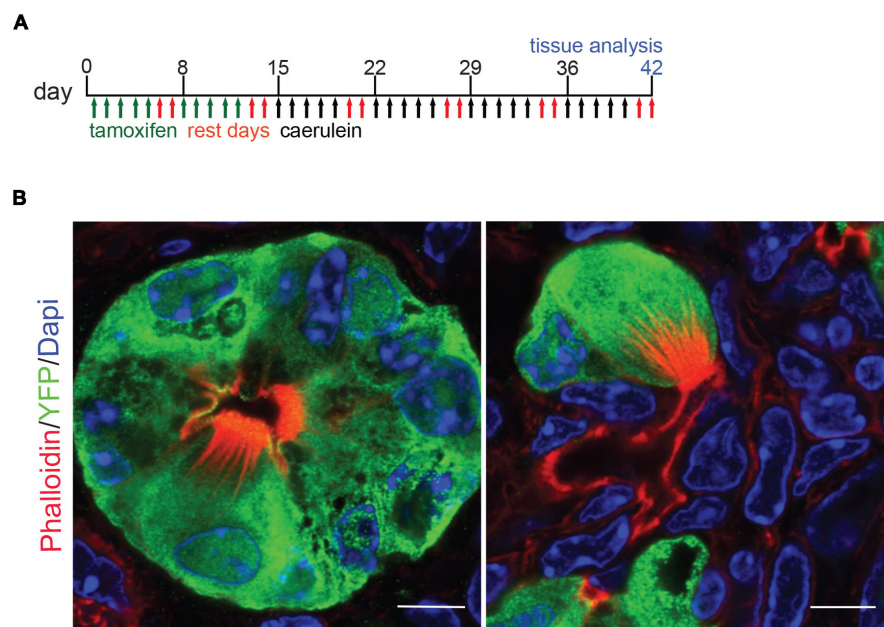
Tuft Cell Formation Is Mouse Strain-Dependent

To determine the function of tuft cells in pancreatitis, we sought to employ a number of genetically engineered mouse models (GEMMs) that would allow us to eliminate tuft cell formation and/or secreted effectors. For the purpose of standardization, however, most GEMMs are typically backcrossed into the inbred C57Bl/6J mouse strain. To first confirm that C57Bl/6J can generate tuft cells in response to chronic injury, we induced pancreatitis with 1–5 cycles of caerulein treatment. Surprisingly, we found that, although C57Bl/6J mice develop pancreatitis and suffer significant loss of pancreas tissue in response to caerulein, similar to CD-1 (**Figures 5A,B**), we were unable to detect Dclk1+ cells with tall columnar, tuft cell morphology (**Figures 5B,C**). To determine if this strain exhibits reduced sensitivity to caerulein treatment or has a sex-specific response, we varied the dose of caerulein (four cycles of either 62.5 μg/kg or 250 μg/kg) and induced injury in both genders (**Supplementary Figure S4**). We found that increasing caerulein dosage leads to the formation of a few cells with tuft cell morphology, but to a lesser extent than identified in CD-1 mice (**Supplementary Figure S4C**). To determine if injury-induced tuft cell formation is unique to CD-1 mice, we evaluated pancreatitis in an additional five mouse strains. In total, we examined seven strains of mice: C57Bl/6J, BALB/c, FVB, CD-1, Swiss Webster, DBA/2, and 129S6. A minimum of three mice from each strain were treated with four cycles of caerulein and examined histologically. All treated mice experienced a decrease in pancreas weight to body weight ratio compared to control mice (of the same strain), and tissue injury and inflammation could be identified by H&E analysis in all strains (**Figures 5D,E** and **Supplementary Figure S5**). Interestingly, we found a significant increase in Dclk1

FIGURE 2 | Transcriptomic analysis of pancreatitis-induced tuft cells in wild type CD1 mice. **(A)** Co-immunofluorescence for phalloidin (red, labels the microvilli and actin rootlets of tuft cells) and Siglec f (green) in the injured pancreas. Scale bar, 5 μm. **(B)** Heat map with hierarchical clustering showing differentially expressed genes in EpCAM+; Siglec f+ tuft cells as compared to EpCAM+; Siglec f-neg non-tuft epithelial cells. **(C)** Confirmation of Siglec f expression and tuft cell markers in sorted EpCAM+; Siglec f+ cells. $n = 5$ mice. **(D)** Gene ontology network analysis of genes differentially up-regulated in tuft cells, as compared to non-tuft epithelial cells, identifies immune cell signaling pathways (labeled in red). $^*p < 0.05$; $^{***}p < 0.005$; $^\#p < 0.001$.

FIGURE 3 | Pancreatitis-induced tuft cells in wild type CD1 mice express cytokine IL-25. **(A)** RNA-seq demonstrating significantly higher expression of *Il25* in tuft cells (EpCAM+; Siglec f+ cells) as compared to non-tuft epithelial cells (EpCAM+; Siglec f-neg cells). **(B)** RT-qPCR confirms significantly higher *Il25* expression in tuft cells. **(C)** Co-immunofluorescence for red fluorescent protein (RFP, red) and phalloidin (green) in $Il25^{F25/F25}$ mice with pancreatitis. Scale bar, 5 μm. $^*p < 0.05$; $^{****}p < 0.001$.

FIGURE 4 | Lineage tracing of pancreatitis tuft cells in wild type mice reveals acinar cell origin. **(A)** Schematic of tamoxifen and caerulein treatment for lineage tracing in *Ptf1aCre*$^{ERTM/+}$; *Rosa*^{YFP} mice. **(B)** Co-immunofluorescence for tuft cell marker phalloidin (red, labels the microvilli and actin rootlets of tuft cells) and YFP, green, in caerulein-treated pancreata. Scale bar, 5 μm.

expression, identified by IHC, in nearly all strains (**Figure 5F**). However, expression levels varied and cellular morphology was often inconsistent with that of tuft cells, demonstrating that Dclk1 is not tuft cell specific (**Figures 5E,F**). Consistent with this, we identified Dclk1 staining in the normal ducts of the pancreas within all strains, which lack tuft cells. Importantly, and consistent with prior reports, these ducts lack tuft cells (**Supplementary Figure S5**; May et al., 2010; Delgiorno et al., 2014; Westphalen et al., 2016). Further, our histological and RNA-seq analyses are consistent in showing that while Dclk1 expression is significantly higher in tuft cells, it is not specific to them (**Figure 2C**).

Due to the lack of specificity of Dclk1 in identifying tuft cells, we evaluated expression of additional tuft cell markers Pou2f3 and Trpm5 (**Figures 6A,B**). Pou2f3 expression is absent from the normal pancreas, but has been reported to occur in response to activation of *Kras*^{G12D} (**Supplementary Figure S6**; Zhang et al., 2018). Consistent with the literature, Trpm5 can be detected in the islets of the normal pancreas; however, expression is absent in the exocrine portion of the tissue (**Supplementary Figure S6**; Colsoul et al., 2010). In response to four cycles of caerulein, we observed a significant increase in Pou2f3 expression in 4 of the 7 strains analyzed. The Pou2f3+ strains also presented with Trpm5 expression consistent with tuft cell formation. While 97% of pancreatitis tuft cells are Pou2f3 positive (189/195 cells, $n = 4$ mice), only 81% of Pou2f3 positive cells (118/145 cells, $n = 4$ mice) were determined to be tuft cells by co-expression of marker Cox1 (conducted in the CD-1 strain). Consistent with this analysis, 79% of Pou2f3+ cells (239/302 cells, $n = 4$ mice) were positive for acetylated α-tubulin (which labels the dense tubulin network found in tuft cells). To confirm tuft cell formation, we conducted

co-immunofluorescence for markers Dclk1, Cox1, and acetylated α-tubulin on treated and control pancreata from all seven strains. By this analysis we confirmed that the CD-1, Swiss Webster, DBA/2, and 129S6 strains do, in fact, form tuft cells in response to chronic injury (**Figure 6C**). These data demonstrate that mouse strains differ significantly in their susceptibility to tuft cell formation in response to injury.

The Epithelial and Stromal Composition of Pancreatitis Varies by Mouse Strain

Our lineage tracing analyses, conducted in CD-1 mice, demonstrate that nearly all pancreatitis tuft cells result from ADM (**Figure 4**). These results led us to hypothesize that the proclivity for acinar cells to undergo this cell state reprograming varies between mouse strains. As an initial test of this hypothesis we compared the relative area occupied by acinar and ductal cells in caerulein-treated pancreata from all seven strains. Amylase is a digestive enzyme produced by acinar cells, while cytokeratin is a structural protein characteristic of ductal cells. Consistent with this hypothesis, we found significantly less amylase expression in mouse strains that form tuft cells in response to injury (48.7 ± 3.8%; CD1, Swiss Webster, DBA/2, 129S6; $n = 5$ for CD1, $n = 3$ for all other strains) vs. those strains that do not (62.1 ± 5.6%; C57BL/6J, BALB/c, FVB; $n = 3$ each) (**Figures 7A,B** and **Supplementary Figure S7**). Cytokeratin expression, however, was not significantly different between the two groups (47.88 ± 9.9% for tuft cell positive stains vs. 48.1 ± 3.4% for tuft cell negative strains) (**Figures 7A,B** and **Supplementary Figure S7**). Interestingly, we found that TC+ strains are characterized by significantly more stromal deposition (collagen, 28.49 ± 10.52%;

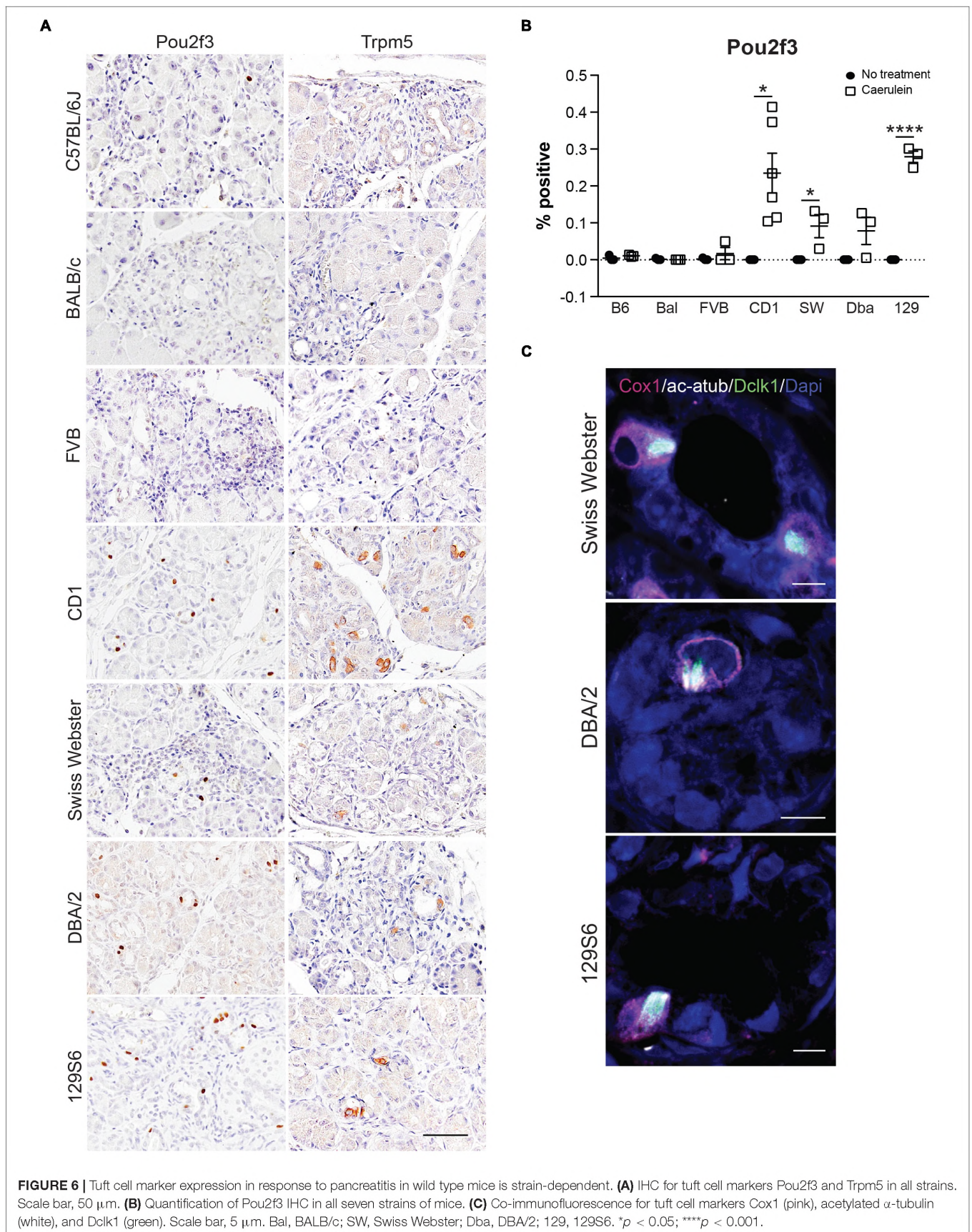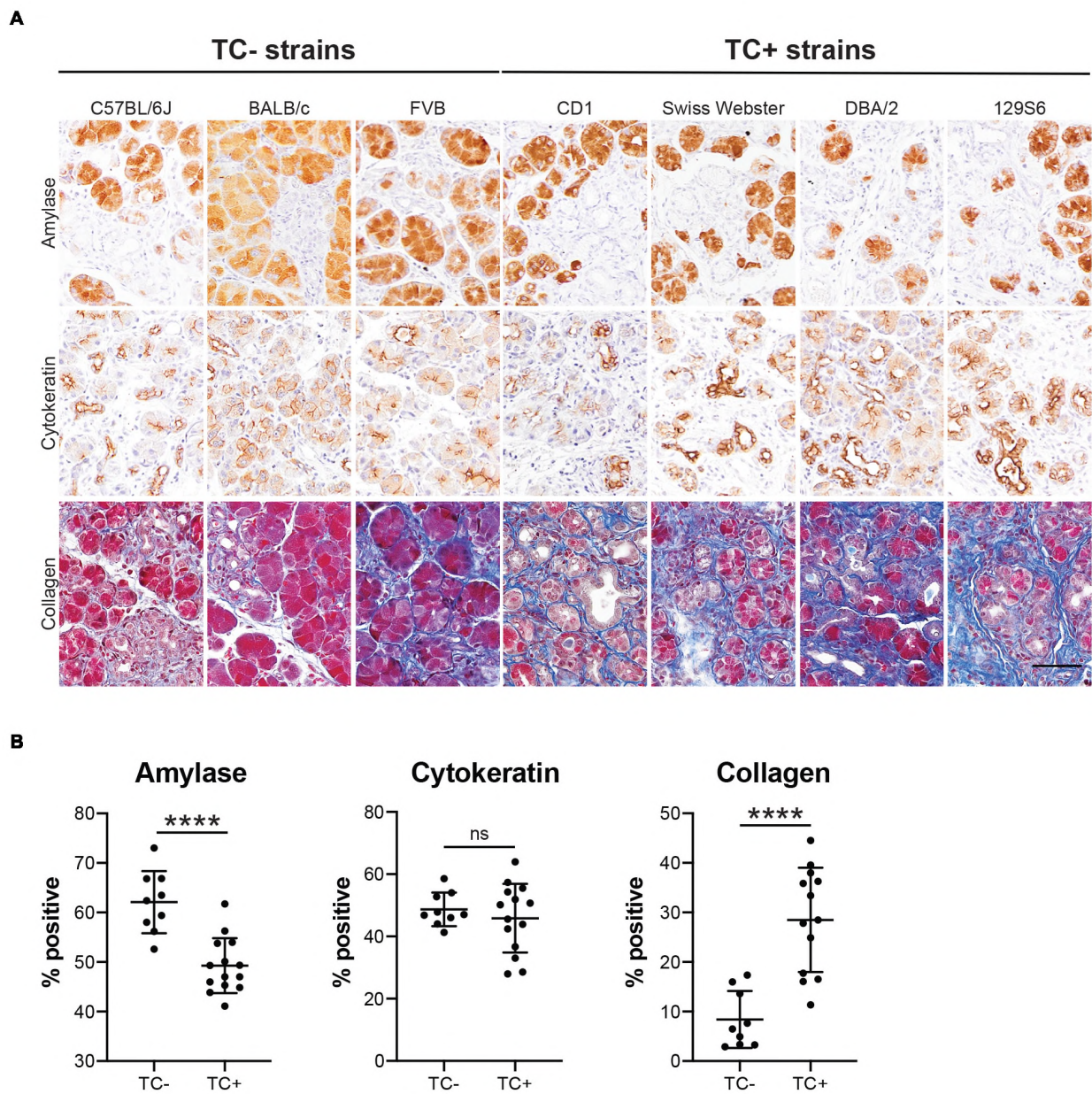**FIGURE 5 |** Tuft cell formation in response to pancreatitis in wild type mice is strain-dependent. **(A)** Pancreas: Body weight ratio (PW/BW) changes in C57BL/6J (B6) and CD1 mice in response to four cycles of caerulein treatment. **(B)** H&E and IHC for tuft cell marker Dclk1 in caerulein-treated C57BL/6J and CD1 mice showing expression consistent with tuft cell morphology (black arrows) as well as non-tuft cells (red arrows), quantified in **(C)**. **(D)** Pancreas: Body weight ratio (PW/BW) changes in an additional five mouse strains in response to four cycles of caerulein treatment. **(E)** H&E and IHC for tuft cell marker Dclk1 in the same caerulein-treated mouse strains. Cells with tuft cell morphology (black arrows), non-tuft cells (red arrows). Dclk1 IHC quantified in **(F)**. Bal, BALB/c; SW, Swiss Webster; Dba, DBA/2; 129, 129S6. Scale bar, 50 μm. *$p < 0.05$, **$p < 0.01$; ***$p < 0.005$; ****$p < 0.001$.

$n = 4$ for CD1, $n = 3$ for all other strains) than TC− strains (8.39 ± 5.74%; $n = 3$ for all strains) (**Figures 7A,B** and **Supplementary Figure S7**). When we evaluated co-expression of amylase and cytokeratin, we were surprised to find cells with

acinar cell morphology that co-expressed both markers in the caerulein-treated pancreata from all seven strains, regardless of tuft cell status (**Figure 8**). Collectively, these data indicate that acinar cells up-regulate cytokeratin expression in response to

FIGURE 6 | Tuft cell marker expression in response to pancreatitis in wild type mice is strain-dependent. **(A)** IHC for tuft cell markers Pou2f3 and Trpm5 in all strains. Scale bar, 50 μm. **(B)** Quantification of Pou2f3 IHC in all seven strains of mice. **(C)** Co-immunofluorescence for tuft cell markers Cox1 (pink), acetylated α-tubulin (white), and Dclk1 (green). Scale bar, 5 μm. Bal, BALB/c; SW, Swiss Webster; Dba, DBA/2; 129, 129S6. $*p < 0.05$; $****p < 0.001$.

FIGURE 7 | Epithelial and stromal marker expression in caerulein-induced pancreatitis varies by mouse strain. **(A)** IHC for acinar cell marker amylase or ductal cell marker cytokeratin (both brown), or collagen staining (Trichrome, blue) in the pancreata of mice treated with four cycles of caerulein, quantified in **(B)**. Scale bar, 50 μm. TC−, measurements from mouse strains lacking tuft cells (C57BL/6J, BALB/c, and FVB); TC+, measurements from mouse strains that form tuft cells in response to caerulein (CD1, Swiss Webster, DBA/2, 129S6). ****$p < 0.01$; ns, not significant.

injury, but do not necessarily undergo metaplasia (ADM). While this is suggestive of varying proclivity for ADM between strains, lineage tracing in each strain will be required to evaluate this hypothesis more thoroughly.

DISCUSSION

Our data show that tuft cell formation occurs in genetically wild type mice as part of the epithelial response to chronic pancreatic injury, and that this process is highly strain dependent. While tubulin kinase Dclk1 is a fairly specific tuft cell marker in the intestines, our data clearly show that non-tuft cells express Dclk1 under conditions of pancreatic injury, consistent with previous studies (Westphalen et al., 2016). Consequently, multiple markers must be used to confirm tuft cell formation, and additional analysis by electron microscopy provides the gold standard for unambiguous identification.

Our studies reveal that nearly all pancreatitis tuft cells arise from acinar cells, identifying a new layer of epithelial

FIGURE 8 | Co-expression of acinar and ductal markers in the normal or injured pancreata of wild type mice. Immunofluorescence for acinar cell marker amylase (red) or ductal cell marker cytokeratin (green) in the pancreata of untreated or treated (four cycles of caerulein) mice from all seven strains. Cells co-positive for amylase and cytokeratin appear yellow. Scale bar, 50 μm.

Strobel et al., 2007). This begs the question of the function of these morphologically distinct and highly specialized cells in pancreatitis. Consistent with a function in recovery, we found that, while two cycles of caerulein treatment is insufficient to induce tuft cell formation, pancreatic tuft cells will form in these mice during the recovery phase (data not shown).

We also show that pancreatitis tuft cells express cytokine IL-25. In the gut, it has been shown that tuft cell-derived IL-25 is required to mount a Th2 immune response to parasite infection. Tuft cell-derived IL-25 stimulates group 2 innate lymphoid cells (ILC2s) to produce IL-5, -9, and -13, promoting type 2 inflammation (Ting and von Moltke, 2019). IL-13 is sufficient to skew the lineage of undifferentiated intestinal epithelial cells toward tuft and mucin-producing goblet cells. Goblet cells then secrete large amounts of mucus, which aids in clearance of the infection (Gerbe et al., 2016; Howitt et al., 2016; von Moltke et al., 2016). While the pancreas is devoid of goblet cells, pancreatitis is characterized by the formation of mucin-producing cells, which may play a role in neutralizing injury and promoting epithelial recovery. Further, IL-25 itself has been shown to suppress tumorigenesis in a number of cancer models, including PDA, consistent with a protective role for tuft cells in pancreas disease (Benatar et al., 2010). While, IL-25 is an attractive candidate to study tuft cell function in pancreatitis, our RNA-seq analysis identified a number of other potential candidates, which also play a role in mediating inflammation and deserve further investigation (**Supplementary File S1**).

Interestingly, we found significant differences between mouse strains in their ability to form tuft cells in response to the same stimuli. All seven strains analyzed experience pancreatitis in response to chronic caerulein treatment, as evidenced by a significant decrease in the pancreas to body weight ratio and inflammation identified histologically, but epithelial heterogeneity was substantially different. It is well reported in the literature that different mouse strains, and even different mouse sub-strains, react to caerulein-induced injury with disparate immune infiltrates and varying severity of disease (Wang et al., 2010; Ulmasov et al., 2013). The root of these differences lies in the intrinsic genetic and epigenetic variations between strains. This poses interesting implications for susceptibility to pancreatitis in patients. This report, to the best of our knowledge, is the first to demonstrate strain-dependent tuft cell formation and susceptibility to ADM. As tuft cells likely play an important role in pancreatitis, genetic susceptibility to tuft cell formation may represent a critical factor in pancreatitis formation, severity, and progression in patients.

DATA AVAILABILITY STATEMENT

The data generated in this study has been deposited in the Gene Expression Omnibus (Accession No. GSE143749).

ETHICS STATEMENT

The animal study was reviewed and approved by Iacuc, the Salk Institute for Biological Studies.

cell plasticity in pancreatic injury. One implication of this discovery is that tuft cells play a role in pancreatitis progression and/or recovery from injury. Previous studies have shown that in response to injury and regeneration, existing acinar cell populations mainly drive the genesis of new exocrine tissue rather than ADM-derived ductal cells (Desai et al., 2007;

AUTHOR CONTRIBUTIONS

FUNDING

ACKNOWLEDGMENTS

SUPPLEMENTARY MATERIAL

The Supplementary Material for this article can be found online at: https://www.frontiersin.org/articles/10.3389/fphys.2020.00088/full#supplementary-material

REFERENCES

Bailey, J. M., Alsina, J., Rasheed, Z. A., McAllister, F. M., Fu, Y. Y., Plentz, R., et al. (2014). DCLK1 marks a morphologically distinct subpopulation of cells with stem cell properties in preinvasive pancreatic cancer. *Gastroenterology* 146, 245–256. doi: 10.1053/j.gastro.2013.09.050

Benatar, T., Cao, M. Y., Lee, Y., Lightfoot, J., Feng, N., Gu, X., et al. (2010). IL-17E, a proinflammatory cytokine, has antitumor efficacy against several tumor types in vivo. *Cancer Immunol. Immunother.* 59, 805–817. doi: 10.1007/s00262-009-0802-8

Bezencon, C., Furholz, A., Raymond, F., Mansourian, R., Metairon, S., Le Coutre, J., et al. (2008). Murine intestinal cells expressing Trpm5 are mostly brush cells and express markers of neuronal and inflammatory cells. *J. Comp. Neurol.* 509, 514–525. doi: 10.1002/cne.21768

Bindea, G., Mlecnik, B., Hackl, H., Charoentong, P., Tosolini, M., Kirilovsky, A., et al. (2009). ClueGO: a cytoscape plug-in to decipher functionally grouped gene ontology and pathway annotation networks. *Bioinformatics* 25, 1091–1093. doi: 10.1093/bioinformatics/btp101

Bornstein, C., Nevo, S., Giladi, A., Kadouri, N., Pouzolles, M., Gerbe, F., et al. (2018). Single-cell mapping of the thymic stroma identifies IL-25-producing tuft epithelial cells. *Nature* 559, 622–626. doi: 10.1038/s41586-018-0346-1

Colsoul, B., Schraenen, A., Lemaire, K., Quintens, R., Van Lommel, L., Segal, A., et al. (2010). Loss of high-frequency glucose-induced Ca2+ oscillations in pancreatic islets correlates with impaired glucose tolerance in Trpm5-/- mice. *Proc. Natl. Acad. Sci. U.S.A.* 107, 5208–5213. doi: 10.1073/pnas.0913107107

Delgiorno, K. E., Hall, J. C., Takeuchi, K. K., Pan, F. C., Halbrook, C. J., Washington, M. K., et al. (2014). Identification and manipulation of biliary metaplasia in pancreatic tumors. *Gastroenterology* 146, 233–244.e5. doi: 10.1053/j.gastro.2013.08.053

Desai, B. M., Oliver-Krasinski, J., De Leon, D. D., Farzad, C., Hong, N., Leach, S. D., et al. (2007). Preexisting pancreatic acinar cells contribute to acinar cell, but not islet beta cell, regeneration. *J. Clin. Invest.* 117, 971–977. doi: 10.1172/jci29988

Filippenko, L. N. (1981). Possibility of formation of brush cells from Type II alveolocytes in rats. *Biull. Eksp. Biol. Med.* 92, 616–620.

Gerbe, F., Sidot, E., Smyth, D. J., Ohmoto, M., Matsumoto, I., Dardalhon, V., et al. (2016). Intestinal epithelial tuft cells initiate type 2 mucosal immunity to helminth parasites. *Nature* 529, 226–230. doi: 10.1038/nature16527

Gerbe, F., van Es, J. H., Makrini, L., Brulin, B., Mellitzer, G., Robine, S., et al. (2011). Distinct ATOH1 and Neurog3 requirements define tuft cells as a new

secretory cell type in the intestinal epithelium. *J. Cell Biol.* 192, 767–780. doi: 10.1083/jcb.201010127

Howitt, M. R., Lavoie, S., Michaud, M., Blum, A. M., Tran, S. V., Weinstock, J. V., et al. (2016). Tuft cells, taste-chemosensory cells, orchestrate parasite type 2 immunity in the gut. *Science* 351, 1329–1333. doi: 10.1126/science.aaf1648

Jarvi, O., and Keyrilainen, O. (1956). On the cellular structures of the epithelial invasions in the glandular stomach of mice caused by intramural application of 20-methylcholantren. *Acta Pathol. Microbiol. Scand. Suppl.* 39(Suppl. 111), 72–73. doi: 10.1111/j.1600-0463.1956.tb06739.x

Kim, D., Langmead, B., and Salzberg, S. L. (2015). HISAT: a fast spliced aligner with low memory requirements. *Nat. Methods* 12, 357–360. doi: 10.1038/nmeth.3317

Lei, W., Ren, W., Ohmoto, M., Urban, J. F. Jr., Matsumoto, I., Margolskee, R. F., et al. (2018). Activation of intestinal tuft cell-expressed Sucnr1 triggers type 2 immunity in the mouse small intestine. *Proc. Natl. Acad. Sci. U.S.A.* 115, 5552–5557. doi: 10.1073/pnas.1720758115

May, R., Sureban, S. M., Lightfoot, S. A., Hoskins, A. B., Brackett, D. J., Postier, R. G., et al. (2010). Identification of a novel putative pancreatic stem/progenitor cell marker DCAMKL-1 in normal mouse pancreas. *Am. J. Physiol. Gastrointest. Liver Physiol.* 299, G303–G310. doi: 10.1152/ajpgi.00146.2010

Miller, C. N., Proekt, I., von Moltke, J., Wells, K. L., Rajpurkar, A. R., Wang, H., et al. (2018). Thymic tuft cells promote an IL-4-enriched medulla and shape thymocyte development. *Nature* 559, 627–631. doi: 10.1038/s41586-018-0345-2

Murtaugh, L. C., and Keefe, M. D. (2015). Regeneration and repair of the exocrine pancreas. *Annu. Rev. Physiol.* 77, 229–249. doi: 10.1146/annurev-physiol-021014-071727

Nadjsombati, M. S., McGinty, J. W., Lyons-Cohen, M. R., Jaffe, J. B., DiPeso, L., Schneider, C., et al. (2018). Detection of succinate by intestinal tuft cells triggers a type 2 innate immune circuit. *Immunity* 49, 33–41.e7. doi: 10.1016/j.immuni.2018.06.016

Pan, F. C., Bankaitis, E. D., Boyer, D., Xu, X., Van de Casteele, M., Magnuson, M. A., et al. (2013). Spatiotemporal patterns of multipotentiality in Ptf1a-expressing cells during pancreas organogenesis and injury-induced facultative restoration. *Development* 140, 751–764. doi: 10.1242/dev.090159

Pertea, M., Kim, D., Pertea, G. M., Leek, J. T., and Salzberg, S. L. (2016). Transcript-level expression analysis of RNA-seq experiments with HISAT, stringtie and ballgown. *Nat. Protoc.* 11, 1650–1667. doi: 10.1038/nprot.2016.095

Picelli, S., Faridani, O. R., Bjorklund, A. K., Winberg, G., Sagasser, S., and Sandberg, R. (2014). Full-length RNA-seq from single cells using Smart-seq2. *Nat. Protoc.* 9, 171–181. doi: 10.1038/nprot.2014.006

Pinho, A. V., Chantrill, L., and Rooman, I. (2014). Chronic pancreatitis: a path to pancreatic cancer. *Cancer Lett.* 345, 203–209. doi: 10.1016/j.canlet.2013.08.015

Rhodin, J., and Dalhamn, T. (1956). Electron microscopy of the tracheal ciliated mucosa in rat. *Z. Zellforsch. Mikrosk. Anat.* 44, 345–412. doi: 10.1007/bf00345847

Ritchie, M. E., Phipson, B., Wu, D., Hu, Y., Law, C. W., Shi, W., et al. (2015). limma powers differential expression analyses for RNA-sequencing and microarray studies. *Nucleic Acids Res.* 43:e47. doi: 10.1093/nar/gkv007

Sah, R. P., Garg, S. K., Dixit, A. K., Dudeja, V., Dawra, R. K., and Saluja, A. K. (2014). Endoplasmic reticulum stress is chronically activated in chronic pancreatitis. *J. Biol. Chem.* 289, 27551–27561. doi: 10.1074/jbc.M113.528174

Saqui-Salces, M., Keeley, T. M., Grosse, A. S., Qiao, X. T., El-Zaatari, M., Gumucio, D. L., et al. (2011). Gastric tuft cells express DCLK1 and are expanded in hyperplasia. *Histochem. Cell Biol.* 136, 191–204. doi: 10.1007/s00418-011-0831-1

Sato, A. (2007). Tuft cells. *Anat. Sci. Int.* 82, 187–199. doi: 10.1111/j.1447-073x.2007.00188.x

Schindelin, J., Arganda-Carreras, I., Frise, E., Kaynig, V., Longair, M., Pietzsch, T., et al. (2012). Fiji: an open-source platform for biological-image analysis. *Nat. Methods* 9, 676–682. doi: 10.1038/nmeth.2019

Schneider, C., O'Leary, C. E., von Moltke, J., Liang, H. E., Ang, Q. Y., Turnbaugh, P. J., et al. (2018). A metabolite-triggered tuft cell-ILC2 circuit drives small intestinal remodeling. *Cell* 174, 271–284.e14. doi: 10.1016/j.cell.2018.05.014

Shu, J., Fu, H., Qiu, G., Kaye, P., and Ilyas, M. (2013). Segmenting overlapping cell nuclei in digital histopathology images. *Conf. Proc. IEEE Eng. Med. Biol. Soc.* 2013, 5445–5448.

Siegel, R. L., Miller, K. D., and Jemal, A. (2019). Cancer statistics, 2019. *CA Cancer J. Clin.* 69, 7–34. doi: 10.3322/caac.21551

Storz, P. (2017). Acinar cell plasticity and development of pancreatic ductal adenocarcinoma. *Nat. Rev. Gastroenterol. Hepatol.* 14, 296–304. doi: 10.1038/nrgastro.2017.12

Strobel, O., Dor, Y., Alsina, J., Stirman, A., Lauwers, G., Trainor, A., et al. (2007). In vivo lineage tracing defines the role of acinar-to-ductal transdifferentiation in inflammatory ductal metaplasia. *Gastroenterology* 133, 1999–2009. doi: 10.1053/j.gastro.2007.09.009

Ting, H. A., and von Moltke, J. (2019). The immune function of tuft cells at gut mucosal surfaces and beyond. *J. Immunol.* 202, 1321–1329. doi: 10.4049/jimmunol.1801069

Ulmasov, B., Oshima, K., Rodriguez, M. G., Cox, R. D., and Neuschwander-Tetri, B. A. (2013). Differences in the degree of cerulein-induced chronic pancreatitis in C57BL/6 mouse substrains lead to new insights in identification of potential risk factors in the development of chronic pancreatitis. *Am. J. Pathol.* 183, 692–708. doi: 10.1016/j.ajpath.2013.05.020

von Moltke, J., Ji, M., Liang, H. E., and Locksley, R. M. (2016). Tuft-cell-derived IL-25 regulates an intestinal ILC2-epithelial response circuit. *Nature* 529, 221–225. doi: 10.1038/nature16161

Wang, J., Ohmuraya, M., Suyama, K., Hirota, M., Ozaki, N., Baba, H., et al. (2010). Relationship of strain-dependent susceptibility to experimentally induced acute pancreatitis with regulation of Prss1 and Spink3 expression. *Lab. Invest.* 90, 654–664. doi: 10.1038/labinvest.2010.44

Westphalen, C. B., Takemoto, Y., Tanaka, T., Macchini, M., Jiang, Z., Renz, B. W., et al. (2016). Dclk1 defines quiescent pancreatic progenitors that promote injury-induced regeneration and tumorigenesis. *Cell Stem Cell* 18, 441–455. doi: 10.1016/j.stem.2016.03.016

Whitcomb, D. C. (2013). Genetic risk factors for pancreatic disorders. *Gastroenterology* 144, 1292–1302. doi: 10.1053/j.gastro.2013.01.069

Yang, D., and Forsmark, C. E. (2017). Chronic pancreatitis. *Curr. Opin. Gastroenterol.* 33, 396–403. doi: 10.1097/MOG.0000000000000377

Zhang, Y., Zoltan, M., Riquelme, E., Xu, H., Sahin, I., Castro-Pando, S., et al. (2018). Immune cell production of interleukin 17 induces stem cell features of pancreatic intraepithelial neoplasia cells. *Gastroenterology* 155, 210–223.e13. doi: 10.1053/j.gastro.2018.03.041

Signaling in the Physiology and Pathophysiology of Pancreatic Stellate Cells – *a* Brief Review of Recent Advances

Agnieszka A. Kusiak[1], Mateusz D. Szopa[1], Monika A. Jakubowska[2†] and Pawel E. Ferdek[1*†]

[1] Faculty of Biochemistry, Biophysics and Biotechnology, Jagiellonian University, Kraków, Poland, [2] Malopolska Centre of Biotechnology, Jagiellonian University, Kraków, Poland

The interest in pancreatic stellate cells (PSCs) has been steadily growing over the past two decades due mainly to the central role these cells have in the desmoplastic reaction associated with diseases of the pancreas, such as pancreatitis or pancreatic cancer. In recent years, the scientific community has devoted substantial efforts to understanding the signaling pathways that govern PSC activation and interactions with neoplastic cells. This mini review aims to summarize some very recent findings on signaling in PSCs and highlight their impact to the field.

Keywords: calcium, Hippo, pancreatic cancer, pancreatic stellate cells, pancreas, PDAC, signaling, Wnt

INTRODUCTION

Since their discovery, pancreatic stellate cells (PSCs) have often been overlooked in favor of other cellular components of the pancreas – pancreatic acinar cells (PACs), ductal cells, and pancreatic islets – that all are present in evident abundance in the tissue architecture and perform obvious exocrine or endocrine functions. Only relatively recently have PSCs gained substantial attention from the scientific community, and this was once it became clear that these cells play important roles in pancreatic pathophysiology. PSCs occupy periacinar space and form a dynamic network in between pancreatic acini. In health, PSCs predominantly occur in a quiescent phenotype and are a minority among cellular components of the pancreas, comprising merely 4–7% of all cells in the organ (Apte et al., 1998). One characteristic propensity of quiescent PSCs is the presence of retinoid droplets in the cytosol (Apte et al., 1998). Upon activation triggered by tissue injury, PSCs undergo a series of morphological alterations, which include the loss of retinoid droplets, increased prominence of the ER network, and elongation of the cellular processes; they also start expressing alpha smooth muscle actin (α-SMA) as well as collagen types I and III, laminin, and fibronectin (Apte et al., 1998; Bachem et al., 1998). As a result, activated PSCs increase in numbers, and their products – extracellular matrix (ECM) components – may become a significant part of the organ. If unbalanced, this mechanism underlies the development of pancreatic fibrosis. This mini review aims to summarize the most recent studies on signaling in PSCs relevant in physiology and pathophysiology of the pancreas.

SIGNALING AND PSC ACTIVATION

Physiologically, the transition of quiescent PSCs into a proliferative, fibrogenic phenotype is an autonomous repair reaction to tissue injury. Since the damage to enzyme-storing PACs is

particularly threatening to the integrity of the tissue, there is an obvious need for an efficient and well-balanced system orchestrating regeneration and containment of the injury with PSC activation at its center. This mechanism is expected to have cross-talks between numerous signaling pathways (**Figure 1**), given that PSC activation may be triggered by various stimuli, such as inflammatory mediators (Mews et al., 2002), alcohol metabolites (Apte et al., 2000), and growth factors, including transforming growth factors TGF-α and TGF-β, platelet-derived growth factor (PDGF) (Apte et al., 1999), or connective tissue growth factor (CTGF) (Gao and Brigstock, 2005). These activating factors are secreted not only by infiltrating immune cells but might also be coming from other sources e.g., acinar cells (PACs) (Masamune and Shimosegawa, 2009). Other pathophysiologically relevant factors associated with PSC activation include hyperglycemia (Nomiyama et al., 2007), hypoxia (Masamune et al., 2008), and oxidative stress (Casini et al., 2000). It is widely accepted that signaling pathways, such as the MAPK/ERK (Jaster et al., 2002; Yoshida et al., 2004), PI3K (McCarroll et al., 2004), Smad (Ohnishi et al., 2004), Jak/STAT (Komar et al., 2017), PKC (Nomiyama et al., 2007), and Hedgehog (Li et al., 2014), play a crucial role in PSC physiology and have been subjects of previous reviews (Masamune and Shimosegawa, 2009). However, recent evidence has indicated that the Hippo and Wnt pathways as well as authophagy and calcium signaling might be equally important players in PSCs. These new findings are briefly described below.
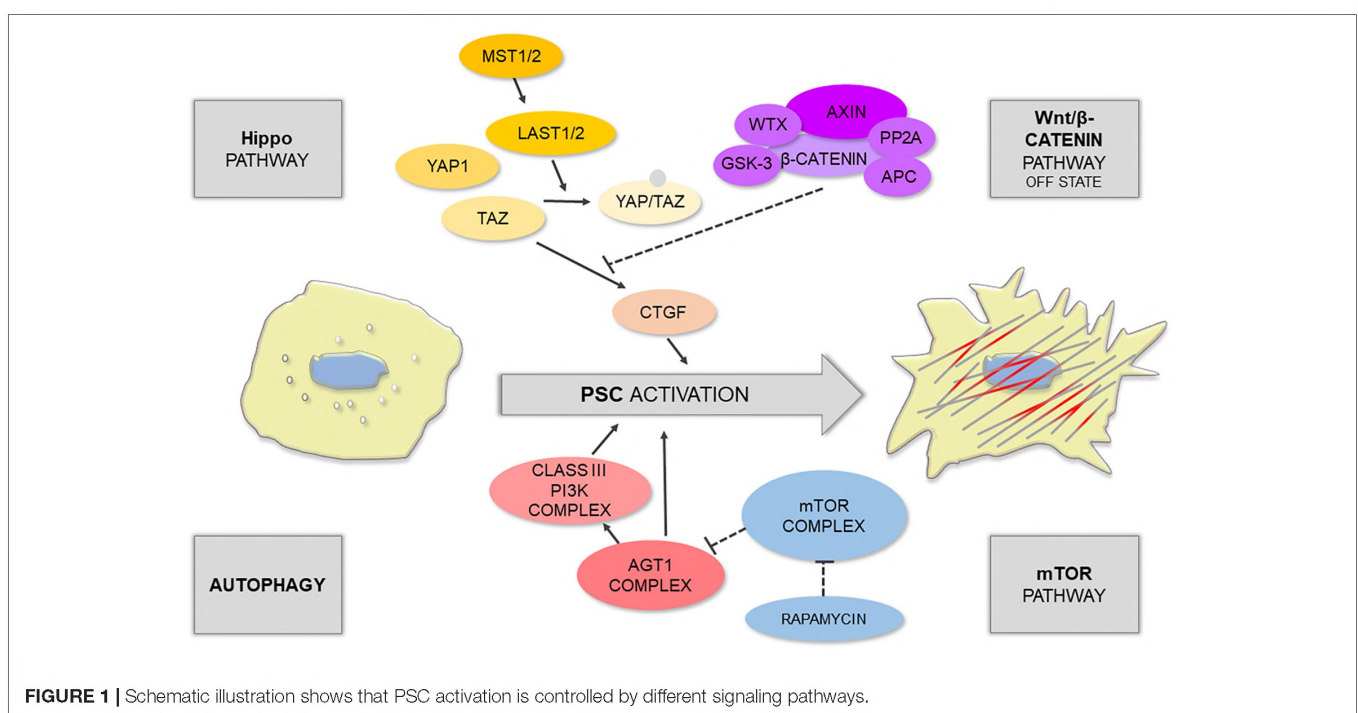
Hippo Signaling Pathway

The Hippo signaling pathway is one of the main restrictors of cell proliferation that tend to promote apoptosis; it can be triggered by numerous microenvironmental cues, such as cell–cell contact,

mechanotransduction, and cellular stress (Meng et al., 2016). During tissue repair, which normally requires cell proliferation, the Hippo pathway is often downregulated by phosphorylation of its main effectors: yes-associated protein 1 (YAP1) and transcriptional co-activator with PDZ-binding motif (TAZ) (Furth et al., 2018). This results in the switched off expression of YAP1/TAZ target genes, particularly CTGF, responsible for PSC activation. Liu J. et al. (2019) have recently demonstrated that acinar-specific deletion of central kinases in Hippo signaling – large tumor suppressor 1 and 2 (LATS1/2) – contributed to inflammation and severe fibrosis *in vivo*, even without the initiation of acinar cell rupture; whereas removal of CTGF with a neutralizing antibody attenuated this effect. The authors have also shown that in the mouse model of caerulein-induced pancreatitis there was an upregulation of secreted phosphoprotein 1 (SPP1) (Liu J. et al., 2019), a previously reported target of YAP1/TAZ involved in fibroinflammatory responses in other organs (Pardo et al., 2005). Interestingly, YAP1 and TAZ activity can be further modulated by the Wnt/β-catenin pathway. For instance, Wnt signaling can activate YAP1/TAZ by preventing their degradation by the β-catenin destruction complex (Hansen et al., 2015). Since the Wnt/β-catenin pathway plays a role in embryonic development as well as in homeostasis of the developed tissues, Wnt signaling becomes particularly important in the pathogenesis of proliferative diseases, including cancer.

Wnt Signaling Pathway

The main factors associated with the Wnt signaling pathway were found both in the endocrine and exocrine pancreas; this includes β-catenin, Wnt2, Wnt5a, and Wnt inhibitors e.g., the secreted frizzled-related protein (SFRP) family (Heller et al., 2003). The distribution of these factors is dependent on the

FIGURE 1 | Schematic illustration shows that PSC activation is controlled by different signaling pathways.

condition of the tissue – that is it changes upon tissue damage and in fibrosis. An analysis of human samples revealed that in the non-fibrotic pancreatic tissue, β-catenin is mainly located at the cell membrane of PACs, inhibitory SFRP4 is present in these cells, and Wnt2 is expressed at a low level (Blauer et al., 2019). In moderate fibrosis, the expression of Wnt2 in PACs increases, and β-catenin can now be found in the acinar nuclei indicating transcriptional activation; whereas in advanced fibrosis, β-catenin mostly localizes to PSCs (Blauer et al., 2019). Interestingly, this distribution pattern can be modeled *in vitro*. PSCs express β-catenin in monocultures, but when co-cultured with PACs, the levels of SFRP4 increase compared to monoculture, and thus PSCs do not exhibit nuclear distribution of β-catenin (Blauer et al., 2019). The above indicates that, in terms of Wnt signaling, a monoculture of PSCs reflects advanced stages of fibrosis, whereas a co-culture of PACs-PSCs has the expression pattern seen in moderate fibrosis. In another study, reversion of activated PSCs to quiescence was associated with upregulation of retinoic acid receptor β (RARβ), an increase in SFRP4 expression, and a reduction in nuclear β-catenin content in these cells (Carapuca et al., 2016). However, other reports suggest that both Wnt2 and SFRP4 might be elevated upon PSC activation (Hu et al., 2014). It is likely that PSCs could utilize multiple mechanisms regulating SFRP4, and thus its role in the interplay between PSCs and PACs, as well as in the process of PSC phenotype transition, is yet to be fully elucidated.

Autophagy

Autophagy is traditionally viewed either as a means for nutrient seeking under stress or as a physiological process for a cell quality check and removal of dysfunctional cellular components (Glick et al., 2010; Bootman et al., 2018). While it is normally pro-survival, disruption of autophagy has been associated with non-apoptotic cell death via the interaction of its main effector Beclin-1 with anti-apoptotic Bcl-2 protein (Pattingre et al., 2005). Just like other autophagy-related proteins (Atg), including Atg1 or Atg5, Beclin-1 acts as an initiator of autophagosome formation (Shibutani et al., 2015). The relationship between PSC activation, pancreatic fibrosis, and autophagy has recently been well documented in the literature; autophagy has been suggested to be a source of energy and molecular material for PSC phenotype transition and ECM deposition (Endo et al., 2017). In highly fibrotic pancreatic solid tumors, cancer cells can stimulate autophagy of PSCs. This leads to the release of non-essential amino acids (NEAA), mainly alanine, from PSCs; NEAA are then used by cancer cells as an alternative (to glucose) energy source (Sousa et al., 2016). However, mouse models revealed that deregulation of Atg5 in the pancreas results in a similar phenotype to that seen in human chronic pancreatitis, indicating that the development of this disease appears to involve defects in autophagy (Diakopoulos et al., 2015). Mammalian target of rapamycin (mTOR) is a very well-known suppressor of autophagy that inhibits this process by regulating the activity of the initiator complex Atg1/ULK1 (Mizushima, 2010). In turn, mTOR can be upregulated by sphingosine-1-phosphate (S1P) or its analog, the immunomodulator fingolimod (FTY720), both of which inhibit autophagy (Thangada et al., 2014). FTY720 has

been shown to suppress PSC activation and autophagy via the mTOR pathway; it can also increase the Bax/Bcl-2 ratio with a simultaneous decrease in the mitochondrial membrane potential (Cui et al., 2019). The mTOR pathway also links autophagy with intracellular calcium signals (Bootman et al., 2018).

Calcium Signaling

Calcium signaling is one of the most universal pathways, regulating virtually every cellular process from excitability and motility to apoptosis (Clapham, 2007). Sophisticated machinery consisting of pumps, ion channels, and active transporters controls Ca^{2+} homeostasis; while spatiotemporal changes in Ca^{2+} concentration encode signals that exert cell responses. In the pancreas, Ca^{2+} signals play a particularly important role in regulating secretion of digestive enzymes by PACs, which has been a relatively frequent subject of research in the past decades (Petersen and Tepikin, 2008). In contrast, Ca^{2+} signaling in PSCs has so far been investigated only by a handful of studies. Nevertheless, recent reports indicate that Ca^{2+} signals are also important in the regulation of PSC physiology, showing a clear cross-talk with other pathways, such as NO signaling (Jakubowska et al., 2016). We already know that PSCs express bradykinin receptor type 2 (BDKRB2) (Ferdek et al., 2016), and pharmacological studies revealed that these cells produce Ca^{2+} responses even to very low doses of bradykinin (Won et al., 2011; Gryshchenko et al., 2016a). Since bradykinin is a well-known pro-inflammatory mediator, BDKRB2 signaling may well play a role in activation of PSCs in diseases of the pancreas (Gryshchenko et al., 2016b). PSCs also express a number of Ca^{2+} channels, particularly those from the family of transient receptor potential (TRP). For example, TRPC6 has been associated with autocrine stimulation of PSCs in hypoxic conditions (Nielsen et al., 2017); whereas another TRP member, TRPC1, was proposed to contribute to pressure-induced activation of these cells (Fels et al., 2016). Deregulated Ca^{2+} signals directly underlie the pathophysiology of acute pancreatitis, and thus it is somewhat surprising that so little is known about the effects that common inducers of pancreatic pathology, such as bile acids and ethanol metabolites, have on Ca^{2+} signaling in PSCs. Given that ethanol induces the expression of TRPV4 in these cells (Zhang et al., 2013), whereas sodium cholate and taurocholate generate noxious and sustained Ca^{2+} signals (Ferdek et al., 2016), the contribution of PSCs in the development of acute pancreatitis might still be underrated by the current dogma.

PSCs IN DISEASES OF THE PANCREAS

Despite being a minority in the normal pancreas, the role of activated PSCs becomes apparent in pathophysiological conditions. It is well established that persistent activation of PSCs is the main contributor to fibrosis in pancreatic diseases, with pancreatic cancer and pancreatitis being the most prevalent. In health, PSCs regulate ECM turnover not only by producing its components but also by secreting key enzymes engaged in EMC remodeling – matrix metalloproteinases (MMP) as well as their inhibitors – tissue inhibitors of metalloproteinases (TIMPs)

(Phillips et al., 2003). PSCs have been shown to activate in response to cytokines upregulated in acute pancreatitis (Mews et al., 2002). Upon activation, the fate of PSCs largely depends on the external stimuli and can follow different scenarios. If the injury is transient, activated PSCs revert to quiescence or become senescent (McCarroll et al., 2003). However, a subpopulation of PSCs may expand excessively when activating factors accumulate or occur in a persistent manner e.g., in chronic pancreatitis (Haber et al., 1999; Masamune et al., 2009). Activated PSCs secrete increased amounts of MMP-2 (Phillips et al., 2003), and this enzyme breaks down normal basement membrane, which then may hasten its replacement by fibril-forming collagen (Friedman, 2000).

Pancreatic cancer – mainly pancreatic ductal adenocarcinoma (PDAC) – remains one of the most serious problems of our modern society. According to the Global Cancer Statistics 2018 (GLOBOCAN 2018), PDAC has been ranked the 11th most frequent cancer worldwide and the 7th most deadly cancer, accounting for 4.5% of all cancer-related deaths (Bray et al., 2018). The hallmark of pancreatic tumorigenesis is a desmoplastic reaction that leads to the formation of fibrotic stroma. The stroma not only provides a hypoxic microenvironment for the neoplastic cells, but it also constitutes a physical barrier that limits the efficacy of drug delivery to the tumor. Despite significant advances in the treatment regimens and surgical procedures, the collagen-rich fibrotic microenvironment of pancreatic cancer is the main reason why chemotherapeutics are largely ineffective and the clinical outcome remains very poor (Dangi-Garimella et al., 2011; Shields et al., 2012). It is becoming increasingly clear that a successful therapy should not only be focused on cancer cells but also target the tumor-associated fibrotic stroma.

Pancreatic stellate cells are the main cellular contributors to the desmoplastic reaction in PDAC. They become progressively activated in the process of tumorigenesis and deposit collagen fibers that embed and protect cancer cells. This collagen-rich microenvironment becomes an integral part of the developing tumor, and the interactions between the stroma and cancer cells are essential practically at every stage of tumorigenesis from its initiation, through progression, and to metastasis. As an example, PSCs have been shown to increase the viability and proliferative capacity of cancer cells as well as reduce gemcitabine-induced apoptosis of these cells. This was attenuated by pharmacological blockade of TGF-β receptor I (TGF-βRI, ALK5) (Liu S.L. et al., 2019). The inhibition of stroma-cancer cell interactions is currently attracting a lot of interest as a promising strategy that may sensitize PDAC to therapy and increase the 5-year survival rate of patients suffering from this disease (Cannon et al., 2018).

SIGNALING IN PSC-CANCER CELL INTERACTIONS

In light of the above, a number of recent studies have been devoted to investigating signaling pathways in tumor–stroma interactions. Yet again, the Hippo pathway stands out as an important player in pancreatic tumorigenesis. YAP1 is expressed by cancer cells as well as is present in the nuclei of PDAC-derived

PSCs, correlating with their activated phenotype. Xiao et al. (2019) have recently demonstrated *in vitro* that depletion of YAP1 in PSCs (via silencing its expression) results in a shift of PSC phenotype toward quiescence, evidenced by a downregulation of markers such as α-SMA and collagen I as well as a decrease in PSC contractility and proliferation. While secreted protein acidic and cysteine rich (SPARC) has previously been associated with the poor outcomes of pancreatic cancer patients (Erkan et al., 2008; Whatcott et al., 2015), very recently SPARC has been identified as a downstream target of YAP1 that mediates its effects on cancer cell proliferation via paracrine signaling (Xiao et al., 2019). Since YAP1 expression shows a strong correlation with the degree of tissue fibrosis in patient samples, YAP1 was suggested as a feasible target in PDAC therapy that, in principle, could inactivate PSCs and limit the development of the tumor-associated stroma (Xiao et al., 2019).

Another recently revealed paracrine factor involved in stroma–cancer cell interactions is leukemia inhibitory factor (LIF) (Ohlund et al., 2017; Bressy et al., 2018; Shi et al., 2019). This cytokine is secreted by activated PSCs in PDAC lesions and acts on the neighboring cancer cells via its receptor LIFR, activating the STAT3 pathway, driving tumor progression and increasing chemoresistance (Shi et al., 2019). Since its circulating and tissue levels increase in PDAC patients, LIF was postulated to be both a novel biomarker and a feasible therapeutic target.

Stroma–cellular interaction may also occur via cell surface receptors such as integrins (Schnittert et al., 2018). Integrin α-11 (ITGA11), a collagen type I–binding receptor, is an interesting example: essentially absent in the healthy pancreas, it becomes expressed within the stromal fraction of PDAC tissues. It has been found that approximately 80% of α-SMA-positive cells are also ITGA11-positive, and knockdown of ITGA11 in PSCs results in attenuation of differentiation, migration, and secretion of ECM components by these cells (Schnittert et al., 2019). Another cell surface protein, integrin α-5 (ITGA5), was also shown to be present in as many as 72% of α-SMA-positive cells in human PDAC tissues, and its high expression was associated with poor prognosis (Kuninty et al., 2019). ITGA5 was demonstrated to play a role in TGF-β–mediated activation of PSCs via Smad2 and FAK pathways; and its knockdown inhibited both PSC-induced cancer cell proliferation *in vitro* and tumor growth *in vivo* (Kuninty et al., 2019). The authors went even one step further and developed a novel ITGA5-antagonizing peptidomimetic (AV3) that could inhibit PSC activation and enhance the cytotoxic effects of gemcitabine in spheroid co-cultures of cancer cell lines with PSCs (Kuninty et al., 2019).

Bcl2-associated athanogene 3 (BAG3) is expressed by multiple cancer types, including PDAC, and correlates with poor prognosis. Recent studies show that this marker is also present in activated PSCs and may promote, via IL−6, TGF−β2, and insulin-like growth factor-binding protein 2 (IGFBP2) signaling, autocrine-driven maintenance of the activated phenotype in these cells (Yuan et al., 2019). *Vice versa*, BAG3−positive PSCs also increase migration and invasion capacity of nearby cancer cells via soluble factors such as IL−8, monocyte chemoattractant protein-1 (MCP-1), TGF−β2, and IGFBP2 (Yuan et al., 2019). A recent report shows that plasminogen activator inhibitor-1

(PAI-1), a common regulator of blood coagulation, cell apoptosis, and migration, is secreted by pancreatic cancer cells and activates PSCs LRP-1/ERK/c-JUN signaling (Wang et al., 2019). Interestingly, knockdown of PAI-1 in cancer cells abolished activation in co-cultured PSCs, indicating that PAI-1 might be one of the key players in PSC – cancer cell interaction (Fang et al., 2012).

While cancer-associated PSCs secrete hepatocyte growth factor (HGF), its receptor c-MET is present on pancreatic cancer cells. Simultaneous inhibition of HGF and c-MET combined with gemcitabine is more effective in reduction of tumor volume in an orthotopic model of pancreatic cancer than chemotherapy alone, indicating a critical role of the HGF/c-MET pathway in PSC–cancer cell interactions (Pothula et al., 2017). What is more, inhibition of HGF, c-MET, and urokinase-type plasminogen activator (uPA) has been shown to decrease the angiogenic properties of endothelial cells, suggesting the role of PSCs and the HGF/c-MET pathway in neoangionesis (Patel et al., 2014). The authors envision that a novel antiangiogenic approach that targets the HGF/c-MET and uPA pathways could be used against pancreatic cancer (Patel et al., 2014).

MECHANOSENSING AND ECM STIFFNESS

The human pancreas is an organ that weights only approximately 100 g (Innes and Carey, 1994), but it produces daily as much as 1 L (or 1 kg) of pancreatic juice, comprising water, bicarbonate, and a variety of digestive enzymes (Pallagi et al., 2015). This substantial difference between the juice mass and the mass of the tissue is associated with mechanical stress in the organ exerted by the fluid pressure on pancreatic duct walls and pancreatic acini. PSCs have recently been attributed to sensing the mechanical properties of pancreatic microenvironment (Cortes et al., 2019b). PSCs control mechanostasis (mechanical homeostasis of the organ in response to various types of forces) not only in the normal tissue but also under pathophysiological conditions like that present in the development of fibrosis (Ferdek and Jakubowska, 2017). Deposition of collagen fibers by activated PSCs, as well as the presence of cross-linking in these fibers, affects the mechanical properties of the pancreatic microenvironment, making it dense and rigid (Cortes et al., 2019a,b). In light of the recent findings, activated PSCs might be able to sense fiber topology, adhesiveness of their surroundings, and viscoelasticity of the stroma (Papalazarou et al., 2018). Stress, strain, and forces that stretch the fibrillary proteins are also mechanosensed by myofibroblast-like cells (Chen et al., 2017). Importantly, the increased matrix stiffness may further promote activation of PSCs, supporting a positive feedback loop that perpetuates formation of the dense fibrotic tumor stroma (Bachem et al., 2005). Therefore, modulation of the mechanical properties of the desmoplastic pancreatic tissue, in order to decrease its density and overcome problems with drug delivery, may become one of key strategies in successful therapy of pancreatic cancer (Papalazarou et al., 2018). Only very recently has tamoxifen, a drug used successfully against

breast cancer cells, been demonstrated to inhibit differentiation of quiescent PSCs into myofibroblasts via the G protein-coupled estrogen receptor (GPER)- and hypoxia-inducible factor-1 alpha (HIF-1α)-mediated mechanism and suppress matrix remodeling (Cortes et al., 2019a,b). Another plausible anti-fibrotic and mechanomodulatory strategy against pancreatic diseases could be targeting YAP and TAZ signal transduction of the Hippo pathway: YAP/TAZ, via their interaction with the cell cytoskeleton, promote cell "stemness," tissue regeneration, and remodeling of the stroma; whereas YAP can modulate fibroinflammatory responses (Martinez et al., 2019).

What is more, activated PSCs express hyaluronan synthase 2 (HAS2) as well as hyaluronidase 1 (HYAL1) and have been identified as an important source of stromal hyaluronic acid (HA) (Junliang et al., 2019). In turn, HA has been attributed to high interstitial fluid pressure and vascular collapse in PDAC desmoplastic reaction (Provenzano et al., 2012). Enzymatic degradation of HA has been shown to reduce the interstitial pressure, restore the microvasculature and enhance the efficacy of chemotherapy (Kultti et al., 2012; Provenzano et al., 2012; Jacobetz et al., 2013). Of note is that HA binds to CD44, commonly expressed by many types of cancer cells, and this interaction promotes tumor-driving signaling and transport activities (Slomiany et al., 2009; Toole, 2009). Since CD44 has also been found on the surface of PDAC cells (Zhao et al., 2016), the full spectrum of HA roles in pancreatic cancer might be even more complex; but this notion requires further investigation.

REVERSION TO QUIESCENCE

Since activation of PSCs can often become part of the pathophysiological process, a number of attempts have been made to either block the phenotype transition in these cells or force already activated PSCs back to quiescence. Treatment with retinol and retinoic acid (both ATRA and 9-RA) was used to inhibit cell proliferation, expression of activation markers and the MAPK signaling pathway in these cells; and retinol even blocked ethanol-induced activation of PSCs (McCarroll et al., 2006). Further, ligands of PPARγ, a nuclear receptor
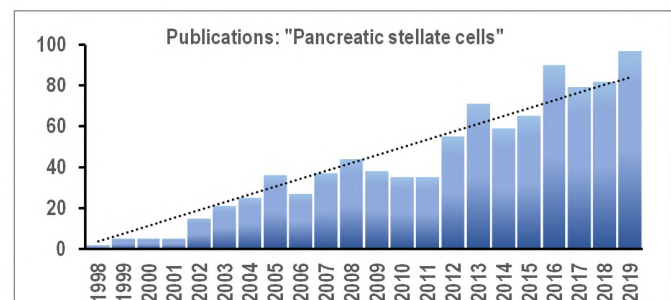
FIGURE 2 | Bar chart shows the number of new scientific papers published each year between 2008 and 2019 with the phrase "pancreatic stellate cells" in the text (based on online search via PubMed.gov). Trend line (dotted): $y = 3.8179x$; $R^2 = 0.914$.

regulating lipid storage and glucose metabolism, inhibited PSC proliferation and decreased expression of α-SMA and MCP-1, suggesting a potential role of PPARγ in the development of pancreatic fibrosis and inflammation (Masamune et al., 2002). More recently, it was shown that vitamin D receptor (VDR) is present in the stroma of human pancreatic tumors, and its ligand, calcipotriol, reduces markers of inflammation and fibrosis in mouse models of pancreatitis and pancreatic cancer (Sherman et al., 2014). A different group demonstrated that while vitamin D2, vitamin D3 and calcipotriol inhibit activation of PSCs *in vitro*, they fail to reverse the phenotype transition after the cells have already been activated (Wallbaum et al., 2018).

CONCLUDING REMARKS

For the last two decades, there has been a steady (linear) increase in the number of papers on PSCs published every year (**Figure 2**). This new field continues to expand, and increasingly more efforts are directed toward uncovering the signaling pathways that control PSC physiology. Since PSC activation underlies the pathogenesis of pancreatic disorders, the signals that induce

phenotype transition in these cells are of particular interest. Targeted manipulation of these signals might prevent or even revert PSC activation and become a useful tool in the therapy of pancreatic diseases.

AUTHOR CONTRIBUTIONS

FUNDING

REFERENCES

Apte, M. V., Haber, P. S., Applegate, T. L., Norton, I. D., Mccaughan, G. W., Korsten, M. A., et al. (1998). Periacinar stellate shaped cells in rat pancreas: identification, isolation, and culture. *Gut* 43, 128–133. doi: 10.1136/gut.43.1.128

Apte, M. V., Haber, P. S., Darby, S. J., Rodgers, S. C., Mccaughan, G. W., Korsten, M. A., et al. (1999). Pancreatic stellate cells are activated by proinflammatory cytokines: implications for pancreatic fibrogenesis. *Gut* 44, 534–541. doi: 10.1136/gut.44.4.534

Apte, M. V., Phillips, P. A., Fahmy, R. G., Darby, S. J., Rodgers, S. C., Mccaughan, G. W., et al. (2000). Does alcohol directly stimulate pancreatic fibrogenesis? Studies with rat pancreatic stellate cells. *Gastroenterology* 118, 780–794. doi: 10.1016/s0016-5085(00)70148-x

Bachem, M. G., Schneider, E., Gross, H., Weidenbach, H., Schmid, R. M., Menke, A., et al. (1998). Identification, culture, and characterization of pancreatic stellate cells in rats and humans. *Gastroenterology* 115, 421–432. doi: 10.1016/s0016-5085(98)70209-4

Bachem, M. G., Schunemann, M., Ramadani, M., Siech, M., Beger, H., Buck, A., et al. (2005). Pancreatic carcinoma cells induce fibrosis by stimulating proliferation and matrix synthesis of stellate cells. *Gastroenterology* 128, 907–921. doi: 10.1053/j.gastro.2004.12.036

Blauer, M., Laaninen, M., Sand, J., and Laukkarinen, J. (2019). Wnt/beta-catenin signalling plays diverse functions during the process of fibrotic remodelling in the exocrine pancreas. *Pancreatology* 19, 252–257. doi: 10.1016/j.pan.2019.02.003

Bootman, M. D., Chehab, T., Bultynck, G., Parys, J. B., and Rietdorf, K. (2018). The regulation of autophagy by calcium signals: Do we have a consensus? *Cell Calcium.* 70, 32–46. doi: 10.1016/j.ceca.2017.08.005

Bray, F., Ferlay, J., Soerjomataram, I., Siegel, R. L., Torre, L. A., and Jemal, A. (2018). Global cancer statistics 2018: GLOBOCAN estimates of incidence and mortality worldwide for 36 cancers in 185 countries. *CA Cancer J. Clin.* 68, 394–424. doi: 10.3322/caac.21492

Bressy, C., Lac, S., Nigri, J., Leca, J., Roques, J., Lavaut, M. N., et al. (2018). LIF drives neural remodeling in pancreatic cancer and offers a new candidate biomarker. *Cancer Res.* 78, 909–921. doi: 10.1158/0008-5472.CAN-15-2790

Cannon, A., Thompson, C., Hall, B. R., Jain, M., Kumar, S., and Batra, S. K. (2018). Desmoplasia in pancreatic ductal adenocarcinoma: insight into pathological function and therapeutic potential. *Genes Cancer* 9, 78–86. doi: 10.18632/genesandcancer.171

Carapuca, E. F., Gemenetzidis, E., Feig, C., Bapiro, T. E., Williams, M. D., Wilson, A. S., et al. (2016). Anti-stromal treatment together with chemotherapy targets multiple signalling pathways in pancreatic adenocarcinoma. *J. Pathol.* 239, 286–296. doi: 10.1002/path.4727

Casini, A., Galli, A., Pignalosa, P., Frulloni, L., Grappone, C., Milani, S., et al. (2000). Collagen type I synthesized by pancreatic periacinar stellate cells (PSC) co-localizes with lipid peroxidation-derived aldehydes in chronic alcoholic pancreatitis. *J. Pathol.* 192, 81–89. doi: 10.1002/1096-9896(2000)9999:9999<::aid-path675>3.0.co;2-n

Chen, Y., Ju, L., Rushdi, M., Ge, C., and Zhu, C. (2017). Receptor-mediated cell mechanosensing. *Mol. Biol. Cell* 28, 3134–3155. doi: 10.1091/mbc.E17-04-0228

Clapham, D. E. (2007). Calcium signaling. *Cell* 131, 1047–1058.

Cortes, E., Lachowski, D., Robinson, B., Sarper, M., Teppo, J. S., Thorpe, S. D., et al. (2019a). Tamoxifen mechanically reprograms the tumor microenvironment via HIF-1A and reduces cancer cell survival. *EMBO Rep.* 2:e46557. doi: 10.15252/embr.201846557

Cortes, E., Sarper, M., Robinson, B., Lachowski, D., Chronopoulos, A., Thorpe, S. D., et al. (2019b). GPER is a mechanoregulator of pancreatic stellate cells and the tumor microenvironment. *EMBO Rep.* 20:e46556. doi: 10.15252/embr.201846556

Cui, L., Li, C., Gao, G., Zhuo, Y., Yang, L., Cui, N., et al. (2019). FTY720 inhibits the activation of pancreatic stellate cells by promoting apoptosis and suppressing autophagy via the AMPK/mTOR pathway. *Life Sci.* 217, 243–250. doi: 10.1016/j.lfs.2018.12.019

Dangi-Garimella, S., Krantz, S. B., Barron, M. R., Shields, M. A., Heiferman, M. J., Grippo, P. J., et al. (2011). Three-dimensional collagen I promotes gemcitabine resistance in pancreatic cancer through MT1-MMP-mediated expression of HMGA2. *Cancer Res.* 71, 1019–1028. doi: 10.1158/0008-5472.CAN-10-1855

Diakopoulos, K. N., Lesina, M., Wormann, S., Song, L., Aichler, M., Schild, L., et al. (2015). Impaired autophagy induces chronic atrophic pancreatitis in mice via sex- and nutrition-dependent processes. *Gastroenterology* 148, 626–638e617. doi: 10.1053/j.gastro.2014.12.003

Endo, S., Nakata, K., Ohuchida, K., Takesue, S., Nakayama, H., Abe, T., et al. (2017). Autophagy is required for activation of pancreatic stellate cells, associated with pancreatic cancer progression and promotes growth of pancreatic tumors in mice. *Gastroenterology* 152, 1492.e24–1506.e24. doi: 10.1053/j.gastro.2017.01.010

Erkan, M., Michalski, C. W., Rieder, S., Reiser-Erkan, C., Abiatari, I., Kolb, A., et al. (2008). The activated stroma index is a novel and independent prognostic

marker in pancreatic ductal adenocarcinoma. *Clin. Gastroenterol. Hepatol.* 6, 1155–1161. doi: 10.1016/j.cgh.2008.05.006

Fang, H., Placencio, V. R., and Declerck, Y. A. (2012). Protumorigenic activity of plasminogen activator inhibitor-1 through an antiapoptotic function. *J. Natl. Cancer Inst.* 104, 1470–1484. doi: 10.1093/jnci/djs377

Fels, B., Nielsen, N., and Schwab, A. (2016). Role of TRPC1 channels in pressure-mediated activation of murine pancreatic stellate cells. *Eur. Biophys. J.* 45, 657–670. doi: 10.1007/s00249-016-1176-4

Ferdek, P. E., and Jakubowska, M. A. (2017). Biology of pancreatic stellate cells - more than pancreatic cancer. *Pflugers Arch.* 469, 1039–1050. doi: 10.1007/s00424-017-1968-0

Ferdek, P. E., Jakubowska, M. A., Gerasimenko, J. V., Gerasimenko, O. V., and Petersen, O. H. (2016). Bile acids induce necrosis in pancreatic stellate cells dependent on calcium entry and sodium-driven bile uptake. *J. Physiol.* 594, 6147–6164. doi: 10.1113/JP272774

Friedman, S. L. (2000). Molecular regulation of hepatic fibrosis, an integrated cellular response to tissue injury. *J. Biol Chem.* 275, 2247–2250. doi: 10.1074/jbc.275.4.2247

Furth, N., Aylon, Y., and Oren, M. (2018). p53 shades of Hippo. *Cell Death Differ.* 25, 81–92. doi: 10.1038/cdd.2017.163

Gao, R., and Brigstock, D. R. (2005). Connective tissue growth factor (CCN2) in rat pancreatic stellate cell function: integrin alpha5beta1 as a novel CCN2 receptor. *Gastroenterology* 129, 1019–1030. doi: 10.1053/j.gastro.2005.06.067

Glick, D., Barth, S., and Macleod, K. F. (2010). Autophagy: cellular and molecular mechanisms. *J. Pathol.* 221, 3–12. doi: 10.1002/path.2697

Gryshchenko, O., Gerasimenko, J. V., Gerasimenko, O. V., and Petersen, O. H. (2016a). Ca2+ signals mediated by bradykinin type 2 receptors in normal pancreatic stellate cells can be inhibited by specific Ca2+ channel blockade. *J. Physiol.* 594, 281–293. doi: 10.1113/jp271468

Gryshchenko, O., Gerasimenko, J. V., Gerasimenko, O. V., and Petersen, O. H. (2016b). Calcium signalling in pancreatic stellate cells: mechanisms and potential roles. *Cell Calcium.* 59, 140–144. doi: 10.1016/j.ceca.2016.02.003

Haber, P. S., Keogh, G. W., Apte, M. V., Moran, C. S., Stewart, N. L., Crawford, D. H., et al. (1999). Activation of pancreatic stellate cells in human and experimental pancreatic fibrosis. *Am. J. Pathol.* 155, 1087–1095. doi: 10.1016/s0002-9440(10)65211-x

Hansen, C. G., Moroishi, T., and Guan, K. L. (2015). YAP and TAZ: a nexus for Hippo signaling and beyond. *Trends Cell Biol.* 25, 499–513. doi: 10.1016/j.tcb.2015.05.002

Heller, R. S., Klein, T., Ling, Z., Heimberg, H., Katoh, M., Madsen, O. D., et al. (2003). Expression of Wnt, Frizzled, sFRP, and DKK genes in adult human pancreas. *Gene Expr.* 11, 141–147. doi: 10.3727/000000003108749035

Hu, Y., Wan, R., Yu, G., Shen, J., Ni, J., Yin, G., et al. (2014). Imbalance of Wnt/Dkk negative feedback promotes persistent activation of pancreatic stellate cells in chronic pancreatitis. *PLoS One* 9:e95145. doi: 10.1371/journal.pone.0095145

Innes, J. T., and Carey, L. C. (1994). Normal pancreatic dimensions in the adult human. *Am. J. Surg.* 167, 261–263. doi: 10.1016/0002-9610(94)90088-4

Jacobetz, M. A., Chan, D. S., Neesse, A., Bapiro, T. E., Cook, N., Frese, K. K., et al. (2013). Hyaluronan impairs vascular function and drug delivery in a mouse model of pancreatic cancer. *Gut* 62, 112–120. doi: 10.1136/gutjnl-2012-302529

Jakubowska, M. A., Ferdek, P. E., Gerasimenko, O. V., Gerasimenko, J. V., and Petersen, O. H. (2016). Nitric oxide signals are interlinked with calcium signals in normal pancreatic stellate cells upon oxidative stress and inflammation. *Open Biol.* 6:160149. doi: 10.1098/rsob.160149

Jaster, R., Sparmann, G., Emmrich, J., and Liebe, S. (2002). Extracellular signal regulated kinases are key mediators of mitogenic signals in rat pancreatic stellate cells. *Gut* 51, 579–584. doi: 10.1136/gut.51.4.579

Junliang, L., Lili, W., Xiaolong, L., Xuguang, L., Huanwen, W., and Zhiyong, L. (2019). High-molecular-weight hyaluronan produced by activated pancreatic stellate cells promotes pancreatic cancer cell migration via paracrine signaling. *Biochem. Biophys. Res. Commun.* 515, 493–498. doi: 10.1016/j.bbrc.2019.05.167

Komar, H. M., Serpa, G., Kerscher, C., Schwoegl, E., Mace, T. A., Jin, M., et al. (2017). Inhibition of Jak/STAT signaling reduces the activation of pancreatic stellate cells in vitro and limits caerulein-induced chronic pancreatitis in vivo. *Sci. Rep.* 7:1787. doi: 10.1038/s41598-017-01973-0

Kultti, A., Li, X., Jiang, P., Thompson, C. B., Frost, G. I., and Shepard, H. M. (2012). Therapeutic targeting of hyaluronan in the tumor stroma. *Cancers* 4, 873–903. doi: 10.3390/cancers4030873

Kuninty, P. R., Bansal, R., De Geus, S. W. L., Mardhian, D. F., Schnittert, J., Van Baarlen, J., et al. (2019). ITGA5 inhibition in pancreatic stellate cells attenuates desmoplasia and potentiates efficacy of chemotherapy in pancreatic cancer. *Sci. Adv.* 5:eaax2770. doi: 10.1126/sciadv.aax2770

Li, X., Wang, Z., Ma, Q., Xu, Q., Liu, H., Duan, W., et al. (2014). Sonic hedgehog paracrine signaling activates stromal cells to promote perineural invasion in pancreatic cancer. *Clin. Cancer Res.* 20, 4326–4338. doi: 10.1158/1078-0432. CCR-13-3426

Liu, J., Gao, M., Nipper, M., Deng, J., Sharkey, F. E., Johnson, R. L., et al. (2019). Activation of the intrinsic fibroinflammatory program in adult pancreatic acinar cells triggered by Hippo signaling disruption. *PLoS Biol.* 17:e3000418. doi: 10.1371/journal.pbio.3000418

Liu, S. L., Cao, S. G., Li, Y., Sun, B., Chen, D., Wang, D. S., et al. (2019). Pancreatic stellate cells facilitate pancreatic cancer cell viability and invasion. *Oncol. Lett.* 17, 2057–2062.

Martinez, B., Yang, Y., Harker, D. M. R., Farrar, C., Mukundan, H., Nath, P., et al. (2019). YAP/TAZ related biomechano signal transduction and cancer metastasis. *Front. Cell Dev. Biol.* 7:199. doi: 10.3389/fcell.2019.00199

Masamune, A., Kikuta, K., Satoh, M., Sakai, Y., Satoh, A., and Shimosegawa, T. (2002). Ligands of peroxisome proliferator-activated receptor-gamma block activation of pancreatic stellate cells. *J. Biol. Chem.* 277, 141–147. doi: 10.1074/jbc.m107582200

Masamune, A., Kikuta, K., Watanabe, T., Satoh, K., Hirota, M., and Shimosegawa, T. (2008). Hypoxia stimulates pancreatic stellate cells to induce fibrosis and angiogenesis in pancreatic cancer. *Am. J. Physiol. Gastrointest. Liver. Physiol.* 295, G709–G717. doi: 10.1152/ajpgi.90356.2008

Masamune, A., and Shimosegawa, T. (2009). Signal transduction in pancreatic stellate cells. *J. Gastroenterol.* 44, 249–260. doi: 10.1007/s00535-009-0013-2

Masamune, A., Watanabe, T., Kikuta, K., and Shimosegawa, T. (2009). Roles of pancreatic stellate cells in pancreatic inflammation and fibrosis. *Clin. Gastroenterol. Hepatol.* 7, S48–S54. doi: 10.1016/j.cgh.2009.07.038

McCarroll, J. A., Phillips, P. A., Kumar, R. K., Park, S., Pirola, R. C., Wilson, J. S., et al. (2004). Pancreatic stellate cell migration: role of the phosphatidylinositol 3-kinase(PI3-kinase) pathway. *Biochem. Pharmacol.* 67, 1215–1225. doi: 10.1016/j.bcp.2003.11.013

McCarroll, J. A., Phillips, P. A., Park, S., Doherty, E., Pirola, R. C., Wilson, J. S., et al. (2003). Pancreatic stellate cell activation by ethanol and acetaldehyde: is it mediated by the mitogen-activated protein kinase signaling pathway? *Pancreas* 27, 150–160. doi: 10.1097/00006676-200308000-00008

McCarroll, J. A., Phillips, P. A., Santucci, N., Pirola, R. C., Wilson, J. S., and Apte, M. V. (2006). Vitamin A inhibits pancreatic stellate cell activation: implications for treatment of pancreatic fibrosis. *Gut* 55, 79–89. doi: 10.1136/gut.2005.064543

Meng, Z., Moroishi, T., and Guan, K. L. (2016). Mechanisms of Hippo pathway regulation. *Genes Dev.* 30, 1–17. doi: 10.1101/gad.274027.115

Mews, P., Phillips, P., Fahmy, R., Korsten, M., Pirola, R., Wilson, J., et al. (2002). Pancreatic stellate cells respond to inflammatory cytokines: potential role in chronic pancreatitis. *Gut* 50, 535–541. doi: 10.1136/gut.50.4.535

Mizushima, N. (2010). The role of the Atg1/ULK1 complex in autophagy regulation. *Curr. Opin. Cell Biol.* 22, 132–139. doi: 10.1016/j.ceb.2009.12.004

Nielsen, N., Kondratska, K., Ruck, T., Hild, B., Kovalenko, I., Schimmelpfennig, S., et al. (2017). TRPC6 channels modulate the response of pancreatic stellate cells to hypoxia. *Pflugers Arch.* 469, 1567–1577. doi: 10.1007/s00424-017-2057-0

Nomiyama, Y., Tashiro, M., Yamaguchi, T., Watanabe, S., Taguchi, M., Asaumi, H., et al. (2007). High glucose activates rat pancreatic stellate cells through protein kinase C and p38 mitogen-activated protein kinase pathway. *Pancreas* 34, 364–372. doi: 10.1097/mpa.0b013e31802f0531

Ohlund, D., Handly-Santana, A., Biffi, G., Elyada, E., Almeida, A. S., Ponz-Sarvise, M., et al. (2017). Distinct populations of inflammatory fibroblasts and myofibroblasts in pancreatic cancer. *J. Exp. Med.* 214, 579–596. doi: 10.1084/jem.20162024

Ohnishi, H., Miyata, T., Yasuda, H., Satoh, Y., Hanatsuka, K., Kita, H., et al. (2004). Distinct roles of Smad2-, Smad3-, and ERK-dependent pathways in transforming growth factor-beta1 regulation of pancreatic stellate cellular functions. *J. Biol. Chem.* 279, 8873–8878. doi: 10.1074/jbc.m309698200

Pallagi, P., Hegyi, P., and Rakonczay, Z. Jr. (2015). The physiology and pathophysiology of pancreatic ductal secretion: the background for clinicians. *Pancreas* 44, 1211–1233. doi: 10.1097/MPA.0000000000000421

Papalazarou, V., Salmeron-Sanchez, M., and Machesky, L. M. (2018). Tissue engineering the cancer microenvironment-challenges and opportunities. *Biophys. Rev.* 10, 1695–1711. doi: 10.1007/s12551-018-0466-8

Pardo, A., Gibson, K., Cisneros, J., Richards, T. J., Yang, Y., Becerril, C., et al. (2005). Up-regulation and profibrotic role of osteopontin in human idiopathic pulmonary fibrosis. *PLoS Med.* 2:e251. doi: 10.1371/journal.pmed.0020251

Patel, M. B., Pothula, S. P., Xu, Z., Lee, A. K., Goldstein, D., Pirola, R. C., et al. (2014). The role of the hepatocyte growth factor/c-MET pathway in pancreatic stellate cell-endothelial cell interactions: antiangiogenic implications in pancreatic cancer. *Carcinogenesis* 35, 1891–1900. doi: 10.1093/carcin/bgu122

Pattingre, S., Tassa, A., Qu, X., Garuti, R., Liang, X. H., Mizushima, N., et al. (2005). Bcl-2 antiapoptotic proteins inhibit Beclin 1-dependent autophagy. *Cell* 122, 927–939. doi: 10.1016/j.cell.2005.07.002

Petersen, O. H., and Tepikin, A. V. (2008). Polarized calcium signaling in exocrine gland cells. *Annu. Rev. Physiol.* 70, 273–299. doi: 10.1146/annurev.physiol.70.113006.100618

Phillips, P. A., Mccarroll, J. A., Park, S., Wu, M. J., Pirola, R., Korsten, M., et al. (2003). Rat pancreatic stellate cells secrete matrix metalloproteinases: implications for extracellular matrix turnover. *Gut* 52, 275–282. doi: 10.1136/gut.52.2.275

Pothula, S. P., Xu, Z., Goldstein, D., Merrett, N., Pirola, R. C., Wilson, J. S., et al. (2017). Targeting the HGF/c-MET pathway: stromal remodelling in pancreatic cancer. *Oncotarget* 8, 76722–76739. doi: 10.18632/oncotarget.20822

Provenzano, P. P., Cuevas, C., Chang, A. E., Goel, V. K., Von Hoff, D. D., and Hingorani, S. R. (2012). Enzymatic targeting of the stroma ablates physical barriers to treatment of pancreatic ductal adenocarcinoma. *Cancer Cell* 21, 418–429. doi: 10.1016/j.ccr.2012.01.007

Schnittert, J., Bansal, R., Mardhian, D. F., Van Baarlen, J., Ostman, A., and Prakash, J. (2019). Integrin alpha11 in pancreatic stellate cells regulates tumor stroma interaction in pancreatic cancer. *FASEB J.* 33, 6609–6621. doi: 10.1096/fj.201802336R

Schnittert, J., Bansal, R., Storm, G., and Prakash, J. (2018). Integrins in wound healing, fibrosis and tumor stroma: High potential targets for therapeutics and drug delivery. *Adv. Drug Deliv. Rev.* 129, 37–53. doi: 10.1016/j.addr.2018.01.020

Sherman, M. H., Yu, R. T., Engle, D. D., Ding, N., Atkins, A. R., Tiriac, H., et al. (2014). Vitamin D receptor-mediated stromal reprogramming suppresses pancreatitis and enhances pancreatic cancer therapy. *Cell* 159, 80–93. doi: 10.1016/j.cell.2014.08.007

Shi, Y., Gao, W., Lytle, N. K., Huang, P., Yuan, X., Dann, A. M., et al. (2019). Targeting LIF-mediated paracrine interaction for pancreatic cancer therapy and monitoring. *Nature* 569, 131–135. doi: 10.1038/s41586-019-1130-6

Shibutani, S. T., Saitoh, T., Nowag, H., Munz, C., and Yoshimori, T. (2015). Autophagy and autophagy-related proteins in the immune system. *Nat. Immunol.* 16, 1014–1024. doi: 10.1038/ni.3273

Shields, M. A., Dangi-Garimella, S., Redig, A. J., and Munshi, H. G. (2012). Biochemical role of the collagen-rich tumour microenvironment in pancreatic cancer progression. *Biochem. J.* 441, 541–552. doi: 10.1042/BJ20111240

Slomiany, M. G., Grass, G. D., Robertson, A. D., Yang, X. Y., Maria, B. L., Beeson, C., et al. (2009). Hyaluronan, CD44, and emmprin regulate lactate efflux and membrane localization of monocarboxylate transporters in human breast carcinoma cells. *Cancer Res.* 69, 1293–1301. doi: 10.1158/0008-5472.CAN-08-2491

Sousa, C. M., Biancur, D. E., Wang, X., Halbrook, C. J., Sherman, M. H., Zhang, L., et al. (2016). Pancreatic stellate cells support tumour metabolism through autophagic alanine secretion. *Nature* 536, 479–483. doi: 10.1038/nature 19084

Thangada, S., Shapiro, L. H., Silva, C., Yamase, H., Hla, T., and Ferrer, F. A. (2014). Treatment with the immunomodulator FTY720 (fingolimod) significantly reduces renal inflammation in murine unilateral ureteral obstruction. *J. Urol.* 191, 1508–1516. doi: 10.1016/j.juro.2013.10.072

Toole, B. P. (2009). Hyaluronan-CD44 interactions in cancer: paradoxes and possibilities. *Clin. Cancer Res.* 15, 7462–7468. doi: 10.1158/1078-0432.ccr-09-0479

Wallbaum, P., Rohde, S., Ehlers, L., Lange, F., Hohn, A., Bergner, C., et al. (2018). Antifibrogenic effects of vitamin D derivatives on mouse pancreatic stellate cells. *World J. Gastroenterol.* 24, 170–178. doi: 10.3748/wjg.v24.i2.170

Wang, H. C., Lin, Y. L., Hsu, C. C., Chao, Y. J., Hou, Y. C., Chiu, T. J., et al. (2019). Pancreatic stellate cells activated by mutant KRAS-mediated PAI-1 upregulation foster pancreatic cancer progression via IL-8. *Theranostics* 9, 7168–7183. doi: 10.7150/thno.36830

Whatcott, C. J., Diep, C. H., Jiang, P., Watanabe, A., Lobello, J., Sima, C., et al. (2015). Desmoplasia in primary tumors and metastatic lesions of pancreatic cancer. *Clin. Cancer Res.* 21, 3561–3568. doi: 10.1158/1078-0432.CCR-14-1051

Won, J. H., Zhang, Y., Ji, B., Logsdon, C. D., and Yule, D. I. (2011). Phenotypic changes in mouse pancreatic stellate cell Ca2+ signaling events following activation in culture and in a disease model of pancreatitis. *Mol. Biol. Cell* 22, 421–436. doi: 10.1091/mbc.E10-10-0807

Xiao, Y., Zhang, H., Ma, Q., Huang, R., Lu, J., Liang, X., et al. (2019). YAP1-mediated pancreatic stellate cell activation inhibits pancreatic cancer cell proliferation. *Cancer Lett.* 462, 51–60. doi: 10.1016/j.canlet.2019.07.015

Yoshida, S., Yokota, T., Ujiki, M., Ding, X. Z., Pelham, C., Adrian, T. E., et al. (2004). Pancreatic cancer stimulates pancreatic stellate cell proliferation and TIMP-1 production through the MAP kinase pathway. *Biochem. Biophys. Res. Commun.* 323, 1241–1245. doi: 10.1016/j.bbrc.2004.08.229

Yuan, Y., Jiang, J. Y., Wang, J. M., Sun, J., Li, C., Liu, B. Q., et al. (2019). BAG3-positive pancreatic stellate cells promote migration and invasion of pancreatic ductal adenocarcinoma. *J. Cell. Mol. Med.* 23, 5006–5016. doi: 10.1111/jcmm.14352

Zhang, L. P., Ma, F., Abshire, S. M., and Westlund, K. N. (2013). Prolonged high fat/alcohol exposure increases TRPV4 and its functional responses in pancreatic stellate cells. *Am. J. Physiol. Regul. Integr. Comp. Physiol.* 304, R702–R711. doi: 10.1152/ajpregu.00296.2012

Zhao, S., Chen, C., Chang, K., Karnad, A., Jagirdar, J., Kumar, A. P., et al. (2016). CD44 Expression Level and Isoform Contributes to Pancreatic Cancer Cell Plasticity, Invasiveness, and Response to Therapy. *Clin. Cancer Res.* 22, 5592–5604. doi: 10.1158/1078-0432.CCR-15-3115

Metaplastic Paneth Cells in Extra-Intestinal Mucosal Niche Indicate a Link to Microbiome and Inflammation

Rajbir Singh[1], Iyshwarya Balasubramanian[1], Lanjing Zhang[1,2,3,4] and Nan Gao[1,3]*

[1] Department of Biological Sciences, Rutgers University, Newark, NJ, United States, [2] Department of Chemical Biology, Ernest Mario School of Pharmacy, Rutgers University, Piscataway, NJ, United States, [3] Rutgers Cancer Institute of New Jersey, New Brunswick, NJ, United States, [4] Department of Pathology, Princeton Medical Center, Plainsboro, NJ, United States

Paneth cells are residents of the intestinal epithelium. Abnormal appearance of Paneth cells has been widely documented in non-intestinal tissues within the digestive tract and even observed in non-gastrointestinal organs. Although metaplastic Paneth cells are part of the overarching pathology of intestinal metaplasia (IM), only a fraction of intestinal metaplastic lesions contain Paneth cells. We survey literature documenting metaplastic Paneth cells to gain insights into mechanism underlying their etiologic development as well as their potential relevance to human health. A synthesized view from this study suggests that the emergence of metaplastic Paneth cells at extra-intestinal mucosal sites likely represents a protective, anti-bacterial, and inflammatory response evoked by an altered microbial activity.

Keywords: Paneth cells, Paneth cell metaplasia, microbiome, intestinal metaplasia, gastritis, Barrett's esophagus

INTRODUCTION

Paneth cells are a group of mature intestinal epithelial cells present in humans and other mammals. They are primarily localized at the base of the crypts of Lieberkühn in the small intestine. These cells were first described by Schwalbe (1872) and later fully characterized by Josef Paneth (1888). Normal Paneth cells differentiate from intestinal stem cells and live for about 60 days (Ireland et al., 2005). Paneth cells can be found in human cecum and ascending colon but are extremely rare in human distal colon and are absent in rodent colonic epithelium (Tanaka et al., 2001). Conventional histological examination identifies Paneth cells as large columnar epithelial cells with characteristic eosinophilic secretory granules densely packed in the cytoplasm. In addition to secretion of growth factors (e.g., Wnt and EGF ligands) (Clevers and Bevins, 2013) to maintain the intestinal stem cell niche (Clevers and Bevins, 2013), Paneth cells secrete numerous antimicrobial peptides (e.g., α-defensins, lysozyme, Reg3A, etc.) (Bevins and Salzman, 2011) to regulate mucosal immune response.

Loss or reduction of Paneth cells are found in ileal Crohn's disease (Wehkamp et al., 2005; Perminow et al., 2010; Adolph et al., 2013), intestinal ischemia (Grootjans et al., 2011), necrotizing enterocolitis (McElroy et al., 2013), pathogenic bacterial infection (Zhang et al., 2012; Conway et al., 2013; White et al., 2017), and graft vs. host disease (Fishbein et al., 2008; Levine et al., 2013; Kroemer et al., 2016). In contrast, abnormal appearance of Paneth cells in other parts of

the gastrointestinal and extra-gastrointestinal region is referred to as Paneth cell metaplasia (PCM). Abundant appearance of Paneth cells in the human distal colons have been extensively documented in literatures published on ulcerative colitis (Tanaka et al., 2001; Bedini et al., 2014; Simmonds et al., 2014), Crohn's disease (Tanaka et al., 2001; Simmonds et al., 2014), and colonic tubular adenoma (Symonds, 1974; Wada et al., 2005; Shi, 2007; Wehkamp and Stange, 2010; Wang et al., 2011a; Mahon et al., 2016). Although these Paneth cell alterations are frequently associated with chronic inflammation, the molecular mechanism and significance of Paneth cell-related pathologies are poorly understood.

Intestinal metaplasia (IM) represents a gastrointestinal pathological condition and is defined as an abnormal presence of intestinal epithelial cells in non-intestinal tissues. Although not all IM contain Paneth cells, metaplastic Paneth cells have been widely reported in diseased upper alimentary tissues such as Barrett's esophagus (BE) (Chen et al., 2015), chronic gastritis (Montero and Loizaga, 1971; Lewin et al., 1976; Rubio et al., 1987; Deveci and Deveci, 2004; Shen et al., 2005), and Brunner's gland (Coutinho et al., 1996). Surprisingly, rare metaplastic Paneth cells were even observed in other gastrointestinal and non-gastrointestinal tissues (Symonds, 1974; Tanaka et al., 2001; Mitsuhashi et al., 2005; Puiman et al., 2011; Gassler, 2017). In addition to briefly summarizing the well-studied PCM in the left colon, which represents a hallmark change in idiopathic inflammatory bowel disease (IBD), this review will analyze literature on metaplastic Paneth cells in upper gastrointestinal or non-gastrointestinal tissues, an area of research that has received little attention. We noted a potential correlation between bacterial activity and the etiologic development of metaplastic Paneth cells within these extra-intestinal mucosal niche.

Metaplastic Paneth Cells in Colon and Its Disease Relevance

Paneth cells are normally present in proximal (right and transverse) colons in human but are extremely rare in the distal (left) colon. Detection of Paneth cells in the left colon were referred to as PCM, and documented in many IBD studies (Lewin, 1969; Bansal et al., 1984; Ajioka et al., 2005; Simmonds et al., 2014). In addition, PCM in other colonic inflammation conditions such as diverticulitis (Sandow and Whitehead, 1979) and radiation colitis (Watanabe, 1978) had also been reported. However, the histogenesis of colonic PCM is not fully understood. Metaplastic Paneth cells in IBD colon were usually found in crypt regions and morphologically identical to normal Paneth cells that reside in the small intestines (Cunliffe et al., 2001). Immuno-histochemical studies indicated that colonic metaplastic Paneth cells expressed antimicrobial peptides: lysozyme (Klockars et al., 1977), sPLA2 (Haapamaki et al., 1997), and α-defensins (Cunliffe et al., 2001). Normal colonic mucosa does not express human alpha defensin 5 (HD5; antimicrobial protein produced by Paneth cells). However, HD5 was detected in colonic crypts of IBD patients' samples, consistent with the occurrence of PCM (Cunliffe et al., 2001).

By reporting significantly higher PCM incidences in the distal colon of IBD patients compared to non-IBD and control patients, Tanaka et al. (2001) proposed an association of colonic Paneth cells with IBD. Regression analysis suggested that repair and regeneration might be the most potent stimuli causing PCM (Tanaka et al., 2001). Moreover, Paneth cells can sense commensal microbiota (Vaishnava et al., 2008) and shape the microbiome (Salzman et al., 2010) to maintain the intestinal homeostasis. Therefore, the presence of PCM could be an adaptive response to protect the damaged colonic epithelium against bacterial invasion. Additionally, Wehkamp et al. (2007) suggested that the antibacterial peptides produced by Paneth cells might counteract bacterial attack as an "on-demand" mechanism.

The detection of Paneth cells in colorectal adenomas was reported as early as 1967 (Gibbs, 1967) and the reported frequencies of such detection varied from 0.2 to 39% in different studies (Bansal et al., 1984; Wada et al., 1994, 2005; Joo et al., 2009; Pai et al., 2013; Mahon et al., 2016). Furthermore, Paneth cells not only produce antimicrobial components but also constitute an important epithelial niche for small intestinal stem cells by producing epithelial growth factor (EGF), transforming growth factor (TGF-α), Wnt3, and Notch ligands (Sato et al., 2011). The IBD patients have an increased risk to develop inflammation-associated colon cancer. Additionally, during repair and regeneration of damaged epithelium in IBD patients, there might be an increased chance of mutation accumulation (cyclic hit model, described in later paragraphs), and the metaplastic Paneth cells may contribute to accelerated epithelial tumorigenesis by providing stem cell growth factor to tumor cells (Chen and Huang, 2014).

Metaplastic Paneth Cells in Gastric Mucosa and Its Disease Relevance

Intestinal metaplasia in human stomach was first reported by Morson (1955) and later recognized as a precursor for gastric cancer in various studies (Morson, 1955; Ming et al., 1967; Matsukura et al., 1979; Segura and Montero, 1983; Shimada et al., 1987). Kawachi et al. (1976) used Tes Tape method to characterize IM by disaccharidase visualization and classified the lesions into two types. In type I IM, also known as the complete IM, goblet cells, Paneth cells, as well as enterocyte enzymes, including sucrase, maltase, trehalase and alkaline phosphatase were present. In type II, the incomplete form of IM, trehalase, alkaline phosphatase, and Paneth cells were absent. Thus, complete metaplasia partially resembles small intestinal epithelium containing Paneth cells whereas incomplete metaplasia resembles colonic epithelium lacking Paneth cells. In their study, out of 96 samples of IM, 57% showed type I IM with the presence of Paneth cells, while 43% were type II lacking Paneth cells (Kawachi et al., 1976).

By using various staining procedures (**Table 1**), Albedi et al. (1984) reported that immature Paneth cells were present in less differentiated IM. Other authors also confirmed the presence of PCM by immunostaining for PSTI (Pancreatic secretory trypsin inhibitor) (Kazal et al., 1948; Bohe et al., 1986, 1987), lysozyme (Heitz and Wegmann, 1980), and human defensin 5

TABLE 1 | Methods used for identification of metaplastic Paneth cells.

Organ	Method of identification	References
Esophagus	Conventional H&E staining	Chen et al., 2015
	H&E, light microscopy and electron microscopy	Schreiber et al., 1978
	H&E, periodic acid-Schiff/Alcian blue	Takubo et al., 1995
	H&E, Lendrum's Phyloxine-tartrazine stain	Thompson et al., 1983
Stomach	Periodic acid-Schiff/Alcian blue at pH 2.5	Abraham et al., 2003
	H&E, Masson's Trichome, Lendrum's Phyloxine-tartrazine, Periodic acid-Schiff/Alcian blue at pH 2.5 and colloidal iron pH 1.9 staining	Albedi et al., 1984
	H&E, Periodic acid-Schiff/Alcian blue at pH 2.5, immunostaining for lysozyme	Deveci and Deveci, 2004
	Immunostaining for lysozyme	Gassler et al., 2002
	Conventional H&E staining	Inada et al., 1997
	H&E, Periodic acid-Schiff/Alcian blue at pH 2.5 and Electron microscopy	Matsubara, 1977
	Immunoelectron microscopy for lysozyme	Ohtani and Sasano, 1988
	Immunostaining for HD5 and HD6	Ostaff et al., 2015
	Conventional H&E staining	Rubio et al., 1987
	Lysozyme immunostaining	Rubio, 2012
Gallbladder	Conventional H&E staining	Albores-Saavedra et al., 1986
	Conventional H&E staining	Bae et al., 2002
	Electron microscopy, H&E, Periodic acid-Schiff	Laitio and Nevalainen, 1975
	Conventional H&E staining	Sakaki et al., 2000
Ovary	Conventional H&E staining	Alrajban et al., 2018
	Conventional H&E staining	Niemiec et al., 1989
Prostate	Conventional H&E staining, immunostaining for lysozyme	Frydman et al., 1992
	Conventional H&E staining	Adlakha and Bostwick, 1994

(Shen et al., 2005). Additionally, Paneth-like cells were reported in gastric adenomas and carcinomas (Heitz and Wegmann, 1980; Ito et al., 1986; Caruso et al., 1989; Rubio, 1989). Although some of these tumors exhibited aggressiveness (Ohtani and Sasano, 1988), the prognostic value of these Paneth-like cells for gastric carcinoma remain unclear.

Inada et al. (1997) further classified gastric IM on the basis of differentiation status into two major classes (i) gastric and intestinal (GI) mixed type; and (ii) solely intestinal (I) type. Six subclasses were further established for the mixed GI type. In this study, they observed the presence and absence of Paneth cells in IM at almost the same incidence rate i.e., 15 and 17%, respectively in fundic mucosa. The incidences of intestinal subtypes with Paneth cells were 17% in fundic and 19% in pyloric mucosa, respectively. The incidences of GI(Su-Pa+) subtypes which are characterized as showing presence of Paneth cells (Pa) and absence of surface mucous cells (Su) were 11% in fundic and 14% in pyloric mucosa (Inada et al., 1997). Within these metaplastic lesions, the presence of Paneth cells near the proliferative zone and the large intracellular granules suggested that these cells were neither chief cells nor pyloric gland cells (Inada et al., 1997).

Matsubara performed morphological characterizations of Paneth cells and reported that Paneth cells in normal small intestinal epithelia contained more phagolysosomes in lower cytoplasm compared to Paneth cells found in IM (Matsubara, 1977). This represented one of the earliest attempts to distinguish intestinal resident cells vs. metaplastic Paneth cells. Gassler et al. (2002) later reported that the expression of calnexin was inversely related to secretory lysozyme in Paneth cells of normal intestinal mucosa but became directly correlated to lysozyme in metaplastic Paneth cells in gastric mucosa. They further identified the expression of proliferative marker Ki67 in metaplastic Paneth cells but not in Paneth cells of normal small intestines. These studies suggested that metaplastic Paneth cells may behave differently from normal Paneth cells (Gassler et al., 2002). However, detailed information at the molecular level is currently absent to distinguish normal from metaplastic Paneth cells.

Most human gastric cancers arise after long-term *Helicobacter pylori* infection via progression of metaplastic changes, first named by Correa (Correa, 1992; Correa and Shiao, 1994; Uemura et al., 2001) with the first metaplastic change that increases risk for progression to cancer being atrophic gastritis, involving loss of acid secreting parietal cells with concomitant pseudopyloric metaplasia (aka SPEM, discussed below) of the remaining cells. Some authors believe IM is a requisite step after atrophy (Correa's hypothesis), whereas others like David Graham (Graham et al., 2019) have suggested IM is more of a reparative lesion, not directly related to carcinogenesis, and atrophy is the more diagnostic risk factor (El-Zimaity et al., 2002). In gastric atrophy, caused by long-term *H. pylori* colonization, mature chief cells that are present at the base of glands are replaced by (metaplastic) cell types that co-express both the chief cell marker and markers of normal mucus-secreting cells residing in the gland neck, such as Trefoil Factor 2, TFF2 (spasmolytic polypeptide). This type of metaplasia was also known as spasmolytic polypeptide-expressing metaplasia (SPEM) or pseudopyloric metaplasia due to the lack of mature chief and parietal cells, resembling antrum or pyloric epithelium

(Goldenring et al., 2011; Saenz and Mills, 2018). During SPEM, the differentiated cells change their fate to a regenerative state by first shutting down the mTORC1 signaling followed by expression of progenitor markers to reactivate mTORC1. This process was named as paligenosis (Jin and Mills, 2018; Willet et al., 2018). In mouse models, SPEM emerged in chronically inflamed stomach and clearly proceeded to give rise to gastric cancer (Fox et al., 1996). Inflammation due to infection or other insults increases paligenotic events. This continuous process of paligenosis increases the risk of accumulation of mutations leading to emergence of a neoplastic or dysplastic clone. This phenomenon was called "cyclical hit model" (Burclaff and Mills, 2018; Saenz and Mills, 2018; Jin and Mills, 2019). Although there is no study that has explicitly studied how Paneth cells originated during the process of metaplasia, a recent study by Leushacke et al. (2017) showed LGR5+ subpopulation of chief cells co-expressed intestinal stem cell and Wnt markers in advanced intestinal type tumors in the corpus. Therefore, metaplastic Paneth cells could be part of the program of IM, the origin of which may relate to infection and inflammation but remain poorly understood.

Although the relevance of metaplastic Paneth cells during gastric mucosal pathogenesis are not clear, the characteristic production of antimicrobial peptides by Paneth cells suggested that the metaplasia might be an adaptive response to bacterial infection. Paneth cells secrete defensins and lysozyme shown to reduce the colonization of *H. pylori* in the stomach (Tanabe et al., 2008). Interestingly, mucosal areas with IM or with pseudo-pyloric metaplasia showed a lack of *H. pylori*, suggesting presence of Paneth cells in the metaplastic mucosa may be an adaptation against bacterial infection (Rubio, 2015). Gastric atrophy is characterized by the loss of chief and parietal cells and during infection this atrophy progresses from antrum to corpus (Kimura et al., 1996; Shichijo et al., 2015). As *H. pylori* infection is associated with IM and a higher risk of cancer, attempts were made to reduce the infection (Fukase et al., 2008; Ogura et al., 2008; Sakitani et al., 2011; Shichijo et al., 2016). Some studies reported that IM did not seem alleviated even after eradication of *H. pylori* infection, suggesting the potentially irreversible nature of IM (Wang et al., 2011b; Kodama et al., 2012; Mera et al., 2018). However, other studies showed that eradication of *H. pylori* somewhat reduced the IM (Correa et al., 2000; Zullo et al., 2000; Kong et al., 2014). In addition, Paneth cell antimicrobial peptides, especially human defensin 5 and 6, were recently found upregulated in gastric mucosa of heavy alcohol users (Ostaff et al., 2015). Thus, IM in gastric mucosa might also be caused by non-bacterial factors such as excessive alcohol use, retrograde bile reflux, aspirin, and anti-inflammatory drugs (Webb et al., 1996; Bresalier, 1998). However, these changes may also indirectly alter the gastric colonization of *H. pylori* or other bacterial species. More studies are required to elucidate these causal relationships.

Metaplastic Paneth Cells in Esophageal Mucosa and Disease Relevance

The presence of Paneth cells in BE was first described by Schreiber et al. (1978), when metaplastic Paneth cells similar to intestinal resident Paneth cells were detected in BE biopsy samples from 4 patients. BE is characterized by a single layer of columnar epithelium replacing the native multi-layered stratified squamous epithelium of distal esophagus. BE is considered as a form of protective adaption from chronic insults, secondary to gastroesophageal reflux disease (Burgess et al., 1971; Naef et al., 1975; Ozzello et al., 1977), and the precursor to most esophageal adenocarcinomas. This esophageal disorder is pathologically manifested by the presence of multiple intestinal epithelial cell lineages including Paneth cells and enteroendocrine cells along with gastric cells (Boulton et al., 2003).

Later, Thompson et al. (1983) exhibited the presence of Paneth cells in 50% of the esophagogastrectomy samples of Barrett's metaplasia and specimens with adenocarcinoma at the gastroesophageal junction. No difference in sex ratio or age range was observed among the samples associated with or without metaplasia. Compared to earlier studies using biopsy samples, sampling error was minimized in this study using esophagogastrectomy. Moreover, various experimental approaches including scanning electron microscopy, specimen radiography, and dissecting microscopy along with regular histochemical techniques were used in this study in comparison to earlier studies that mainly relied on histologic analysis.

In the last decade, immunostaining for various antimicrobial peptides was used to identify Paneth cells. Shen et al. (2005) reported human defensin 5 immunostaining as a tool for identification of IM in BE as well as in gastric IM. Under normal conditions, human defensin 5 is present in intestinal Paneth cells, and is generally confined to the small intestinal epithelium. However, the expression of defensin 5 was also observed in IM. The frequency of human defensin 5 staining was higher in gastric IM compared to BE. This difference was attributed to higher *H. pyloric* infection in stomach compared to esophagus (Shen et al., 2005).

Rubio also reported the presence of PCM in BE by detecting expression of lysozyme and other Paneth cell-specific antimicrobial proteins (Rubio, 2012). In a recent study, Chen et al. (2015) conducted a large study on 757 esophageal biopsy specimens, and reported that 31% of this cohort with IM contained metaplastic Paneth cells. These results were in accordance with previous reports showing a similar frequency of PCM in BE (Schreiber et al., 1978; Thompson et al., 1983; Takubo et al., 1995). Moreover, the highest incidence of PCM in BE was observed in indefinite dysplasia and low grade dysplasia samples. Additionally, in their follow-up study, they showed PCM was associated with reduced disease regression and suggested it as a potential marker for identification of severe disease (Chen et al., 2015). Moreover, presence of metaplastic Paneth cell products such as antimicrobial peptides may accelerate the cascade of BE by altering the expression of E-cadherin, thereby reducing the cell-cell interaction (Nomura et al., 2013).

Similar to gastric IM, BE was also viewed as an adaptation following chronic inflammation or injury to the esophageal epithelium. Bile acid was reported as one of the major contributor to the development of BE in animal models (Clark et al., 1994; Quante et al., 2012). Patients with gastroesophageal reflux disease often received proton pump inhibitors, which could cause

reduced gastric acid secretion leading to bacterial overgrowth in BE. Additionally, it was reported that BE biopsies were highly associated with presence of bacteria compared to esophageal biopsies without BE (Osias et al., 2004). Two different types of microbiome were observed in esophageal biopsies: type I was dominated by genus *Streptococcus* and present with phenotypically normal esophagus; and type II contained Gram-negative anaerobes that were correlated with BE (Yang et al., 2009). Other studies also reported the presence of residential bacterial population in gastroesophageal reflux disease and BE. One study showed the presence of Bacteroidetes, Firmicutes, Proteobacteria, and Actinobacteria (Pei et al., 2005), while the other reported 46 bacterial species including high levels of *Campylobacter consisus* and *Campylobacter rectus* (Macfarlane et al., 2007). Liu et al. (2013) also observed Firmicutes, Proteobacteria, *Bacteroides*, *Fusobacterium*, and Actinobacter in 6 cases of BE. These studies suggested a potential rational toward a self defense mechanism against pathogenic bacteria. Therefore, presence of metaplastic Paneth-like cells in these lesions may represent an adaptive antibacterial response by the infected mucosa. However, besides an antibacterial role, defensins were also proposed to reduce E-cadherin in esophageal epithelium to possibly accelerate the BE pathogenesis (Nomura et al., 2013).

Appearance of Paneth Cells in Other Gastrointestinal and Non-gastrointestinal Organs

Intestinal metaplasia has also been observed in several other gastrointestinal tissues. Although IM in gallbladder is very rare, complete IM was reported in gallbladder as early as 1967 (Jarvi and Lauren, 1967). Laitio and Nevalainen (1975) studied 100 gallbladders following cholecystectomies to remove gallstones. One specimen showed the presence of Paneth cells. Electron microscopy of this sample showed Paneth cells in columnar shape with apical cytoplasm occupied by secretory granules and well-developed Golgi apparatus. Later, Albores-Saavedra et al. (1986) reported that 3 out of 49 gallbladder samples showed the presence of Paneth cells. The presence of similar morphology in the IM in gallbladder to those in the stomach suggested that gastric and gallbladder epithelia have the same potential to differentiate into similar cell lineages. Although the IM of gallbladder containing Paneth cells was suspected to be associated with carcinoma development, the presence of higher immunoreactivity of lysozyme in non-dysplastic mucosa than in carcinoma did not support the hypothesis. Furthermore, the frequency of observing Paneth cells was found to be lowest in gallbladder cancer tissues compared to non-neoplastic mucosa, suggesting an inverse correlation of PCM to gallbladder cancer (Yamamoto et al., 1989). This observation was consistent with a recent comprehensive case-control study of 1,900 colorectal adenomas showing metaplastic Paneth cells in distal colorectal adenomas were inversely associated with synchronous advanced adenoma and carcinoma (Mahon et al., 2016). Sakaki et al. (2000) observed a case of gallbladder adenocarcinoma with extensive PCM.

Moreover, PCM was also observed in intestinal type cholangiocarcinoma associated with hepatolithiasis in large hepatic bile duct (Bae et al., 2002). Abnormal cholesterol and bile acid metabolism and secretion are common pathophysiological defects in gallbladder-related diseases. The presence of metaplastic Paneth cells in these diseases could be attributed to the presence of bacterial community. Bile-acid metabolism was reported to be regulated by the gut microbiome, thus the role of microbiota in disease cannot be overruled (Abeysuriya et al., 2008; Wang et al., 2009; Sayin et al., 2013). Similarly, the presence of microbiota in lithogenic bile could also promote inflammation and gall stones (White et al., 2006; Capoor et al., 2008; Sekirov et al., 2010) and microbiota association with gallstones was well reported (Kaufman et al., 1989; Lee et al., 1999; Maurer et al., 2005; Saltykova et al., 2016). Additionally, various microbes have also been isolated from bile in patients with cholesterol stones (Stewart et al., 1987; Cull and Beck, 1988; Darko and Archampong, 1994). Although, no study has established a direct correlation of PCM and the presence of bacteria in gallbladder related diseases, existing studies showed the presence of bacterial communities in lithogenic bile (Abeysuriya et al., 2008) and metaplastic Paneth cells in gallbladder with gallstones (Laitio and Nevalainen, 1975). Therefore, the presence of Paneth cells could be a protective mechanism against the pathogenic bacteria in lithogenic bile.

Alrajban et al. (2018) reported the first PCM in Krukenberg tumors, which represents 1–2% of ovarian tumors and are characterized by the presence of metastatic adenocarcinoma cells. A poorly differentiated carcinoma was observed to contain a mixture of signet ring malignant cells with eosinophilic cytoplasm characteristic of PCM. PCM was also observed in the lining of urethral diverticulum (Niemiec et al., 1989), a condition in which a variable sized pouch is formed. The *E. coli* was the most common organism among other enteric gram-negative bacteria isolated from urethral diverticulum patients (Ljungqvist et al., 2007; Greiman et al., 2019). Since urethral diverticulum is connected to the urethra and filled during urination, the metaplastic change in urethral lining could be due to exposure to irritants like bacterial colonization and retained urine. Thus, the metaplastic Paneth cells could again be an anti-bacterial response in this scenario. The reported presence of Paneth cells in neovaginitis (van der Sluis et al., 2016) might suggest a similar adaptive response to combat bacterial presence.

Intestinal metaplasia has been described in both benign and malignant prostate glands following estrogen therapy (Bainborough, 1952; Maung et al., 1988). Paneth cell-like metaplasia of prostate gland was first reported by Frydman et al. (1992). Adlakha and Bostwick later reported that these Paneth cell-like changes resembled intestinal Paneth cells by light microscopy. However, they lacked lysozyme immunoreactivity, and retained many prostate markers. Since these Paneth-like cells were positive for neuroendocrine markers, they were called "neuroendocrine cells with large eosinophilic granules" (Adlakha and Bostwick, 1994). PCM was also found in epididymis disorders (Nevalainen et al., 2001; Nistal et al., 2007). Together, these Paneth-like cells may represent transformed normal or neoplastic prostate cells.

The association of infection and inflammation had been investigated in many prostate cancer studies. In a recent study, Shrestha et al. (2018) showed that urine samples of patients with biopsy-proven prostate cancer had increased bacterial clusters frequently associated with other urogenital infections such as prostatitis and bacterial vaginosis (Massari et al., 2019). Additionally, a recent study testing prostatic fluid from prostate cancer and non-prostate cancer patients showed the presence of microbes in both samples, but revealed a difference in microbial species (Ma et al., 2019). Similarly, the presence of microbiota within tumoral, peritumoral and non-tumoral prostate tissue has also been reported (Cavarretta et al., 2017). Thus, whether emergence of Paneth like cells in prostate pathology represented another form of protective mechanism against bacteria may require future investigation.

CLOSING REMARKS

The mucosa of the gastrointestinal tract is continuously challenged by various micro-environmental factors ranging from pathogenic and opportunistic bacteria, and their products, to harsh secretions with digestive properties. In turn, human body has developed defense mechanisms like peristalsis, continuous revival of lining epithelium, and production of antimicrobial peptides, such as those secreted by the Paneth cells. The ectopic expression and secretion of these antimicrobial peptides in non-intestinal mucosa where they are normally absent illustrates a robust tissue plasticity in adaptation to infection and injury. Future studies are necessary to delineate the responsible microbial signaling pathways that invoke such unusual cellular metaplasia. The impact of these widely emerged metaplastic Paneth cells on the progression of inflammatory diseases and cancers warrants in-depth investigation such as using Paneth cell lineage tracing approaches (Yu et al., 2018).

AUTHOR CONTRIBUTIONS

RS, IB, LZ and NG conceptualized the manuscript. RS and NG drafted the manuscript. IB and LZ edited the manuscript.

FUNDING

REFERENCES

Abeysuriya, V., Deen, K. I., Wijesuriya, T., and Salgado, S. S. (2008). Microbiology of gallbladder bile in uncomplicated symptomatic cholelithiasis. *Hepatobiliary Pancreat. Dis. Int.* 7, 633–637.

Abraham, S. C., Park, S. J., Lee, J. H., Mugartegui, L., and Wu, T. T. (2003). Genetic alterations in gastric adenomas of intestinal and foveolar phenotypes. *Mod. Pathol.* 16, 786–795. doi: 10.1097/01.mp.0000080349.37658.5e

Adlakha, H., and Bostwick, D. G. (1994). Paneth cell-like change in prostatic adenocarcinoma represents neuroendocrine differentiation: report of 30 cases. *Hum. Pathol.* 25, 135–139. doi: 10.1016/0046-8177(94)90268-2

Adolph, T. E., Tomczak, M. F., Niederreiter, L., Ko, H. J., Bock, J., and Martinez-Naves, E. (2013). Paneth cells as a site of origin for intestinal inflammation. *Nature* 503, 272–276.

Ajioka, Y., Nishikura, K., and Watanabe, G. (2005). [Pathomorphology of ulcerative colitis]. *Nihon Rinsho* 63, 763–769.

Albedi, F. M., Lorenzetti, E., Contini, M., and Nardi, F. (1984). Immature Paneth cells in intestinal metaplasia of gastric mucosa. *Appl. Pathol.* 2, 43–48.

Albores-Saavedra, J., Nadji, M., Henson, D. E., Ziegels-Weissman, J., and Mones, J. M. (1986). Intestinal metaplasia of the gallbladder: a morphologic and immunocytochemical study. *Hum. Pathol.* 17, 614–620. doi: 10.1016/s0046-8177(86)80134-4

Alrajban, W. A., Khubrani, R. A., Almalki, M. S., Almassri, A., and Alrikabi, A. C. (2018). Extensive Paneth cell metaplasia in an ovarian Krukenberg tumor: report of an unusual case and literature review. *J. Surg. Case Rep.* 2018:rjy323.

Bae, J. Y., Park, Y. N., Nakanuma, Y., Lee, W. J., Kim, J. Y., and Park, C. (2002). Intestinal type cholangiocarcinoma of intrahepatic large bile duct associated with hepatolithiasis–a new histologic subtype for further investigation. *Hepatogastroenterology* 49, 628–630.

Bainborough, A. R. (1952). Squamous metaplasia of prostate following estrogen therapy. *J. Urol.* 68, 329–336. doi: 10.1016/s0022-5347(17)68202-8

Bansal, M., Fenoglio, C. M., Robboy, S. J., and King, D. W. (1984). Are metaplasias in colorectal adenomas truly metaplasias? *Am. J. Pathol.* 115, 253–265.

Bedini, O. A., Naves, A., San Miguel, P., Quispe, A., and Guida, C. (2014). [Metaplasic Paneth cells in ulcerative colitis]. *Acta Gastroenterol. Latinoam.* 44, 285–289.

Bevins, C. L., and Salzman, N. H. (2011). Paneth cells, antimicrobial peptides and maintenance of intestinal homeostasis. *Nat. Rev. Microbiol.* 9, 356–368. doi: 10.1038/nrmicro2546

Bohe, M., Borgstrom, A., Lindstrom, C., and Ohlsson, K. (1986). Pancreatic endoproteases and pancreatic secretory trypsin inhibitor immunoreactivity in human Paneth cells. *J. Clin. Pathol.* 39, 786–793. doi: 10.1136/jcp.39.7.786

Bohe, M., Lindstrom, C. G., and Ohlsson, K. (1987). Varying occurrence of gastroduodenal immunoreactive pancreatic secretory trypsin inhibitor. *J. Clin. Pathol.* 40, 1345–1348. doi: 10.1136/jcp.40.11.1345

Boulton, R. A., Usselmann, B., Mohammed, I., and Jankowski, J. (2003). Barrett's esophagus: environmental influences in the progression of dysplasia. *World J. Surg.* 27, 1014–1017. doi: 10.1007/s00268-003-7054-0

Bresalier, R. S. (1998). *Helicobacter pylori* and gastric cancer: a not so simple association. *Gastroenterology* 114, 408–409. doi: 10.1016/s0016-5085(98)70495-0

Burclaff, J., and Mills, J. C. (2018). Plasticity of differentiated cells in wound repair and tumorigenesis, part II: skin and intestine. *Dis. Model Mech.* 11:dmm035071. doi: 10.1242/dmm.035071

Burgess, J. N., Payne, W. S., Andersen, H. A., Weiland, L. H., and Carlson, H. C. (1971). Barrett esophagus: the columnar-epithelial-lined lower esophagus. *Mayo Clin. Proc.* 46, 728–734.

Capoor, M. R., Rajni, D. N., Khanna, G., Krishna, S. V., Chintamani, M. S., and Aggarwal, P. (2008). Microflora of bile aspirates in patients with acute cholecystitis with or without cholelithiasis: a tropical experience. *Braz. J. Infect. Dis.* 12, 222–225.

Caruso, R. A., La Spada, F., Casablanca, G., and Rigoli, L. (1989). Lysozyme and mucins in gastric adenomas. *J. Clin. Pathol.* 42, 827–833. doi: 10.1136/jcp.42.8.827

Cavarretta, I., Ferrarese, R., Cazzaniga, W., Saita, D., Luciano, R., Ceresola, E. R., et al. (2017). The microbiome of the prostate tumor microenvironment. *Eur. Urol.* 72, 625–631.

Chen, S., and Huang, E. H. (2014). The colon cancer stem cell microenvironment holds keys to future cancer therapy. *J. Gastrointest. Surg.* 18, 1040–1048. doi: 10.1007/s11605-014-2497-1

Chen, W., Frankel, W. L., Cronley, K. M., Yu, L., Zhou, X., and Yearsley, M. M. (2015). Significance of Paneth cell metaplasia in Barrett esophagus: a morphologic and clinicopathologic study. *Am. J. Clin. Pathol.* 143, 665–671. doi: 10.1309/ajcpvujmcvbc9pkm

Clark, G. W., Smyrk, T. C., Mirvish, S. S., Anselmino, M., Yamashita, Y., Hinder, R. A., et al. (1994). Effect of gastroduodenal juice and dietary fat on the development of Barrett's esophagus and esophageal neoplasia: an experimental rat model. *Ann. Surg. Oncol.* 1, 252–261. doi: 10.1007/bf02303531

Clevers, H. C., and Bevins, C. L. (2013). Paneth cells: maestros of the small intestinal crypts. *Annu. Rev. Physiol.* 75, 289–311. doi: 10.1146/annurev-physiol-030212-183744

Conway, K. L., Kuballa, P., Song, J. H., Patel, K. K., Castoreno, A. B., Yilmaz, O. H., et al. (2013). Atg16l1 is required for autophagy in intestinal epithelial cells and protection of mice from *Salmonella* infection. *Gastroenterology* 145, 1347–1357. doi: 10.1053/j.gastro.2013.08.035

Correa, P. (1992). Human gastric carcinogenesis: a multistep and multifactorial process–First American cancer society award lecture on cancer epidemiology and prevention. *Cancer Res.* 52, 6735–6740.

Correa, P., Fontham, E. T., Bravo, J. C., Bravo, L. E., Ruiz, B., Zarama, G., et al. (2000). Chemoprevention of gastric dysplasia: randomized trial of antioxidant supplements and anti-*Helicobacter pylori* therapy. *J. Natl. Cancer Inst.* 92, 1881–1888. doi: 10.1093/jnci/92.23.1881

Correa, P., and Shiao, Y. H. (1994). Phenotypic and genotypic events in gastric carcinogenesis. *Cancer Res.* 54, 1941s–1943s.

Coutinho, H. B., Robalinho, T. I., Coutinho, V. B., Amorin, A. M., Almeida, J. R., Filho, J. T., et al. (1996). Immunocytochemical demonstration that human duodenal Brunner's glands may participate in intestinal defence. *J. Anat.* 189(Pt 1), 193–197.

Cull, D. L., and Beck, D. E. (1988). Routine bile cultures during elective cholecystectomy. *South Med. J.* 81, 1358–1360. doi: 10.1097/00007611-198811000-00006

Cunliffe, R. N., Rose, F. R., Keyte, J., Abberley, L., Chan, W. C., and Mahida, Y. R. (2001). Human defensin 5 is stored in precursor form in normal Paneth cells and is expressed by some villous epithelial cells and by metaplastic Paneth cells in the colon in inflammatory bowel disease. *Gut* 48, 176–185. doi: 10.1136/gut.48.2.176

Darko, R., and Archampong, E. Q. (1994). The microflora of bile in Ghanaians. *West Afr. J. Med.* 13, 113–115.

Deveci, M. S., and Deveci, G. (2004). Altered distribution of metaplastic Paneth, gastrin and pancreatic acinar cells in atrophic gastritic mucosa with endocrine cell lesions. *Tohoku J. Exp. Med.* 202, 13–22. doi: 10.1620/tjem.202.13

El-Zimaity, H. M., Ota, H., Graham, D. Y., Akamatsu, T., and Katsuyama, T. (2002). Patterns of gastric atrophy in intestinal type gastric carcinoma. *Cancer* 94, 1428–1436. doi: 10.1002/cncr.10375

Fishbein, T., Novitskiy, G., Mishra, L., Matsumoto, C., Kaufman, S., Goyal, S., et al. (2008). NOD2-expressing bone marrow-derived cells appear to regulate epithelial innate immunity of the transplanted human small intestine. *Gut* 57, 323–330. doi: 10.1136/gut.2007.133322

Fox, J. G., Li, X., Cahill, R. J., Andrutis, K., Rustgi, A. K., Odze, R., et al. (1996). Hypertrophic gastropathy in *Helicobacter felis*-infected wild-type C57BL/6 mice and p53 hemizygous transgenic mice. *Gastroenterology* 110, 155–166. doi: 10.1053/gast.1996.v110.pm8536852

Frydman, C. P., Bleiweiss, I. J., Unger, P. D., Gordon, R. E., and Brazenas, N. V. (1992). Paneth cell-like metaplasia of the prostate gland. *Arch. Pathol. Lab Med.* 116, 274–276.

Fukase, K., Kato, M., Kikuchi, S., Inoue, K., Uemura, N., Okamoto, S., et al. (2008). Effect of eradication of *Helicobacter pylori* on incidence of metachronous gastric carcinoma after endoscopic resection of early gastric cancer: an open-label, randomised controlled trial. *Lancet* 372, 392–397. doi: 10.1016/s0140-6736(08)61159-9

Gassler, N. (2017). Paneth cells in intestinal physiology and pathophysiology. *World J. Gastrointest. Pathophysiol.* 8, 150–160. doi: 10.4291/wjgp.v8.i4.150

Gassler, N., Schnolzer, M., Rohr, C., Helmke, B., Kartenbeck, J., Grunewald, S., et al. (2002). Expression of calnexin reflects paneth cell differentiation and function. *Lab. Invest.* 82, 1647–1659. doi: 10.1097/01.lab.0000041709.42598.4a

Gibbs, N. M. (1967). Incidence and significance of argentaffin and paneth cells in some tumours of the large intestine. *J. Clin. Pathol.* 20, 826–831. doi: 10.1136/jcp.20.6.826

Goldenring, J. R., Nam, K. T., and Mills, J. C. (2011). The origin of pre-neoplastic metaplasia in the stomach: chief cells emerge from the Mist. *Exp. Cell Res.* 317, 2759–2764. doi: 10.1016/j.yexcr.2011.08.017

Graham, D. Y., Rugge, M., and Genta, R. M. (2019). Diagnosis: gastric intestinal metaplasia - what to do next? *Curr. Opin. Gastroenterol.* 35, 535–543. doi: 10.1097/mog.0000000000000576

Greiman, A. K., Rolef, J., and Rovner, E. S. (2019). Urethral diverticulum: a systematic review. *Arab J. Urol.* 17, 49–57. doi: 10.1080/2090598x.2019.1589748

Grootjans, J., Hodin, C. M., De Haan, J. J., Derikx, J. P., Rouschop, K. M., Verheyen, F. K., et al. (2011). Level of activation of the unfolded protein response correlates with Paneth cell apoptosis in human small intestine exposed to ischemia/reperfusion. *Gastroenterology* 140, 529–539.e3. doi: 10.1053/j.gastro.2010.10.040

Haapamaki, M. M., Gronroos, J. M., Nurmi, H., Alanen, K., Kallajoki, M., and Nevalainen, T. J. (1997). Gene expression of group II phospholipase A2 in intestine in ulcerative colitis. *Gut* 40, 95–101. doi: 10.1136/gut.40.1.95

Heitz, P. U., and Wegmann, W. (1980). Identification of neoplastic Paneth cells in an adenocarcinoma of the stomach using lysozyme as a marker, and electron microscopy. *Virchows Arch. A Pathol. Anat. Histol.* 386, 107–116. doi: 10.1007/bf00432648

Inada, K., Nakanishi, H., Fujimitsu, Y., Shimizu, N., Ichinose, M., Miki, K., et al. (1997). Gastric and intestinal mixed and solely intestinal types of intestinal metaplasia in the human stomach. *Pathol. Int.* 47, 831–841. doi: 10.1111/j.1440-1827.1997.tb03714.x

Ireland, H., Houghton, C., Howard, L., and Winton, D. J. (2005). Cellular inheritance of a Cre-activated reporter gene to determine Paneth cell longevity in the murine small intestine. *Dev. Dyn.* 233, 1332–1336. doi: 10.1002/dvdy.20446

Ito, H., Hata, J., Yokozaki, H., Nakatani, H., Oda, N., and Tahara, E. (1986). Tubular adenoma of the human stomach. An immunohistochemical analysis of gut hormones, serotonin, carcinoembryonic antigen, secretory component, and lysozyme. *Cancer* 58, 2264–2272. doi: 10.1002/1097-0142(19861115)58:10<2264::aid-cncr2820581018>3.0.co;2-f

Jarvi, O., and Lauren, P. K. (1967). Intestinal metaplasia in the mucosa of the gallbladder and common bile duct with additional observations on pancreas heterotopy. *Ann. Med. Exp. Biol. Fenn.* 45, 213–223.

Jin, R. U., and Mills, J. C. (2018). Are gastric and esophageal metaplasia relatives? The case for Barrett's stemming from SPEM. *Dig. Dis. Sci.* 63, 2028–2041. doi: 10.1007/s10620-018-5150-0

Jin, R. U., and Mills, J. C. (2019). The cyclical hit model: how paligenosis might establish the mutational landscape in Barrett's esophagus and esophageal adenocarcinoma. *Curr. Opin. Gastroenterol.* [Epub ahead of print].

Joo, M., Shahsafaei, A., and Odze, R. D. (2009). Paneth cell differentiation in colonic epithelial neoplasms: evidence for the role of the Apc/beta-catenin/Tcf pathway. *Hum. Pathol.* 40, 872–880. doi: 10.1016/j.humpath.2008.12.003

Kaufman, H. S., Magnuson, T. H., Lillemoe, K. D., Frasca, P., and Pitt, H. A. (1989). The role of bacteria in gallbladder and common duct stone formation. *Ann. Surg.* 209, 584–591;discussion591–582.

Kawachi, T., Kurisu, M., Numanyu, N., Sasajima, K., and Sano, T. (1976). Precancerous changes in the stomach. *Cancer Res.* 36, 2673–2677.

Kazal, L. A., Spicer, D. S., and Brahinsky, R. A. (1948). Isolation of a crystalline trypsin inhibitor-anticoagulant protein from pancreas. *J. Am. Chem. Soc.* 70, 3034–3040. doi: 10.1021/ja01189a060

Kimura, K., Satoh, K., Ido, K., Taniguchi, Y., Takimoto, T., and Takemoto, T. (1996). Gastritis in the Japanese stomach. *Scand. J. Gastroenterol. Suppl.* 214, 17–20; discussion 21–23.

Klockars, M., Reitamo, S., Reitamo, J. J., and Moller, C. (1977). Immunohistochemical identification of lysozyme in intestinal lesions in ulcerative colitis and Crohn's disease. *Gut* 18, 377–381. doi: 10.1136/gut.18.5.377

Kodama, M., Murakami, K., Okimoto, T., Sato, R., Uchida, M., Abe, T., et al. (2012). Ten-year prospective follow-up of histological changes at five points on the gastric mucosa as recommended by the updated Sydney system after

Helicobacter pylori eradication. *J. Gastroenterol.* 47, 394–403. doi: 10.1007/s00535-011-0504-9

Kong, Y. J., Yi, H. G., Dai, J. C., and Wei, M. X. (2014). Histological changes of gastric mucosa after *Helicobacter pylori* eradication: a systematic review and meta-analysis. *World J. Gastroenterol.* 20, 5903–5911.

Kroemer, A., Elsabbagh, A. M., Matsumoto, C. S., Zasloff, M., and Fishbein, T. M. (2016). The microbiome and its implications in intestinal transplantation. *Curr. Opin. Organ Transplant.* 21, 135–139. doi: 10.1097/mot.0000000000000278

Laitio, M., and Nevalainen, J. (1975). An electron microscopic study of intestinal metaplasia in human gallbladder. *Beitr. Pathol.* 155, 297–308. doi: 10.1016/s0005-8165(75)80123-5

Lee, D. K., Tarr, P. I., Haigh, W. G., and Lee, S. P. (1999). Bacterial DNA in mixed cholesterol gallstones. *Am. J. Gastroenterol.* 94, 3502–3506. doi: 10.1111/j.1572-0241.1999.01614.x

Leushacke, M., Tan, S. H., Wong, A., Swathi, Y., Hajamohideen, A., Tan, L. T., et al. (2017). Lgr5-expressing chief cells drive epithelial regeneration and cancer in the oxyntic stomach. *Nat. Cell Biol.* 19, 774–786. doi: 10.1038/ncb3541

Levine, J. E., Huber, E., Hammer, S. T., Harris, A. C., Greenson, J. K., Braun, T. M., et al. (2013). Low Paneth cell numbers at onset of gastrointestinal graft-versus-host disease identify patients at high risk for nonrelapse mortality. *Blood* 122, 1505–1509. doi: 10.1182/blood-2013-02-485813

Lewin, K. (1969). The Paneth cell in disease. *Gut* 10, 804–811. doi: 10.1136/gut.10.10.804

Lewin, K. J., Dowling, F., Wright, J. P., and Taylor, K. B. (1976). Gastric morphology and serum gastrin levels in pernicious anaemia. *Gut* 17, 551–560. doi: 10.1136/gut.17.7.551

Liu, N., Ando, T., Ishiguro, K., Maeda, O., Watanabe, O., Funasaka, K., et al. (2013). Characterization of bacterial biota in the distal esophagus of Japanese patients with reflux esophagitis and Barrett's esophagus. *BMC Infect. Dis.* 13:130. doi: 10.1186/1471-2334-13-130

Ljungqvist, L., Peeker, R., and Fall, M. (2007). Female urethral diverticulum: 26-year followup of a large series. *J. Urol.* 177, 219–224; discussion 224.

Ma, X., Chi, C., Fan, L., Dong, B., Shao, X., Xie, S., et al. (2019). The microbiome of prostate fluid is associated with prostate cancer. *Front. Microbiol.* 10:1664. doi: 10.3389/fmicb.2019.01664

Macfarlane, S., Furrie, E., Macfarlane, G. T., and Dillon, J. F. (2007). Microbial colonization of the upper gastrointestinal tract in patients with Barrett's esophagus. *Clin. Infect. Dis.* 45, 29–38. doi: 10.1086/518578

Mahon, M., Xu, J., Yi, X., Liu, X., Gao, N., and Zhang, L. (2016). Paneth cell in adenomas of the distal colorectum is inversely associated with synchronous advanced adenoma and carcinoma. *Sci. Rep.* 6:26129.

Massari, F., Mollica, V., Di Nunno, V., Gatto, L., Santoni, M., Scarpelli, M., et al. (2019). The human microbiota and prostate cancer: friend or foe? *Cancers* 11:E459.

Matsubara, F. (1977). Morphological study of the Paneth cell. Paneth cells in intestinal metaplasia of the stomach and duodenum of man. *Acta Pathol. Jpn.* 27, 677–695. doi: 10.1111/j.1440-1827.1977.tb00185.x

Matsukura, N., Kawachi, T., Sugimura, T., Nakadate, M., and Hirota, T. (1979). Induction of intestinal metaplasia and carcinoma in the glandular stomach of rats by N-alkyl-N'-nitro-N-nitrosoguanidines. *Gan* 70, 181–185.

Maung, R., Kelly, J. K., and Grace, D. A. (1988). Intestinal metaplasia and dysplasia of prostatic urethra secondary to stricture. *Urology* 32, 361–363. doi: 10.1016/0090-4295(88)90246-4

Maurer, K. J., Ihrig, M. M., Rogers, A. B., Ng, V., Bouchard, G., Leonard, M. R., et al. (2005). Identification of cholelithogenic enterohepatic *Helicobacter* species and their role in murine cholesterol gallstone formation. *Gastroenterology* 128, 1023–1033. doi: 10.1053/j.gastro.2005.01.008

McElroy, S. J., Underwood, M. A., and Sherman, M. P. (2013). Paneth cells and necrotizing enterocolitis: a novel hypothesis for disease pathogenesis. *Neonatology* 103, 10–20. doi: 10.1159/000342340

Mera, R. M., Bravo, L. E., Camargo, M. C., Bravo, J. C., Delgado, A. G., Romero-Gallo, J., et al. (2018). Dynamics of *Helicobacter pylori* infection as a determinant of progression of gastric precancerous lesions: 16-year follow-up of an eradication trial. *Gut* 67, 1239–1246. doi: 10.1136/gutjnl-2016-311685

Ming, S. C., Goldman, H., and Freiman, D. G. (1967). Intestinal metaplasia and histogenesis of carcinoma in human stomach. Light and electron microscopic study. *Cancer* 20, 1418–1429. doi: 10.1002/1097-0142(196709)20:9<1418::aid-cncr2820200908>3.0.co;2-z

Mitsuhashi, J., Mikami, T., Saigenji, K., and Okayasu, I. (2005). Significant correlation of morphological remodeling in ulcerative colitis with disease duration and between elevated p53 and p21 expression in rectal mucosa and neoplastic development. *Pathol. Int.* 55, 113–121. doi: 10.1111/j.1440-1827.2005.01802.x

Montero, C., and Loizaga, J. M. (1971). Disulphide groups in Paneth cell granules of enteoid metaplasia in chronic gastritis. *Histochem. J.* 3, 399–402. doi: 10.1007/bf01005022

Morson, B. C. (1955). Carcinoma arising from areas of intestinal metaplasia in the gastric mucosa. *Br. J. Cancer* 9, 377–385. doi: 10.1038/bjc.1955.36

Naef, A. P., Savary, M., and Ozzello, L. (1975). Columnar-lined lower esophagus: an acquired lesion with malignant predisposition. Report on 140 cases of Barrett's esophagus with 12 adenocarcinomas. *J. Thorac. Cardiovasc. Surg.* 70, 826–835. doi: 10.1016/s0022-5223(19)39666-7

Nevalainen, T. J., Shah, V. I., De Peralta-Venturina, M., and Amin, M. B. (2001). Absence of group II phospholipase A2, a Paneth cell marker, from the epididymis. *APMIS* 109, 295–298. doi: 10.1034/j.1600-0463.2001.d01-123.x

Niemiec, T. R., Mercer, L. J., Stephens, J. K., and Hajj, S. N. (1989). Unusual urethral diverticulum lined by colonic epithelium with Paneth cell metaplasia. *Am. J. Obstet. Gynecol.* 160, 186–188. doi: 10.1016/0002-9378(89)90116-6

Nistal, M., Marino-Enriquez, A., and De Miguel, M. P. (2007). Granular changes (Paneth cell-like) in epididymal epithelial cells are lysosomal in nature and are not markers of obstruction. *Histopathology* 50, 944–947. doi: 10.1111/j.1365-2559.2007.02690.x

Nomura, Y., Tanabe, H., Moriichi, K., Igawa, S., Ando, K., Ueno, N., et al. (2013). Reduction of E-cadherin by human defensin-5 in esophageal squamous cells. *Biochem. Biophys. Res. Commun.* 439, 71–77. doi: 10.1016/j.bbrc.2013.08.026

Ogura, K., Hirata, Y., Yanai, A., Shibata, W., Ohmae, T., Mitsuno, Y., et al. (2008). The effect of *Helicobacter pylori* eradication on reducing the incidence of gastric cancer. *J. Clin. Gastroenterol.* 42, 279–283.

Ohtani, H., and Sasano, N. (1988). Ultrastructural immunolocalization of lysozyme in paneth-like cells in undifferentiated (gastric)-type carcinoma of the stomach. *Acta Pathol. Jpn.* 38, 861–871. doi: 10.1111/j.1440-1827.1988.tb02358.x

Osias, G. L., Bromer, M. Q., Thomas, R. M., Friedel, D., Miller, L. S., Suh, B., et al. (2004). Esophageal bacteria and Barrett's esophagus: a preliminary report. *Dig. Dis. Sci.* 49, 228–236.

Ostaff, M. J., Schafer, C., Courth, L., Stebe, S. R., Ott, G., Stange, E. F., et al. (2015). Chronic heavy alcohol use is associated with upregulated paneth cell antimicrobials in gastric mucosa. *Clin. Transl. Gastroenterol.* 6:e103. doi: 10.1038/ctg.2015.26

Ozzello, L., Savary, M., and Roethlisberger, B. (1977). Columnar mucosa of the distal esophagus in patients with gastroesophageal reflux. *Pathol. Annu.* 12(Pt 1), 41–86.

Pai, R. K., Rybicki, L. A., Goldblum, J. R., Shen, B., Xiao, S. Y., and Liu, X. (2013). Paneth cells in colonic adenomas: association with male sex and adenoma burden. *Am. J. Surg. Pathol.* 37, 98–103. doi: 10.1097/pas.0b013e318267b02e

Paneth, J. (1888). Ueber die secernirenden zellen des dunndarm-epithels. *Arch. Mikrosk. Anat.* 31, 113–191. doi: 10.1007/bf02955706

Pei, Z., Yang, L., Peek, R. M. Jr., Levine, S. M., Pride, D. T., and Blaser, M. J. (2005). Bacterial biota in reflux esophagitis and Barrett's esophagus. *World J. Gastroenterol.* 11, 7277–7283.

Perminow, G., Beisner, J., Koslowski, M., Lyckander, L. G., Stange, E., Vatn, M. H., et al. (2010). Defective paneth cell-mediated host defense in pediatric ileal Crohn's disease. *Am. J. Gastroenterol.* 105, 452–459. doi: 10.1038/ajg.2009.643

Puiman, P. J., Burger-Van Paassen, N., Schaart, M. W., De Bruijn, A. C., De Krijger, R. R., Tibboel, D., et al. (2011). Paneth cell hyperplasia and metaplasia in necrotizing enterocolitis. *Pediatr. Res.* 69, 217–223. doi: 10.1203/pdr.0b013e3182092a9a

Quante, M., Bhagat, G., Abrams, J. A., Marache, F., Good, P., Lee, M. D., et al. (2012). Bile acid and inflammation activate gastric cardia stem cells in a mouse model of Barrett-like metaplasia. *Cancer Cell* 21, 36–51. doi: 10.1016/j.ccr.2011.12.004

Rubio, C. A. (1989). Paneth cell adenoma of the stomach. *Am. J. Surg. Pathol.* 13, 325–328. doi: 10.1097/00000478-198904000-00008

Rubio, C. A. (2012). Lysozyme is up-regulated in columnar-lined Barrett's mucosa: a possible natural defence mechanism against Barrett's esophagus-associated pathogenic bacteria. *Anticancer Res.* 32, 5115–5119.

Rubio, C. A. (2015). Increased production of lysozyme associated with bacterial proliferation in Barrett's Esophagitis, Chronic Gastritis, Gluten-induced Atrophic duodenitis (celiac disease), lymphocytic colitis, collagenous colitis, ulcerative colitis and Crohn's colitis. *Anticancer Res.* 35, 6365–6372.

Rubio, C. A., Kato, Y., Sugano, H., and Kitagawa, T. (1987). Intestinal metaplasia of the stomach in Swedish and Japanese patients without ulcers or carcinoma. *Jpn. J. Cancer Res.* 78, 467–472.

Saenz, J. B., and Mills, J. C. (2018). Acid and the basis for cellular plasticity and reprogramming in gastric repair and cancer. *Nat. Rev. Gastroenterol. Hepatol.* 15, 257–273. doi: 10.1038/nrgastro.2018.5

Sakaki, M., Hirokawa, M., Sano, T., Horiguchi, H., Wakatsuki, S., and Ogata, S. (2000). Gallbladder adenocarcinoma with florid neuroendocrine cell nests and extensive paneth cell metaplasia. *Endocr. Pathol.* 11, 365–371.

Sakitani, K., Hirata, Y., Watabe, H., Yamada, A., Sugimoto, T., Yamaji, Y., et al. (2011). Gastric cancer risk according to the distribution of intestinal metaplasia and neutrophil infiltration. *J. Gastroenterol. Hepatol.* 26, 1570–1575. doi: 10.1111/j.1440-1746.2011.06767.x

Saltykova, I. V., Petrov, V. A., Logacheva, M. D., Ivanova, P. G., Merzlikin, N. V., Sazonov, A. E., et al. (2016). Biliary microbiota, gallstone disease and infection with *Opisthorchis felineus*. *PLoS Negl. Trop. Dis.* 10:e0004809. doi: 10.1371/journal.pntd.0004809

Salzman, N. H., Hung, K., Haribhai, D., Chu, H., Karlsson-Sjoberg, J., Amir, E., et al. (2010). Enteric defensins are essential regulators of intestinal microbial ecology. *Nat. Immunol.* 11, 76–83.

Sandow, M. J., and Whitehead, R. (1979). The Paneth cell. *Gut* 20, 420–431.

Sato, T., Van Es, J. H., Snippert, H. J., Stange, D. E., Vries, R. G., Van Den Born, M., et al. (2011). Paneth cells constitute the niche for Lgr5 stem cells in intestinal crypts. *Nature* 469, 415–418. doi: 10.1038/nature09637

Sayin, S. I., Wahlstrom, A., Felin, J., Jantti, S., Marschall, H. U., Bamberg, K., et al. (2013). Gut microbiota regulates bile acid metabolism by reducing the levels of tauro-beta-muricholic acid, a naturally occurring FXR antagonist. *Cell Metab.* 17, 225–235. doi: 10.1016/j.cmet.2013.01.003

Schreiber, D. S., Apstein, M., and Hermos, J. A. (1978). Paneth cells in Barrett's esophagus. *Gastroenterology* 74, 1302–1304. doi: 10.1016/0016-5085(78)90711-4

Schwalbe, G. (1872). Beitrage zur kenntnis der drusen in den darmwandungen insbesondere der Brunner'schen drusen. *Arch. Mikr. Anat.* 8, 92–139.

Segura, D. I., and Montero, C. (1983). Histochemical characterization of different types of intestinal metaplasia in gastric mucosa. *Cancer* 52, 498–503. doi: 10.1002/1097-0142(19830801)52:3<498::aid-cncr2820520320>3.0.co;2-8

Sekirov, I., Russell, S. L., Antunes, L. C., and Finlay, B. B. (2010). Gut microbiota in health and disease. *Physiol. Rev.* 90, 859–904.

Shen, B., Porter, E. M., Reynoso, E., Shen, C., Ghosh, D., Connor, J. T., et al. (2005). Human defensin 5 expression in intestinal metaplasia of the upper gastrointestinal tract. *J. Clin. Pathol.* 58, 687–694. doi: 10.1136/jcp.2004.022426

Shi, J. (2007). Defensins and Paneth cells in inflammatory bowel disease. *Inflamm. Bowel Dis.* 13, 1284–1292. doi: 10.1002/ibd.20197

Shichijo, S., Hirata, Y., Niikura, R., Hayakawa, Y., Yamada, A., Ushiku, T., et al. (2016). Histologic intestinal metaplasia and endoscopic atrophy are predictors of gastric cancer development after *Helicobacter pylori* eradication. *Gastrointest. Endosc.* 84, 618–624. doi: 10.1016/j.gie.2016.03.791

Shichijo, S., Hirata, Y., Sakitani, K., Yamamoto, S., Serizawa, T., Niikura, R., et al. (2015). Distribution of intestinal metaplasia as a predictor of gastric cancer development. *J. Gastroenterol. Hepatol.* 30, 1260–1264. doi: 10.1111/jgh.12946

Shimada, S., Maeno, M., Misumi, A., Takano, S., and Akagi, M. (1987). Antigen reversion of glycogen phosphorylase isoenzyme in carcinoma and proliferative zone of intestinal metaplasia of the human stomach. An immunohistochemical study. *Gastroenterology* 93, 35–40. doi: 10.1016/0016-5085(87)90310-6

Shrestha, E., White, J. R., Yu, S. H., Kulac, I., Ertunc, O., De Marzo, A. M., et al. (2018). Profiling the urinary microbiome in men with positive versus negative biopsies for prostate cancer. *J. Urol.* 199, 161–171. doi: 10.1016/j.juro.2017.08.001

Simmonds, N., Furman, M., Karanika, E., Phillips, A., and Bates, A. W. (2014). Paneth cell metaplasia in newly diagnosed inflammatory bowel disease in children. *BMC Gastroenterol.* 14:93. doi: 10.1186/1471-230X-14-93

Stewart, L., Smith, A. L., Pellegrini, C. A., Motson, R. W., and Way, L. W. (1987). Pigment gallstones form as a composite of bacterial microcolonies and pigment solids. *Ann. Surg.* 206, 242–250. doi: 10.1097/00000658-198709000-00002

Symonds, D. A. (1974). Paneth cell metaplasia in diseases of the colon and rectum. *Arch. Pathol.* 97, 343–347.

Takubo, K., Nixon, J. M., and Jass, J. R. (1995). Ducts of esophageal glands proper and paneth cells in Barrett's esophagus: frequency in biopsy specimens. *Pathology* 27, 315–317. doi: 10.1080/00313029500169213

Tanabe, H., Sato, T., Watari, J., Maemoto, A., Fujiya, M., Kono, T., et al. (2008). Functional role of metaplastic paneth cell defensins in *Helicobacter pylori*-infected stomach. *Helicobacter* 13, 370–379. doi: 10.1111/j.1523-5378.2008.00621.x

Tanaka, M., Saito, H., Kusumi, T., Fukuda, S., Shimoyama, T., Sasaki, Y., et al. (2001). Spatial distribution and histogenesis of colorectal Paneth cell metaplasia in idiopathic inflammatory bowel disease. *J. Gastroenterol. Hepatol.* 16, 1353–1359. doi: 10.1046/j.1440-1746.2001.02629.x

Thompson, J. J., Zinsser, K. R., and Enterline, H. T. (1983). Barrett's metaplasia and adenocarcinoma of the esophagus and gastroesophageal junction. *Hum. Pathol.* 14, 42–61. doi: 10.1016/s0046-8177(83)80045-8

Uemura, N., Okamoto, S., Yamamoto, S., Matsumura, N., Yamaguchi, S., Yamakido, M., et al. (2001). *Helicobacter pylori* infection and the development of gastric cancer. *N. Engl. J. Med.* 345, 784–789.

Vaishnava, S., Behrendt, C. L., Ismail, A. S., Eckmann, L., and Hooper, L. V. (2008). Paneth cells directly sense gut commensals and maintain homeostasis at the intestinal host-microbial interface. *Proc. Natl. Acad. Sci. U.S.A.* 105, 20858–20863. doi: 10.1073/pnas.0808723105

van der Sluis, W. B., Neefjes-Borst, E. A., Bouman, M. B., Meijerink, W. J., De Boer, N. K., Mullender, M. G., et al. (2016). Morphological spectrum of neovaginitis in autologous sigmoid transplant patients. *Histopathology* 68, 1004–1012. doi: 10.1111/his.12894

Wada, R., Kuwabara, N., and Suda, K. (1994). Incidence of Paneth cells in colorectal adenomas of Japanese descendants in Hawaii. *J. Gastroenterol. Hepatol.* 9, 286–288. doi: 10.1111/j.1440-1746.1994.tb01727.x

Wada, R., Yamaguchi, T., and Tadokoro, K. (2005). Colonic Paneth cell metaplasia is pre-neoplastic condition of colonic cancer or not? *J. Carcinog.* 4:5.

Wang, D., Peregrina, K., Dhima, E., Lin, E. Y., Mariadason, J. M., and Augenlicht, L. H. (2011a). Paneth cell marker expression in intestinal villi and colon crypts characterizes dietary induced risk for mouse sporadic intestinal cancer. *Proc. Natl. Acad. Sci. U.S.A.* 108, 10272–10277. doi: 10.1073/pnas.1017668108

Wang, D. Q., Cohen, D. E., and Carey, M. C. (2009). Biliary lipids and cholesterol gallstone disease. *J. Lipid Res.* 50(Suppl.), S406–S411.

Wang, J., Xu, L., Shi, R., Huang, X., Li, S. W., Huang, Z., et al. (2011b). Gastric atrophy and intestinal metaplasia before and after *Helicobacter pylori* eradication: a meta-analysis. *Digestion* 83, 253–260. doi: 10.1159/000280318

Watanabe, H. (1978). Experimentally induced intestinal metaplasia in Wistar rats by X-ray irradiation. *Gastroenterology* 75, 796–799. doi: 10.1016/0016-5085(78)90460-2

Webb, P. M., Yu, M. C., Forman, D., Henderson, B. E., Newell, D. G., Yuan, J. M., et al. (1996). An apparent lack of association between *Helicobacter pylori* infection and risk of gastric cancer in China. *Int. J. Cancer* 67, 603–607. doi: 10.1002/(sici)1097-0215(19960904)67:5<603::aid-ijc2>3.0.co;2-y

Wehkamp, J., Salzman, N. H., Porter, E., Nuding, S., Weichenthal, M., Petras, R. E., et al. (2005). Reduced Paneth cell alpha-defensins in ileal Crohn's disease. *Proc. Natl. Acad. Sci. U.S.A.* 102, 18129–18134.

Wehkamp, J., Schmid, M., and Stange, E. F. (2007). Defensins and other antimicrobial peptides in inflammatory bowel disease. *Curr. Opin. Gastroenterol.* 23, 370–378. doi: 10.1097/mog.0b013e328136c580

Wehkamp, J., and Stange, E. F. (2010). Paneth's disease. *J. Crohns Colitis* 4, 523–531.

White, J. R., Gong, H., Pope, B., Schlievert, P., and Mcelroy, S. J. (2017). Paneth-cell-disruption-induced necrotizing enterocolitis in mice requires live bacteria and occurs independently of TLR4 signaling. *Dis. Model Mech.* 10, 727–736. doi: 10.1242/dmm.028589

White, J. S., Hoper, M., Parks, R. W., Clements, W. D., and Diamond, T. (2006). Patterns of bacterial translocation in experimental biliary obstruction. *J. Surg. Res.* 132, 80–84. doi: 10.1016/j.jss.2005.07.026

Willet, S. G., Lewis, M. A., Miao, Z. F., Liu, D., Radyk, M. D., Cunningham, R. L., et al. (2018). Regenerative proliferation of differentiated cells by mTORC1-dependent paligenosis. *EMBO J.* 37:e98311.

Yamamoto, M., Nakajo, S., and Tahara, E. (1989). Dysplasia of the gallbladder. Its histogenesis and correlation to gallbladder adenocarcinoma. *Pathol. Res. Pract.* 185, 454–460.

Yang, L., Lu, X., Nossa, C. W., Francois, F., Peek, R. M., and Pei, Z. (2009). Inflammation and intestinal metaplasia of the distal esophagus are associated with alterations in the microbiome. *Gastroenterology* 137, 588–597. doi: 10.1053/j.gastro.2009.04.046

Yu, S., Tong, K., Zhao, Y., Balasubramanian, I., Yap, G. S., Ferraris, R. P., et al. (2018). Paneth cell multipotency induced by notch activation following injury. *Cell Stem Cell* 23, 46–59. doi: 10.1016/j.stem.2018.05.002

Zhang, C., Sherman, M. P., Prince, L. S., Bader, D., Weitkamp, J. H., Slaughter, J. C., et al. (2012). Paneth cell ablation in the presence of *Klebsiella pneumoniae* induces necrotizing enterocolitis (NEC)-like injury in the small intestine of immature mice. *Dis. Model Mech.* 5, 522–532. doi: 10.1242/dmm. 009001

Zullo, A., Rinaldi, V., Hassan, C., Diana, F., Winn, S., Castagna, G., et al. (2000). Ascorbic acid and intestinal metaplasia in the stomach: a prospective, randomized study. *Aliment. Pharmacol. Ther.* 14, 1303–1309. doi: 10.1046/j.1365-2036.2000.00841.x

Advantages of publishing in Frontiers

OPEN ACCESS
Articles are free to read
for greatest visibility
and readership

FAST PUBLICATION
Around 90 days
from submission
to decision

HIGH QUALITY PEER-REVIEW
Rigorous, collaborative,
and constructive
peer-review

TRANSPARENT PEER-REVIEW
Editors and reviewers
acknowledged by name
on published articles

Frontiers
Avenue du Tribunal-Fédéral 34
1005 Lausanne | Switzerland

Visit us: www.frontiersin.org
Contact us: info@frontiersin.org | +41 21 510 17 00

REPRODUCIBILITY OF RESEARCH
Support open data
and methods to enhance
research reproducibility

DIGITAL PUBLISHING
Articles designed
for optimal readership
across devices

FOLLOW US
@frontiersin

IMPACT METRICS
Advanced article metrics
track visibility across
digital media

EXTENSIVE PROMOTION
Marketing
and promotion
of impactful research

LOOP RESEARCH NETWORK
Our network
increases your
article's readership